STUDIES OF PLATINUM POLYYNYL COMPLEXES: ELABORATION OF NOVEL "CLICK" CYCLOADDUCTS AND FLUOROUS AND POLYGON BASED PLATINUM POLYYNEDIYL SYSTEMS

A Dissertation

by

MELISSA CATHERINE CLOUGH

Submitted to the Office of Graduate Studies of
Texas A&M University
in partial fulfillment of the requirements for the degree of

DOCTOR OF PHILOSOPHY

Approved by:

Chair of Committee,	John Gladysz
Committee Members,	Donald Darensbourg
	François Gabbaï
	Hung-Jue Sue
Head of Department,	David Russell

December 2012

Major Subject: Chemistry

ABSTRACT

The major directions of this dissertation involve (1) the syntheses and characterization of molecular polygons incorporating sp-hybridized carbon linkers and L_2Pt corners (L_2 = *cis*-1,3-diphosphine), (2) the development of protected carbon chain complexes featuring fluorous phosphine ligands and (3) click reactions of metal terminal polyynyl complexes and further metallations of the resulting triazole rings. A brief overview is provided in Chapter I.

Chapter II details the syntheses of molecular squares containing bidendate diphosphine ligands of the formula $R_2C(CH_2PPh_2)_2$ where R = Me, Et, *n*-Bu, *n*-Dec, Bn, and *p*-tolCH_2 (general designation dppp*), in which the R_2 groups are intended to circumvent the solubility issues encountered by others. Their syntheses involve double substitutions of the dimesylate compounds $R_2C(CH_2OMs)_2$ using $KPPh_2$. Building blocks of the formulae (dppp*)$PtCl_2$ and (dppp*)$Pt((C{\equiv}C)_2H)_2$ are synthesized and characterized, including one crystal structure of the latter. The target complexes are accessed by reactions of (dppp*)$PtCl_2$ with (dppp*)$Pt((C{\equiv}C)_2H)_2$ under Sonogashira type conditions. Six new squares of the formula $[(R_2C(CH_2PPh_2)_2)Pt(C{\equiv}C)_2]_4$ are characterized including two crystal structures. Further topics include approaches to higher homologues and cyclocarbon synthesis.

Chapter III focuses on carbon chain complexes bearing fluorous phosphine ligands of the formula $P((CH_2)_mR_{fn})_3$ (R_{fn} = $(CF_2)_{n-1}CF_3$; *m/n* = 2/8, 3/8, and 3/10). Precursors of the formula *trans*-$(C_6F_5)((R_{fn}(CH_2)_m)_3P)_2PtCl$ are synthesized and characterized, including one crystal structure, which reveals phase separation of the fluorous and non-fluorous domains. Reactions with butadiyne give *trans*-

$(C_6F_5)((R_{fn}(CH_2)_m)_3P)_2Pt(C{\equiv}C)_2H$. Oxidative homocouplings afford the target complexes *trans,trans*-$(C_6F_5)((R_{fn}(CH_2)_m)_3P)_2Pt(C{\equiv}C)_4(C_6F_5)(P((CH_2)_mR_{fn})_3)_2Pt$. Cyclic voltammetry indicates irreversible oxidations of the title compounds, in contrast to partially reversible oxidations of non-fluorous analogues.

Chapter IV focuses on multimetallic complexes achieved by click reactions in metal coordination spheres. The copper catalyzed click reaction between *trans*-$(C_6F_5)(p\text{-}tol_3P)_2Pt(C{\equiv}C)_2H$ (1) and $(\eta^5\text{-}C_5H_4N_3)Re(CO)_3$ affords the bimetallic 1,2,3-triazole *trans*-$(C_6F_5)(p\text{-}tol_3P)_2PtC{\equiv}CC{=}CHN((\eta^5\text{-}C_5H_4)Re(CO)_3)N{=}N$. Further reactions with $Re(CO)_5OTf$ and $Re(CO)_5Br$ give trimetallated adducts, which represent the first species of this type. An alternative route to a trimetallic complex involves the twofold cycloaddition of the diazide $(\eta^5\text{-}C_5H_4N_3)_2Fe$ and 1, giving $(\eta^5\text{-}C_5H_4NN{=}N\text{-}C(trans\text{-}(C{\equiv}C)Pt(Pp\text{-}tol_3)_2(C_6F_5){=}CH)_2Fe$. The crystal structures of the di and trimetallic complexes are compared, but attempts to achieve a fourth metallation involving the =CH groups are unsuccessful. However, when the triazolium salt $[trans\text{-}(C_6F_5)(p\text{-}tol_3P)_2PtC{\equiv}CC{=}CHN(CH_2C_6H_5)N{=}N(Me)]^+ I^-$ is treated with Ag_2O and $[Rh(COD)Cl]_2$, a =CRh adduct is obtained. The success of =CH metallation is correlated to the ^1H NMR chemical shift, indicative of an electronic effect.

ACKNOWLEDGEMENTS

I would first like to thank my research advisor, Dr. John Gladysz. For years, he has lavished his efforts on my research and recently much time and effort on this dissertation. I have learned a great deal from him. The process of writing a dissertation, although never a fun experience, has been a very lucrative one with him. I would also like to thank my committee members, Dr. Don Darensbourg, Dr. François Gabbaï, and Dr. Hung-Jue Sue for their precious time.

The Gladysz group has been a constant source of support. First and foremost, thanks to Dr. Sébastien Gauthier and Dr. Yoshihiro Kobayashi who taught me during my early graduate school years. I can't imagine not having had them as mentors when I first came to College Station. I want to thank Dr. Juan Guerrero-Leal, who, during his post-doctoral position, was of immeasurable help to me. I want to thank Dr. Paul Zeits, who throughout most of my graduate school career, was always a source of immense knowledge and guided me in so many ways. I want to thank Georgette Lang and Kyle Lewis for being the best bench mates I could ask for. To everyone else in the Gladysz group, I'm grateful for your guidance, help, and birthday cake surprises. I also want to acknowledge the Bluemel group members for their assistance.

I want to thank those special friends whom I met on the first day of graduate school and friends I have made on the way. Without them, I wouldn't have had a family in College Station.

Finally, I would like to thank Dr. Nattamai Bhuvanesh, who has proven to be a very skilled and helpful crystallographer throughout this process.

DEDICATION

I dedicate this dissertation to my family. My parents, Cristina and Daniel Clough, have invested immeasurable efforts to ensure that I succeed and continue to be happy. My sister, Christiane, and her family have kept me sane throughout the process. My nephew, Angelo, has always been my number one fan. Finally, my baby sister, Michelle, even though she doesn't understand why I or anyone would enjoy the subject of chemistry, has always been there for me in countless ways. I cannot thank my family enough for their continual support.

TABLE OF CONTENTS

LIST OF FIGURES

LIST OF SCHEMES

SCHEME Page

LIST OF TABLES

NOMENCLATURE

δ	chemical shift in ppm
ν	stretching mode (IR)
$\{^1H\}$	proton decoupled
Å	Angstrom
APCI	atmospheric pressure chemical ionization
Avg	average
Bn	benzyl
br	broad
Bu	butyl
Bipy	bipyridine
Calcd	calculated
CHCA	α-cyano-4-hydroxycinnamic acid
Cp	cyclopentadienyl
C_{sp}	sp hybridized carbon atom
d	doublet (NMR), days
DCTB	*trans*-2-(3-(4-*t*-butyl-phenyl)-2-methyl-2-propenylidene)malononitrile
Dec	decyl
DMF	dimethylformamide
DMSO	dimethylsulfoxide
dppe	1,2-bis(diphenylphosphino) ethane
dppp	diphenylphosphino propane
Et	ethyl
equiv	equivalent

ESI	electrospray ionization
h	hour
HPLC	high pressure liquid chromatography
i	*ipso*
$^{i}J_{jk}$	scalar coupling constant for coupling of nucleus j with nucleus k through i bonds
IR	infrared
M	metal, mol/L
m	multiplet (NMR), medium (IR)
m	meta
MALDI	matrix assisted laser desorption ionization
Me	methyl
min	minutes
MS	mass spectrometry
n	normal, number of units
NMR	nuclear magnetic resonance
nr	no reaction
o	ortho
OAc	acetate
p	para
ppm	parts per million
py	pyridine
q	quartet
R	organic group
rt	room temperature

s	singlet (NMR), strong (IR)
sept	septet
t	triplet
t	tertiary
Tf	triflate
TFA	trifluoroacetic acid
THAP	2',4',6'-trihydroxyacetophenone monohydrate
THF	tetrahydrofuran
THT	tetrahydrothiophene
TLC	thin layer chromatography
TMEDA	tetramethylethylenediamine
tol	tolyl
UV	ultraviolet
V	volume
vis	visible
vs	very strong
v/v	volume/volume
w	weak

CHAPTER I

INTRODUCTION

Graphite and diamond are the two most ubiquitous and well understood allotropes of carbon. More recently, the carbon allotrope class of fullerenes has been explored, with such work leading to the 1996 Nobel Prize and applications in many different fields.[1] These allotropes, shown in Figure 1.1, are much better understood than the putative carbon allotrope carbyne based on sp hybridized carbon.[2]

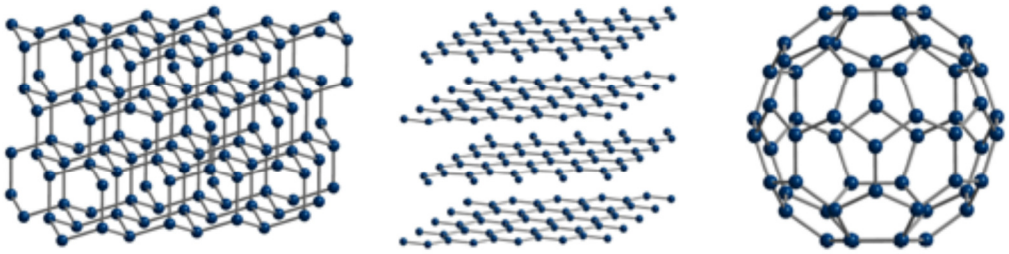

Figure 1.1. Three allotropes of carbon: diamond (left), graphite (middle), and buckminsterfullerene (right).

The polymer carbyne theoretically has two forms, polyyne ($H(C{\equiv}C)_nH$) and cumulene ($H_2C{=}(C{=}C)_n{=}CH_2$), and could also prove to hold beneficial properties, such as conductance and use as a wire in molecular electronics. To date, no direct evidence has been found for the isolation of carbyne as a bulk material.[3] Calculations have shown that the polyynic chain, with alternating single and triple bonds, is more stable than the cumulenic analogue, composed entirely of double bonds.[4]

This research aims to exploit the chemistry of the polyynediyl moiety to further understand its properties, reactivity, and possible uses. The reactivity of terminal polyynes is of special interest and falls into three categories for this study: (1) heterocoupling reactions with metal halides, (2) oxidative homocoupling reactions, and (3) click reactions with azides. These reaction types are extensively used in this research and are further discussed below.

The first involves a Sonogashira[5,6] type reaction between a terminal alkyne or polyynediyl complex and a metal halide to produce a new carbon-metal bond. This is the organometallic version of the typical Sonogashira reaction, which is widely used in organic chemistry to heterocouple a terminal alkyne and an aryl or vinyl halide to form a new carbon-carbon bond using copper and palladium catalysts.

The second type of reaction is a homocoupling reaction between two terminal poyynes. To accomplish this type of transformation, Hay conditions are often employed,[7] although several other coupling methods, such as the Glaser or Eglington (introduced in 1869 and 1959, respectively), are possible.[8,9] The Hay coupling method uses a copper (I) chloride-TMEDA complex as the catalyst in the presence of molecular oxygen. The TMEDA is added to facilitate catalyst solubility in the chosen solvent. This method was introdueced in 1962 and is preferred due to the increase in solubility of the copper catalyst system. The product is derived from a formal sp^3 carbon-hydrogen bond cleavage to form a new C_{sp}-C_{sp} linkage.

Lastly, copper catalyzed click reactions involving terminal alkynes or polyynes and azides result in the formation of 1,2,3-triazoles generated via two new carbon-nitrogen bonds.[10] A generalized summary of the three transformations is offered in Figure 1.2.

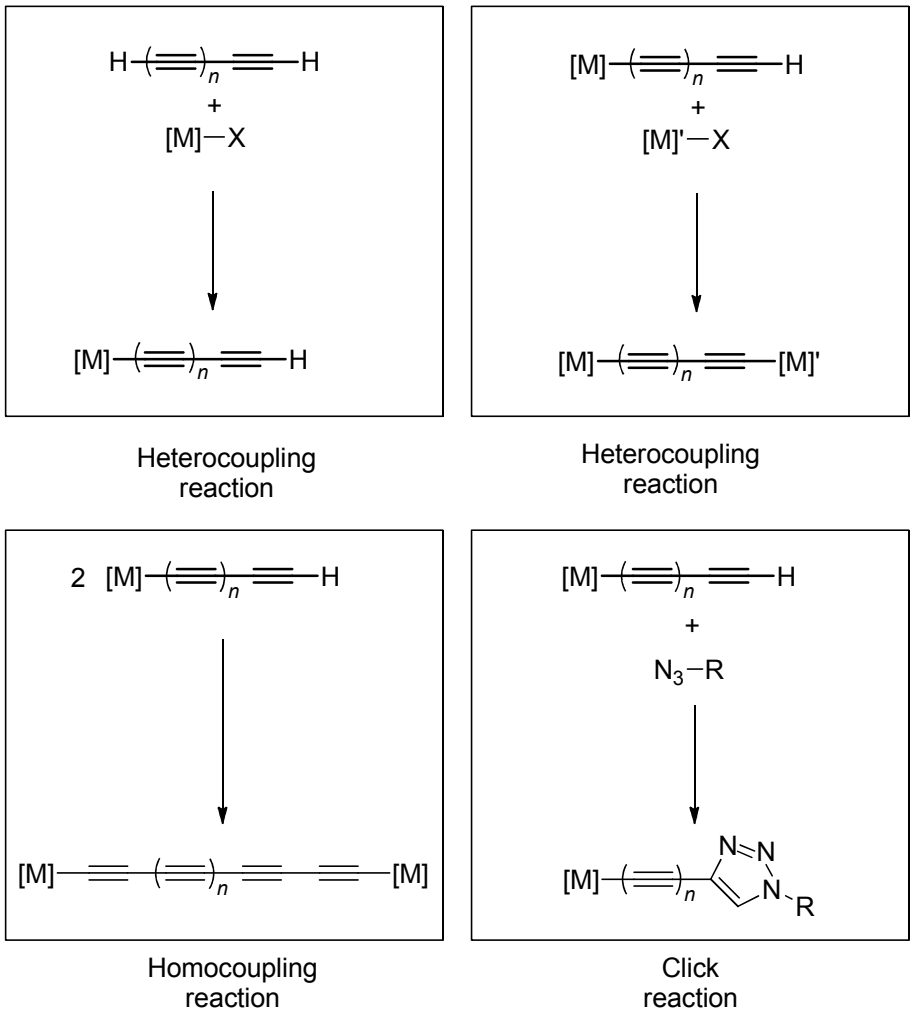

Figure 1.2. Copper catalyzed transformations of terminal polyynes.

This research consists of three components. Metal capped polyynyl or polyynediyl complexes are of interest and each chapter is concerned with a different type of ligand system on the metal and/or a different type of polyyne transformation.

Chapter II focuses on molecular polygons incorporating polyynediyl chains as the linear linkers. This work explores the concept of self assembly and supramolecular

chemistry, a topic of great interest to synthetic chemists.[11] Also involved in this work is the development and use of specialized bidentate diphosphines.

Chapter III focuses on polyynyl and polyynediyl systems comprised of four and eight sp carbon atoms bearing highly fluorous phosphines. Both the hetero and homocoupling reactions are successfully used to give complexes with novel phase properties.

Chapter IV focuses on click reactions with terminal polyynes. Since the terminal polyynes incorporate an organometallic moiety, this represents one of relatively few in-depth examinations of click reactions that occur within metal coordination spheres. Additionally, further functionalizations on the resulting triazole rings are possible, leading to the incorporation of metals at other heterocycle sites.

More generally, this research will focus on copper catalyzed transformations of terminal polyynes to form complexes that bear 2, 8, and 16 sp carbon atoms.

CHAPTER II

MOLECULAR POLYGONS EMPLOYING POLYYNEDIYL LINKERS AND BIDENTATE DIPHOSPHINE CONTAINING CORNERS

INTRODUCTION

1. Self assembly processes. Self assembly processes have been of interest for many years, and see much use in the construction of supramolecular architectures.[11-14] A self assembly process is a process in which various components are combined to form a highly specific aggregate.[15] Biological chemists are all too familiar with self assembly processes as they are necessary for the proliferation of biological systems. Synthetic chemists have been attracted to such phenomena, and have applied self-assembly to a variety of different targets.[16-18]

Self assembly products are typically constructed by combining highly specific and symmetrical subunits. Thus, self assembly or self organization can be approached in a methodical manner. Accordingly, these types of phenomena can be classified into three distinct groups as shown in Figure 2.1: statistical, amplified, and absolute.[19] The statistical classification assumes no organization; *i.e.*, the subunits of the polygon have no statistical reason to form product *x* over product *y*. The amplified approach takes into consideration certain variables such as subunit design and reaction temperature. The ideal case, or the absolute approach, utilizes subunits that are sufficiently encoded with enough electronic and steric parameters to guarantee a single self assembly product.

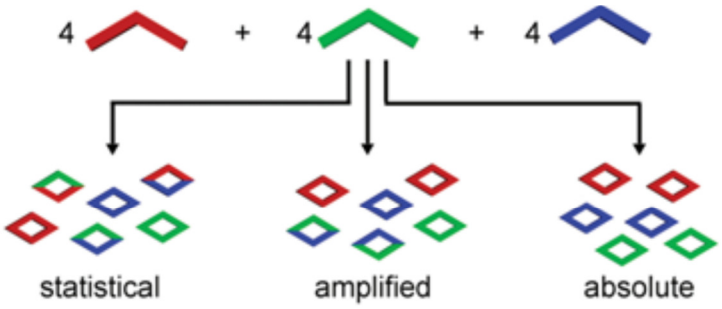

Figure 2.1. Classification of self assembly processes that can occur with a mixture of subunits: statistical (left), amplified (middle), and absolute (right).

The design of highly specific subunits is an integral part of approaching the ideal, or absolute, case. For instance, as shown in Figure 2.2, in the case of a self assembly product that adopts a square configuration, a combination of a linear unit and an angular unit with an angle at or near 90° would be desired. However, to build a pentagonal architecture, for example, an angular unit with an angle at or near 108° would be utilized.[13]

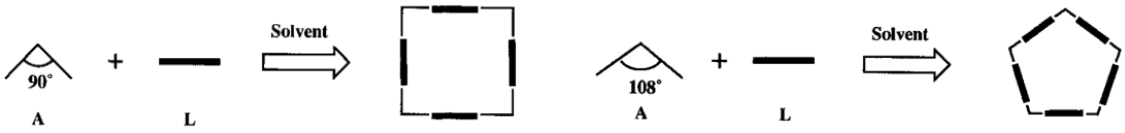

Figure 2.2. Schematic representation of square (left) and pentagon (right) angular and linear building blocks.

Due to the relatively well defined and understood nature of metal coordination spheres, coordination chemistry is often employed to construct well defined subunits.

This approach gives way to an efficient directed assembly of the desired aggregate, as the components are chosen for their particular bonding properties.

2. Molecular polygons and their applications. Self assembly processes can be utilized in the synthesis of molecular polygons. One type of molecular polygon, molecular squares, is of interest to synthetic chemists. Molecular squares first gained interest in 1990 when Ogura synthesized an organometallic molecular square shown in Figure 2.3 which was comprised of square planar palladium corners with 4,4'-bipy linkers (bipy = bipyridine). This octacationic square had the capability of encapsulating a guest molecule in solution, which was evidenced by high field shifts of the square signals in the ^{1}H NMR spectrum upon addition of 1,3,5-trimethoxybenzene.[20,21]

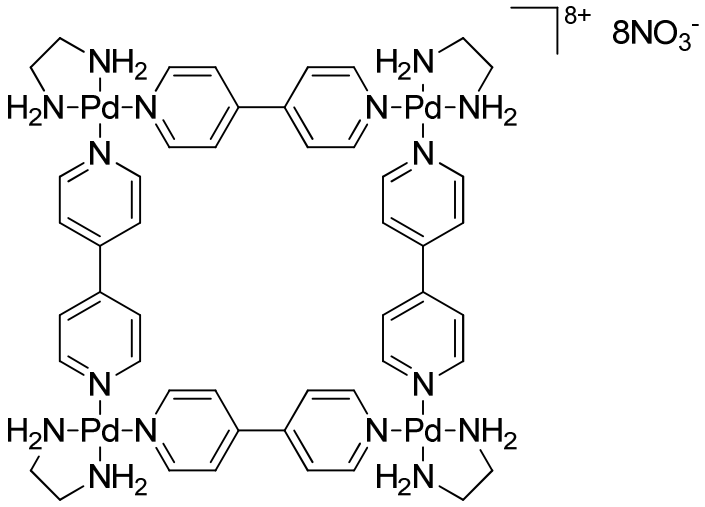

Figure 2.3. Ogura's molecular square capable of solution encapsulation.

Since Ogura's example, numerous molecular squares and other polygons have been synthesized that span an array of transition metals. Likewise, applications of molecular squares have since been extended to various uses, one of which being needed

an anti-cancer agent in biological chemistry. A molecular rectangle synthesized by Chi, comprised of ruthenium corners, is shown in Figure 2.4. Two possible isomers are possible for this rectangle, with one isomer depicted. It was demonstrated to have higher cytotoxicity against various human cancer cell lines than that of the reference drug, *cis*-platin ($(H_3N)_2PtCl_2$). As illustrated at the right in Figure 2.4, the rectangle was ca. four times more efficient at cancer cell destruction than *cis*-platin at a concentration of 30 μM.[22]

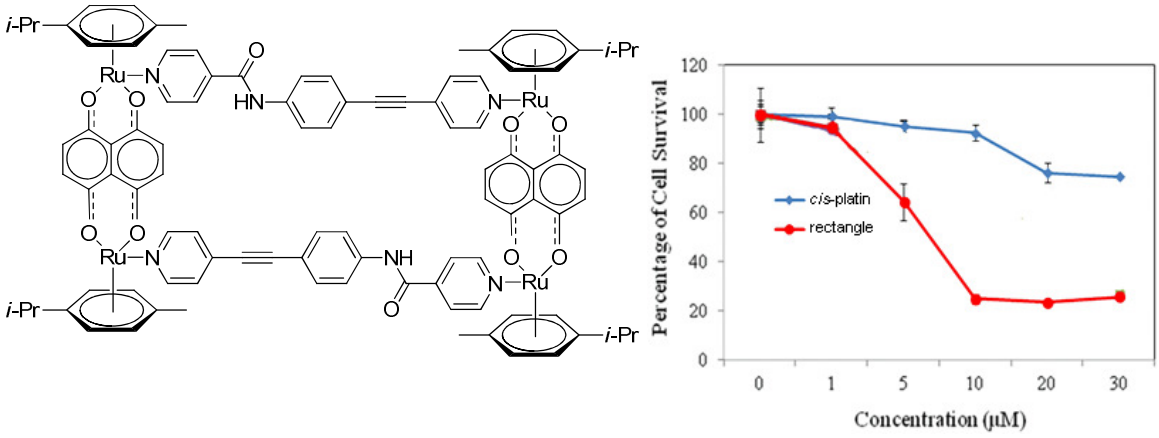

Figure 2.4. Chi's tetrametallic molecular rectangle (left) and a cytotoxicity study versus that of *cis*-platin against human lung cancer cells (right).

Many applications have been sought for molecular squares and rectangles, as evidenced by the examples given above. Molecular squares have been used as guests for an array of host molecules. A heterobimetallic palladium and platinum based square with dppf (1,1'-diphenylphosphino ferrocene) as the phosphine ligands was synthesized by Chi and shown to selectively sense electron deficient guests, such as nitroaromatics. As illustrated in Figure 2.5, the host behavior was exhibited by fluorescence quenching in

solution. Electron rich aromatic guests such as benzene and xylene were unresponsive in fluorescence quenching experiments. However, 1,3,5-trinitrobenzene, a highly electron deficient aromatic guest, exhibited a high degree of fluorescence quenching, indicating interaction with the square's electron rich linkers.[23]

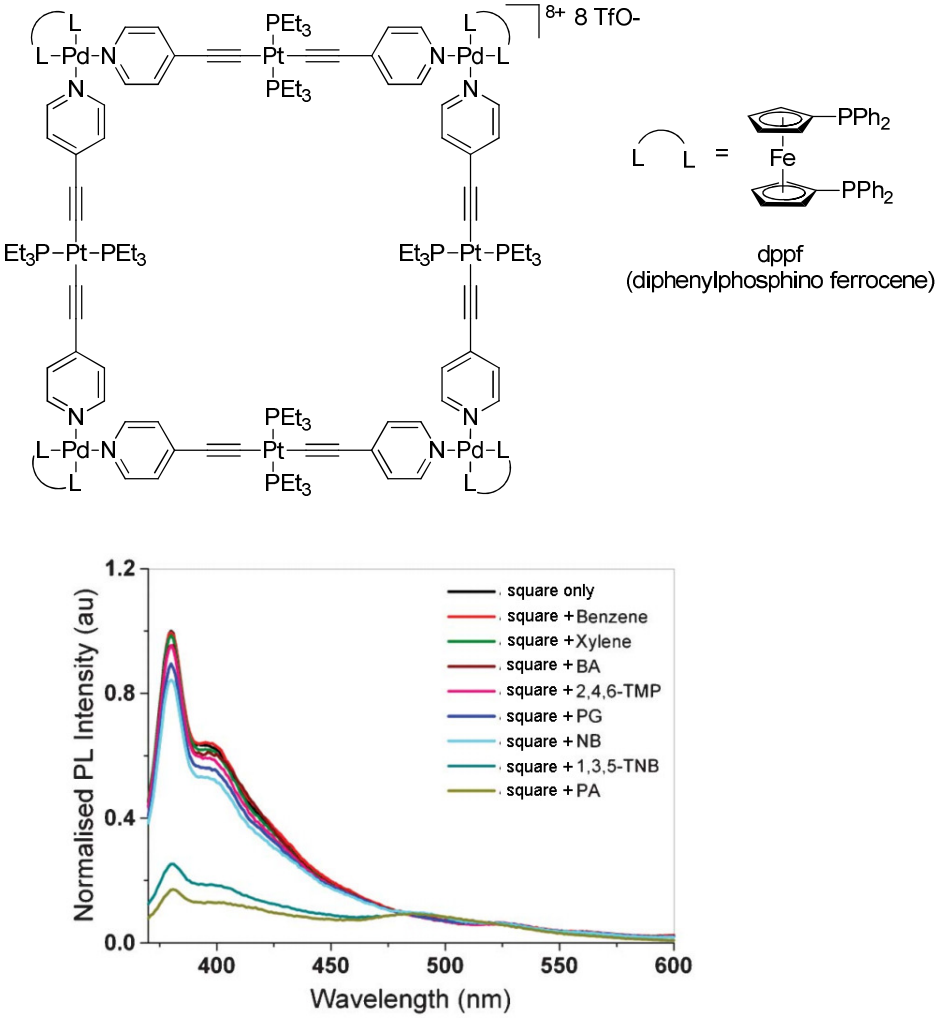

Figure 2.5. Chi's trimetallic molecular square (top) and fluorescence quenching (bottom) using various aromatic guest molecules. BA = benzoic acid, 2,4,6-TMP = 2,4,6-trimethylphenol, PG = phloroglucinol, 4-NB = 4-nitrobenzene, 1,3,5-TNB = 1,3,5-trinitrobenzene, and PA = picric acid.

Another type of guest applicable to the molecular polygon arena is fullerene, or C_{60}. Hosts for C_{60} were initially sought for use in separation from larger analogues such as C_{70} and C_{120} with effective hosts incorporating π-electron rich substituents.[24] Mukherjee synthesized a bimetallic molecular square using iron and palladium corners and an organic linker with alkyne functionality. Similar to the fluorescence studies in Figure 2.5, Mukherjee showed that fluorescence quenching of his molecular square occurred upon the addition of C_{60}. The crystal structure of this square established a bowl shape, and a model of the square and fullerene complex can be seen in Figure 2.6, in which a 3.32 Å distance between the square and fullerene is indicative of π-π interaction.[25]

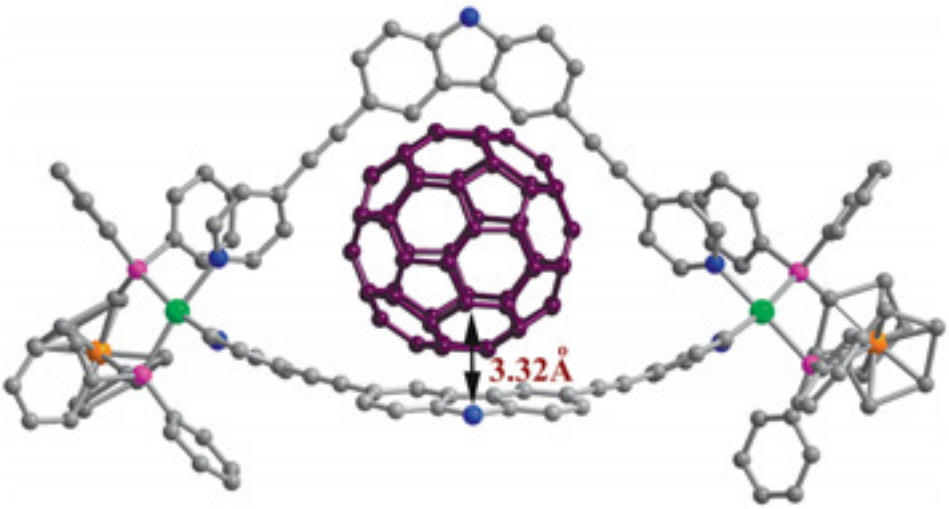

Figure 2.6. Mukherjee's model of host-guest interaction between his molecular square and a fullerene molecule.

Molecular squares often exhibit cavities via uniform channels formed from stacking. These cavities, along with the host-guest chemistry theme, can provide a means for sensing, processing, or transporting.[26] There is much interest in molecular squares as sensors, in which NMR spectroscopy is employed to investigate solution phase interactions.[20,21,27,28] Such interactions can also be investigated by luminescence[29,30] or electrochemical[28,31] methods.

3. Neutral molecular squares. As evidenced by the examples above, molecular polygons are often synthesized as cationic species using amine based donor ligands. Neutral polygons are also of interest, as they would have solubility in less polar solvents. Neutral molecular squares can be accessed by employing phosphine ligands and formally anionic donor ligands on the metal center. Furthermore, of particular interest to this project is a neutral square utilizing polyynediyl chains as the linear units. As shown in Figure 2.7, the first squares of this type were reported in 1998 by Young, in which corners of the formulae *cis*-$(R_3P)_2PtCl_2$ and *cis*-$(R_3P)_2Pt((C{\equiv}C)_2H)_2$ were combined in the presence of CuI and $HNEt_2$ to achieve the C_4-sided square.[32] Also synthesized was a similar square with a platinum metal center incorporated into the linker, a strategy also seen in Figure 2.5 above.

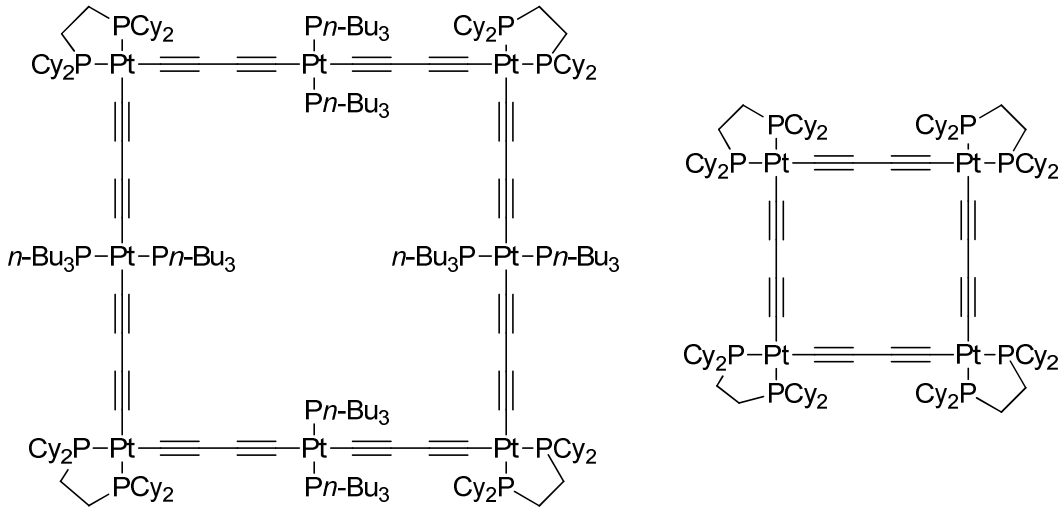

Figure 2.7. Young's neutral molecular squares based on bidentate diphosphines.

4. Cyclo[*n*]carbons. In addition to their uses in host-guest chemistry, transformations involving molecular squares can also be of interest. Molecular squares with polyyne based linkers can serve as precursors to cyclo[*n*]carbons, in which *n* indicates the number of carbons in the ring.[33] As shown in Scheme 2.1, the existence of cyclo[18]carbon has been demonstrated by Diederich. Its formation was observed by time of flight mass spectrometry via a retro Diels-Alder reaction using a purely organic triangle.[34] Similarly, Diederich detected cyclo[*n*]carbons with *n* = 18, 24, and 30 upon using higher homologues. Interestingly, the said cyclo[*n*]carbons coalesced to the fullerene ions C_{60} and C_{70}.[35]

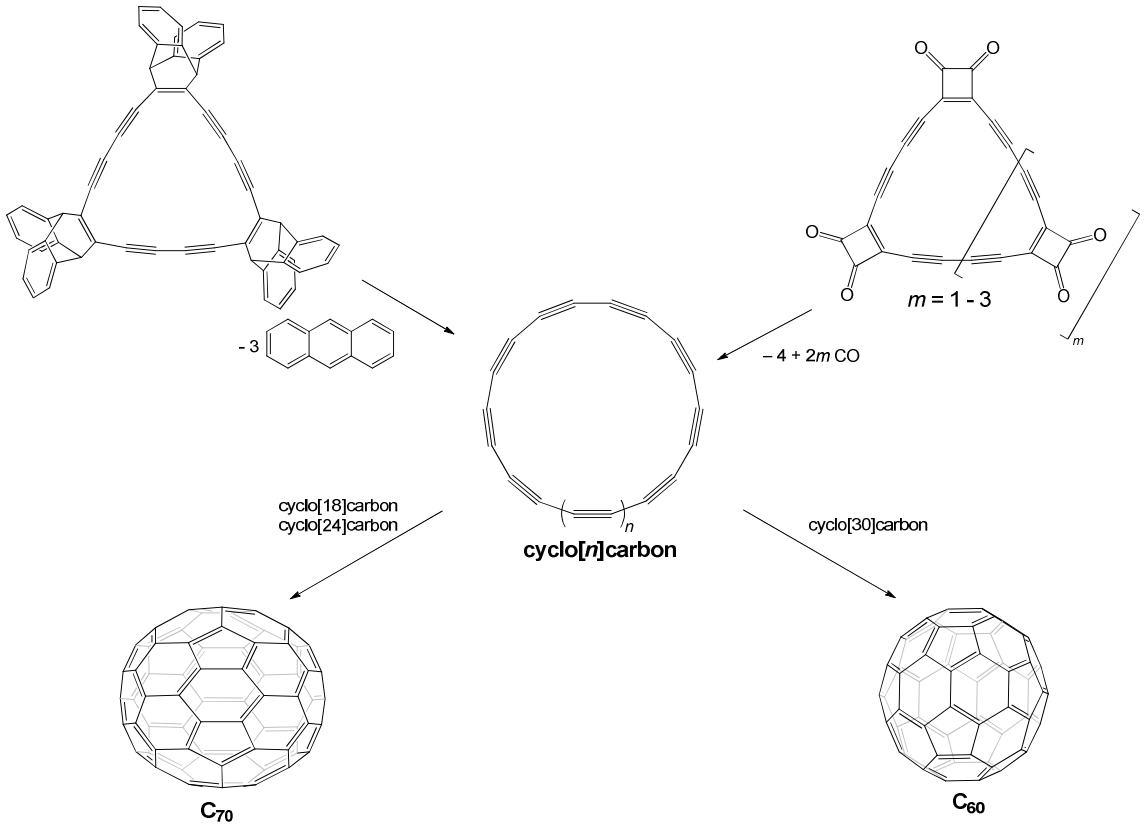

Scheme 2.1. Diederich's formation of cyclo[*n*]carbons as evidenced by mass spectrometry.

Accordingly, a metal center can be extruded from an organometallic square and the two neighboring carbon atoms can be coupled to form a new carbon-carbon bond. This has been demonstrated on platinum complexes using I_2, Br_2, and $HgCl_2$. As shown in Scheme 2.2, Iwamoto reported platinum extrusion and subsequent carbon-carbon bond formation between the aromatic ligands on a platinum based square using Br_2.[36] The resulting crude mixture was not analyzed by $^{31}P\{^1H\}$ NMR, so the organometallic byproduct was not described.

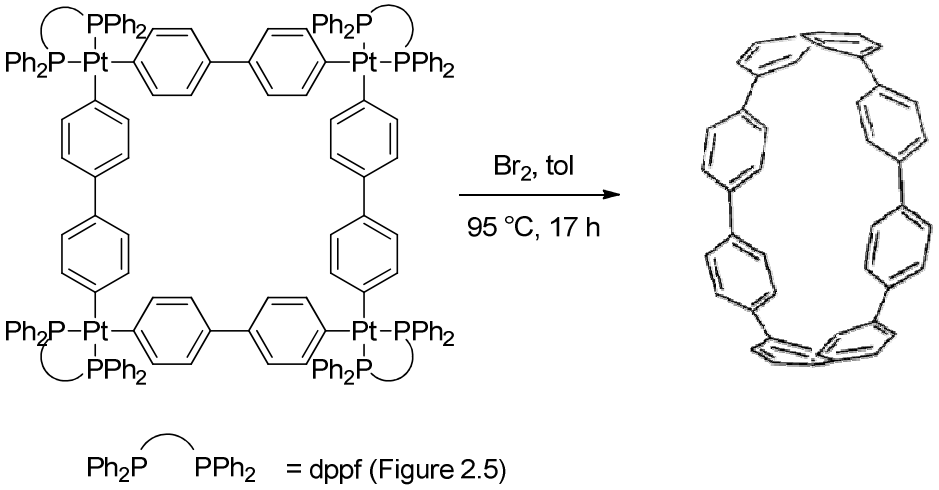

Scheme 2.2. Iwamoto's formation of [8]cycloparaphenylene by the elimination of platinum to induce a carbon-carbon bond.

Similarly, as shown in Scheme 2.3, Hill demonstrated an analogous reaction in which a *cis*-bis(butadiynyl) platinum complex was treated with $HgCl_2$ to form a polyyne capped with tungsten metal centers.[37]

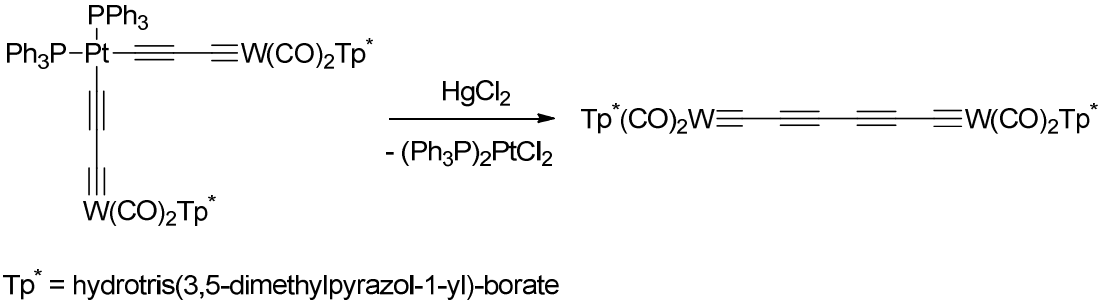

Scheme 2.3. Hill's formation of a tungsten capped polyyne by the extrusion of the platinum metal center using $HgCl_2$.

Bauerle demonstrated, as depicted at the top in Scheme 2.4, that I_2 was effective in a similar reaction. The platinum metal centers in bis(alkynyl) complexes were extruded with I_2 and the neighboring carbons subsequently formed a new carbon-carbon bond.[38] Although not described or spectroscopically observed, the byproduct, presumably (dppp)PtI_2, was removed via column chromatography. The described methods of metal extrusion could potentially be implemented with a molecular square employing polyyne chains as the linkers, in which these reactions would occur four times as shown at the bottom in Scheme 2.4. The resulting product would theoretically be the desired cyclo[*n*]carbon, with the stability of the ring being the limiting factor in terms of its observation and isolation.

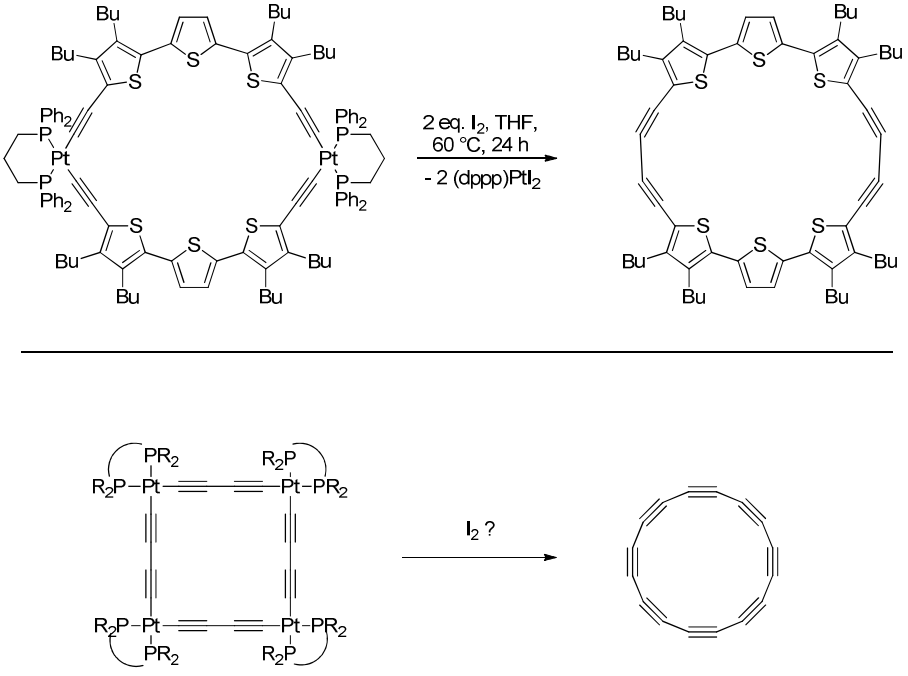

Scheme 2.4. Bauerle's elimination of platinum from a diplatinum complex to induce a carbon-carbon bond (top) and a possible pathway to cyclo[16]carbon using a C_4-sided square by the same methodology (bottom).

5. Aims of this project. Neutral molecular squares incorporating platinum on the corners and polyyne chains as the linear units were sought. One of the drawbacks of organometallic molecular squares is their often insoluble nature in common organic solvents (e.g. CH_2Cl_2, $CHCl_3$, etc.). Since earlier attempts to synthesize squares using dppp (1,3-bis(diphenylphosphino)propane) resulted in poorly soluble materials,[39,40] methods to circumvent this problem were sought. One possible approach to overcome this drawback is the utilization of bidentate diphosphine ligands that have been functionalized with lipophilic substituents. With a higher degree of solubility, crystals may be realized.

6. Earlier results. Earlier results from the Gladysz group utilized palladium and platinum square corners. The anticipated product would have alternating palladium and platinum corners in the C_4-sided square, as indicated on the left of Scheme 2.5. Accordingly, the complex (dppp)Pt($(C\equiv C)_2H)_2$ was combined with an equimolar amount of (dppp)$PdCl_2$ in the presence of CuCl and $HNEt_2$. Instead of observing the anticipated product, evidence for a platinum triangle was observed, with no palladium being incorporated into the polygon.[40] The IR and $^{13}C\{^1H\}$ NMR spectra indicated a C_8 carbon chain, but no crystal structure was obtained.

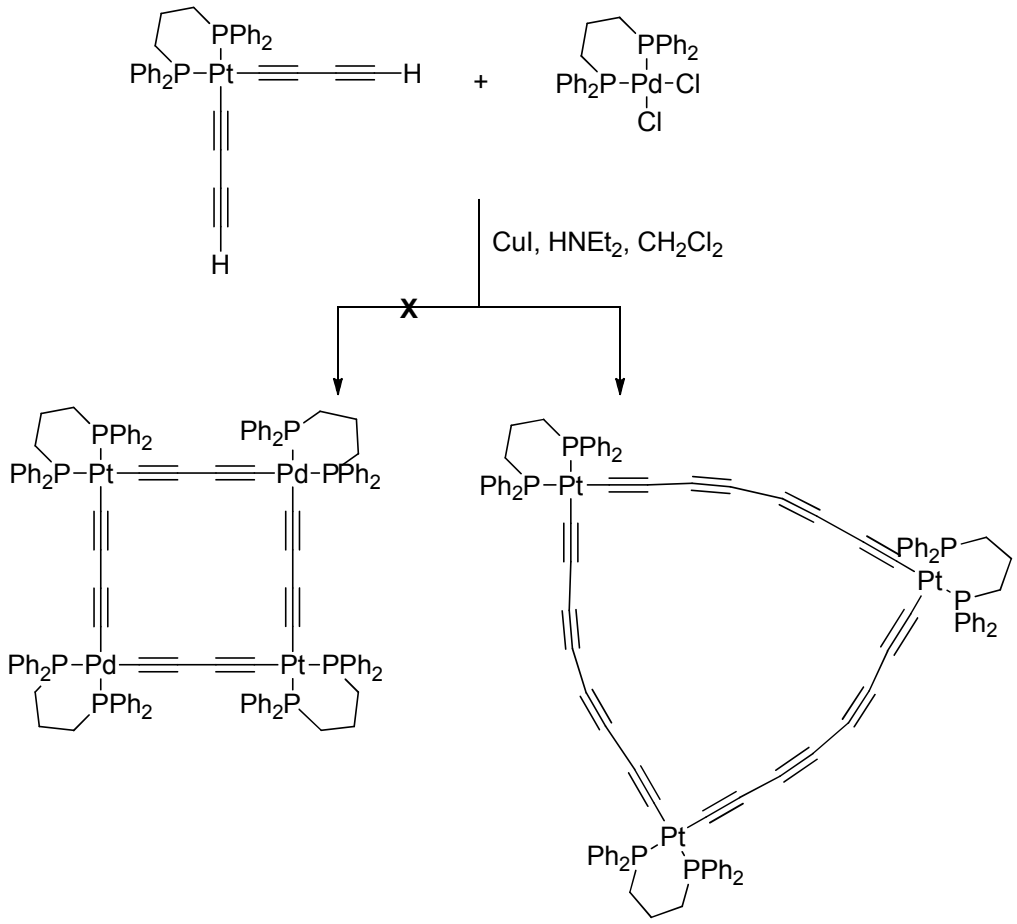

Scheme 2.5. Previously attempted synthesis of a bimetallic square.

7. Diphosphine and platinum starting materials. Six different 2,2-geminally disubstituted dppp ligands were used in this chapter. As shown at the top of Scheme 2.6, the dimethyl derivative was previously reported and is synthesized from 1,3-dichloro-2,2-dimethylpropane.[41] Also previously reported are the syntheses of the diethyl and dibenzyl diphosphines, shown at the bottom of Scheme 2.6. These syntheses commence with commercially available diols and conversions to the bidentate diphosphines are accomplished in two steps using MsCl and $KPPh_2$, respectively.[42] The syntheses of the new bidentate diphosphines for this chapter will follow the same methodologies.

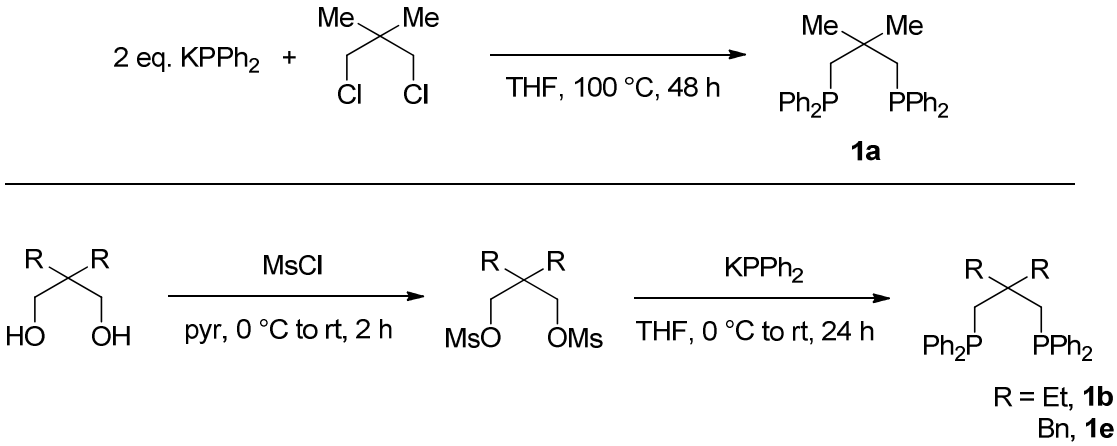

Scheme 2.6. Previously reported syntheses of the bidentate diphosphines **1a**, **1b**, and **1e**.

.

The platinum functionality is accessed by *cis/trans*-(*p*-tol$_3$P)$_2$PtCl$_2$, which has been previously synthesized as a mixture of isomers as shown in Scheme 2.7.[43,44] The starting platinum complex is red, and the reaction mixture becomes a white suspension, giving the white *cis*/*trans* mixture upon workup. The two isomers are distinguishable by NMR spectroscopy. In the $^{31}P\{^{1}H\}$ NMR spectrum, they give very different chemical shifts and coupling constants, with the *cis* isomer exhibiting a signal at δ 13.7 ppm ($^{1}J_{PPt}$ = 2691 Hz) and the *trans* at δ 19.6 ppm ($^{1}J_{PPt}$ = 2609 Hz) in $CDCl_3$. The former is the kinetic product and is the dominant isomer. A bis(butadiynyl) complex is accessed by a reaction with butadiyne as shown at the bottom in Scheme 2.7. Even though the educt is a mixture of isomers, *trans*-(*p*-tol$_3$P)$_2$Pt((C≡C)$_2$H)$_2$ is exclusively isolated, as assigned by $^{31}P\{^{1}H\}$ NMR spectroscopy.[45]

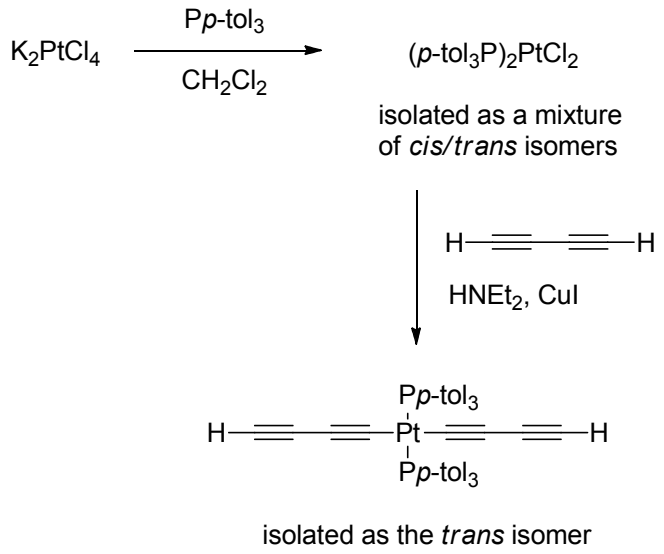

Scheme 2.7. Previously reported syntheses of *cis/trans*-(*p*-$tol_3P)_2PtCl_2$ and *trans*-(*p*-$tol_3P)_2Pt((C{\equiv}C)_2H)_2$.

RESULTS

1. Diphosphine syntheses. The bidentate diphosphines sought for this study are variations of 1,3-bis(diphenylphosphino)propane (dppp). Functionalization has been realized at the 2-position to give six different diphosphines shown in Figure 2.8. Collectively, these ligands are given the generic designation dppp*. These include the previously reported diphosphines $Me_2C(CH_2PPh_2)_2$ (**1a**),[46] $Et_2C(CH_2PPh_2)_2$ (**1b**),[46] and $Bn_2C(CH_2PPh_2)_2$ (**1e**),[42] synthesized as in Scheme 2.6 above, and the new diphosphines *n*-$Bu_2C(CH_2PPh_2)_2$ (**1c**), *n*-$Dec_2C(CH_2PPh_2)_2$ (**1d**), and (*p*-$tolCH_2)_2C(CH_2PPh_2)_2$ (**1f**). The last three feature longer *n*-alkyl chains or substituted benzyl groups.

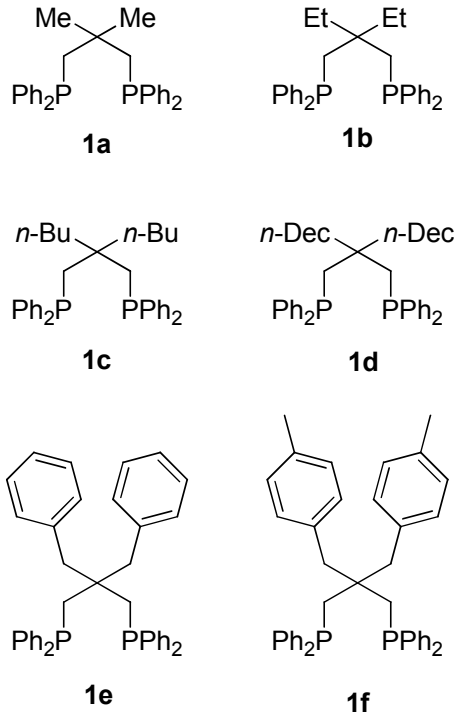

Figure 2.8. Summary of the bidentate diphosphines **1a-f** used in this study.

The use of these specialized bidentate diphosphines serves two purposes: (1) to increase solubility of the resulting molecular square, and equally as important, (2) to ensure that the corner building blocks adopt *cis* configurations at the square planar platinum metal center.

The syntheses of the new diphosphines involve the reaction of $KPPh_2$ with the corresponding dimesylates. Depending on the commercial availability of suitable starting materials, either two or four steps are required. For example, as shown in Scheme 2.8, **1c** is synthesized from the commercially available diol in two steps and in good overall yield (74%).

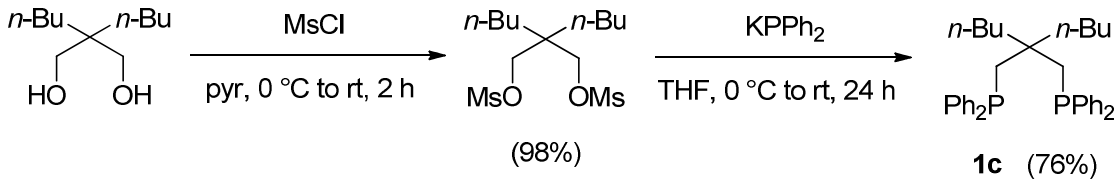

Scheme 2.8. Synthesis of the bidentate diphosphine **1c**.

As described in Scheme 2.9, the bidentate diphosphines **1d** and **1f** were synthesized from diethyl malonate. The first step involved proton abstraction using NaH and subsequent addition of two equiv. of the alkyl or aryl bromide. The resulting 1,3-diesters were easily reduced to 1,3-diols using $LiAlH_4$. Subsequent treatment with MsCl gave the dimesylate compounds. Finally, reactions with $KPPh_2$ consummated the diphosphine syntheses in good yields.

All diphosphines were white solids with the exception of **1d**, which was an oil and could not be crystallized. Workups were done in air, with the exception of **1e** and **1f**, whose workups needed to be done under an inert atmosphere to avoid oxidation. After workups, all diphosphines were air stable as solids or oils, but readily oxidized in solution when exposed to air.

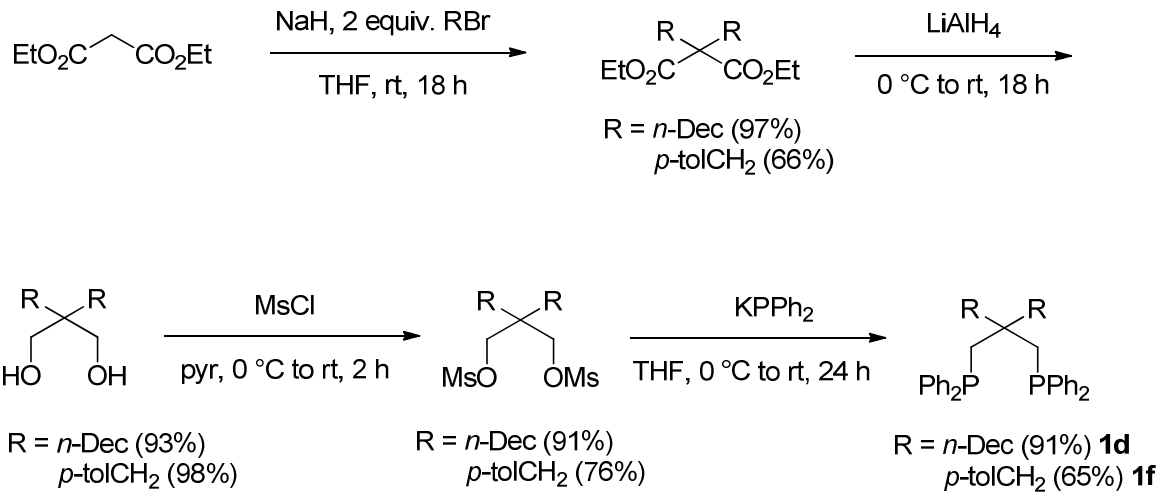

Scheme 2.9. Syntheses of the bidentate diphosphines **1d** and **1f**.

The new bidentate diphosphines were characterized by NMR (^{1}H, $^{13}C\{^{1}H\}$, and $^{31}P\{^{1}H\}$) and IR spectroscopies, mass spectrometry, and microanalyses. The $^{31}P\{^{1}H\}$ NMR chemical shifts of the entire series are summarized in Table 2.1.

Table 2.1. $^{31}P\{^{1}H\}$ NMR data (δ, ppm; $CDCl_3$) for the 1,3-diphosphines.

diphosphine	$^{31}P\{^{1}H\}$ NMR
1a	–26.2
1b	–26.2
1c	–25.8
1d	–25.8
1e	–26.3
1f	–26.2

2. Square Corners. Attention was then turned to the syntheses of the platinum square "corners." These can be categorized into two groups: (a) the dichloride derived corners and (b) the bis(butadiynyl) derived corners. As shown in Scheme 2.10, the former were accessed by reactions of the bidentate diphosphines with *cis/trans*-(*p*-$tol_3P)_2PtCl_2$ in CH_2Cl_2. The resulting complexes **2a-f** were compelled to adopt *cis* conformations, ensuring their viabilities as "corners." Solubilities proved to be an issue. On one hand, their low solubilities ensured facile workups, which often simply entailed washing with Et_2O, MeOH, and hexanes. On the other hand, they could not be chromatographed on silica gel, as they had an apparent R_f value of zero using even very polar solvents. Complexes **2a-f** were isolated as air stable white solids in good yields (74-94%). They were characterized by NMR (^1H, $^{13}C\{^1H\}$, and $^{31}P\{^1H\}$) and IR spectroscopies, mass spectrometry, and microanalyses. The $^{31}P\{^1H\}$ NMR data for the dichloride complexes are summarized in Table 2.2.

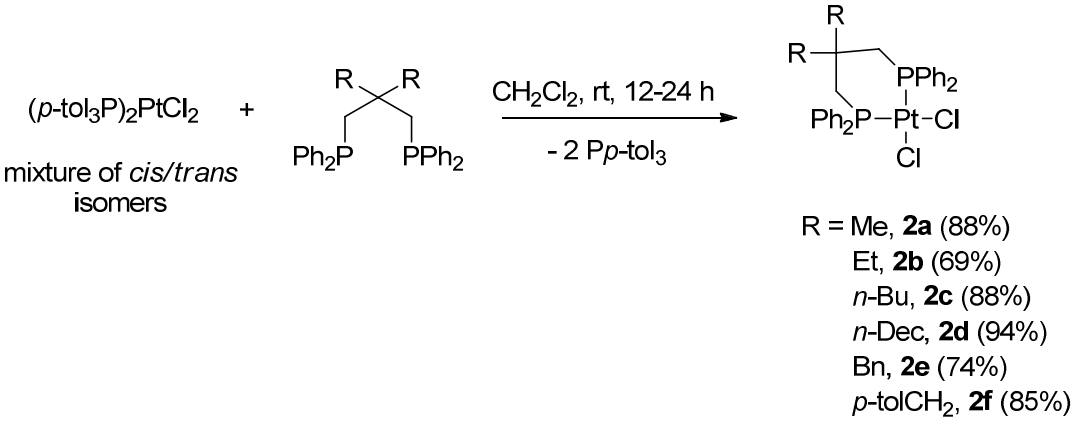

Scheme 2.10. Syntheses of the dichloride square corners **2a-f**.

Table 2.2. $^{31}P\{^{1}H\}$ NMR data (δ, ppm; $CDCl_3$) for the dichloride complexes.

complex	$^{31}P\{^{1}H\}$ ($^{1}J_{PPt}$ (Hz))
2a	–1.3 (3431)
2b	–2.5 (3429)
2c	–2.6 (3419)
2d	–2.7 (3417)
2e	–2.0 (3376)
2f	–2.0 (3386)

The syntheses of the bis(butadiynyl)complexes can be achieved via two methods. As shown in Scheme 2.11, in method A the butadiynyl ligands were introduced prior to the bidentate diphosphines. Thus, *trans*-(*p*-$tol_3P)_2Pt((C{\equiv}C)_2H)_2$ (see synthesis in Scheme 2.7) was combined with **1a-d** to afford the bis(butadiynyl) complexes **3a-d**. Alternatively, using method B shown in Scheme 2.12, the diphosphine dichloride complexes **2a-f** were treated with an excess of butadiyne in the presence of CuI and $HNEt_2$ to afford **3a-f**. The products were isolated as tan or light yellow solids in good yields (58-87%) following silica gel chromatography.

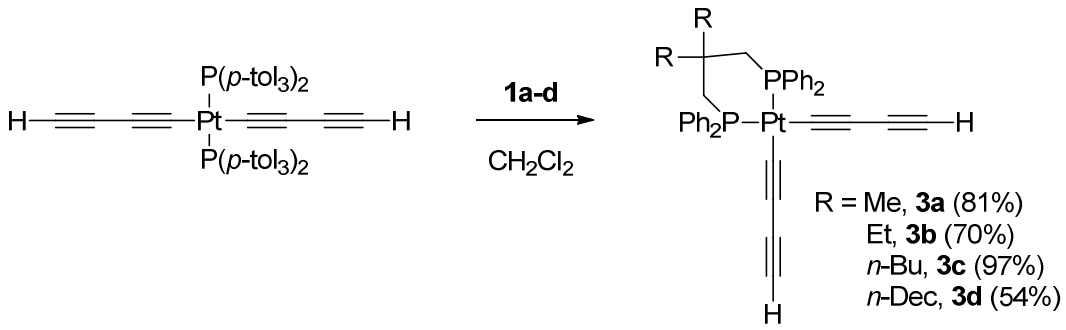

Scheme 2.11. Syntheses of the bis(butadiynyl) square corners using method A.

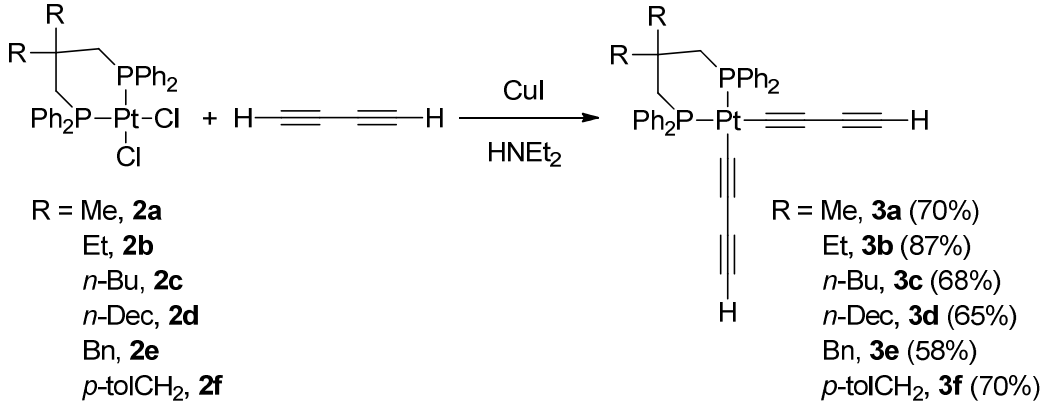

Scheme 2.12. Syntheses of the bis(butadiynyl) square corners using method B.

An assessment of the methods A and B, as summarized in Table 2.3, demonstrates that they are comparable in terms of isolated yields.

Table 2.3. Yields of bis(butadiynyl) complexes **3a-f**.

Complex	Method A (%)	Method B (%)
3a	81	70
3b	70	87
3c	97	68
3d	54	65
3e	-	58
3f	-	70

The $^{1}J_{PPt}$ values of the bis(butadiynyl) complexes **3a-f** vastly differ from their dichloride analogues **2a-f**. As summarized in Table 2.4, the former fall into the range of 2100-2300 Hz, whereas the latter are 3300-3500 Hz (see Table 2.2).

Table 2.4. $^{31}P\{^{1}H\}$ NMR data (δ, ppm; $CDCl_3$) for the bis(butadiynyl) complexes.

R	$^{31}P\{^{1}H\}$ ($^{1}J_{PPt}$ (Hz))
3a	–4.9 (2224)
3b	–6.2 (2231)
3c	–6.5 (2227)
3d	–6.6 (2221)
3e	–4.8 (2192)
3f	–3.3 (2196)

Interestingly, these *cis* complexes were much less stable than the precursor *trans*-(*p*-$tol_3P)_2Pt((C{\equiv}C)_2H)_2$. As shown in Figure 2.9, even an NMR tube solution of **3b** discolored from yellow to brown over a period of 48 h. This behavior was observed with all of the other bis(butadiynyl) complexes, but not observed with *trans*-(*p*-$tol_3P)_2Pt((C{\equiv}C)_2H)_2$.

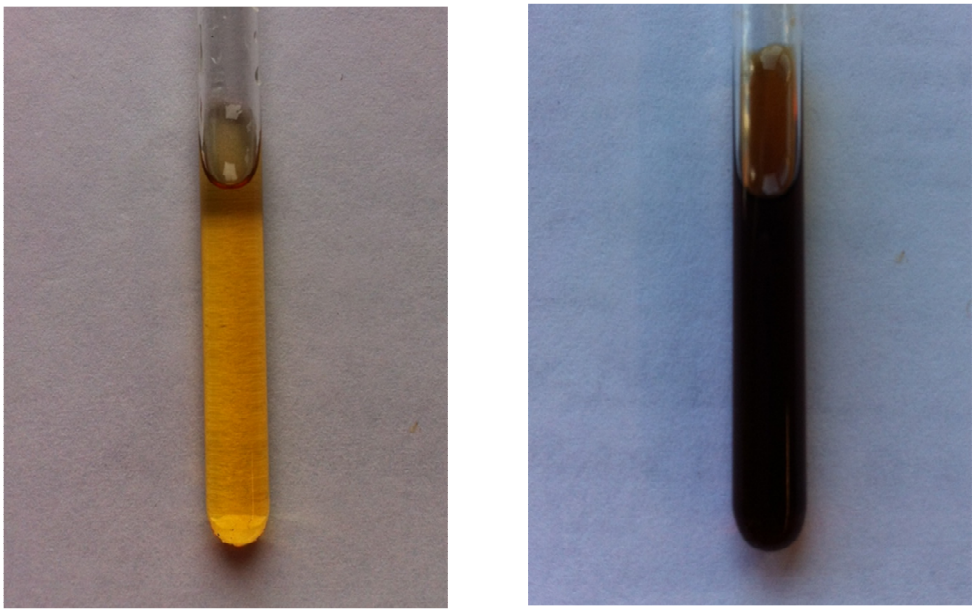

Figure 2.9. Decomposition of **3b**: t = 0 h (left) and t = 48 h (right).

Single crystals of the solvate **3a**·CH_2Cl_2 were grown from a CH_2Cl_2 solution at –20 °C. X-ray data were collected and the structure refined as summarized in Table 2.11. Thermal ellipsoid plots of **3a** are shown in Figure 2.10 and salient features are analyzed in the discussion section.

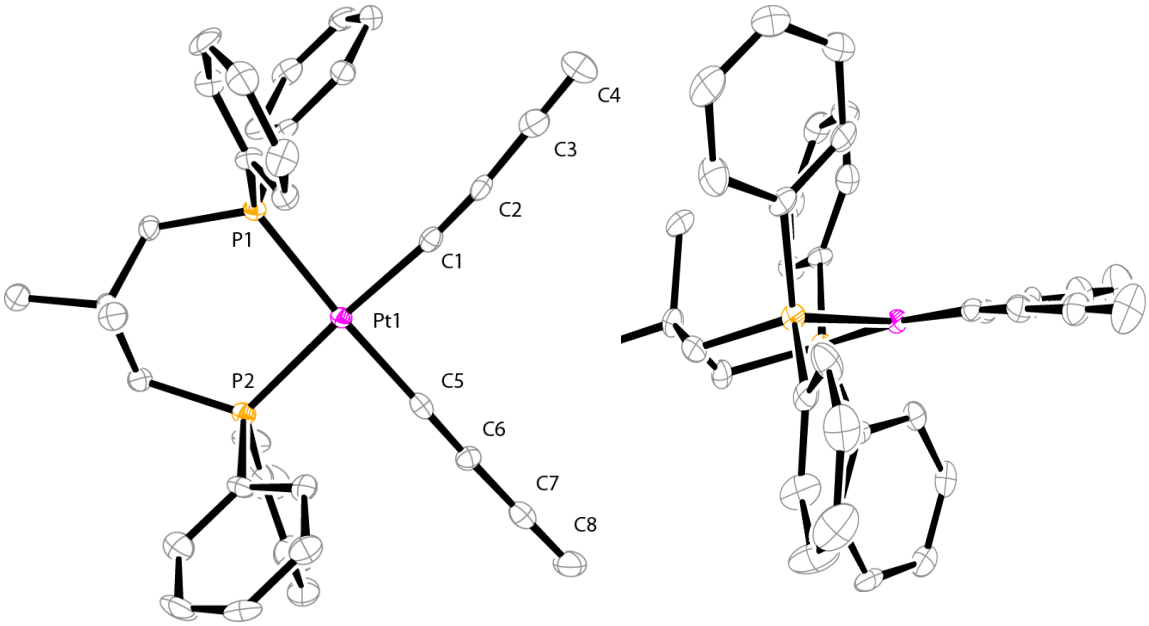

Figure 2.10. Thermal ellipsoid plots (50% probability level) of **3a**·CH_2Cl_2 with solvate molecule omitted.

3. Reactions of 2 and 3. The title compounds, molecular polygons, were sought next. As depicted in Scheme 2.13, equimolar quantities of **2** and **3** were reacted under standard Sonogashira coupling conditions, as exemplified in Scheme 2.7 above. However, the transformations in Scheme 2.13 required elevated temperatures (55 °C) and extended time periods (48 h) to go to completion.

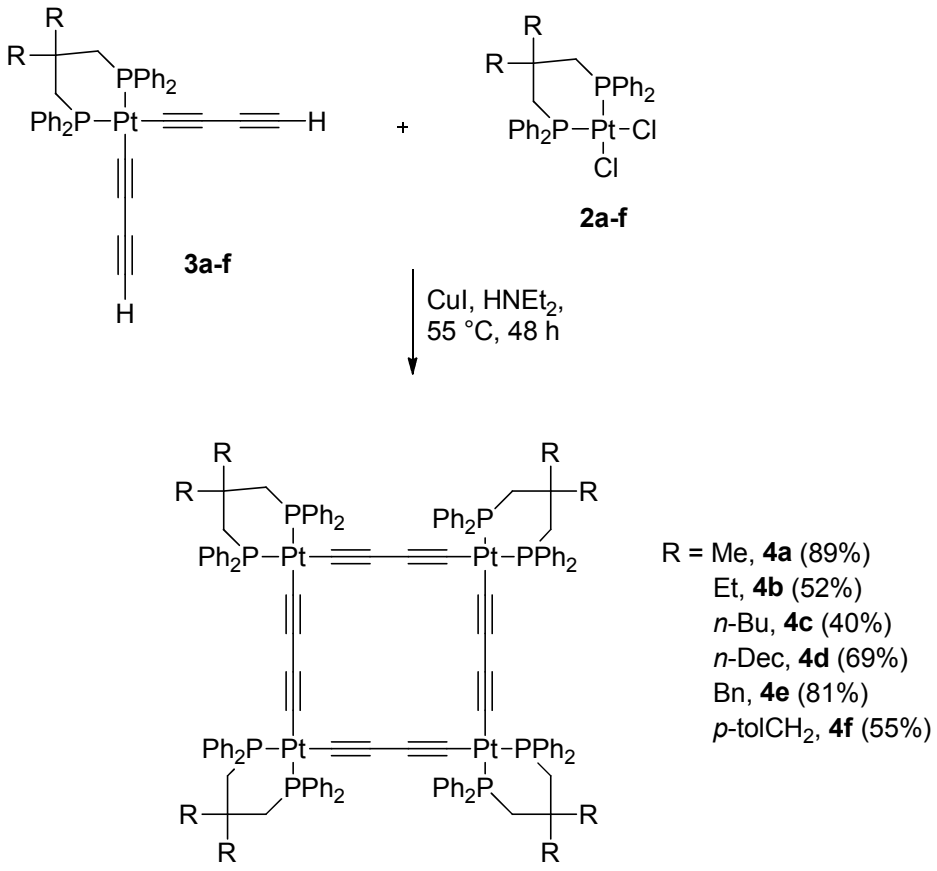

Scheme 2.13. Syntheses of the C_4-sided squares **4a-f**.

The resulting C_4-sided squares **4a-f** were isolated as air stable solids in good yields (40-89%) by extraction with CH_2Cl_2 and subsequent washing with various solvents such as hexanes and MeOH. Complexes **4a-f** were characterized by NMR (^1H, $^{13}C\{^1H\}$, and $^{31}P\{^1H\}$) and IR spectroscopies and mass spectrometry. ^1H NMR spectra showed the disappearance of the characteristic ≡C-H functionality. Purifications via column chromatography were not possible as further described in section 8 below, so no microanalyses are reported. The $^{31}P\{^1H\}$ NMR chemical shifts are summarized in Table

2.5. The $^{13}C\{^1H\}$ NMR spectra of **4a-f** show an interesting feature: unlike the parent complexes **3a-f**, the PtC≡*C* carbon is downfield with respect to the Pt*C*≡C carbon. Importantly, no evidence for other polygons, such as a trimer or tetramer, was observed by mass spectrometry, indicating that the squares were preferentially formed over other polygons. Further details regarding mass spectrometry analyses are offered in section 7 below.

Table 2.5. $^{31}P\{^1H\}$ NMR data (δ, ppm; $CDCl_3$) for the C_4-sided squares.

square	$^{31}P\{^1H\}$ ($^1J_{PPt}$ (Hz))
4a	–6.1 (2142)
4b	–7.7 (2243)
4c	–7.8 (2224)
4d	–8.6 (2236)
4e	–4.8 (2192)
4f	–4.6 (2205)

The solubilities of **4a-f** were assayed in a variety of solvents. Some data are summarized in Table 2.6, and show that the 1,3-diphosphine substituents had dramatic effects. When the diphosphine backbone substituents reached four carbon atoms, solubility was no longer a problem.

Table 2.6. Solubility of C_4-sided squares in various solvents.

square	DMSO	CH_2Cl_2	Et_2O	hexanes
4a	soluble	slightly soluble	insoluble	insoluble
4b	soluble	slightly soluble	insoluble	insoluble
4c	soluble	soluble	insoluble	insoluble
4d	soluble	soluble	soluble	insoluble
4e	soluble	soluble	soluble	insoluble
4f	soluble	soluble	soluble	insoluble

Single crystals of a solvate of **4a** were grown from a DMSO solution layered with EtOAc. X-ray data were collected and the structure refined as summarized in Table 2.12 and the experimental section. A thermal ellipsoid plot is shown at the top in Figure 2.11. The square selectively crystallized with DMSO molecules, but these were removed using PLATON. Further details are provided in the experimental section.

Similarly, single crystals of a solvate of the diethyl dppp* system **4b** were grown from a CH_2Cl_2 solution layered with toluene and Et_2O. X-ray data were collected and the structure refined as summarized in Table 2.13 and the experimental section. A thermal ellipsoid plot of **4b** is shown at the bottom in Figure 2.11. The solvent molecules of **4b** (CH_2Cl_2 and possibly toluene or Et_2O) were found to be disordered and were also removed using PLATON.

Table 2.7 compares key crystallographic features of **4a** and **4b**. These are analyzed in the discussion section.

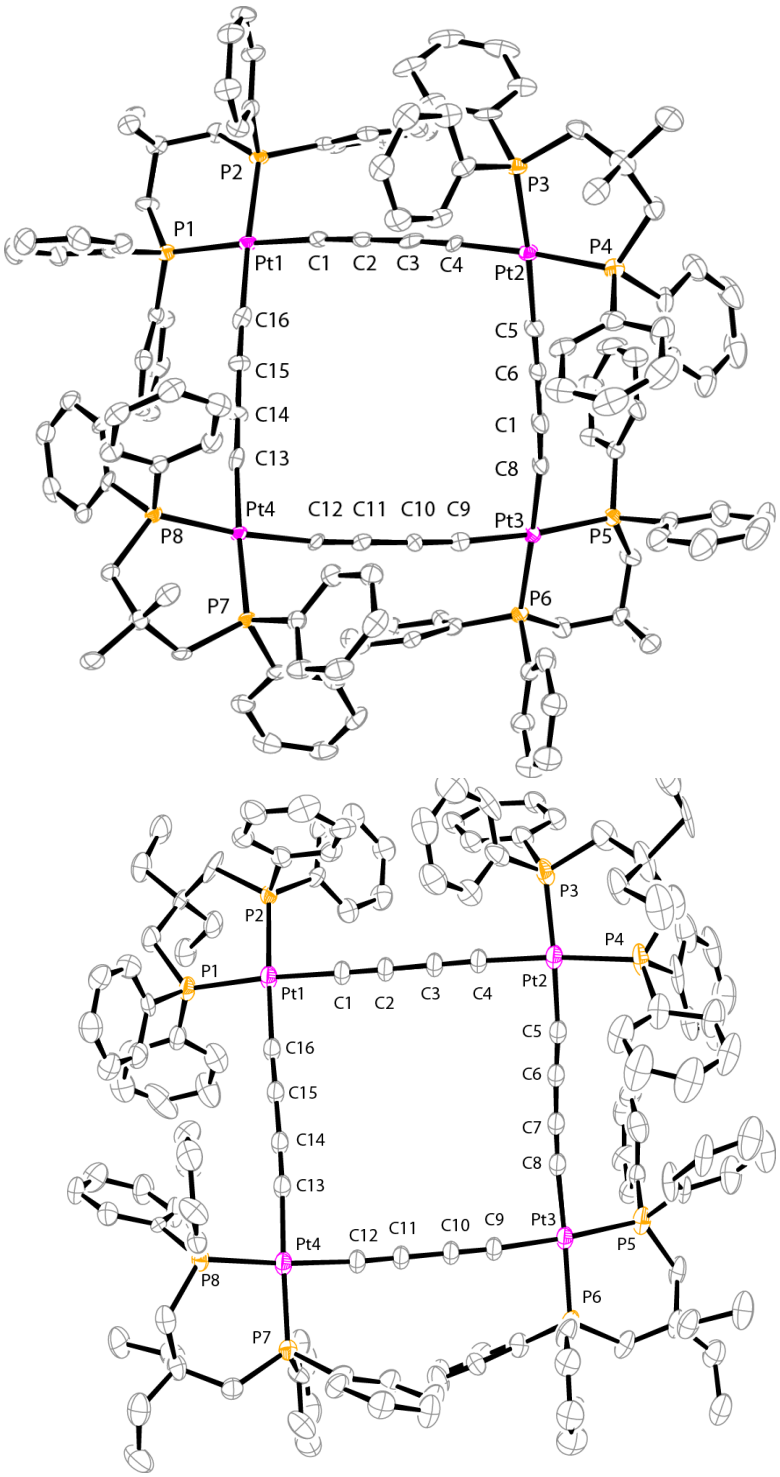

Figure 2.11. Thermal ellipsoid plots (50% probability) of squares **4a** (top) and **4b** (bottom)**.**

Table 2.7. Key crystallographic distances [Å] and angles [°] for C_4-sided squares.

	4a	**4b**[a]
Pt1-C1	2.006(6)	2.030(12)
Pt1-C16	1.998(7)	2.017(9)
Pt2-C4	2.001(6)	2.047(12)
Pt2-C5	2.010(6)	2.019(10)
Pt3C8	2.008(6)	2.031(10)
Pt3-C9	2.009(6)	1.999(11)
Pt4-C12	2.022(6)	2.028(12)
Pt4-C13	1.998(7)	2.026(9)
Avg Pt-C	2.007(8)[b]	2.025(14)[b]
Pt1-P1	2.2825(15)	2.266(3)
Pt1-P2	2.2819(15)	2.283(3)
Pt2-P3	2.2811(15)	2.287(3)
Pt2-P4	2.2809(16)	2.267(3)
Pt3-P5	2.2770(15)	2.273(3)
Pt3-P6	2.2812(15)	2.276(3)
Pt4-P7	2.2770(14)	2.288(2)
Pt4-P8	2.2787(15)	2.265(3)
Avg Pt-P	2.2800(2)[b]	2.276(9)[b]
C1≡C2	1.232(9)	1.158(14)
C2-C3	1.376(9)	1.359(16)
C3≡C4	1.212(9)	1.209(9)
C5≡C6	1.192(8)	1.204(3)
C6-C7	1.408(9)	1.355(14)
C7≡C8	1.187(8)	1.206(13)
C9≡C10	1.208(8)	1.204(15)
C10-C11	1.376(9)	1.387(16)
C11≡C12	1.181(8)	1.185(15)
Avg C≡C	1.202 (18)[b]	1.194(20)[b]
C16-Pt1-C1	86.1(2)	88.5(4)
C4-Pt2-C5	88.6(2)	87.4(4)
C8-Pt3-C9	86.5(2)	86.6(4)
C12-Pt4-C13	88.2(2)	88.3(3)
Avg C-P-C angle	87.4(1.2)[b]	87.7(9)[b]

Table 2.7. (Continued)

	4a	**4b**[a]
Pt1-C1-C2	176.5(5)	172.3(10)
C1-C2-C3	177.4(7)	177.9(12)
C2-C3-C4	177.9(6)	177.5(11)
C3-C4-Pt2	176.6(5)	174.4(9)
Pt2-C5-C6	179.4(6)	176.2(10)
C5-C6-C7	177.9(7)	179.3(12)
C6-C7-C8	177.0(8)	179.1(13)
C7-C8-Pt3	173.6(5)	177.5(10)
Pt3-C9-C10	174.7(5)	176.4(10)
C9-C10-C11	177.7(7)	178.7(13)
C10-C11-C12	179.6(8)	178.2(12)
C11-C12-Pt4	174.1(5)	172.1(10)
Pt4-C13-C14	176.9(5)	175.3(10)
C13-C14-C15	177.9(7)	178.7(12)
C14-C15-C16	177.6(7)	179.5(13)
C15-C16-Pt2	177.0(5)	176.4(11)
Bowing parameter 1[c]	7.419	7.402
Bowing parameter 2[d]	7.373	7.649
Pt1-Pt3	10.144	10.577
Pt2-Pt4	9.734	10.706

[a] The atomic numbering for the diphosphine atoms in **4b** have been changed from those in the CIF files to facilitate comparison of structural features with **4a**. [b] this represents the standard deviation of the averaged values. [c] distance between the C2-C3 and C10-C11 centroids. [d] distance between the C6-C7 and C14-C15 centroids.

4. Chain extension of square corner. Precursors to molecular squares with more than four sp carbon atoms in the linkers were sought. To increase the length, a chain extension reaction was employed. As summarized in Scheme 2.14, this reaction lengthened the polyyne chain by two carbon atoms and involved an oxidative cross

coupling of *trans*-(*p*-tol$_3$P)$_2$Pt((C≡C)$_2$H)$_2$ and excess HC≡CSiEt$_3$ to give *trans*-(*p*-tol$_3$P)$_2$Pt((C≡C)$_3$SiEt$_3$)$_2$, which was previously reported in a thesis.[47] The *trans* stereochemistry was assigned on the basis of $^{31}P\{^1H\}$ NMR, similar to the methodology used in Scheme 2.7. Subsequent substitution of the P*p*-tol$_3$ ligands by the diphosphine **1c** gave the extended corner building block **5c** in good yield (82%). This diphosphine was chosen based on the solubility data presented in Table 2.6. Since longer terminal polyyne chains are inherently less stable, the SiEt$_3$ moiety was retained as a protecting group.

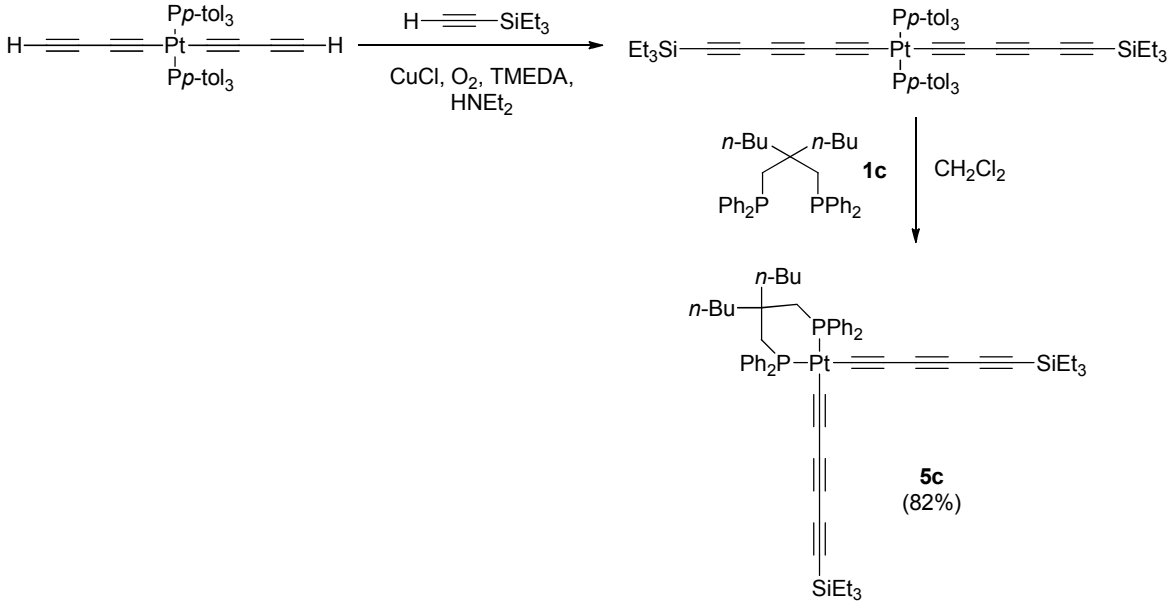

Scheme 2.14. Chain extension reaction of square corner complex **5c**.

5. Reaction of 3c and 5c. Larger molecular squares were next sought. Reactions of the platinum triethylsilylpolyynyl complexes L$_3$Pt(C≡C)$_n$SiEt$_3$ with wet *n*-Bu$_4$N$^+$ F$^-$

have been shown to effect protodesilylation, generating the corresponding terminal polyyne complex in situ.[48] Accordingly, the synthesis of a C_6-sided square, outlined in Scheme 2.15, was attempted. Complex **5c** was first treated with wet *n*-Bu_4N^+ F^-. This could be conveniently monitored by TLC. When no **5c** remained, the dichloride complex **2c** and a copper catalyst were subsequently added. These conditions are analogous to the Sonogashira-type conditions employed in the syntheses of the C_4-sided squares shown in Scheme 2.13.

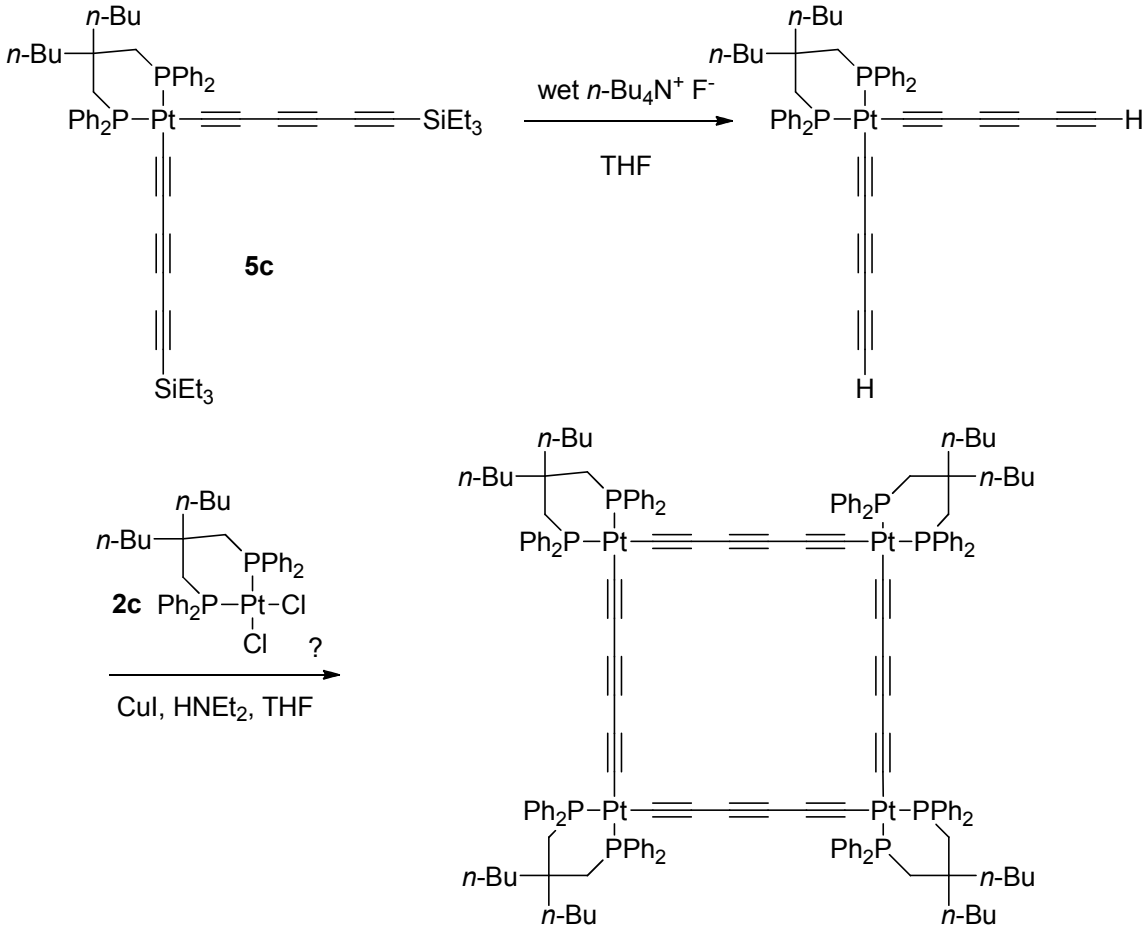

Scheme 2.15. Approach to a C_6-sided square involving *in situ* deprotection of **5c** and subsequent addition of **2c**.

Scheme 2.16 summarizes the results of three runs of Scheme 2.15. First, **5c** was dissolved in THF with stirring. Then wet *n*-Bu_4N^+ F^- was added and the reaction was monitored by TLC. When no starting material remained, CuI, $HNEt_2$, and an equimolar amount of **2c** were added. Over time, all material remained in solution. The solvents were removed and the residue was washed with Et_2O and hexanes. The isolated solid was soluble in CH_2Cl_2 and $CHCl_3$. The $^{31}P\{^1H\}$ NMR spectrum in $CDCl_3$ showed two broad and closely spaced singlets at δ –6.5 ppm and –6.7 ppm ($^1J_{PPt}$ = 2189 Hz), indicating a mixture of products in a 38:62 ratio. The overall concentration of platinum complexes in this reaction was 0.00542 M.

The possibility that multiple polygons had formed was considered. In an attempt to enhance selectivity, a reaction was conducted similarly to that above but at a concentration of 0.00227 M. The $^{31}P\{^1H\}$ NMR spectrum in $CDCl_3$ showed two broad and closely spaced singlets at δ –6.3 ppm and –6.6 ppm ($^1J_{PPt}$ = 2218 Hz) indicating a mixture of products in a 50:50 ratio. Mass spectral analysis ($MALDI^+$) showed the presence of both the trimeric triangle and tetrameric square at *m/z* 2374 and 3165, respectively. These are depicted at the bottom of Scheme 2.16.

The reaction was again repeated similarly to that above at an even more dilute concentration, 0.00106 M. After workup, the $^{31}P\{^1H\}$ NMR spectrum in $CDCl_3$ showed two broad and closely spaced singlets at δ –6.4 ppm and –6.6 ppm ($^1J_{PPt}$ = 2214 Hz), indicating a mixture of products in a 41:59 ratio. In all three cases, it was not possible to separate the products by silica gel, alumina, or florisil column chromatography, as they all gave apparent R_f values of zero in various solvents. Additional chromatography details are offered in section 8 below.

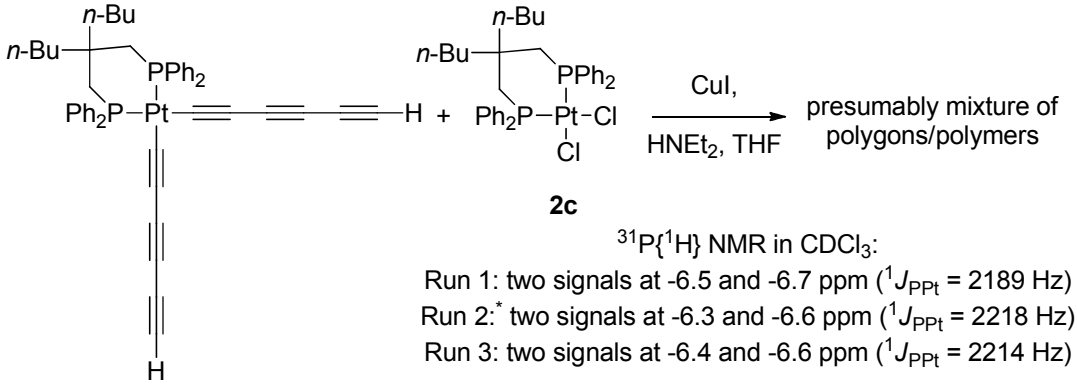

accessed *in situ* from **5c** using wet *n*-Bu_4N^+ F^- per Scheme 2.15

2c

$^{31}P\{^1H\}$ NMR in $CDCl_3$:
Run 1: two signals at -6.5 and -6.7 ppm ($^1J_{PPt}$ = 2189 Hz)
Run 2:* two signals at -6.3 and -6.6 ppm ($^1J_{PPt}$ = 2218 Hz)
Run 3: two signals at -6.4 and -6.6 ppm ($^1J_{PPt}$ = 2214 Hz)

* MS (MALDI$^+$, *m/z*): 2374; indicative of trimer
3165; indicative of tetramer

Results of run 2 indicate:

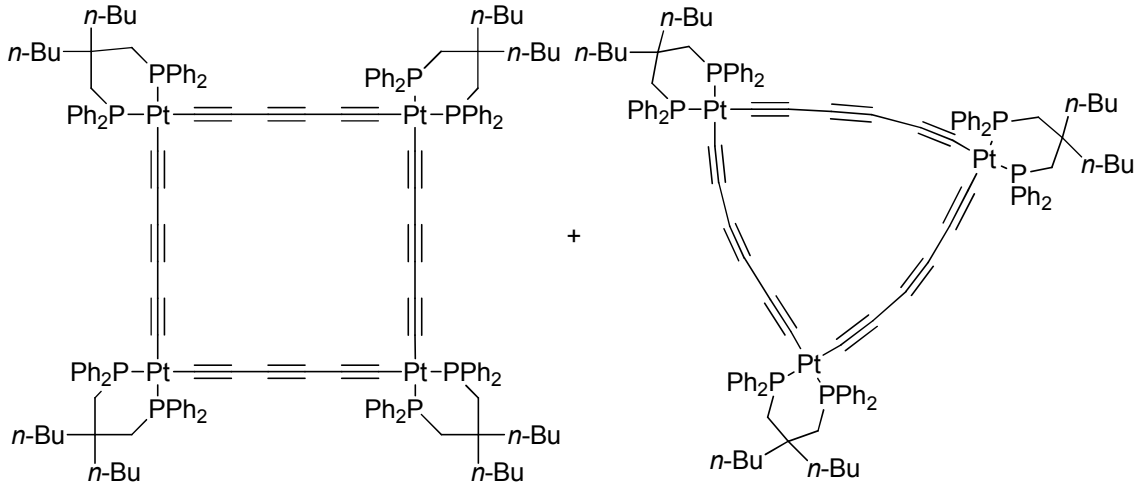

Scheme 2.16. Reaction of **5c** and **2c**.

6. Homocoupling reactions of (dppp*)Pt($(C\equiv C)_2H)_2$. Molecular squares with eight carbons in the polyyne chain were sought. Hay homocoupling is a viable method of linking $L_3Pt(C\equiv C)_nH$ type complexes to generate platinum capped polyynediyl complexes.[48] This method utilizes CuCl as the catalyst in the presence of TMEDA and

oxygen. Scheme 2.17 illustrates a four fold Hay homocoupling approach to a C_8-sided square.

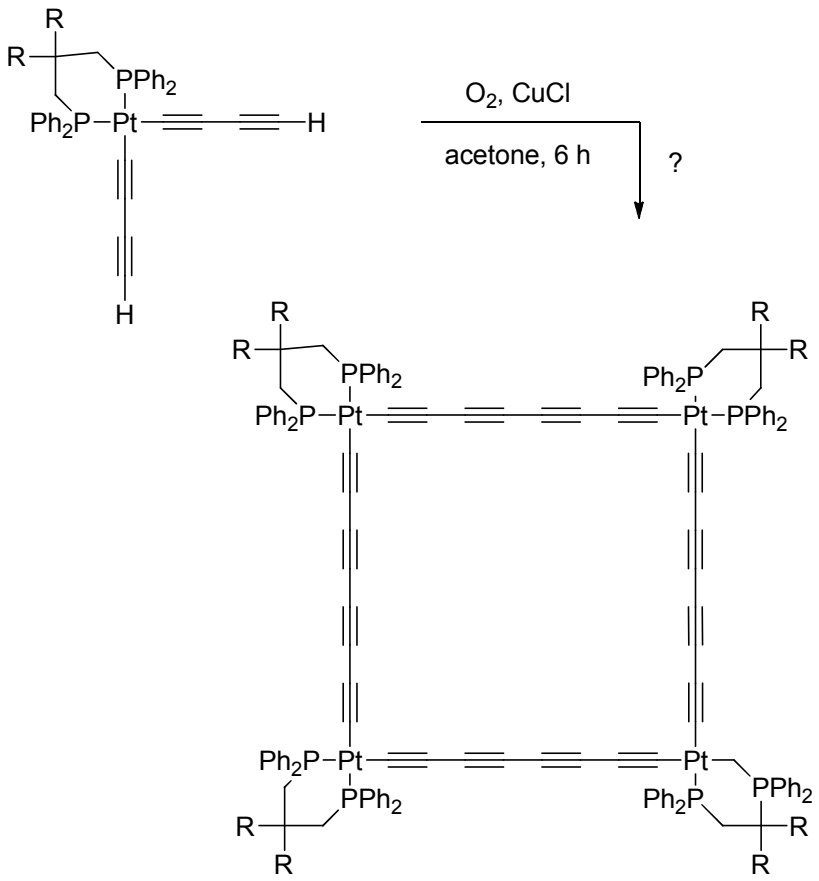

Scheme 2.17. Proposed route to C_8-sided squares.

The first attempt is shown in Scheme 2.18. An acetone solution of **3a** was aspirated with oxygen. The reaction was cooled to 0 °C and then heated to 50 °C. The catalyst solution was added. After 6 h, the solvent was removed and only a brown

insoluble solid remained and could not be characterized by NMR spectroscopy. The IR spectrum showed signals around 2140 cm^{-1}, indicating the presence of sp carbon atoms.

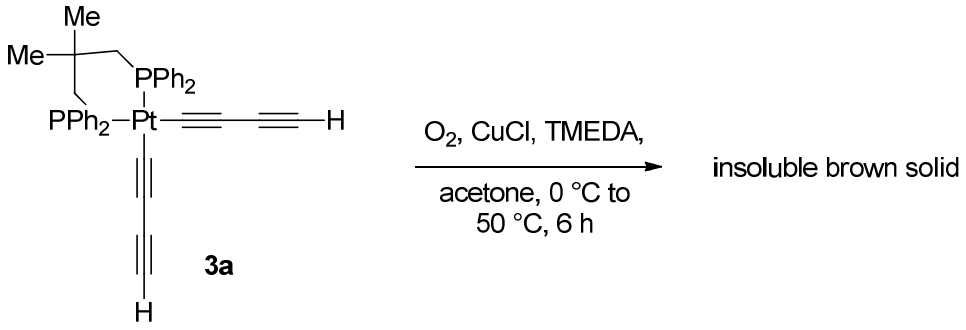

Scheme 2.18. Attempted synthesis of a C_8-sided square using **3a**.

The second and third attempts are shown in Scheme 2.19. Here **3c** was used, based on the data presented in Table 2.6, in hopes that the solubility problems encountered in Scheme 2.18 could be avoided. The reactions were carried out at 40 °C under otherwise identical conditions. The first run in Scheme 2.19 was stirred for 7 h, after which a brown solid resulted. There were no solubility problems, with the solid readily dissolving in CH_2Cl_2 and $CHCl_3$. It was washed with Et_2O and water. The $^{31}P\{^1H\}$ NMR spectrum in $CDCl_3$ showed two broad overlapping signals at δ –6.2 ppm and –6.6 ppm ($^1J_{PPt}$ = 2206 Hz), establishing a mixture of products.

The reaction was repeated a second time under the same conditions but stopped after 6 h. The $^{31}P\{^1H\}$ NMR spectrum in CD_2Cl_2 from the second attempt showed four signals at δ –5.9 ppm, –6.1 ppm, –6.3 ppm, and –6.4 ppm ($^1J_{PPt}$ = 2206 Hz),

establishing a mixture of products. The IR spectrum showed signals around 2145 cm^{-1}, indicating the presence of sp carbon atoms. The products could not be separated by column chromatography, as further described in section 8 below.

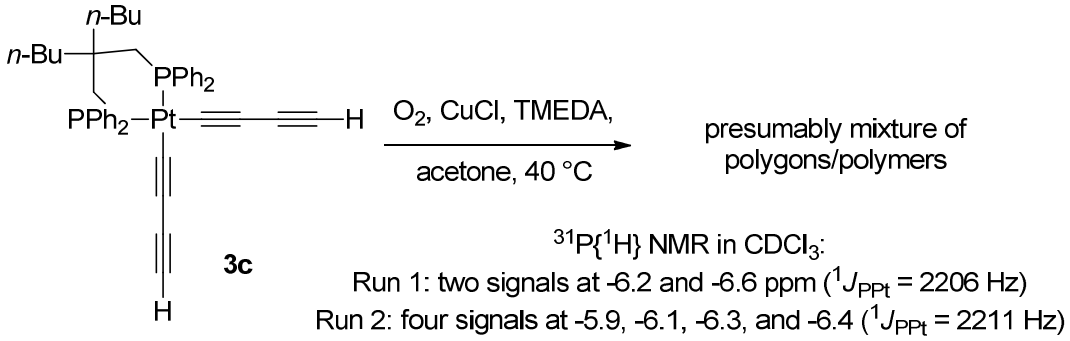

Scheme 2.19. Attempted syntheses of a C_8-sided square using **3c**.

As shown in Scheme 2.20, the synthesis of a C_8-sided square using **3d** was also attempted, since the resulting product would also have a high degree of solubility based on the data in Table 2.6. The reaction was carried out at 40 °C under otherwise identical conditions. The reaction was stirred for 5 h and the solvents were removed. A brown solid resulted and was extracted with CH_2Cl_2 and washed with water. The $^{31}P\{^1H\}$ NMR spectrum in $CDCl_3$ showed three broad overlapping signals at δ –6.2 ppm, –6.3 ppm, and –6.6 ppm ($^1J_{PPt}$ = 2219 Hz), establishing a mixture of products. The IR spectrum showed bands around 2144 cm^{-1}, indicating the presence of sp carbon atoms. Similar problems were encountered with column chromatography as above.

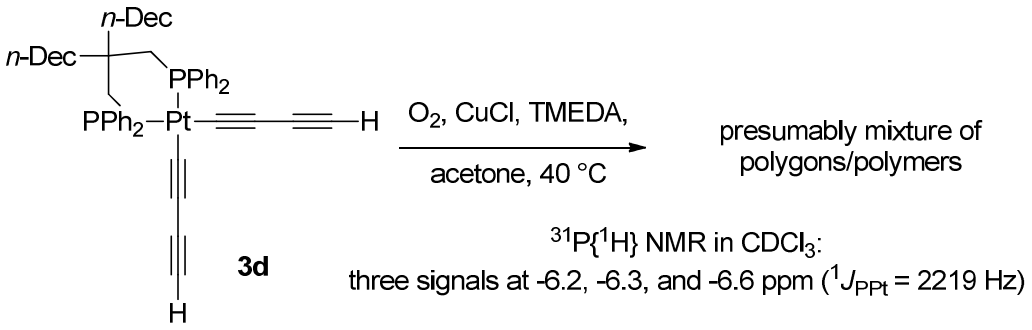

Scheme 2.20. Attempted synthesis of a C_8-sided square using **3d**.

An alternative route to a C_8-sided square was next considered. In principle, approaches analogous to those in Schemes 2.13 and 2.16 could be employed. This would require a bis(octatetraynyl) complex, or the $SiEt_3$ derivative. Scheme 2.21 depicts an attempt to synthesize the platinum complex *trans*-(*p*-$tol_3P)_2Pt((C{\equiv}C)_4SiEt_3)_2$ via a chain extension reaction with excess $H(C{\equiv}C)_2SiEt_3$ under Hay conditions. This is analogous to the chain extension reaction shown in Scheme 2.15, in which *trans*-(*p*-$tol_3P)_2Pt((C{\equiv}C)_3SiEt_3)_2$ was successfully synthesized from the same platinum starting material.

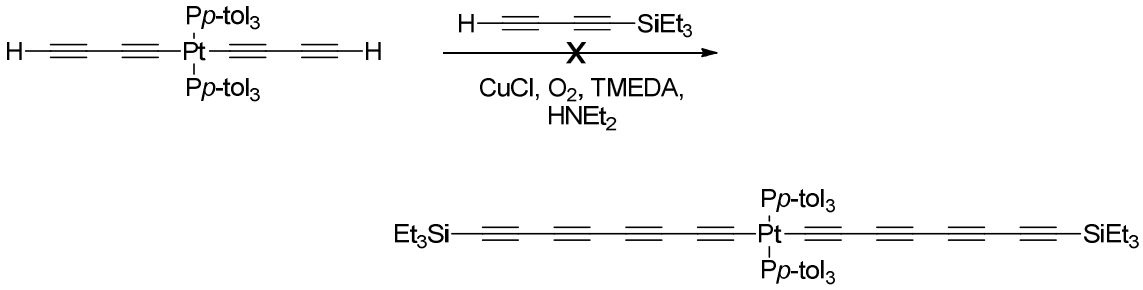

Scheme 2.21. Attempt to extend the polyyne chain to eight sp carbon atoms.

No tractable product could be isolated from this attempt. During the course of the reaction, the solution became black, in contrast to the successful cross coupling in Scheme 2.15. After column chromatography, a considerable amount (ca. 54% based upon $H(C{\equiv}C)_2SiEt_3$) of the byproduct $Et_3Si(C{\equiv}C)_4SiEt_3$ was isolated, resulting from the homocoupling of $H(C{\equiv}C)_2SiEt_3$. The remaining material isolated from the column showed $^{31}P\{^1H\}$ signals in $CDCl_3$ at δ 16.9 ppm, 16.8 ppm, and 16.5 ppm, all with $^1J_{PPt}$ = 2451 Hz, which could not be separated by column chromatography or HPLC.

7. Mass spectrometry. The squares analyzed in this chapter via mass spectrometry were ionized by MALDI, or matrix assisted laser desorption ionization. The platinum containing complexes in this chapter could not be ionized by ESI, or electrospray ionization, under the conditions that were successful for those in Chapter IV. MALDI is often more appropriate for large molecules. An alternative ionization method, APCI, or atmospheric pressure chemical ionization, has been shown to be an effective ionization method for bis(butadiynyl) complexes in a previous thesis,[39] but the *m/z* values corresponding to the squares in this chapter were too high for the APCI method. Thus, all mass spectrometry analyses of platinum containing complexes in this

chapter were conducted using MALDI. The use of different matrices can sometimes affect the results. For example, in Scheme 2.16, signals for the trimer and tetramer were observed when using a THAP matrix (THAP = 2',4',6'-trihydroxyacetophenone monohydrate). However, when the sample was analyzed using a DCTB matrix, these signals were not observed (DCTB = *trans*-2-(3-(4-*t*-butyl-phenyl)-2-methyl-2-propenylidene)malononitrile.

The dichloride corners **2a-f** did not give detectable molecular ions, but $[M - Cl]^+$ ions were observed in all cases. The bis(butadiynyl) complexes **3a-f** afforded $[M + K]^+$, $[M + Na]^+$, $[M + H]^+$, and/or $[M + Cu]^+$ ions (none of the metal ions were deliberately added to the sample). The squares **4a-d** and **4f** yielded $[M + H]^+$, $[M + K]^+$, and/or $[M + Cu]^+$ ions. Importantly, other possible polygons (triangles and pentagons, for example) were never detected in the mass spectra of the C_4-sided squares. Table 2.8 summarizes the various ions observed and matrices used. Although no strict trends can be assigned, it can be noted that the compounds in this study generally ionize the best using a DCTB matrix. This matrix was often used first and in cases where it failed, THAP was used instead. Although not employed as frequently, another successful matrix was CHCA (α-cyano-4-hydroxycinnamic acid). TFA (trifluoroacetic acid) was sometimes added to promote ionization. Importantly, there was no rhyme or reason regarding the presence or absence of certain ions, e.g., $[M + Na]^+$ and $[M + K]^+$. These are attributed to impurities in the solvent used to dissolve the matrix. The solvents used for these analyses were HPLC grade but not dried or distilled.

Table 2.8. Matrices employed for MALDI$^+$ mass spectrometry and observed ions, $[M + X]^+$, $[M - X]^+$, and/or $[M]^+$.

Compound	±X	Successful matrices	Unsuccessful matrices
A. *Phosphine or phosphine precursors*			
n-$Bu_2C(CH_2OMs)_2$	+K, $-CH_3$	DCTB	-
1c	+2O, +O, +	DCTB + 1% TFA	-
n-$Dec_2C(CH_2OMs)_2$	+Na	THAP	DCTB
1d	+2O, +O, +H	DCTB + 1% TFA	-
$BnC(CH_2OMs)_2$	+K	DCTB	-
(*p*-$tolCH_2)_2C(CO_2Et)_2$	+Na, +H	DCTB	-
(*p*-$tolCH_2)_2C(CH_2OH)_2$	+Na	DCTB	-
1f	+O, +	DCTB	-
B. *Dichloride complexes*			
2a	–Cl	DCTB	-
2b	–Cl	DCTB, THAP, CHCA	-
2c	–Cl	DCTB + 1% TFA	-
2d	–Cl	DCTB + 1% TFA	-
2e	–Cl	DCTB	-
2f	–Cl	DCTB	-
C. *Bis(ethynyl), Bis(butadiynyl), and bis(hexatriynyl) complexes*			
3a	+K, +Na, +H	THAP	DCTB
3b	+Na, +H, $-(C\equiv C)_2H$	CHCA	-
3c	+K	DCTB + 1% TFA	-
3d	+Cu	DCTB + 1% TFA	-
3e	+Cu	DCTB	-
3f	+K, +Na, +H	DCTB	-
5b	+K, +Na, +H	THAP	DCTB
6	$-C\equiv CSiEt_3$, $-2C\equiv CSiEt_3$	DCTB	-
7	H	DCTB	-
D. *Polygons*			
4a	Cu, +K, +H	DCTB	-
4b	+Cu, +H / +K	DCTB, THAP, CHCA / DCTB	- / THAP, CHCA
4c	+K	DCTB	-
4d	+Cu / +H	DCTB, THAP, CHCA / DCTB, THAP	- / CHCA
4f	+Cu	THAP	DCTB
Reaction of **5c** + **3c**	+	THAP	DCTB

8. Silica Gel Behavior. Attempts to chromatograph the squares and mixtures of products proved to be unsuccessful. Supports investigated included silica gel, basic and neutral alumina, and florisil. The following descriptions are generalized behaviors and were seen for both squares (see Scheme 2.13) and product mixtures (see Schemes 2.16, and 2.18-2.20) using various diphosphines. Thus, the described behavior on chromatography supports is not specific for the size of the polygon or for the bidentate diphosphine used.

Interestingly, the squares and mixtures did not move on any of the supports eluted with various solvents such as CH_2Cl_2 and EtOAc, giving an apparent R_f value of zero. Because of this, even HPLC was not a promising method to separate these samples. They exhibited peculiar behavior when introduced on a silica gel column. Hot extractions of "square infused" silica gel samples (collected from the tops of the silica gel columns after attempted chromatography) were carried out using CH_2Cl_2, THF, Et_2O, and acetonitrile. According to $^{31}P\{^1H\}$ NMR analyses, these were unsuccesful. Furthermore, a soxlet extractor was used to conduct a continuous extraction. The silica gel samples were extracted using CH_2Cl_2 (bp 40 °C), but no squares or polygons were removed from the samples as assayed by $^{31}P\{^1H\}$ NMR spectroscopy after 6 h. Similar soxlet extractions were attempted using THF (bp 66 °C), and the resulting $^{31}P\{^1H\}$ NMR spectra showed decomposition products of the molecular squares, likely due to the extended time at elevated temperature. The "square infused" silica gel samples were also probed using IR spectroscopy in hopes that the interactions between the silica gel and the square could be observed. Unfortunately this method was not sensitive enough to detect any changes in the square or silica gel.

Next, a very polar solvent, MeOH, was evaluated as a co-eluent. Interestingly, the squares did move with CH_2Cl_2/hexanes/MeOH (7:2:1 v/v/v) as the eluent. However,

in each case, a new complex formed and the mass of the square diminished, rendering this an inefficient method for separation. For example, **4c** (original $^{31}P\{^{1}H\}$ NMR spectrum showed a singlet at δ –7.8 ppm in $CDCl_3$) was passed through a silica gel column with CH_2Cl_2/hexanes/MeOH (7:2:1 v/v/v). The solvents were removed from the eluate and the residue showed significant mass loss (ca. 26%). The $^{31}P\{^{1}H\}$ NMR spectrum of the residue in $CDCl_3$ revealed singlets at δ –7.4 and –7.8 ppm, indicating the formation of a new product. The structure of this material remained elusive, as the IR spectrum was virtually unchanged. The mass spectrum did not reveal a new product, as only the ions associated with **4c** were apparent. Efforts to determine the identity of this new product were not further pursued.

9. Cyclocarbon synthesis. Next, attention was turned to the possibility of cyclocarbon formation using the squares **4a-f**, with the anticipated product being cyclo[16]carbon. First, a methodology presented in the introduction was assayed, using a model complex. As shown in Scheme 2.22, *cis/trans*-(*p*-$tol_3P)_2PtCl_2$ and $HC{\equiv}CSiEt_3$ were reacted to give *trans*-(*p*-$tol_3P)_2Pt(C{\equiv}CSiEt_3)_2$ (**6**). Substitution of the P*p*-tol_3 ligands by **1c** gave the new model complex **7**, characterized analogously to the related complexes in Schemes 2.11 and 2.12. Complex **7** featured two carbon chains with just two sp carbon atoms.

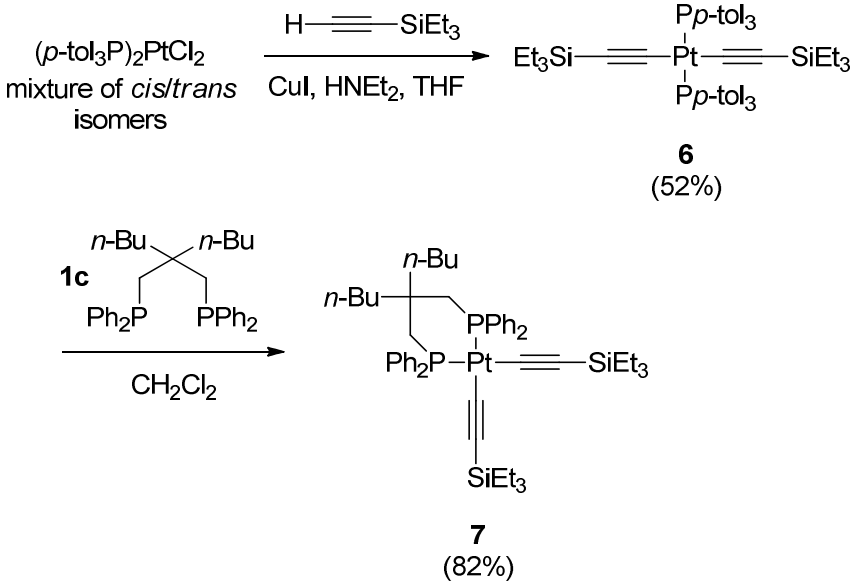

Scheme 2.22. Synthesis of cyclocarbon model complex **7**.

The model complex was treated with I_2 as shown in Scheme 2.23, in accordance with the reaction conditions presented by Bauerle (refer to Scheme 2.4); *i.e.* at 60 °C in THF for 24 h.

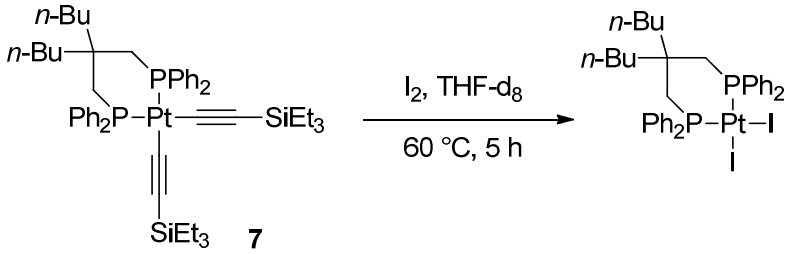

Scheme 2.23. Treatment of model complex **7** with I_2**.**

The $^{31}P\{^{1}H\}$ spectrum in $CDCl_3$ indicated complete transformation within 24 h as the signal was observed to shift from δ –6.1 ppm ($^{1}J_{PPt}$ = 2155 Hz) to δ –8.1 ppm ($^{1}J_{PPt}$ = 3205 Hz). This is indicative of the formation of a platinum diiodide complex. A previously reported complex, (dppp)PtI_2, showed a $^{31}P\{^{1}H\}$ NMR signal at –9.3 ppm with a similar coupling constant ($^{1}J_{PPt}$ = 3208 Hz).[49] This coupling constant is very similar to those of the *cis*-dichloride complexes **2a-f** (see Table 2.2). A slight change in chemical shifts for the $SiEt_3$ moieties in the ^{1}H NMR spectrum was observed, suggestive of $Et_3Si(C{\equiv}C)_2SiEt_3$ formation. This crude reaction mixture was analyzed by mass spectrometry and showed an ion at *m/z* 846 corresponding to the $[M - I]^+$ ion ($MALDI^+$).

Accordingly, as shown in Scheme 2.24, this reaction was attempted with **4a** as well as analogous reactions using Br_2 and $HgCl_2$.

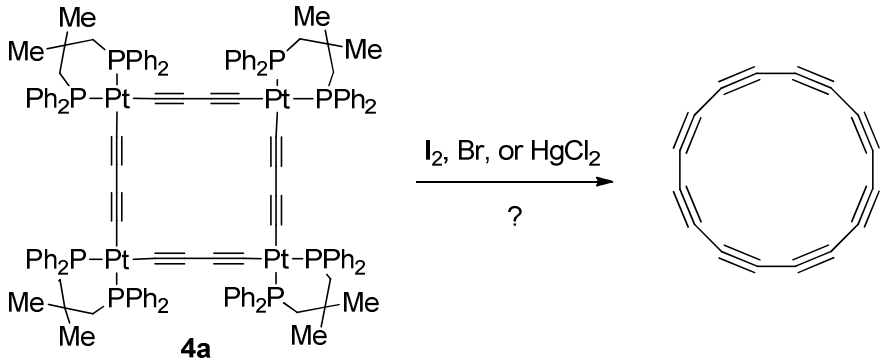

Scheme 2.24. Attempted demetallations of **4a** using various oxidants to form cyclo[16]carbon.

These transformations were carried out under the same conditions as the literature reported procedures. Solvents were removed from the reaction mixtures and

the resulting residues were analyzed by mass spectrometry for the formation of cyclo[16]carbon (*m/z* = 192) and for the possible persistence of the square (*m/z* = 2732). The results from these experiments are outlined in Table 2.9.

Table 2.9. MALDI$^+$ mass spectrometry analyses of attempted demetallation reactions of **4a** using various oxidants.

Oxidant	MS peaks (*m/z*)
I_2	197.19, 227.05, 671.01, 764.93
Br_2	167.00, 246.92, 294.62, 332.99, 467.77, 526.98
$HgCl_2$	167.09, 307.10, 363.50, 637.28, 670.78

According to the data in Table 2.8, cyclo[16]carbon was either not formed or not stable under the given reaction conditions. Importantly, the molecular square **4a** appeared to be consumed.

10. Host Guest Chemistry. Finally, the viability of the molecular squares as hosts for small molecules was tested. Figure 2.12 depicts the small molecules chosen for this study. The screening data can be summarized as follows.

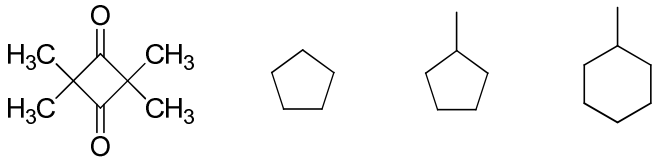

Figure 2.12. Small molecules investigated for host guest behavior. From left to right: tetramethyl cyclobutanedione, cyclopentane, methylcyclopentane, and methylcyclohexane.

10.1. Tetramethyl cyclobutanedione. The guest was combined with **4b** in $CDCl_3$ in a 50:50 molar ratio to give concentrations of 4.4×10^{-3} M for **4b** and 4.4×10^{-3} M for the guest. No shift was observed in the ^{1}H NMR spectrum. Hence, other potential guests were screened.

10.2. Cyclopentane. This guest was combined with **4b** as above to give concentrations of 5.5×10^{-3} M for **4b** and 5.5×10^{-3} M for the guest. The ^{1}H NMR spectrum showed a signal at δ 1.50 ppm, as compared to δ 1.54 for free cyclopentane at a comparable concentration in $CDCl_3$ (Δδ 0.04 ppm). This is suggestive of solution-based interactions between the square and cyclopentane.

10.3. Methylcyclopentane. This guest was combined with **4b** as above to give concentrations of 1.2×10^{-3} M for **4b** and 1.2×10^{-3} M for the guest. The ^{1}H NMR spectrum in $CDCl_3$ showed a methylcyclopentane CH_3 signal at δ 0.96 ppm, as compared to δ 0.98 for free methylcyclopentane at a comparable concentration in $CDCl_3$ (Δδ 0.02 ppm). This is suggestive of solution-based interactions between **4b** and methylcyclopentane. The ^{1}H NMR spectra of the CH_3 regions are shown in Figure 2.13.

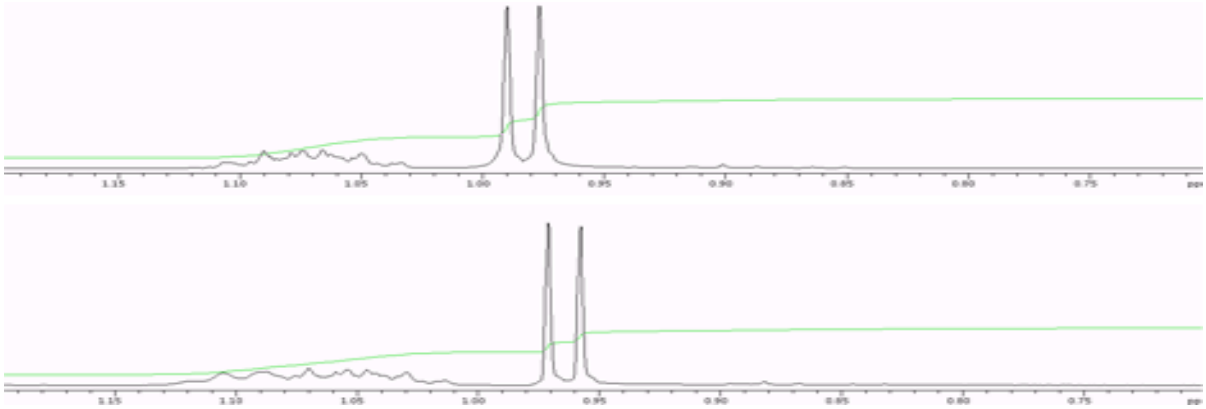

Figure 2.13. ^{1}H NMR spectra (partial, $CDCl_3$) of the CH_3 region of free methylcyclopentane (top) and of methylcyclopentane with **4b** (bottom).

10.4. Methylcyclohexane. This guest was combined with **4b** as above to give concentrations of 9.0×10^{-4} M for **4b** and 9.0×10^{-4} M for the guest. The ^{1}H NMR spectrum in $CDCl_3$ showed a methylcyclohexane CH_3 signal at δ 0.85 ppm, as compared to δ 0.89 ppm for free methylcyclohexane at a comparable concentration in $CDCl_3$ (Δδ 0.04 ppm). This is suggestive of solution-based interactions between **4b** and methylcyclohexane. The ^{1}H NMR spectra of the CH_3 regions are shown in Figure 2.14.

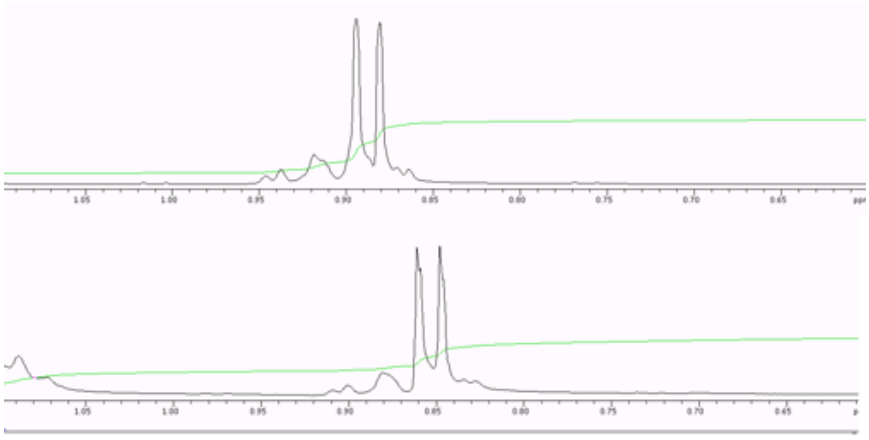

Figure 2.14. ^{1}H NMR spectra (partial, $CDCl_3$) of the CH_3 region of free methylcyclohexane (top) and of methylcyclohexane with **4b** (bottom).

DISCUSSION

1. Outlook on molecular polygons and cyclocarbons. This work has added to the repertoire of neutral molecular squares employing polyyne chains as the linkers (Scheme 2.13). The new squares demonstrate an efficient strategy to circumvent the problem of solubility by using functionalized bidentate diphosphines. However, challenges remain with squares or polygons with linkers of more than four sp carbon atoms.

None of the reactions in Schemes 2.16, 2.19, and 2.20 gave evidence for the selective formation of a higher homologue. In this context, it is important to recognize that other types of byproducts are possible besides higher or lower order polygons. For example, Figure 2.15 shows additional structures – closed species derived from six to eight corners and linkers (left) as well as acyclic intermediates from interrupted

macrocyclizations (right) – that may be derived from the cross coupling and homocoupling reactions employed.

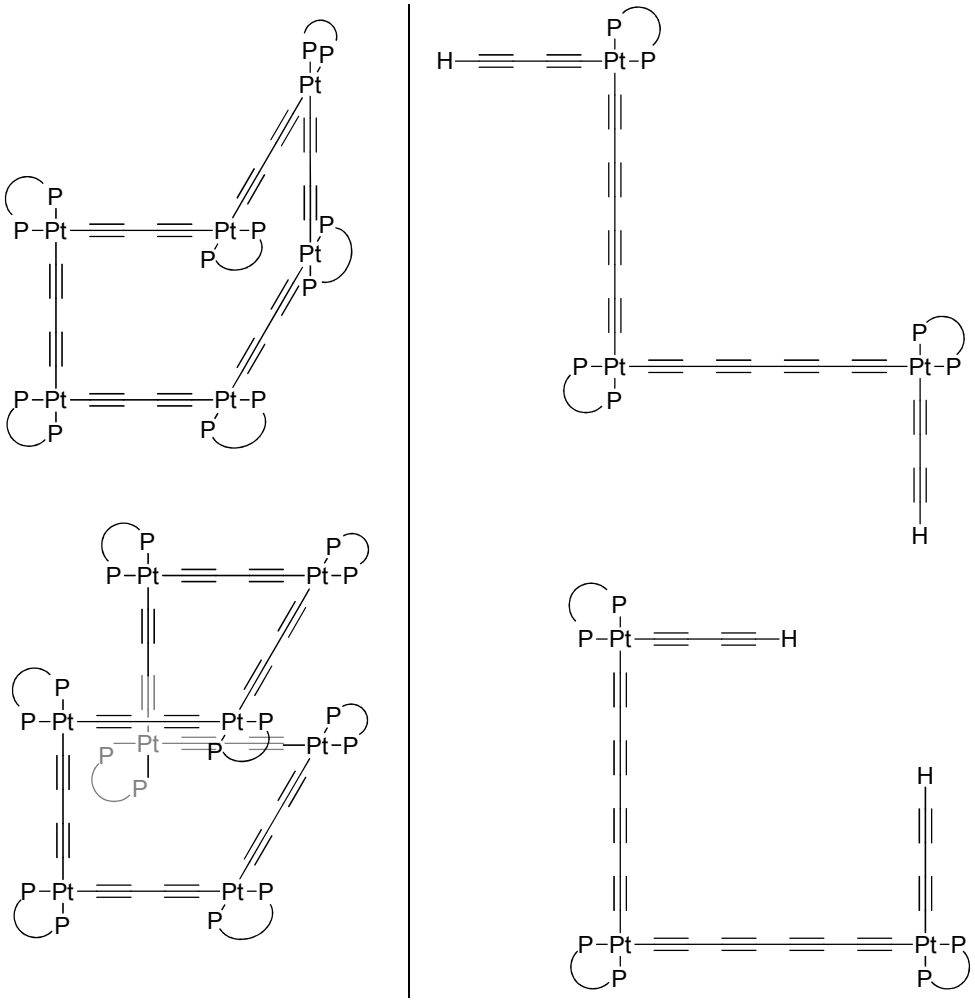

Figure 2.15. Some possible byproducts in attempted syntheses of molecular squares.

The mass spectrometric evidence for multiple polygon formation, i.e. the triangle and the square in Scheme 2.16, suggests that selectivity may be a problem in syntheses

of polygons with longer linkers. The $^{31}P\{^{1}H\}$ NMR chemical shifts for the products in Scheme 2.16 (δ –6.3 to –6.7 ppm, $CDCl_3$) are close to that of the square with the butadiynyl linkers and corresponding phosphine in Scheme 2.13 (δ –7.8 ppm; **4c** in Table 2.5). This downfield trend (C_6 to C_4) is consistent with that observed for analogous $L_nPtC{\equiv}CC{\equiv}CPtL_n$, $L_nPtC{\equiv}CC{\equiv}CC{\equiv}CPtL_n$, and $L_nPtC{\equiv}CC{\equiv}CC{\equiv}CC{\equiv}CPtL_n$ species. For example, the $^{31}P\{^{1}H\}$ chemical shifts for the corresponding polyynediyl complexes with L_nPt = $(C_6F_5)(p\text{-}tol_3P)_2Pt$ are 16.3, 17.2, and 17.6 ppm (δ, $CDCl_3$), respectively.[50] Perhaps a better comparison, the series with L_nPt = $(C_6F_5)(Et_3P)_2Pt$ exhibit $^{31}P\{^{1}H\}$ chemical shifts of 12.5,[51] 14.0,[52] and 13.2[51] ppm (δ, $CDCl_3$), respectively.

The formation of one polygon over another can be due to a number of factors. Note that in both Schemes 2.13 and 2.16, a triangle cannot form without a ligand redistribution reaction (starting materials or intermediates). However, a square complex could equilibrate to a triangle. In many self assembly reactions, triangles are favored for entropic reasons,[53] although strain, concentration, and temperature also play roles.

In any case, the preceding work indicates that the corner starting materials for higher polygons likely require additional coding to ensure a single product. Perhaps the strategic role of the lipophilic bidentate diphosphines can somehow be expanded, varying for example the bite angle and probing the effect in selectivity. Alternatively, guest molecules that would template a certain polygon size might be considered. As demonstrated in section 10, the butadiynediyl polygons do exhibit host behavior.

If the isolation of a higher homologue is achieved, the methods described in this chapter towards the formation of a cyclocarbon can be attempted. In the case of a C_6-sided molecular square, a cyclo[24]carbon would result, whose stability could be greater

than that of cyclo[16]carbon. In the case of a C_8-sided molecular square, this would make cyclo[32]carbon attainable.

2. Thermal and mass spectrometry data. Typical of these platinum complexes is a gradual decomposition upon heating, rather than a sharp melting point. Color changes are frequently observed, as detailed in the experimental section. A typical melting point trace is shown in Figure 2.16, in which decomposition of **2a** is gradual over a span of 50 °C, indicated by the red trace. The y-axis represented in Figure 2.16 indicates a change in intensity observed by the optical camera, which is capable of detecting changes in the optical characteristics of the capillary sample.

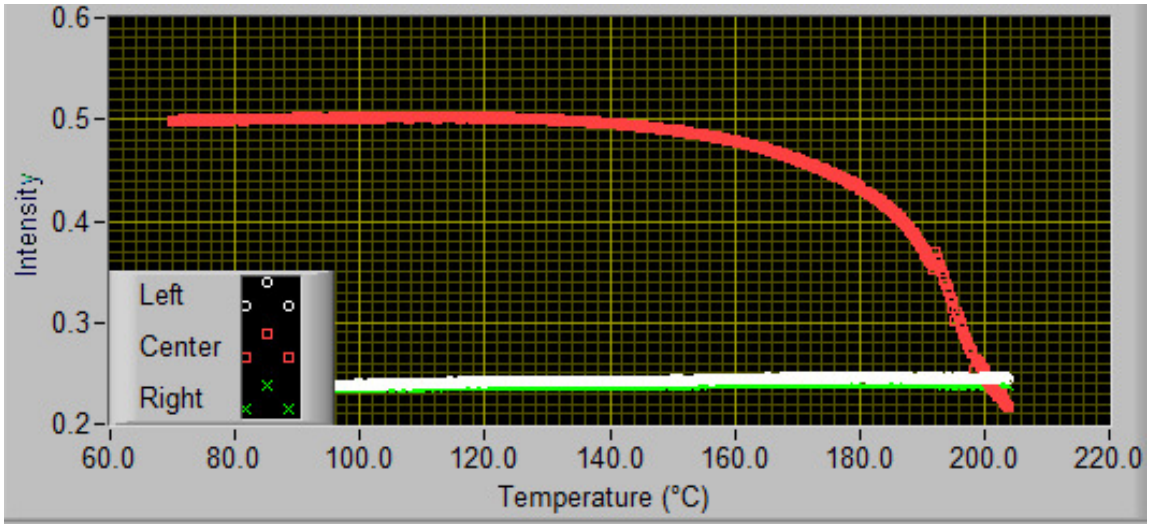

Figure 2.16. Melting point trace of square **2a** in red.

An interesting feature of sp-carbon based polygons or corners is their ability to coordinate suitable metals. Lang demonstrated that related bis(ethynyl) or bis(polyynyl) complexes were able to act as chelating ligands, or "tweezers", to coinage metals.[54-56]

This behavior has also been observed by Bruce, in which a platinum bis(butadiynyl) complex bound silver(I) and copper(I) species in a similar manner.[57] Figure 2.17 shows the structures of representative tweezer-like complexes. In all cases, the coinage metal binds in an η^2 fashion to both M(C≡C) units. The titanium complexes were characterized by X-ray crystallography, while Bruce's evidence involved mass spectrometry.

Although mass spectrometry does not establish structure, several bis(butadiynyl) complexes prepared in this study exhibited $[M + Na]^+$, $[M + K]^+$, or $[M + Cu]^+$ ions under MALDI conditions. Accordingly, analogous tweezer-like structures are suggested in Figure 2.18. As summarized in Table 2.8, nearly all of the square complexes behaved similarly.

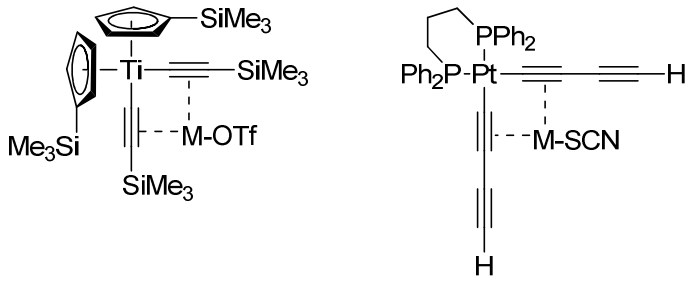

Figure 2.17. Some previously reported copper and silver complexes of molecular tweezers.

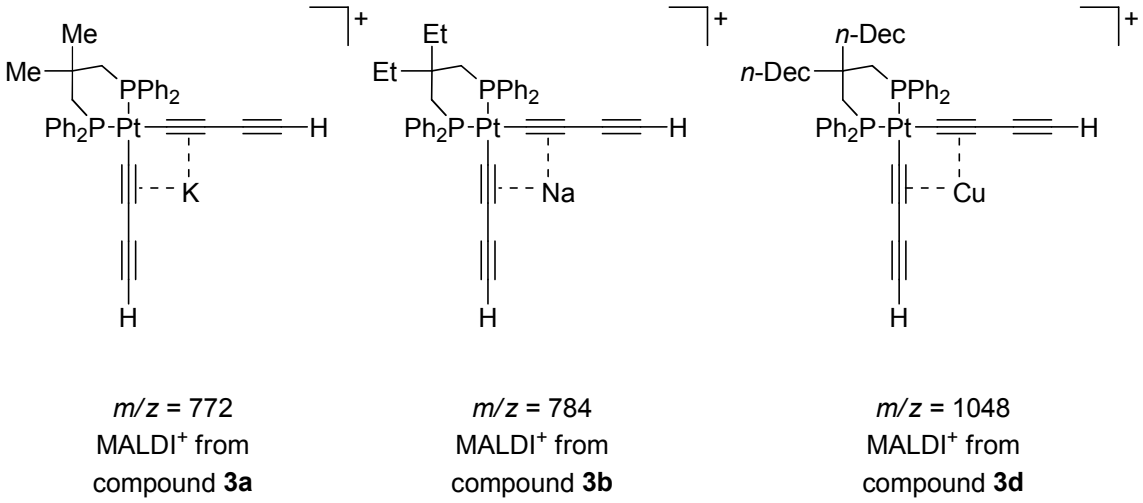

m/z = 772
MALDI$^+$ from
compound **3a**

m/z = 784
MALDI$^+$ from
compound **3b**

m/z = 1048
MALDI$^+$ from
compound **3d**

Figure 2.18. Plausible structures for various ions observed via mass spectrometry.

3. Crystal structure analysis of bis(butadiynyl) complex 3a·CH_2Cl_2. To assess the effect of functionalization at the 2-position on the diphosphine backbone, a comparison of the structure of **3a**·CH_2Cl_2 to that of the unsubstituted analogue, (dppp)Pt($(C{\equiv}C)_2H)_2$ (**8**), reported earlier by Bruce,[57] can be informative. The bidentate diphosphine in **8** has no substituent at the 2-position. The thermal ellipsoid plots of **3a**·CH_2Cl_2 and **8**·CH_2Cl_2 are depicted side by side in Figure 2.19.

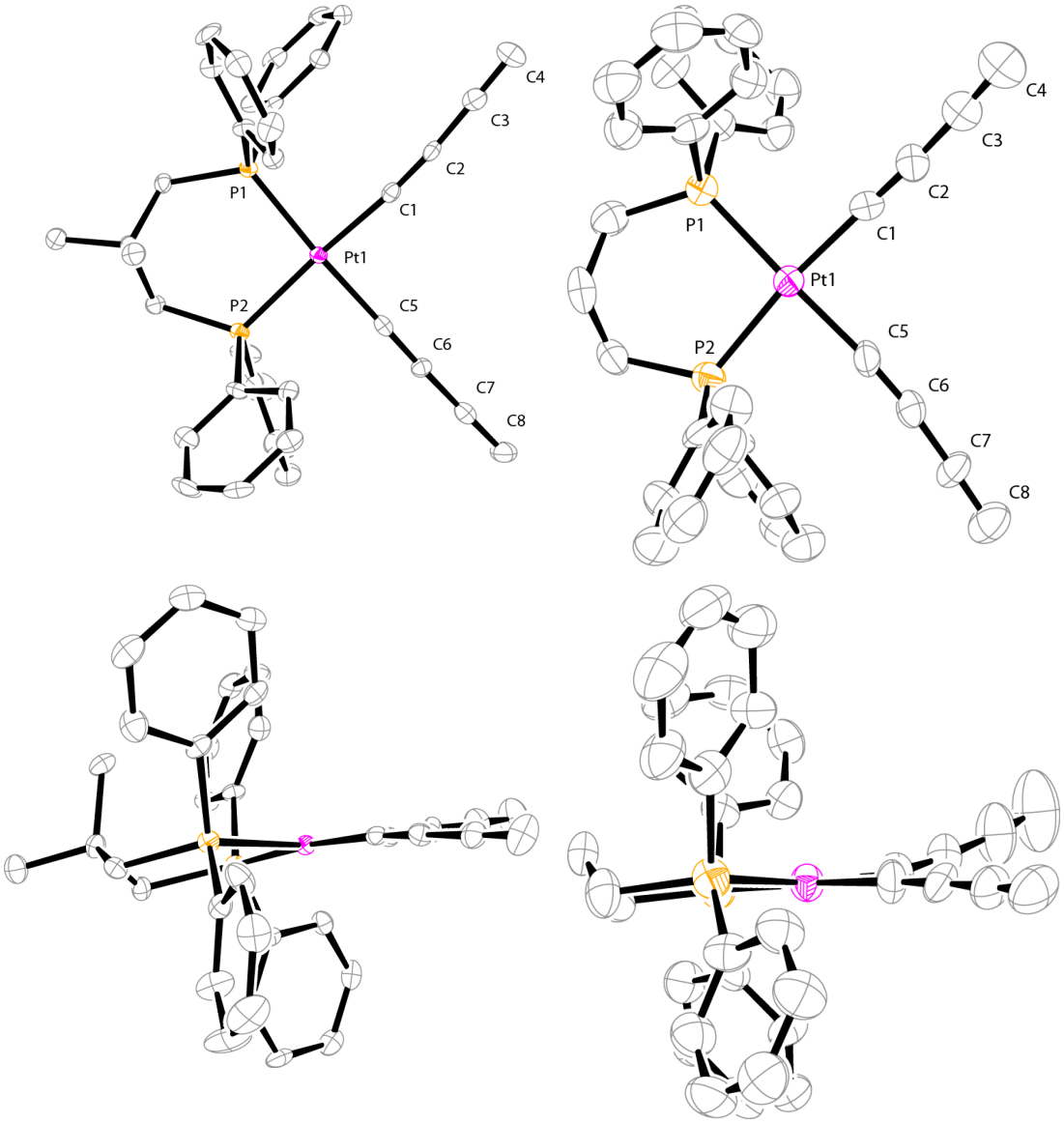

Figure 2.19. Thermal ellipsoid diagrams (50% probability level) of **3a**·CH_2Cl_2 (left) and **8**·CH_2Cl_2 (right) with solvent molecules omitted.

Table 2.10. Key crystallographic distances [Å] and angles [°] for platinum bis(butadiynyl) complexes.

	3a·CH_2Cl_2 [a]	**8**·CH_2Cl_2 [a]
Pt1-C1	1.998(4)	1.997(9)
Pt1-C5	2.007(4)	2.002(9)
Pt1-P1	2.2906(11)	2.304(2)
Pt1-P2	2.2870(11)	2.305(2)
C1≡C2	1.214(6)	1.212(12)
C5≡C6	1.178(6)	1.183(13)
C3≡C4	1.2121(6)	1.170(13)
C7≡C8	1.193(6)	1.172(19)
Avg C≡C	1.199(17)	1.189(14)
Pt···C4	5.757	5.678
Pt···C8	5.779	5.768
C4···C8	8.585	8.169
C1-Pt1-C5	90.58(16)	88.9(3)
C2-Pt1-C6	91.06	92.99
C3-Pt1-C7	95.25	93.06
C4-Pt1-C8	96.19	91.99
Pt1-C1-C2	174.1(4)	175.2(8)
C1-C2-C3	175.4(5)	173.6(9)
C2-C3-C4	179.4(6)	178.1(10)
Pt1-C5-C6	175.9(4)	171.0(8)
C5-C6-C7	177.9(4)	175.2(10)
C6-C7-C8	179.0(5)	175.7(13)
P1-Pt-P2	96.05(4)	97.03(8)

[a] The atomic numbering for **3a**·CH_2Cl_2 and **8**·CH_2Cl_2 have been changed from those in the CIF files to facilitate comparison of structural features.

From the data in Table 2.10, we can see that a substitution at the 2-position on the diphosphine backbone imparts a number of changes. The average C≡C bond length

in **3a**·CH_2Cl_2 is 0.01 Å longer than that in **8**·CH_2Cl_2. The platinum phosphorous bond distances in **8**·CH_2Cl_2 are slightly longer, indicative of less electron donation from the phosphorous ligands. The P-Pt-P angle in **8**·CH_2Cl_2 is significantly smaller than the same angle in **3a**·CH_2Cl_2 with values of 88.9(3) and 90.58(16), respectively.

The platinum center of **3a**·CH_2Cl_2 is coordinated in a slightly distorted square planar arrangement, with *trans* C-Pt-P angles of 173.74(12)° and 174.56(11)°. The six membered chelate ring is not planar, and instead adopts a chair-like conformation, as seen in Figure 2.19.

Figure 2.20 illustrates the staking of **3a**·CH_2Cl_2 in the crystal lattice.

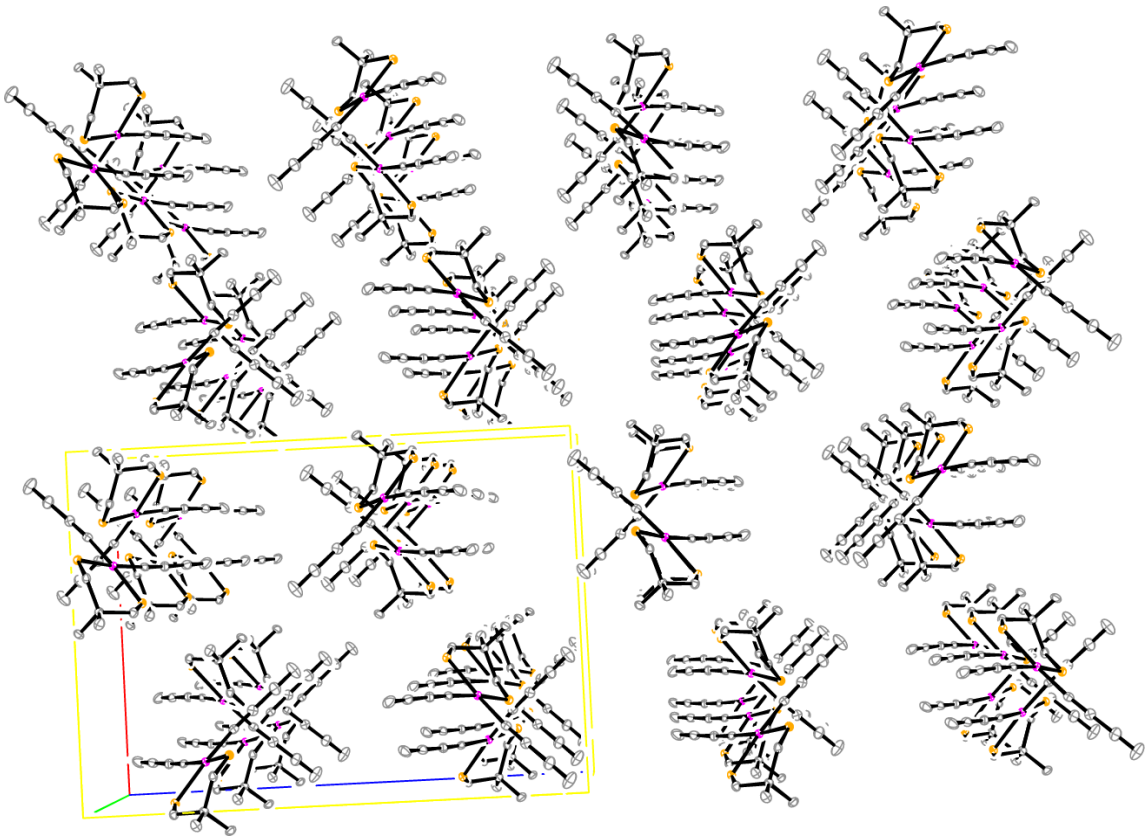

Figure 2.20. Thermal ellipsoid diagram (50% probability level) of **3a** showing stacking behavior.

4. Crystal structure analysis of molecular squares. One starting point is to focus on geometrical features special to the square moieties. One obvious issue concerns the planarity of the polygons. Importantly, both **4a** and **4b** exhibit significant puckering, as shown by the butterfly-like motifs in Figure 2.21. Here, the diphosphine ligands have been removed for clarity.

A puckering angle was measured by creating two mean planes, with the first being defined by Pt1, C1, C8, and Pt3 and the second by Pt1, C16, C9, and Pt3 (refer to Figure 2.11 for atom numbering). Square **4a** was found to have a puckering angle of 116.26° whereas this value in **4b** was 141.96°. An alternative indicator of puckering can be offered by the Pt-Pt distances in Table 2.7. Whereas **4a** exhibits a Pt2-Pt4 distance of 9.734 Å, this measurement in **4b** is elongated to 10.706, indicating less puckering of the square backbone.

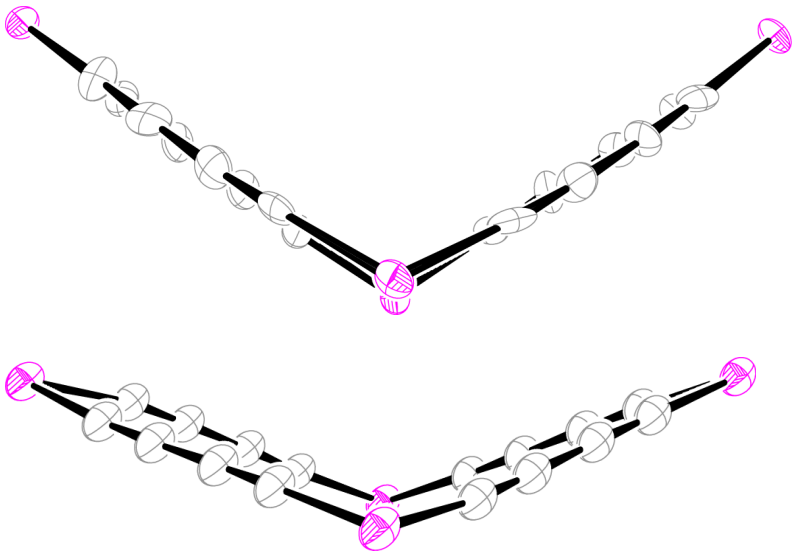

Figure 2.21. Thermal ellipsoid diagram (50% probability level) highlighting the puckered rings of **4a** (top) and **4b** (bottom), with puckering angles of 116.26° and 141.96°, respectively. Diphosphine ligands omitted for clarity.

Another obvious issue concerns the "bowing" of each side of the square. Varying degrees of "curvature" are apparent in Figure 2.11, and a parameter can be defined as illustrated in Figure 2.22. The distances between the bond midpoints indicated are also affected by the puckering, but the two values from a given molecule can be rigorously compared. Whereas **4a** shows two bowing parameters of approximately equal value (7.419 and 7.373 Å), **4b** does not (7.402 and 7.649 Å). Furthermore, the latter bowing parameter in **4b** (7.649 Å) is much greater than that of **4a**, while the former (7.402 Å) is comparable. This largely reflects a more "stretched out" or less folded core.

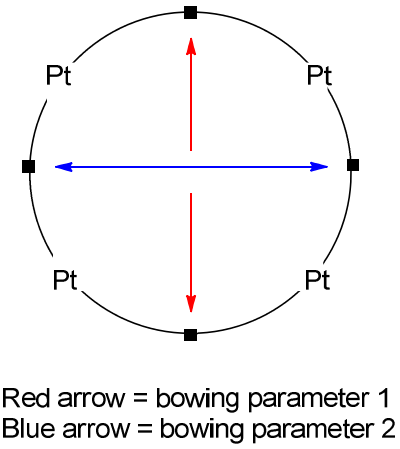

Figure 2.22. Graphical definition of the bowing parameters in Table 2.7. The dark squares indicate the midpoints of the polyynediyl ligands, approximated as the midpoints of the central ≡C-C≡ bond.

Anderson has crystallized a similar square with no substituents on the diphosphine backbone, [(dppp)Pt(C≡C)$_2$]$_4$.[58] He also observed a butterfly-like conformation, with a puckering angle intermediate between those of **4a** and **4b**: 134.79°. The bowing parameters (7.507 and 7.380 Å) were quite close to those of **4a**. Anderson also found, similarly to the case with **4a** and **4b**, a variety of solvent molecules (water, acetonitrile, and ethanol) in the crystal lattice. These also proved difficult to refine.

The crystal lattices of **4a** and **4b** also feature a number of interesting differences. Square **4a** exhibits uniform channels in the crystal lattice. Square **4b** does not, as the square backbones are not neatly stacked. Instead, the squares translate in adjacent layers, which blocks uniform channels. Thermal ellipsoid diagrams are shown in Figures 2.23 and 2.24 to illustrate channel behavior and lack thereof for **4a** and **4b**, respectively.

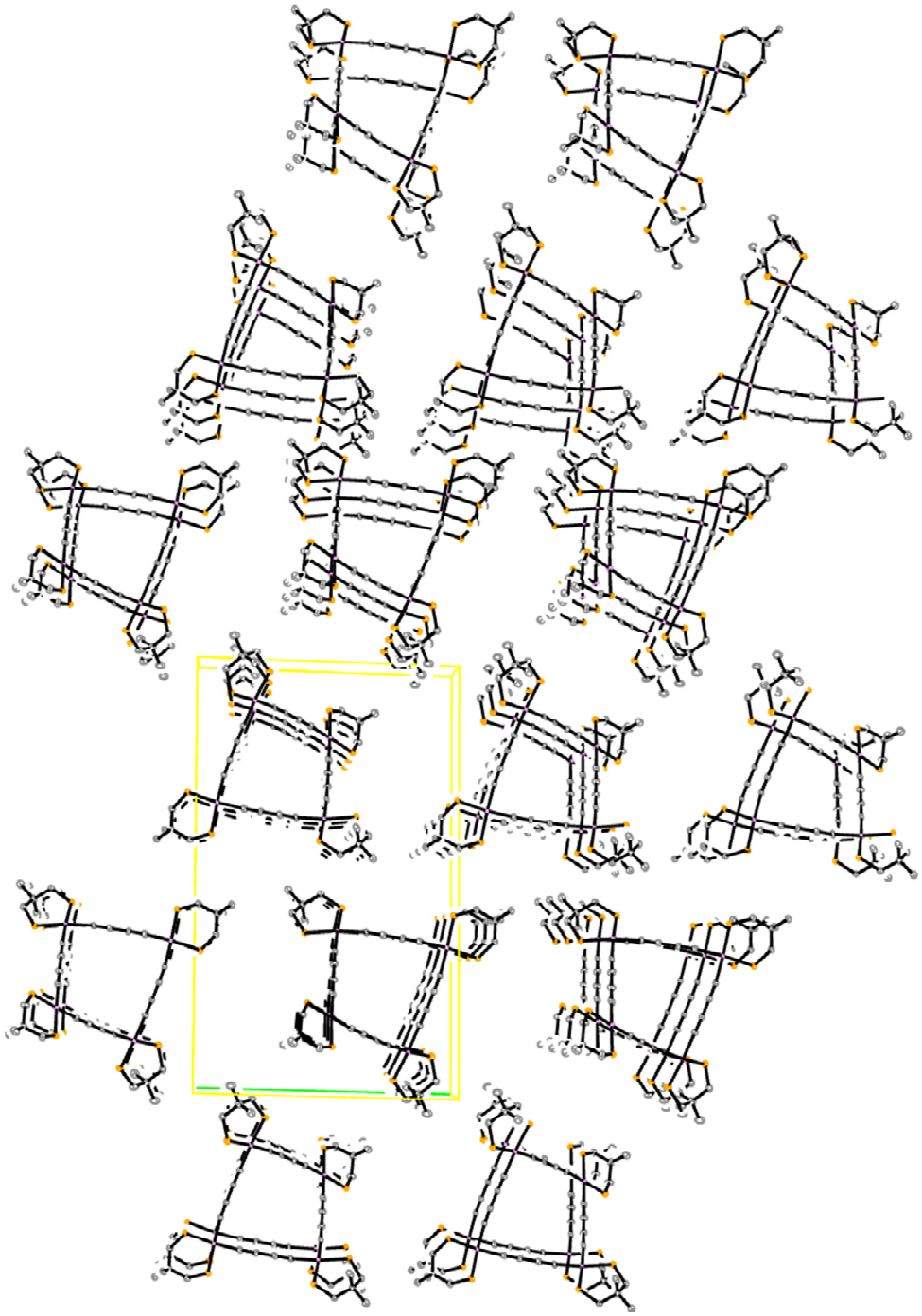

Figure 2.23. Thermal ellipsoid diagram (50% probability level) of **4a** showing the stacking of squares to form uniform channels with *p*-tol substituents omitted for clarity.

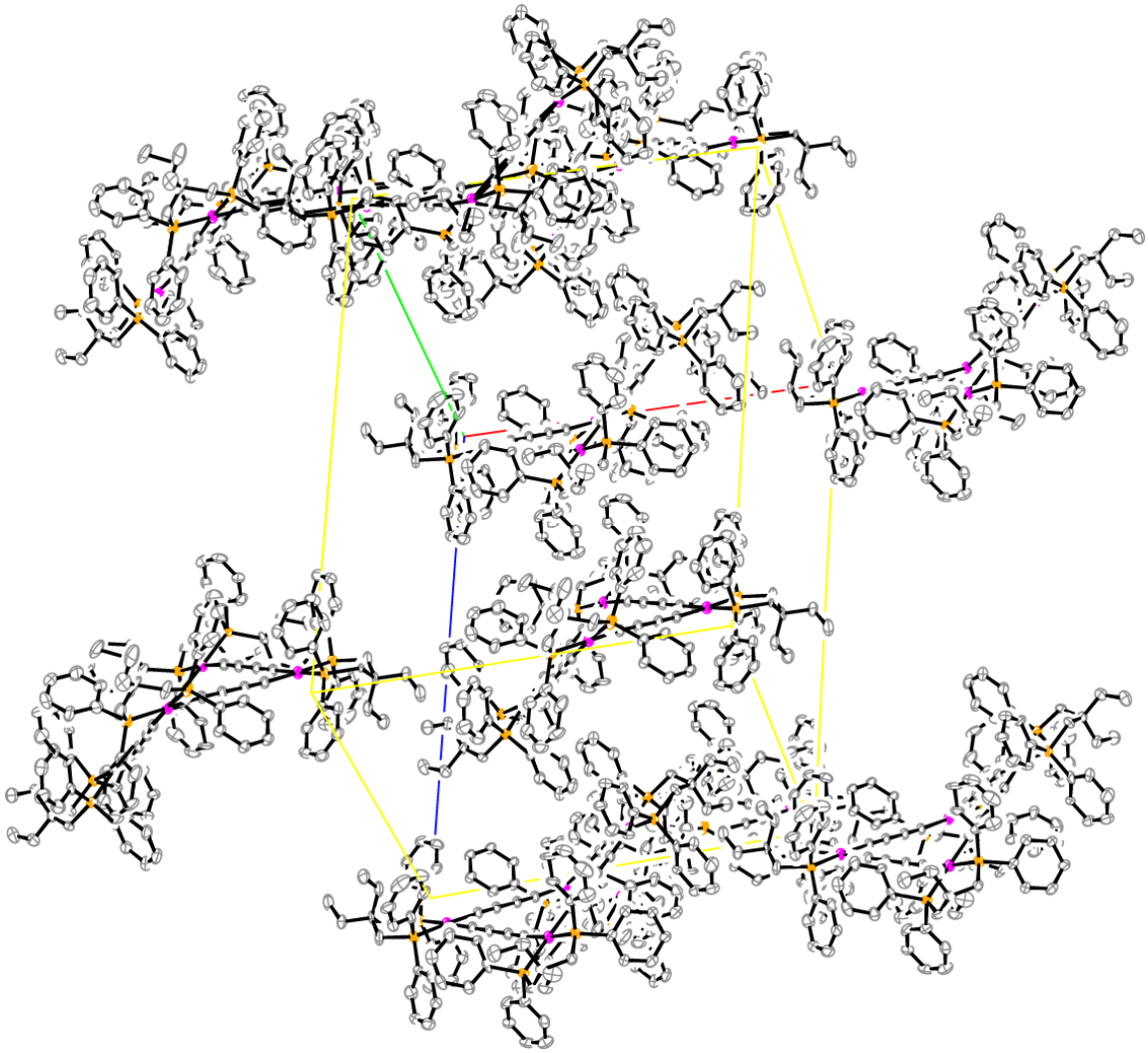

Figure 2.24. Thermal ellipsoid diagram (50% probability level) of **4b** showing the absence of stacking and uniform channels.

In this context, the folds of **4a** are "nested" and adopt two packing motifs. Two views of **4a** down different axes are offered in Figure 2.25, which illustrate this "nesting" behavior. However, **4b** shows less systematic packing with regard to folding patterns.

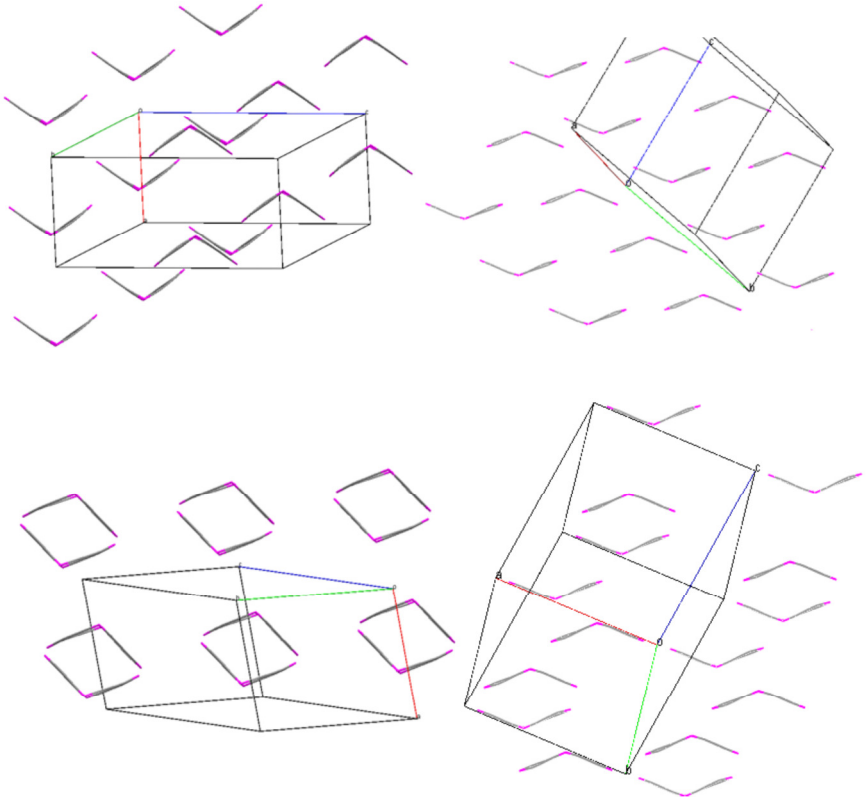

Figure 2.25. Packing diagrams of **4a** (left) and **4b** (right) illustrating folding relationships with diphosphine ligands omitted. Views down the Pt1-Pt3 (top) and Pt2-Pt4 (bottom) axes.

CONCLUSION

This study has expanded the chemistry of neutral molecular polygons involving polyynediyl chains as linkers and diphosphines as ligands on the metal corners. The problems of solubility of neutral molecular squares have been circumvented with the use of functionalized bidentate diphosphines. This has enabled the crystallization of two C_4 sided complexes, and the X-ray structural data establish a number of interesting features. Although higher homologues of C_4 sided systems could not be separated and independently characterized, mass spectrometry provided good evidence for such

squares and triangles (see Scheme 2.16). If efficient workups can be developed in the future, additional significant advances in this field will be possible.

EXPERIMENTAL

General: All reactions were carried out in under an inert atmosphere using standard Schlenk and vacuum line techniques unless noted. All workups were carried out in air unless noted. Chemicals were treated as follows: CH_2Cl_2 (ACS grade, Fisher Scientific; reaction solvent) and THF (ACS grade, Fisher Scientific), dried and degassed using a Glass Contour solvent purification system; acetone (ACS grade, BDH), distilled from $CaSO_4$; CH_2Cl_2 (ACS grade, EMD Chemicals; chromatography/workups), hexanes (ACS grade, Macron Chemicals), $HNEt_2$ (99+%, Alfa Aesar), MeOH (anhydrous, 99.8% EMD), EtOH (Koptec), toluene (ACS grade, Macron chemicals), EtOAc (ACS grade, Macron chemicals), petroleum ether (ACS grade, Fisher), acetonitrile (ACS grade, EMD), HCl (Fisher), Et_2O (ACS grade, JT Baker), $LiAlH_4$ (97%, Alfa Aesar), CuI (99.999%, Alfa Aesar), $HC{\equiv}CSiEt_3$ (97%, Acros), CuCl (99.999%, Alfa Aesar), *n*-Bu_4N^+ F^- (1.0 M in THF, 5 wt% water, Acros), TMEDA (tetramethylethylenediamine, 99%, Acros), *n*-$Bu_2C(CH_2OH)_2$ (97%, Aldrich), pyridine (anhydrous, 99.8%, EMD), $KPPh_2$ (0.5 M in THF, Aldrich), NaH (99%, Alfa Aesar), diethyl malonate (99%, Aldrich), MsCl (>98.0%, Fluka), *p*-tolCH_2Br (99%, Alfa Aesar), alumina (neutral, Brockmann I, 50-200 μm), and silica gel (Acros, Silicycle, or Fluoroflash), used as received.

NMR spectra were recorded on a Varian NMRS 500 MHz spectrometer at ambient probe temperatures and referenced as follows: ^1H NMR, residual $CHCl_3$ (δ, 7.26 ppm), residual $CDHCl_2$ (δ, 5.38 ppm), residual C_6D_5H (δ, 7.15 ppm); $^{13}C\{^1H\}$

NMR, internal $CDCl_3$ (δ, 77.0 ppm), internal C_6D_6 (δ, 128.0 ppm); $^{31}P\{^1H\}$ external H_3PO_4 (δ, 0.00 ppm). Melting and thermal behavior was assayed using an OptiMelt MPA 100 apparatus. Microanalyses were conducted by Atlantic Microlab. IR spectra were recorded on a Shimadzu IRAffinity-1 spectrometer with a Pike MIRacle ATR system (diamond/ZnSe crystal).

***n*-$Bu_2C(CH_2OMs)_2$**. A Schlenk flask was charged with *n*-$Bu_2C(CH_2OH)_2$ (5.0264 g, 25.694 mmol mmol) and pyridine (30 mL) with stirring. The flask was cooled to 0 °C and MsCl (6.17 mL, 9.13 mmol, 79.7 mmol) was added dropwise. The cold bath was removed. After 2 h, water (20 mL) was added. The mixture was extracted with CH_2Cl_2 (2 × 20 mL). The extract was washed with aqueous HCl (pH = 4, 20 mL), saturated aqueous $NaHCO_3$ (20 mL), and water (20 mL) and then dried (Na_2SO_4). The solvent was removed by rotary evaporation. Then CH_2Cl_2 (20 mL) and petroleum ether (20 mL) were added and the solution was stored at 3 °C. The precipitate was collected by filtration, washed with cold CH_2Cl_2 (10 mL), and dried by oil pump vacuum to give *n*-$Bu_2C(CH_2OMs)_2$ as a white solid (8.9326 g, 25.930 mmol, 98%), mp 60-61 °C. Anal. Calcd. for $C_{13}H_{28}O_6S_2$ (344.49 g/mol): C, 45.32; H, 8.19. Found: C, 45.40; H, 8.18.

NMR (δ (ppm), $CDCl_3$): ^1H 4.02 (s, 4H, OCH_2), 3.02 (s, 6H, SCH_3), 1.29-1.24 (m, 8H, $CH_2CH_2CH_2CH_3$), 1.22-1.18 (m, 4H, CH_2CH_3), 0.88 (t, $^3J_{HH}$ = 7.4 Hz, 6H, CH_3); $^{13}C\{^1H\}$ 70.7 (s, OCH_2), 40.4 (s, SCH_3), 37.3 (s, $CH_2CH_2CH_2CH_3$), 29.6 (s, $C(CH_2)_4$), 24.5 (s, $CH_2CH_2CH_3$), 23.3 (s, CH_2CH_3), 14.1 (s, CH_2CH_3).

IR (cm^{-1}, powder film): 2931 (w), 2870 (w), 1471 (w), 1350 (s), 1172 (s), 980 (s), 864 (s), 350 (s).

MS ($MALDI^+$, matrix DCTB):[59] 383 ($[\mathbf{M} + K]^+$, 60%), 329 ($[\mathbf{M} - CH_3]^+$, 100%).

***n*-$Bu_2C(CH_2PPh_2)_2$ (1c)**. A Schlenk flask was charged with $KPPh_2$ (60.00 mL, 0.5 M in THF; 30 mmol) with stirring and cooled to 0 °C. A solution of *n*-$Bu_2C(CH_2OMs)_2$ (2.067 g, 6.000 mmol) in THF (30 mL) was added. After 48 h, the solvent was removed by rotary evaporation. Then water (20 mL) and EtOH (20 mL) were added. The mixture was extracted with CH_2Cl_2 (2 × 20 mL) and the extract was dried ($MgSO_4$). The solvent was removed by rotary evaporation to give a clear oil. Then MeOH (15 mL) was added and the flask was stored at 3 °C. The precipitate was collected by filtration, washed with cold MeOH (5 mL), and dried by oil pump vacuum to give **1c** as a white solid (2.390 g, 4.555 mmol, 76%), mp 85-88 °C. Anal. Calcd. for $C_{35}H_{42}P_2$ (524.66 g/mol): C, 80.12; H, 8.07. Found: C, 79.89; H, 7.89.

NMR (δ (ppm), $CDCl_3$): ^{1}H 7.42-7.49 (m, 8H, *o* to P), 7.22-7.30 (m, 12H, *m* and *p* to P), 2.32-2.41 (d, $^2J_{HP}$ = 7.8 Hz, 4H, PCH_2), 1.31-1.40 (m, 4H, CH_2CH_2CH_2CH_3), 0.70-0.96 (m, 8H, CH_2CH_2CH_3), 0.61 (t, $^3J_{HH}$ = 7.3 Hz, 6H, CH_3); ^{13}C{^{1}H} 140.3 (d, $^2J_{CP}$ = 14.1 Hz, *o* to P), 133.6-133.3 (m, *J* = 21.4 Hz, *J* = 1.5 Hz, *i* to P),[60] 128.5-128.3 (2 m, *p* and *m* to P), 40.2 (t, $^1J_{CP}$ = 11.2 Hz, P*C*H_2),[61] 39.6 (t, $^2J_{CP}$ = 7.7 Hz, *C*$(CH_2)_4$), 39.4-39.2 (m, *C*H_2CH_2CH_2CH_3), 25.7 (s, *C*H_2CH_2CH_3), 23.2 (s, *C*H_2CH_3), 14.1 (s, *C*H_3); ^{31}P{^{1}H} –25.8 (s).

IR (cm^{-1}, powder film): 2924 (w), 2862 (w), 1589 (w), 1435 (w), 1435 (w), 1188 (w), 1064 (w), 918 (w), 825 (w), 741 (w), 694 (w).

MS (MALDI$^+$, matrix DCTB + 1% TFA):[59] 557 ([**1c** + 2O]$^+$, 6%), 539 ([**1c** + O]$^+$, 20%), 525 ([**1c**]$^+$, 30%).

***n*-$Dec_2C(CH_2OMs)_2$.** A Schlenk flask was charged with *n*-$Dec_2C(CH_2OH)_2$ (18.5899 g, 52.1646 mmol)[62] and pyridine (120 mL) with stirring. The flask was cooled to 0 °C and MsCl (12.11 mL, 17.93 g, 156.6 mmol) was added dropwise. The cold bath

was removed. After 3 h, water (75 mL) was added. The mixture was extracted with CH_2Cl_2 (100 mL). The extract was washed with aqueous HCl (pH = 4, 20 mL), saturated aqueous $NaHCO_3$ (20 mL), and water (20 mL), and then dried (Na_2SO_4). The solvent was removed by oil pump vacuum to give *n*-$Dec_2C(CH_2OMs)_2$ as a white solid (24.2973 g, 47.3807 mmol, 91%), mp 58-60 °C. Anal. Calcd. for $C_{25}H_{52}O_6S_2$ (512.81 g/mol): C, 58.55; H, 10.22. Found: C, 58.55; H, 10.18.

NMR (δ (ppm), $CDCl_3$): ^{1}H 4.02 (s, 4H, OCH_2), 3.03 (s, 6H, SCH_3), 1.32-1.20 (m, 36H, (CH_2)$_9$CH_3), 0.87 (t, $^3J_{HH}$ = 7.6 Hz, 6H, CH_2CH_3); ^{13}C{^{1}H} 70.4 (s, OCH_2), 40.3 (s, SCH_3), 37.1 (s, $C(CH_2)_4$), 31.8 (s, CH_2), 30.0 (s, CH_2), 29.7 (s, CH_2), 29.5 (s, CH_2), 29.4 (s, CH_2), 29.3 (s, CH_2), 29.2 (s, CH_2), 22.6 (s, CH_2), 22.2 (s, CH_2), 14.3 (s, CH_2CH_3).

IR (cm^{-1}, powder film): 2916 (m), 2846 (m), 1466 (w), 1350 (s), 1327 (s), 1180 (s), 1165 (s), 957 (s), 833 (s), 795 (w).

MS (MALDI$^+$, matrix THAP):[59] 535 ([**M** + Na]$^+$, 60%).

***n*-$Dec_2C(CH_2PPh_2)_2$ (1d).** A Schlenk flask was charged with $KPPh_2$ (60.00 mL, 0.5 in THF; 30 mmol) with stirring and cooled to 0 °C. Then *n*-$Dec_2C(CH_2OMs)_2$ (6.1523 g, 11.997 mmol) was added as a solid. After 4 d, the solvent was removed by rotary evaporation. Then water (50 mL) and EtOH (20 mL) were added. The mixture was extracted with CH_2Cl_2 (50 mL) and the extract was dried ($MgSO_4$). The solvent was removed by rotary evaporation to give a yellow oil. The oil was chromatographed on a silica gel column (30 × 4.5 cm) eluted with 1:1 v/v CH_2Cl_2/hexanes. The product containing fractions were combined and the solvents were removed by oil pump vacuum to give **1d** as a clear oil (7.5606 g, 10.910 mmol, 91%). Anal. Calcd. for $C_{47}H_{66}P_2$ (692.97 g/mol): C, 81.46; H, 9.60. Found: C, 81.08; H, 9.34.

NMR (δ (ppm), $CDCl_3$): ^1H 7.52-7.44 (m, 8H, *o* to P), 7.34-7.25 (m, 12H, *m* and *p* to P), 1.55-0.73 (m, 42H, $(CH_2)_9CH_3$); $^{13}C\{^1H\}$ 134.6 (virtual t,[63] $^2J_{CP}$ = 5.1 Hz, *o* to P), 131.1 (s, *p* to P), 131.5 (s, *p* to P), 128.6 (m, *J* = 72.9 Hz, *J* = 6.9 Hz, *i* to P),[60] 128.8 (virtual t,[63] $^3J_{CP}$ = 5.8 Hz, *m* to P), 41.1 (s, CH_2), 40.5 (t, $^2J_{CP}$ = 6.9 Hz, $C(CH_2)_4$), 35.9 (t, $^1J_{CP}$ = 20.3 Hz, PCH_2),[61] 32.0 (s, CH_2), 29.7 (s, 2 × CH_2), 29.6 (s, CH_2), 29.4 (s, CH_2), 29.3 (s, CH_2), 22.8 (s, CH_2), 22.6 (s, CH_2), 14.3 (s, CH_3); $^{31}P\{^1H\}$ –25.8 (s).

IR (cm^{-1}, neat oil): 3055 (w), 2924 (s), 2854 (s), 2323 (w), 1458 (w), 1188 (s), 802 (w), 740 (s), 694 (s), 509 (s), 478 (s).

MS (MALDI$^+$, matrix DCTB + 1% TFA):[59] 724 ([**1d** + O]$^+$), 708 ([**1d** + 2O]$^+$), 693 ([**1d** + H]$^+$, 30%).

$Bn_2C(CH_2OMs)_2$. A round bottom flask was charged with $Bn_2C(CH_2OH)_2$ (0.9525 g, 3.715 mmol)[64] and pyridine (2 mL) with stirring. The flask was cooled to 0° and MsCl (0.86 mL, 1.2 g, 11 mmol) was added dropwise. The cold bath was removed. After 2 h, water (10 mL) was added. The mixture was extracted with CH_2Cl_2 (3 × 10 mL). The extract was washed with aqueous HCl (pH = 4, 10 mL), saturated aqueous $NaHCO_3$ (10 mL), and water (10 mL), and then dried (Na_2SO_4). The solvent was removed by oil pump vacuum to give $Bn_2C(CH_2OMs)_2$ as a white solid (1.1703 g, 2.8165 mmol, 76%), mp 112-114 °C. Anal. Calcd. for $C_{19}H_{24}O_6S_2$ (412.52 g/mol): C, 55.32; H, 5.86. Found: C, 55.71; H, 5.82.

NMR (δ (ppm), $CDCl_3$): ^1H 7.30-7.11 (m, 10H, C_6H_5), 3.93 (s, 4H, OCH_2), 2.93 (s, 6H, CH_3), 2.74 (s, 4H, $CH_2C_6H_5$); $^{13}C\{^1H\}$ 135.2 (s, *i* to CH_2), 130.8 (s, *o* to CH_2), 128.8 (s, *m* to CH_2),[65] 127.3 (s, *p* to CH_2), 69.8 (s, CH_2O), 42.3 (s, $C(CH_2)_4$), 38.3 (s, $CH_2C_6H_5$), 37.4 (s, CH_3).

IR (cm^{-1}, powder film): 3032 (w), 2932 (w), 1497 (w), 1458 (w), 1327 (s), 1172 (s), 941 (s), 848 (w), 817 (s), 732 (s), 702 (s).

MS (MALDI$^+$, matrix DCTB):[59] 451 ([**M** + K]$^+$, 100%).

(*p*-tolCH$_2$)$_2$C(CO$_2$Et)$_2$. A three necked flask was fitted with a condenser, charged with diethyl malonate (6.3305 g, 23.950 mmol) and THF (30 mL) with stirring, and cooled to 0 °C. Then NaH (1.687 g, 27.759 mmol, 57% oil dispersion) was added. After 0.5 h, *p*-tolCH$_2$Br (4.4954 g, 24.292 mmol) was added. The mixture was refluxed. After 18 h, the sample was cooled and aqueous NH_4Cl (20 mL) was added. The mixture was extracted with Et_2O (3 × 30 mL) and the extract was dried (Na_2SO_4). The solvents were removed by rotary evaporation. The residue was chromatographed on a silica gel column (30 × 4.5 cm) with 1:1 v/v CH_2Cl_2/hexanes as the eluent. The product containing fractions were combined and the solvents were removed by oil pump vacuum to give (*p*-tolCH$_2$)$_2$C(CO$_2$Et)$_2$ as a clear oil (5.7998 g, 15.740 mmol, 66%). Anal. Calcd. for $C_{23}H_{28}O_4$ (368.47 g/mol): C, 74.97; H, 7.66. Found: C, 75.22; H, 7.56.

NMR (δ (ppm), $CDCl_3$): ^{1}H 7.11-7.03 (m, 8H, C_6H_4), 4.09 (q, $^3J_{HH}$ = 7.2 Hz, 4H, CH_2CH_3), 3.15 (s, 4H, $CH_2C_6H_4$), 2.29 (s, 6H, $C_6H_4CH_3$), 1.16 (t, $^3J_{HH}$ = 7.3 Hz, 6H, CH_2CH_3); ^{13}C{^{1}H} 171.3 (s, CO_2), 136.6 (s, *p* to CH_2), 133.4 (s, *i* to CH_2), 130.2 (s, *o* to CH_2), 129.1 (s, *m* to CH_2),[65] 61.3 (s, CH_2CH_3), 60.4 (s, $C(CH_2C_6H_5)_2$), 38.6 (s, $CH_2C_6H_5$), 21.2 (s, $C_6H_5CH_3$), 14.1 (s, CH_2CH_3).

IR (cm^{-1}, neat oil): 2978 (w), 1728 (s), 1705 (s), 1604 (m), 1512 (m), 1442 (m), 1242 (m), 1196 (s), 1165 (s), 1111 (m), 1070 (w), 848 (w), 810 (s), 750 (m).

MS (MALDI$^+$, matrix DCTB):[59] 369 ([**M** + H]$^+$, 100%).

(*p*-tolCH$_2$)$_2$C(CH$_2$OH)$_2$. A Schlenk flask was fitted with a condenser, charged with (*p*-tolCH$_2$)$_2$C(CO$_2$Et)$_2$ (1.9705 g, 5.3478 mmol) and Et$_2$O (5 mL) with stirring, and cooled to 0 °C. A suspension of LiAlH$_4$ (0.6075 g, 16.01 mmol) in Et$_2$O (20 mL) was added dropwise. After 2 h, the mixture was refluxed. After 18 h, the sample was cooled and aqueous HCl (pH = 4, 20 mL) was added. The mixture was extracted with Et$_2$O (3 × 20 mL). The extract was washed with water (20 mL) and dried (Na$_2$SO$_4$). The solvent was removed by oil pump vacuum to give (*p*-tolCH$_2$)$_2$C(CH$_2$OH)$_2$ as a white solid (1.4879 g, 5.2358 mmol, 98%), mp 96-97 °C. Anal. Calcd. for C$_{19}$H$_{24}$O$_2$ (284.39 g/mol): C, 80.24; H, 8.51. Found: C, 80.54; H, 8.54.

NMR (δ (ppm), CDCl$_3$): ^{1}H 7.11-7.05 (m, 8H, C$_6$*H*$_4$), 3.53 (s, 4H, C*H*$_2$O), 2.66 (s, 4H, C*H*$_2$C$_6$H$_4$), 2.31 (s, 6H, C*H*$_3$), 1.78 (broad s, 2H, O*H*); ^{13}C{^{1}H} 135.8 (s, *p* to CH$_2$), 134.7 (s, *i* to CH$_2$), 130.6 (s, *o* to CH$_2$), 129.0 (s, *m* to CH$_2$),[65] 67.2 (s, *C*H$_2$O), 43.4 (s, *C*(CH$_2$)$_4$), 38.9 (s, *C*H$_2$C$_6$H$_4$), 21.2 (s, *C*H$_3$).

IR (cm^{-1}, powder film): 3310 (br), 2862 (w), 1898 (w), 1512 (m), 1450 (w), 1365 (w), 1234 (w), 1080 (w), 1018 (s), 802 (w), 663 (w).

MS (MALDI$^+$, matrix DCTB):[59] 307 ([**M** + Na]$^+$, 100%).

(*p*-tolCH$_2$)$_2$C(CH$_2$OMs)$_2$. A round bottom flask was charged with (*p*-tolCH$_2$)$_2$C(CH$_2$OH)$_2$ (1.0162 g, 3.5759 mmol) and pyridine (2 mL) with stirring. The flask was cooled to 0 °C and MsCl (0.83 mL, 1.23 g, 10.7 mmol) was added dropwise. The cold bath was removed. After 2.5 h, water (5 mL) was added. The mixture was extracted with CH$_2$Cl$_2$ (15 mL). The extract was washed with aqueous HCl (pH = 4, 5 mL), saturated aqueous NaHCO$_3$ (5 mL), and water (5 mL), and then dried (Na$_2$SO$_4$). The solvent was removed by rotary evaporation give a yellow oil. Then CH$_2$Cl$_2$ (20 mL) was added and the solution was stored at 3 °C. The precipitate was collected by

filtration, washed with cold CH_2Cl_2 (10 mL), and dried by oil pump vacuum to give (*p*-tolCH_2)$_2$C(CH_2OMs)$_2$ as a white solid (1.1703 g, 2.165 mmol, 76%), mp 122-124 °C. Anal. Calcd. for $C_{21}H_{28}O_6S_2$ (440.57 g/mol): C, 57.25; H, 6.41. Found: C, 56.61; H, 6.52.

NMR (δ (ppm), $CDCl_3$): ^{1}H 7.10-7.00 (m, 8H, C_6H_4), 3.92 (s, 4H, OCH_2), 2.96 (s, 6H, SCH_3), 2.71 (s, 4H, C$H_2C_6H_5$), 2.26 (s, 6H, $C_6H_5CH_3$); ^{13}C{^{1}H} 136.7 (s, *i* to CH_3), 131.9 and 130.5 (2 s, *i* and *p* to CH_2), 129.2 (s, *o* to CH_3),[65] 69.8 (s, OCH_2), 42.1 (s, *C*(CH_2)$_4$), 37.5 (s, SCH_3 or $CH_2C_6H_5$), 37.2 (s, SCH_3 or $CH_2C_6H_5$), 21.0 (s, $C_6H_5CH_3$).

IR (cm^{-1}, powder film): 3024 (w), 2939 (w), 1635 (w), 1512 (w), 1465 (w), 1350 (s), 1168 (s), 1041 (m), 948 (s), 826 (s), 748 (m), 687 (w).

MS (ESI$^+$):[59] 441 ([**M** + H]$^+$, 40%).

(*p*-tolCH_2)$_2$C(CH_2PPh_2)$_2$ (1f). A Schlenk flask was charged with $KPPh_2$ (7.60 mL, 0.5 M in THF; 4 mmol) with stirring and cooled to 0 °C. A solution of (*p*-tolCH_2)$_2$C(CH_2OMs)$_2$ (0.5962 g, 1.35 mmol) in THF (20 mL) was added. After 48 h, the solvent was removed by oil pump vacuum. All workup steps were conducted under nitrogen. Water (30 mL) and EtOH (3 mL) were added. The mixture was extracted with Et_2O (3 × 30 mL) and the extract was dried ($MgSO_4$). The solvent was removed by oil pump vacuum to give a yellow oil. The oil was layered with MeOH and stored at –35 °C for 3 d. The precipitate was collected by filtration and dried by oil pump vacuum to give **1f** as a white solid (0.5459 g, 0.8794 mmol, 65%), mp 140-143 °C. Anal. Calcd. for $C_{43}H_{42}P_2$ (620.74 g/mol): C, 83.20; H, 6.82. Found: C, 83.20; H, 6.83.

NMR (δ (ppm), $CDCl_3$): ^{1}H 7.34-7.29 (m, 8H, *o* to P), 7.28-7.23 (m, 12H, *m* and *p* to P), 7.07 and 6.99 (2 d, $^3J_{HH}$ = 7.1 Hz, 4H and 4H, *o* or *m* to CH_2), 2.93 (s, 4H,

$C_6H_4CH_2$), 2.31 (s, 6H, CH_3), 2.09 (d, $^2J_{HP}$ = 2.7 Hz, 4H, PCH_2); $^{13}C\{^1H\}$ 140.0 (d, $^2J_{CP}$ = 14.2 Hz, *o* to P), 135.3 (d, $^1J_{CP}$ = 39.7 Hz, *i* to P), 133.1 (d, $^3J_{CP}$ = 16.7 Hz, *m* to P), 131.3, 128.5, 128.4, 128.3, 128.2 (5 s, *p* to P, *o* to CH_2, *i* to CH_2, *m* to CH_2, and *p* to CH_2), 44.0 (t, $^2J_{CP}$ = 6.9 Hz, $C(CH_2)_4$), 43.2 (s, $CH_2C_6H_4$), 36.7 (t, $^1J_{CP}$ = 12.2 Hz, PCH_2),[61] 21.0 (s, CH_3); $^{31}P\{^1H\}$ –26.1 (s).

IR (cm^{-1}, powder film): 1581 (w), 1512 (m), 1481 (w), 1435 (m), 1188 (m), 1072 (w), 825 (w), 794 (w), 740 (s), 695 (s).

MS (MALDI$^+$, matrix DCTB):[59] 636 ([**1f** + O]), 621 ([**1f**]$^+$, 100%).

($Me_2C(CH_2PPh_2)_2$)$PtCl_2$ (2a). A Schlenk flask was charged with *cis/trans*-(*p*-$tol_3P)_2PtCl_2$ (1.0034 g, 1.14 mmol),[44] $Me_2C(CH_2PPh_2)_2$ (**1a**;[46] 0.615 g, 1.23 mmol), and CH_2Cl_2 (20 mL) with stirring. After 24 h, the solvent was removed by rotary evaporation. The residue was washed with Et_2O (100 mL), EtOH (100 mL), and hexanes (100 mL), and dried by oil pump vacuum to give **2a** as a white solid (0.7047 g, 0.9980 mmol, 88%), which slightly darkened at 250 °C and blackened at 375 °C. Anal. Calcd. for $C_{29}H_{30}Cl_2P_2Pt$ (706.08 g/mol): C, 49.30; H, 4.28. Found: C, 47.84; H, 4.34.[66]

NMR (δ (ppm), CD_2Cl_2): ^1H 7.92-7.79 (m, 8H, *o* to P), 7.50-7.37 (m, 12H, *m* and *p* to P), 2.31 (d, $^2J_{HP}$ = 9.7 Hz, 4H, PCH_2), 0.55 (s, 6H, CH_3); $^{13}C\{^1H\}$ 134.7 (virtual t,[63] $^2J_{CP}$ = 5.6 Hz, *o* to P), 131.9 (s, *p* to P), 129.3 (m, *J* = 73.7 Hz, *J* = 7.0 Hz, *i* to P),[60] 129.0 (virtual t,[63] $^3J_{CP}$ = 5.6 Hz, *m* to P), 35.4 (s, $C(CH_3)_2$), 32.3 (t, $^1J_{CP}$ = 8.7 Hz, PCH_2),[61] 30.0 (s, CH_3); $^{31}P\{^1H\}$ –1.3 (s, $^1J_{PPt}$ = 3431 Hz).[67]

IR (cm^{-1}, powder film): 2954 (w), 1481 (m), 1435 (s), 1103 (s), 840 (s), 802 (s), 748 (s), 694 (s).

MS (MALDI$^+$, matrix DCTB):[59] 670 ([**2a** – Cl]$^+$, 60%).

($Et_2C(CH_2PPh_2)_2$)$PtCl_2$ (2b). A Schlenk flask was charged with *cis/trans*-(*p*-$tol_3P)_2PtCl_2$ (1.1272 g, 1.2887 mmol),[44] $Et_2C(CH_2PPh_2)_2$ (**2a**;[46] 0.6308 g, 1.2887 mmol), and CH_2Cl_2 (30 mL) with stirring. After 24 h, the solvent was removed by rotary evaporation. The residue was washed with Et_2O (110 mL), water (20 mL), and hexanes (90 mL), and dried by oil pump vacuum to give **2b** as a white solid (0.6519 g, 0.6887 mmol, 69%), which yellowed at 230 °C, browned at 305 °C, and blackened at 355 °C. Anal. Calcd. for $C_{31}H_{34}Cl_2P_2Pt$ (734.54 g/mol): C, 50.69; H, 4.67 Found: C, 49.38; H, 4.80.[66]

NMR (δ (ppm), $CDCl_3$): ^{1}H 7.86-7.98 (m, 8H, *o* to P), 7.39-7.50 (m, 12H, *m* and *p* to P), 2.35 (d, $^2J_{HP}$ = 9.2 Hz, 4H, PCH_2), 1.05 (q, $^3J_{HH}$ = 6.9 Hz, 4H, CH_2CH$_3$), 0.29 (t, $^3J_{HH}$ = 6.9 Hz, 6H, CH_3); ^{13}C{^{1}H} 134.3 (virtual t,[63] $^2J_{CP}$ = 4.9 Hz, *o* to P), 133.2 (s, *p* to P), 131.2 (m, *J* = 75.3 Hz, *J* = 7.2 Hz, *i* to P),[60] 128.5 (virtual t,[63] $^2J_{CP}$ = 5.5 Hz, *m* to P), 50.1 (s, *C*H$_2$CH$_3$), 35.0 (t, $^1J_{CP}$ = 23.4 Hz, P*C*H$_2$),[61] 31.4 (t, $^2J_{CP}$ = 6.3 Hz, *C*(CH$_2$)$_4$), 6.5 (s, *C*H$_3$); ^{31}P{^{1}H} –2.5 (s, $^1J_{PPt}$ = 3429 Hz).[67]

IR (cm^{-1}, powder film): 1481 (w), 1435 (m), 1103 (m), 817 (w), 740 (m), 717 (w), 694 (s), 555 (m), 523 (m).

MS (MALDI$^+$, matrix DCTB, THAP, or CHCA):[59] 698 ([**2b** – Cl]$^+$, 100%).

(*n*-$Bu_2C(CH_2PPh_2)_2$)$PtCl_2$ (2c). A Schlenk flask was charged with *cis/trans*-(*p*-$tol_3P)_2PtCl_2$ (1.0067 g, 1.1509 mmol),[44] **1c** (0.8073 g, 1.539 mmol), and CH_2Cl_2 (30 mL) with stirring. After 2 d, the solvent was removed by rotary evaporation. The residue was washed with Et_2O (110 mL), water (20 mL), and hexanes (90 mL), and dried by oil pump vacuum to give **2c** as a white solid (0.7975 g, 1.009 mmol, 88%), which yellowed at 160 °C, browned at 250 °C, and liquefied at 295 °C. Anal. Calcd. for $C_{35}H_{42}Cl_2P_2Pt$ (790.65 g/mol): C, 53.17; H, 5.35; Found: C, 52.93; H, 5.31.

NMR (δ (ppm)): ^{1}H ($CDCl_3$) 7.80-7.98 (m, 8H, *o* to P), 7.41-7.50 (m, 12H, *m* and *p* to P), 2.31 (d, $^{2}J_{HP}$ = 9.0 Hz, 4H, PCH_2), 0.82-0.98 (m, 4H, CH_2CH_2CH_2CH_3), 0.59-0.67 (m, 8H, CH_2CH_2CH_3), 0.52 (t, $^{3}J_{HH}$ = 7.0 Hz, 6H, CH_3); ^{13}C{^{1}H} (CD_2Cl_2) 133.9 (virtual t,[63] $^{2}J_{CP}$ = 4.4 Hz, *o* to P), 130.8 (s, *p* to P), 129.0 (m, *J* = 71.3 Hz, *J* = 6.0 Hz, *i* to P),[60] 127.9 (virtual t,[63] $^{3}J_{CP}$ = 5.1 Hz, *m* to P), 40.5 (t, $^{1}J_{CP}$ = 11.8 Hz, P*C*H_2),[61] 39.8 (t, $^{2}J_{CP}$ = 8.3 Hz, *C*$(CH_2)_4$), 28.0 (s, *C*H_2CH_2CH_2CH_3), 24.1 (s, *C*H_2CH_2CH_3), 22.1 (*C*H_2CH_3), 12.9 (s, *C*H_3); ^{31}P{^{1}H} ($CDCl_3$) –2.6 (s, $^{1}J_{PPt}$ = 3419 Hz).[67]

IR (cm^{-1}, powder film): 2931 (m), 2862 (m), 1435 (s), 1102 (s), 995 (m), 817 (m), 748 (s), 725 (s), 694 (s).

MS (MALDI^{+}, matrix DCTB + 1% TFA):[59] 754 ([**2c** – Cl]$^{+}$, 100%).

(*n*-Dec$_2$C(CH$_2$PPh$_2$)$_2$)PtCl$_2$ (2d). A Schlenk flask was charged with *cis/trans*-(*p*-tol$_3$P)$_2$PtCl$_2$ (2.1346 g, 2.4404 mmol),[44] **1d** (1.6891 g, 2.4375 mmol), and CH_2Cl_2 (40 mL) with stirring. After 2 d, the solvent was removed by rotary evaporation. The residue was washed with Et_2O (50 mL), water (50 mL), and hexanes (100 mL), and dried by oil pump vacuum to give **2d** as a white solid (2.1976 g, 2.2917 mmol, 94%), which yellowed at 190 °C and liquefied at 235 °C. Anal. Calcd. for $C_{47}H_{66}Cl_2P_2Pt$ (958.96 g/mol): C, 58.87; H, 6.94; Found: C, 58.90; H, 6.81.

NMR (δ (ppm)): ^{1}H ($CDCl_3$) 8.03-7.86 (m, 8H, *o* to P), 7.53-7.42 (m, 12H, *m* and *p* to P), 2.37 (d, $^{2}J_{HP}$ = 8.3 Hz, 4H, PCH_2), 1.34-0.55 (m, 42H, (CH_2)$_9$CH_3); ^{13}C{^{1}H} (CD_2Cl_2) 134.2 (virtual t,[63] $^{2}J_{CP}$ = 4.4 Hz, *o* to P), 131.1 (s, *p* to P), 129.7 (m, *J* = 70.4 Hz, *J* = 7.3 Hz, *i* to P),[60] 128.4 (virtual t,[63] $^{3}J_{CP}$ = 5.1 Hz, *m* to P), 40.8 (s, *C*H_2), 40.3 (t, $^{2}J_{CP}$ = 7.3 Hz, *C*$(CH_2)_4$), 35.8 (t, $^{1}J_{CP}$ = 20.6 Hz, P*C*H_2),[61] 31.8 (s, *C*H_2),

29.4 (s, CH_2), 29.3 (s, CH_2), 29.2 (s, CH_2), 29.1 (s, CH_2), 22.6 (s, CH_2), 22.4 (s, CH_2), 21.3 (s, CH_2), 14.1 (s, CH_3); $^{31}P\{^1H\}$ ($CDCl_3$) –2.6 (s, $^1J_{PPt}$ = 3417 Hz).[67]

IR (cm^{-1}, powder film): 2942 (s), 2854 (s), 1458 (w), 1435 (s), 1103 (s), 840 (m), 817 (m), 748 (s), 725 (s), 694 (s).

MS (MALDI$^+$, matrix DCTB + 1% TFA):[59] 922 ([**2d** – Cl]$^+$, 100%).

($Bn_2C(CH_2PPh_2)_2$)$PtCl_2$ (2e). A Schlenk flask was charged with *cis/trans*-(*p*-$tol_3P)_2PtCl_2$ (0.2507 g, 0.2866 mmol),[44] $Bn_2C(CH_2PPh_2)_2$ (**1e**;[42] 0.2473 g, 0.4173 mmol), and CH_2Cl_2 (20 mL) with stiring. After 18 h, the solvent was removed by rotary evaporation. The residue was washed with Et_2O (700 mL) and hexanes (200 mL), and dried by oil pump vacuum to give **2e** as a white powder (0.1828 g, 0.2129 mmol, 74%), which yellowed at 225 °C. Anal. Calcd. for $C_{41}H_{38}Cl_2P_2Pt$ (858.68 g/mol): C, 57.35; H, 4.46; Found: C, 57.35; H, 4.57.

NMR (δ (ppm), CD_2Cl_2): ^1H 7.65-7.20 (m, 30H, C_6H_5), 2.61 (s, 4H, $CH_2C_6H_5$), 2.45 (d, $^2J_{HP}$ = 7.9 Hz, 4H, PCH_2); $^{13}C\{^1H\}$ 136.4 (s, *i* to CH_2), 134.5 (virtual t,[63] $^2J_{CP}$ = 4.6 Hz, *o* to P), 131.8 (s, *p* to P), 131.7 (s, *m* to CH_2), 130.1 (m, *J* = 76.0 Hz, *J* = 8.2 Hz, *i* to P),[60] 129.9 (s, *o* to CH_2), 128.9 (virtual t,[63] $^3J_{CP}$ = 4.0 Hz, *m* to P), 127.7 (s, *p* to CH_2), 48.5 (t, $^2J_{CP}$ = 6.4 Hz, $C(CH_2)_4$), 42.7 (s, $CH_2C_6H_5$), 31.3 (t, $^1J_{CP}$ = 25.4 Hz, PCH_2);[61] $^{31}P\{^1H\}$ –2.0 ($^1J_{PPt}$ = 3376 Hz).[67]

IR (ATR, cm^{-1}): 3024 (w), 2361 (s), 2160 (m), 1435 (s), 1096 (s), 694 (s), 493 (s).

MS (MALDI$^+$, matrix DCTB):[59] 822 ([**2e** – Cl]$^+$, 100%).

((*p*-tolCH_2)$_2C(CH_2PPh_2)_2$)$PtCl_2$ (2f). A Schlenk flask was charged with *cis/trans*-(*p*-$tol_3P)_2PtCl_2$ (0.5224 g, 0.5972 mmol),[44] **1f** (0.5183 g, 0.8350 mmol), and

CH_2Cl_2 (40 mL) with stirring. After 3 d, the solvent was removed by rotary evaporation. The residue was washed with Et_2O (700 mL) and dried by oil pump vacuum to give **2f** as a white solid (0.4511 g, 0.5087 mmol, 85%), which yellowed at 275 °C. Anal. Calcd. for $C_{43}H_{42}Cl_2P_2Pt$ (886.73 g/mol): C, 58.24; H, 4.77; Found: C, 56.08; H, 4.77.[66]

NMR (δ (ppm), CD_2Cl_2): ^{1}H 7.62-7.55 (m, 8H, *o* to P), 7.49-7.33 (m, 8H, *m* and *p* to P), 7.09 and 6.78 (2 d, $^3J_{HH}$ = 8.0 Hz, 4H and 4H, C_6H_4), 2.56 (s, 4H, $CH_2C_6H_4CH_3$), 2.42 (d, $^2J_{HP}$ = 8.0 Hz, 4H, PCH_2), 2.34 (s, 6H, CH_3); $^{13}C\{^1H\}$ 136.9 (s, *p* to P), 133.9 (virtual t,[63] $^2J_{CP}$ = 5.0, *o* to P), 132.7 (s, *m* to CH_2), 131.1 (s, *i* to CH_2), 131.0 (s, *o* to CH_2), 129.6 (m, *J* = 70.1 Hz, *J* = 6.9 Hz, *i* to P),[60] 129.1 (s, *p* to CH_2), 128.3 (virtual t,[63] $^3J_{CP}$ = 6.2 Hz, *m* to P), 47.5 (t, $^2J_{CP}$ = 6.0 Hz, $C(CH_2)_4$), 42.1 (s, $CH_2C_6H_4$), 30.3 (t, $^1J_{CP}$ = 21.0 Hz, PCH_2),[61] 20.7 (s, CH_3); $^{31}P\{^1H\}$ –2.0 ($^1J_{PPt}$ = 3386 Hz).[67]

IR (cm^{-1}, powder film): 3047 (w), 2361 (s), 1512 (w), 1435 (s), 794 (s), 733 (s), 602 (s).

MS (MALDI$^+$, matrix DCTB):[59] 850 ([**2f** – Cl]$^+$, 100%).

$(Me_2C(CH_2PPh_2)_2)Pt((C{\equiv}C)_2H)_2$ (3a). A: A Schlenk flask was charged with *trans*-$(p\text{-}tol_3P)_2Pt((C{\equiv}C)_2H)_2$ (0.4115 g, 0.4563 mmol),[45] **1a** (0.2339 g, 0.4562 mmol), and CH_2Cl_2 (20 mL) with stirring. After 48 h, the solvent was removed and the residue was chromatographed on a silica gel column (30 × 4.5 cm) eluted with 1:1 v/v CH_2Cl_2/hexanes. The solvents were removed from the product containing fractions by oil pump vacuum to give **3a** as an off-white solid (0.3158 g, 0.3919 mmol, 81%).

B: A Schlenk flask was charged with **2a** (0.5445 g, 0.6993 mmol), CuI (0.0371 g, 0.1948 mmol), and $HNEt_2$ (30 mL) with stirring and cooled to –42 °C (CO_2/acetonitrile). Then butadiyne (1.7731 g, 35.46 mmol in 44 mL THF)[68] was added.

After 30 min, the cold bath was removed. After 3 h, the solvents were removed and the residue was chromatographed on a silica gel column (30 × 4.5 cm) eluted with 1:1 v/v CH_2Cl_2/hexanes. The solvents were removed from the product containing fractions by oil pump vacuum to give **3a** as an off-white solid (0.3946 g, 0.4897 mmol, 70%), which yellowed at 135 °C and blackened at 165 °C. Anal. Calcd. for $C_{37}H_{32}P_2Pt$ (733.68 g/mol): C, 60.57; H, 4.40. Found: C, 60.30; H, 4.63.

NMR (δ (ppm), $CDCl_3$): ^{1}H 7.85-7.75 (m, 8H, *o* to P), 7.50-7.37 (m, 12H, *m* and *p* to P), 2.33 (d, $^2J_{HP}$ = 10 Hz, 4H, PCH_2), 1.64 (s, 2H, ≡C*H*), 0.73 (s, 6H, CH_3); ^{13}C{^{1}H} 133.9 (virtual t,[63] $^2J_{CP}$ = 5.2 Hz, *o* to P), 131.4 (s, *p* to P), 130.9 (m, *J* = 68.8 Hz, *J* = 8.2 Hz, *i* to P),[60] 128.5 (virtual t,[63] $^2J_{CP}$ = 6.4 Hz, *m* to P), 95.4 (dd, $^2J_{CP}$ = 146.6 Hz, $^2J_{CP}$ = 18.2 Hz, Pt*C*≡C), 91.9 (m, *J* = 18.4 Hz, PtC≡*C*),[69] 71.7 (s, *C*≡CH), 61.6 (s, ≡*C*H), 37.3 (t, $^1J_{CP}$ = 18.9 Hz, P*C*H$_2$),[61] 33.1 (t, $^2J_{CP}$ = 8.3 Hz, *C*(CH$_2$)$_4$), 21.4 (s, *C*H$_3$); ^{31}P{^{1}H} –4.9 (s, $^1J_{PPt}$ = 2224 Hz).[67]

IR (cm^{-1}, powder film): 3299 (s), 2960 (s), 2922 (s), 2146 (s, $\nu_{C\equiv C}$), 1918 (m).

MS (MALDI$^+$, matrix THAP):[59] 772 ([**3a** + K]$^+$, 30%), 756 ([**3a** + Na]$^+$, 100%), 734 ([**3a** + H]$^+$, 90%).

($Et_2C(CH_2PPh_2)_2$)Pt($(C\equiv C)_2H)_2$ (3b). A: A Schlenk flask was charged with *trans*-(*p*-tol$_3$P)$_2$Pt($(C\equiv C)_2H)_2$ (1.0366 g, 1.1493 mmol),[45] **1b** (05347 g, 1.1411 mmol), and CH_2Cl_2 (100 mL) with stirring. After 48 h, the solvent was removed and the residue was chromatographed on a silica gel column (30 × 4.5 cm) eluted with 1:1 v/v CH_2Cl_2/hexanes. The solvents were removed from the product containing fractions by oil pump vacuum to give **3b** as an off-white solid (0.6088 g, 0.7992 mmol, 70%).

B: A Schlenk flask was charged with **2b** (0.3059 g, 0.4165 g), CuI (00223 g, 0.1171 mmol), and $HNEt_2$ (13 mL) with stirring and cooled to –42 °C

(CO_2/acetonitrile). Then butadiyne (0.5806 g, 11.61 mmol in 13.4 mL THF)[68] was added. After 30 min, the cold bath was removed. After 3 h, the solvents were removed and the residue was chromatographed on a silica gel column (30 × 4.5 cm) eluted with 1:1 v/v CH_2Cl_2/hexanes. The solvents were removed from the product containing fractions by oil pump vacuum to give **3b** as an off-white solid (0.2760 g, 0.3624 mmol, 87%), which yellowed at 114 °C, darkened at 127 °C, and blackened at 142 °C. Anal. Calcd. for $C_{39}H_{36}P_2Pt$ (761.73 g/mol): C, 61.49; H, 4.76; Found: C, 61.19; H, 4.71.

NMR (δ (ppm), $CDCl_3$): ^{1}H 7.89-7.74 (m, 8H, *o* to P), 7.49-7.37 (m, 12H, *m* and *p* to P), 2.32 (d, $^2J_{HP}$ = 7.0 Hz, 4H, PCH_2), 1.63 (s, 2H, ≡C*H*), 1.14 (q, $^3J_{HH}$ = 7.4 Hz, 4H, CH_2CH$_3$), 0.33 (t, $^3J_{HH}$ = 7.4 Hz, 6H, CH_3); ^{13}C{^{1}H} 134.1 (virtual t,[63] $^2J_{CP}$ = 6.0 Hz, *o* to P), 131.5 (m, *J* = 68.3 Hz, *J* = 8.9 Hz, *i* to P),[60] 130.8 (s, *p* to P), 128.5 (virtual t,[63] $^2J_{CP}$ = 5.5 Hz, *m* to P), 95.7 (dd, $^2J_{CP}$ = 149.0 Hz, $^2J_{CP}$ = 20.0 Hz, Pt*C*≡C), 91.7 (m, *J* = 17.8 Hz, PtC≡*C*),[69] 71.8 (s, *C*≡CH), 61.3 (s, ≡*C*H), 41.5 (s, *C*H$_2$CH$_3$), 33.8 (t, $^1J_{CP}$ = 18.8 Hz, P*C*H$_2$),[61] 32.4 (t, $^2J_{CP}$ = 8.6 Hz, *C*(CH$_2$)$_4$), 6.7 (s, *C*H$_3$); ^{31}P{^{1}H} –5.6 (s, $^1J_{PPt}$ = 2257 Hz).[67]

IR (cm^{-1}, powder film): 3047 (m), 2962 (m), 2191 (m, $\nu_{C\equiv C}$), 1435 (s), 1381 (m), 1095 (s), 925 (m), 825 (m), 740 (s).

MS (MALDI$^+$, matrix CHCA):[59] 784 ([**3b** + Na]$^+$, 50%), 762 ([**3b** + H]$^+$, 50%), 712 ([**3b** – (C≡C)$_2$H]$^+$, 50%).

(*n*-Bu$_2$C(CH$_2$PPh$_2$)$_2$)Pt((C≡C)$_2$H)$_2$ (3c). A: A Schlenk flask was charged with *trans*-(*p*-tol$_3$P)$_2$Pt((C≡C)$_2$H)$_2$ (0.4498 g, 0.4987 mmol),[45] **1a** (0.2676 g, 0.5101 mmol), and CH_2Cl_2 (60 mL) with stirring. After 48 h, the solvent was removed and the residue was chromatographed on a silica gel column (30 × 4.5 cm) eluted with 1:1 v/v

CH_2Cl_2/hexanes. The solvents were removed from the product containing fractions by oil pump vacuum to give **3c** as an off-white solid (0.3936 g, 0.4813 mmol, 97%).

B: A Schlenk flask was charged with **2c** (0.4965 g, 0.6280 mmol), CuI (0.0362g, 0.190 mmol), and $HNEt_2$ (20 mL) with stirring and cooled to –42 °C (CO_2/acetonitrile). Then butadiyne (0.0362g, 0.190 mmol in 5.2 mL THF)[68] was added. After 30 min, the cold bath was removed. After 3 h, the solvents were removed and the residue was chromatographed on a silica gel column (30 × 4.5 cm) eluted with 1:1 v/v CH_2Cl_2/hexanes. The solvents were removed from the product containing fractions by oil pump vacuum to give **3c** as an off-white solid (0.3507 g, 0.4291 mmol, 68%), which yellowed at 129 °C and blackened at 139 °C. Anal. Calcd. for $C_{43}H_{44}P_2Pt$ (817.84 g/mol): C, 63.15; H, 5.42; Found: C, 63.17; H, 5.43.

NMR (δ (ppm), $CDCl_3$): ^{1}H 7.75-7.88 (m, 8H, *o* to P), 7.37-7.47 (m, 12H, *m* and *p* to P), 2.29 (d, $^1J_{HP}$ = 7.2 Hz, 4H, PCH_2), 1.56 (s, 2H, ≡C*H*), 1.05-0.95 (m, 4H, CH_2CH$_2$CH$_2$CH$_3$), 0.76-0.67 (m, 8H, CH_2CH_2CH$_3$), 0.52 (t, $^3J_{HH}$ = 7.3 Hz, 6H, CH_3); ^{13}C{^{1}H} 134.1 (virtual t,[63] $^2J_{CP}$ = 5.7 Hz, *o* to P), 130.9 (s, *p* to P), 129.2 (m, *J* = 68.2 Hz, *J* = 8.7 Hz, *i* to P),[60] 128.5 (virtual t,[63] $^3J_{CP}$ = 5.4 Hz, *m* to P), 96.1 (dd, $^2J_{CP}$ = 148.0 Hz, $^2J_{CP}$ = 19.2 Hz, PtC≡C), 91.6 (m, *J* = 18.2 Hz, PtC≡*C*),[69] 72.0 (s, *C*≡CH), 61.2 (s, ≡*C*H), 40.6 (t, $^2J_{CP}$ = 6.8 Hz, *C*(CH$_2$)$_4$), 34.9 (t, $^1J_{CP}$ = 19.0 Hz, P*C*H$_2$),[61] 24.7 (s, *C*H$_2$CH$_2$CH$_2$CH$_3$), 22.7 (s, *C*H$_2$CH$_2$CH$_3$), 22.1 (*C*H$_2$CH$_3$), 13.7 (s, *C*H$_3$); ^{31}P{^{1}H} –6.4 (s, $^1J_{PPt}$ = 2225 Hz).[67]

IR (cm^{-1}, powder film): 2931 (s), 2862 (s), 2152 (s, $\nu_{C\equiv C}$), 1435 (m), 1103 (m), 810 (m), 725 (s), 692 (s), 563 (s).

MS (MALDI$^+$, matrix DCTB + 1% TFA):[59] 856 ([**3c** + K]$^+$, 100%).

(*n*-Dec$_2$C(CH$_2$PPh$_2$)$_2$)Pt((C≡C)$_2$H)$_2$ (3d). A: A Schlenk flask was charged with *trans*-(*p*-tol$_3$P)$_2$Pt((C≡C)$_2$H)$_2$ (1.0782 g, 1.1950 mmol),[45] **1d** (0.8303 g, 1.198 mmol), and CH_2Cl_2 (100 mL) with stirring. After 48 h, the solvent was removed and the residue was chromatographed on a silica gel column (30 × 4.5 cm) eluted with 1:1 v/v CH_2Cl_2/hexanes. The solvents were removed from the product containing fractions by oil pump vacuum to give **3d** as an off-white solid (0.6305 g, 0.6393 mmol, 54%).

B: A Schlenk flask was charged with **2d** (0.6333 g, 0.6601 mmol), CuI (0.01856 g, 0.1848 mmol), THF (50 mL), and $HNEt_2$ (50 mL) with stirring and cooled to –45 °C (acetonitrile/CO_2). Then butadiyne (1.3202 g, 26.404 mmol in 16 mL THF)[68] was added. After 1 h, the cold bath was removed. After 4 h, the solvents were removed and the residue was chromatographed on a silica gel column (30 × 4.5 cm) eluted with 1:1 v/v CH_2Cl_2/hexanes. The solvents were removed from the product containing fractions by oil pump vacuum to give **3d** as an off-white solid (0.4262 g, 0.4322 mmol, 65%), which liquefied at 120 °C and blackened at 140 °C. Anal. Calcd. for $C_{55}H_{68}P_2Pt$ (986.16 g/mol): C, 66.99; H, 6.95; Found: C, 66.89; H, 7.02.

NMR (δ (ppm)): ^{1}H ($CDCl_3$) 7.82-7.71 (m, 8H, *o* to P), 7.44-7.35 (m, 12H, *m* and *p* to P), 2.30 (d, $^1J_{HP}$ = 9.1 Hz, 4H, PC*H*$_2$), 1.55 (s, 2H, ≡C*H*), 1.21-0.87 (m, 46H, (C*H*$_2$)$_9$C*H*$_3$); ^{13}C{^{1}H} (CD_2Cl_2) 134.0 (virtual t,[63] $^2J_{CP}$ = 5.8 Hz, *o* to P), 131.4 (m, *J* = 68.5 Hz, *J* = 9.0 Hz, *i* to P),[60] 130.7 (s, *p* to P), 128.3 (virtual t,[63] $^3J_{CP}$ = 5.3 Hz, *m* to P), 95.8 (dd, $^2J_{CP}$ = 147.2 Hz, $^2J_{CP}$ = 19.0 Hz, Pt*C*≡C), 91.5 (m, *J* = 17.9 Hz, PtC≡*C*),[69] 71.8 (s, *C*≡CH), 61.1 (s, ≡*C*H), 41.1 (s, *C*H$_2$), 40.5 (t, $^2J_{CP}$ = 7.1 Hz, *C*(CH$_2$)$_4$), 34.6 (t, $^1J_{CP}$ = 18.2 Hz, P*C*H$_2$),[61] 31.8 (s, *C*H$_2$), 29.5 (s, *C*H$_2$), 29.4 (s, *C*H$_2$), 29.2 (s, *C*H$_2$), 29.1 (s, *C*H$_2$), 22.6 (s, *C*H$_2$), 22.5 (s, *C*H$_2$), 21.3 (s, *C*H$_2$), 14.0 (s, *C*H$_3$); ^{31}P{^{1}H} ($CDCl_3$) –6.6 (s, $^1J_{PPt}$ = 2221 Hz).[67]

IR (cm^{-1}, powder film): 3294 (m), 2924 (s), 2854 (s), 2152 (s, $\nu_{C\equiv C}$), 1458 (m), 1435 (s), 1103 (s), 825 (m), 810 (m), 725 (s), 695 (s).

MS ($MALDI^+$, matrix DCTB + 1% TFA):[59] 1048 ([**3d** + Cu]$^+$, 100%).

$(Bn_2C(CH_2PPh_2)_2)Pt((C\equiv C)_2H)_2$ (3e). A Schlenk flask was charged with *trans*-$(p\text{-}tol_3P)_2Pt((C\equiv C)_2H)_2$ (0.2016 g, 0.3401 mmol),[45] **1e** (0.2793 g, 0.4712 mmol), and CH_2Cl_2 (20 mL) with stirring. After 48 h, the solvent was removed and the residue was chromatographed on a silica gel column (30 × 4.5 cm) eluted with 1:1 v/v CH_2Cl_2/hexanes. The solvents were removed from the product containing fractions by oil pump vacuum to give **3e** as an off-white solid (0.1745 g, 0.1970 mmol, 58%), which yellowed at 124 °C, blackened at 141 °C and liquefied at 248 °C. Anal. Calcd. for $C_{49}H_{40}P_2Pt$ (885.87 g/mol): C, 66.43; H, 4.55; Found: C, 64.30; H, 4.84.[66]

NMR (δ (ppm), $CDCl_3$): ^{1}H 7.47-7.90 (m, 30H, C_6H_5), 2.72 (s, 4H, $CH_2C_6H_5$), 2.36 (d, $^1J_{HP}$ = 6.6 Hz, 4H, PCH_2), 1.70 (s, 2H, ≡C*H*); $^{13}C\{^1H\}$ 136.4 (s, *i* to CH_2), 133.7 (virtual t,[63] $^2J_{CP}$ = 5.6 Hz, *o* to P), 131.7 (s, *p* to P), 130.9 (m, *J* = 86.7 Hz, *J* = 10.2 Hz, *i* to P),[60] 130.8 (s, *m* to CH_2), 129.6 (s, *o* to CH_2), 128.6 (s, *m* to P),[65] 127.2 (s, *p* to CH_2), 91.6 (dd, $^2J_{CP}$ = 145.6 Hz, $^2J_{CP}$ = 22.1 Hz, Pt*C*≡C), 92.8 (m, *J* = 18.1 Hz, PtC≡*C*),[69] 71.8 (s, *C*≡CH), 61.9 (s, ≡*C*H), 48.9 (t, $^2J_{CP}$ = 6.7 Hz, $C(CH_2)_4$), 42.7 (s, $CH_2C_6H_5$), 28.9 (t, $^1J_{CP}$ = 18.1 Hz, PCH_2);[61] $^{31}P\{^1H\}$ −3.5 ($^1J_{PPt}$ = 2204 Hz).[67]

IR (cm^{-1}, powder film): 3294 (m), 2152 (s, $\nu_{C\equiv C}$), 2090 (w), 1485 (m), 1435 (s), 1095 (s), 810 (w), 740 (s), 694 (s).

MS ($MALDI^+$, matrix DCTB):[59] 976 ([**3e** + Cu]$^+$, 60%).

$((p\text{-}tolCH_2)_2C(CH_2PPh_2)_2)Pt((C\equiv C)_2H)_2$ (3f). A Schlenk flask was charged with *trans*-$(p\text{-}tol_3P)_2Pt((C\equiv C)_2H)_2$ (0.3259 g, 0.5250 mmol),[45] **1f** (0.4299 g, 0.4766 mmol), and CH_2Cl_2 (40 mL) with stirring. After 48 h, the solvent was removed and the

residue was chromatographed on a silica gel column (30 × 4.5 cm) eluted with 1:1 v/v CH_2Cl_2/hexanes. The solvents were removed from the product containing fractions by oil pump vacuum to give **3f** as an off-white solid (0.3346 g, 0.3661 mmol, 70%), which yellowed at 124 °C, blackened at 143 °C and liquefied at 248 °C. Anal. Calcd. for $C_{51}H_{44}P_2Pt$ (913.93 g/mol): C, 67.02; H, 4.85; Found: C, 67.03; H, 4.90.

NMR (δ (ppm), $CDCl_3$): ^{1}H 7.43-7.36 (m, 8H, *o* to P), 7.34-7.18 (m, 12H, *m* and *p* to P), 7.14 and 6.96 (2 d, 4H and 4H, $^3J_{HH}$ = 7.3 Hz, C_6H_4), 2.68 (4H, s, $CH_2C_6H_4$), 2.44-2.35 (m, 10H, CH_3 and PCH_2), 1.72 (s, 2H, ≡C*H*); ^{13}C{^{1}H} 137.0 (s, *m* to CH_2), 133.8 (virtual t,[63] $^2J_{CP}$ = 6.2 Hz, *o* to P), 133.3 (s, *p* to P), 131.6 (s, *i* to CH_2), 131.6, (m, *J* = 69.9 Hz, *J* = 10.0 Hz, *i* to P),[60] 131.3 (s, *o* to CH_2), 130.8 (s, *p* to CH_2), 128.5 (virtual t,[63] $^3J_{CP}$ = 5.0 Hz, *m* to P), 96.3 (dd, $^2J_{CP}$ = 146.4 Hz, $^2J_{CP}$ = 19.4 Hz, PtC≡C), 92.7 (m, *J* = 18.4 Hz, PtC≡*C*),[69] 71.9 (s, PtC≡C*C*), 61.9 (s, ≡*C*H), 48.5 (t, $^2J_{CP}$ = 6.1 Hz, *C*$(CH_2)_4$), 42.7 (s, *C*$H_2C_6H_4$), 28.8 (t, $^2J_{CP}$ = 19.7 Hz, P*C*H_2),[61] 21.2 (s, *C*H_3); ^{31}P{^{1}H} −3.3 ($^1J_{PPt}$ = 2196 Hz).[67]

IR (cm^{-1}, powder film): 3045 (w), 2908 (w), 2152 (s, $\nu_{C\equiv C}$), 1512 (w), 1481 (w), 1435 (s), 1095 (s), 802 (s), 799 (m), 740 (s), 686 (s).

MS (MALDI$^+$, matrix THAP):[59] 952 ([**3f** + K]$^+$, 30%), 936 ([**3f** + Na]$^+$, 90%), 914 ([**3f** + H]$^+$, 100%).

[$(Me_2C(CH_2PPh_2)_2)Pt(C\equiv C)_2]_4$ (4a). A Schlenk flask was charged with **2a** (0.2915 g, 0.4126 mmol), **3a** (0.3039 g, 0.4142 mmol), THF (150 mL), $HNEt_2$ (60 mL), and CuI (0.0079 g, 0.41 mmol) with stirring and heated to 55 °C. After 3 d, the solvents were removed by rotary evaporation. Then water (150 mL) was added. The mixture was extracted with CH_2Cl_2 (3 × 100 mL). The extracts were dried ($MgSO_4$). The solvent was

removed by oil pump vacuum to give **4a** as a cream colored solid (0.5001 g, 0.1829 mmol, 89%), which darkened at 160 °C and blackened at 187 °C.

NMR (δ (ppm), $CDCl_3$): ^{1}H 7.69-7.56 (m, 32H, *m* to P), 7.25-7.18 (m, 16H, *p* to P), 7.12-7.01 (m, 32H, *o* to P), 2.21 (d, $^2J_{HP}$ = 8.2 Hz, 16H, PCH_2), 0.69 (s, 24H, CH_3); ^{13}C{^{1}H} 133.8 (virtual t,[63] $^2J_{CP}$ = 5.6 Hz, *o* to P), 132.5 (m, *J* = 71.1 Hz, *J* = 6.9 Hz, *i* to P),[60] 130.0 (s, *p* to P), 128.0 (virtual t,[63] $^3J_{CP}$ = 5.8 Hz, *m* to P), 96.9 (m, *J* = 16.9 Hz, PtC≡*C*),[69] 91.8 (dd, $^2J_{CP}$ = 141.1 Hz, $^2J_{CP}$ = 21.1 Hz, Pt*C*≡C), 37.8 (t, $^2J_{CP}$ = 7.1 Hz, *C*$(CH_2)_4$), 35.7 (t, $^1J_{CP}$ = 18.4 Hz, P*C*H_2),[61] 32.6 (s, *C*H_3); ^{31}P{^{1}H} –6.1 (s, $^1J_{PPt}$ = 2219 Hz).[67]

IR (cm^{-1}, powder film): 3047 (w), 2955 (w), 2150 (w, $\nu_{C\equiv C}$), 1550 (m), 1433 (s), 1261 (w), 1150 (s), 833 (m), 806 (s).

MS (MALDI$^+$, matrix DCTB):[59] 2795 ([**4a** + Cu]$^+$, 100%), 2771 ([**4a** + K]$^+$, 70%), 2733 ([**4a** + H]$^+$, 40%).

[$(Et_2C(CH_2PPh_2)_2)Pt(C\equiv C)_2]_4$ (4b). A Schlenk flask was charged with **2b** (0.2475 g, 0.3370 mmol), **3b** (0.2565 g, 0.3367 mmol), THF (150 mL), $HNEt_2$ (60 mL), and CuI (0.0115 g, 0.0604 mmol) with stirring and heated to 55 °C. After 3 d, the solvents were removed by rotary evaporation. Then water (20 mL) was added. The mixture was extracted with CH_2Cl_2 (50 mL). The extract was dried ($MgSO_4$). The solvent was removed by rotary evaporation. The residue was washed with THF (10 mL) and dried by oil pump vacuum to give **4b** as a tan solid (0.8201 g, 0.2881 mmol, 52%), which yellowed at 140 °C, browned at 174 °C, blackened at 197 °C, and liquefied at 263 °C.

NMR (δ (ppm), $CDCl_3$): ^{1}H 7.69-7.56 (m, 32H, *m* to P), 7.22-7.16 (m, 16H, *p* to P), 7.11-7.00 (m, 32H, *o* to P), 2.20 (d, $^2J_{HP}$ = 9.9 Hz, 16H, PCH_2), 1.09 (q, $^3J_{HH}$ = 7.1

Hz, 16H, CH_2CH$_3$), 0.21 (t, $^3J_{HH}$ = 7.2 Hz, 24H, CH_3); ^{13}C{^{1}H} 134.0 (virtual t,[63] $^2J_{CP}$ = 6.2 Hz, *o* to P), 132.7 (m, *J* = 71.1 Hz, *J* = 6.8 Hz, *i* to P),[60] 130.0 (s, *p* to P), 128.1 (virtual t,[63] $^3J_{CP}$ = 6.2 Hz, *m* to P), 96.8 (m, *J* = 21.0 Hz, PtC≡*C*),[69] 91.4 (dd, $^2J_{CP}$ = 144.9 Hz, $^2J_{CP}$ = 19.9 Hz, Pt*C*≡C), 41.4 (s, *C*H$_2$CH$_3$), 34.5 (t, $^1J_{CP}$ = 17.6 Hz, P*C*H$_2$),[61] 31.6 (t, $^2J_{CP}$ = 6.4 Hz, *C*(CH$_2$)$_4$), 6.5 (s, *C*H$_3$); ^{31}P{^{1}H} –7.7 (s, $^1J_{PPt}$ = 2243 Hz).[67]

IR (cm^{-1}, powder film): 3047 (m), 2962 (w), 2191 (m, $\nu_{C\equiv C}$), 1435 (s), 1095 (s), 925 (m), 825 (m), 740 (s), 694 (s).

MS (MALDI$^+$, matrix DCTB, THAP, or CHCA):[59] 2907 ([**4b** + Cu]$^+$, 100%), 2883 ([**4b** + K]$^+$, 20%), 2845 ([**4b** + H]$^+$, 70%).

[(*n*-Bu$_2$C(CH$_2$PPh$_2$)$_2$)Pt(C≡C)$_2$]$_4$ (4c). A Schlenk flask was charged with **2c** (0.2565 g, 0.3422 mmol), **3c** (0.2661 g, 0.3254 mmol), THF (150 mL), HNEt$_2$ (60 mL), and CuI (0.09 g, 0.047 mmol) with stirring and heated to 55 °C. After 3 d, the solvents were removed by rotary evaporation. Then water (20 mL) was added. The mixture was extracted with CH_2Cl_2 (3 × 20 mL). The extracts were dried ($MgSO_4$) and the solvent was removed by rotary evaporation. The solid was washed with hexanes (20 mL) and MeOH (20 mL) and dried by oil pump vacuum to give **4c** as a tan solid (0.0516 g, 0.0168 mmol, 40%), which darkened at 132 °C and blackened at 169 °C.

NMR (δ (ppm), $CDCl_3$): ^{1}H 7.70-7.61 (m, 32H, *m* to P), 7.23-7.17 (m, 16H, *p* to P), 7.06-7.00 (m, 32H, *o* to P), 2.24 (d, $^2J_{HP}$ = 9.5 Hz, 16H, PCH_2), 1.39-1.30 (m, 16H, CH_2CH$_2$CH$_2$CH$_3$), 1.00-0.91 (m, 16H, CH_2CH$_2$CH$_3$), 0.74-0.66 (m, 16H, CH_2CH$_3$), 0.60-0.49 (m, 24H, CH_3); ^{13}C{^{1}H} 134.6 (virtual t,[63] $^2J_{CP}$ = 8.4 Hz, *o* to P), 132.4 (m, *J* = 69.9 Hz, *J* = 6.9 Hz, *i* to P),[60] 130.3 (s, *p* to P), 128.2 (virtual t,[63] $^3J_{CP}$ = 6.1 Hz, *m* to P), 105.2 (s, PtC≡*C*),[70] 96.9 (s, Pt*C*≡C),[70] 40.8 (t, $^2J_{CP}$ = 7.0 Hz, *C*(CH$_2$)$_4$), 35.4 (t,

$^1J_{CP}$ = 18.0 Hz, P*C*H_2),[61] 25.1, (s, *C*H_2CH$_2$CH$_2$CH$_3$), 22.8 (s, *C*H_2CH$_2$CH$_2$CH$_3$), 13.8 (s, *C*H_2CH$_3$), 12.0 (s, *C*H_3); ^{31}P{^{1}H} –8.5 (s, $^1J_{PPt}$ = 2247 Hz).[67]

IR (cm^{-1}, powder film): 2931 (m), 2862 (m), 2160 (m, $\nu_{C\equiv C}$), 2098 (m, $\nu_{C\equiv C}$), 1620 (m), 1435 (s), 1095 (s), 995 (m), 810 (m), 725 (s).

MS (MALDI$^+$, matrix DCTB):[59] 3107 ([**4c** + K]$^+$, 100%).

[(*n*-Dec$_2$C(CH$_2$PPh$_2$)$_2$)Pt(C≡C)$_2$]$_4$ (4d). A Schlenk flask was charged with **2d** (0.3984 g, 0.4155 mmol), **3d** (0.4071 g, 0.4128 mmol), CuI (0.0117 g, 0.1163 mmol), HNEt$_2$ (60 mL), and THF (200 mL) with stirring and heated to 55 °C. After 2 d, the solvents were removed by rotary evaporation. Then water was added and the mixture was extracted with CH_2Cl_2 (3 × 30 mL). The extracts were dried ($MgSO_4$). The solvent was removed by oil pump vacuum to give **4d** as a tan solid (0.2627 g, 0.0702 mmol, 69%), which darkened at 125 °C and liquefied at 135 °C.

NMR (δ (ppm), $CDCl_3$): ^{1}H 7.72-7.65 (m, 32H, *m* to P), 7.20-7.14 (m, 16H, *p* to P), 7.10-7.03 (m, 32H, *o* to P), 2.23 (d, $^1J_{HP}$ = 7.0 Hz, 16H, PC*H*$_2$), 1.33-0.50 (m, 168H, (C*H*$_2$)$_9$C*H*$_3$); ^{13}C{^{1}H} 134.1 (virtual t,[63] $^2J_{CP}$ = 5.6 Hz, *o* to P), 132.6 (m, *J* = 69.0 Hz, *J* = 8.7 Hz, *i* to P),[60] 130.0 (s, *p* to P), 128.0 (virtual t,[63] $^3J_{CP}$ = 5.3 Hz, *m* to P), 96.5 (m, *J* = 15.1 Hz, PtC≡*C*),[69] 91.3 (dd, $^2J_{CP}$ = 146.1 Hz, $^2J_{CP}$ = 20.1 Hz, Pt*C*≡C), 41.0 (s, *C*H$_2$), 40.5 (t, $^2J_{CP}$ = 6.8 Hz, *C*(CH$_2$)$_4$), 35.2 (t, $^1J_{CP}$ = 19.9 Hz, P*C*H$_2$),[61] 31.9 (s, *C*H$_2$), 29.6 (s, *C*H$_2$), 29.5 (s, *C*H$_2$), 29.3 (s, *C*H$_2$), 29.2 (s, *C*H$_2$), 22.7 (s, *C*H$_2$), 22.6 (s, *C*H$_2$), 21.5 (s, *C*H$_2$), 14.1 (s, *C*H$_3$); ^{31}P{^{1}H} –8.6 (s, $^1J_{PPt}$ = 2240 Hz).[67]

IR (cm^{-1}, powder film): 2924 (s), 2854 (s), 2160 (m, $\nu_{C\equiv C}$), 1458 (m), 1435 (s), 1257 (s), 1095 (s), 1018 (s), 802 (s), 725 (s), 694 (s).

MS (MALDI$^+$, matrix DCTB, THAP, or CHCA):[59] 3804 ([**4d** + Cu]$^+$, 100%), 3742 ([**4d** + H]$^+$, 30%).

[($Bn_2C(CH_2PPh_2)_2$)$Pt(C{\equiv}C)_2$]$_4$ (4e). A Schlenk flask was charged with **2e** (0.0513 g, 0.05974 mmol), **3e** (0.0529 g, 0.05972 mmol), CuI (0.0040 g, 0.021 mmol), $HNEt_2$ (10 mL), and THF (25 mL) and heated to 55 °C. After 2 d, the solvents were removed by rotary evaporation. Then water (30 mL) was added and the mixture was extracted with CH_2Cl_2 (3 × 20 mL). The extracts were dried ($MgSO_4$). The solvent was removed by rotary evaporation to give **4e** as a tan solid (0.0809 g, 0.0242 mmol, 81%), %), which darkened at 169 °C and blackened at 190 °C.

NMR (δ (ppm), $CDCl_3$): ^{1}H 7.36-7.16 (m, 64H, *o* and *m* to P), 7.14-7.10 (m, 16H, *o* to CH_2), 7.08-7.03 (m, 8H, *p* to CH_2), 6.99-6.90 (m, 32H, *p* to P and *m* to CH_2), 2.57 (s, 16H, C*H*$_2$C$_6$H$_5$), 2.27 (d, $^1J_{HP}$ = 6.9 Hz, 16H, PC*H*$_2$); ^{13}C{^{1}H} 136.4 (s, *i* to CH_2), 133.7 (virtual t,[63] $^2J_{CP}$ = 6.8 Hz, *o* to P), 132.1 (m, *J* = 68.9 Hz, *J* = 19.4 Hz, *i* to P),[60] 131.2 (s, *p* to P), 130.2 (s, *m* to CH_2), 128.9 (s, *o* to CH_2), 128.8 (virtual t,[63] $^2J_{CP}$ = 5.4 Hz, *m* to P), 127.2 (s, *p* to CH_2), 97.6 (m, *J* = 19.9 Hz, PtC≡*C*),[69] 92.5 (dd, $^2J_{CP}$ = 149.0 Hz, $^2J_{CP}$ = 19.1 Hz, Pt*C*≡C), 43.4 (t, $^2J_{CP}$ = 7.9 Hz, *C*(CH$_2$)$_4$), 29.5 (t, $^1J_{CP}$ = 17.0 Hz, P*C*H$_2$),[61] 14.3 (s, *C*H$_2$C$_6$H$_5$); ^{31}P{^{1}H} –4.8 ($^1J_{PPt}$ = 2192 Hz).[67]

IR (cm^{-1}, powder film): 2963 (w), 2160 (w, $\nu_{C\equiv C}$), 2013 (w, $\nu_{C\equiv C}$), 1381 (w), 918 (s), 794 (s).

[((*p*-tolCH$_2$)$_2$C(CH$_2$PPh$_2$)$_2$)Pt(C≡C)$_2$]$_4$ (4f). A Schlenk flask was charged with **2f** (00.0586 g, 0.0661 mmol), **3f** (0.0613 g, 0.0671 mmol), CuI (0.0022 g, 0.012 mmol), $HNEt_2$ (10 mL), and THF (25 mL) with stirring and heated to 55 °C. After 2 d, the solvents were removed by rotary evaporation. Then water (30 mL) was added and the mixture was extracted with CH_2Cl_2 (20 mL). The exract was dried ($MgSO_4$). The solvent was removed by rotary evaporation to give **4f** as a tan solid (0.0629 g, 0.0182 mmol, 55%), which darkened at 161 °C and blackened at 179 °C.

NMR (δ (ppm), $CDCl_3$): ^{1}H 7.32-7.27 (m, 32H, *m* to P), 7.15-7.06 (m, 16H, *p* to P), 7.03 (d, $^3J_{HH}$ = 7.2 Hz, 16H, C_6H_4), 6.96-6.93 (m, 32H, *o* to P), 6.84 (d, $^3J_{HH}$ = 7.2 Hz, 16H, C_6H_4), 2.56 (s, 16H, $CH_2C_6H_4$), 2.35 (s, 24H, CH_3), 2.27 (d, $^2J_{HP}$ = 7.6 Hz, 16H, PCH_2); $^{13}C\{^1H\}$ 136.6 (s, *p* to CH_2), 133.5 (virtual t,[63] $^2J_{CP}$ = 7.2 Hz, *o* to P), 133.5 (s, *m* to CH_2), 132.4 (m, *J* = 70.2 Hz, *J* = 7.9 Hz, *i* to P),[60] 131.3 (s, *i* to CH_2), 129.0 (s, *o* to CH_2), 128.9 (s, *p* to P), 128.2 (virtual t,[63] $^2J_{CP}$ = 5.2 Hz, *m* to P), 97.5 (m, *J* = 16.9 Hz, PtC≡*C*),[69] 88.4 (dd, $^2J_{CP}$ = 149.6 Hz, $^2J_{CP}$ = 18.1 Hz, Pt*C*≡C), 43.5 (t, $^2J_{CP}$ = 8.9 Hz, *C*$(CH_2)_4$), 42.2 (s, *C*$H_2C_6H_4$), 29.7 (t, $^1J_{CP}$ = 18.7 Hz, P*C*H_2),[61] 21.1 (s, *C*H_3); $^{31}P\{^1H\}$ –4.6 (s, $^1J_{PPt}$ = 2172 Hz).[67]

IR (ATR, cm^{-1}): 2963 (m), 2360 (m), 2160 (w, $\nu_{C\equiv C}$), 2029 (m, $\nu_{C\equiv C}$), 1558 (m), 1257 (s), 1095 (s), 1018 (s), 802 (s), 694 (s).

MS (MALDI$^+$, matrix THAP):[59] 3515 ([**4f** + Cu]$^+$, 100%).

(*n*-$Bu_2C(CH_2PPh_2)_2$)$Pt((C\equiv C)_3SiEt_3)_2$ (5b). A Schlenk flask was charged with (*p*-$tol_3P)_2Pt((C\equiv C)_3SiEt_3)_2$ (0.1395 g, 0.1209 mmol),[47] **1c** (0.0719 g, 0.1370 mmol), and CH_2Cl_2 (20 mL) with stirring. After 48 h, the solvent was removed by rotary evaporation. The residue was chromatographed on an alumina column (30 × 4.5 cm) eluted with 1:4 v/v CH_2Cl_2/hexanes, then with 1:2 v/v CH_2Cl_2/hexanes. The solvents were removed from the product containing fractions by oil pump vacuum to give **5b** as a yellow solid (0.1082 g, 0.09877 mmol, 82%), mp 119-126 °C. Anal. Calcd. for $C_{59}H_{72}P_2PtSi_2$ (1094.41 g/mol): C, 64.75; H, 6.63; Found: C, 64.54; H, 6.56.

NMR (δ (ppm), $CDCl_3$): ^{1}H 7.84-7.74 (m, 8H, *o* to P), 7.49-7.39 (m, 12H, *m* and *p* to P), 2.35 (d, $^1J_{HP}$ = 6.7 Hz, 4H, PCH_2), 1.02-0.96 (m, 4H, $CH_2CH_2CH_2CH_3$), 0.94 (t, $^3J_{HH}$ = 7.1 Hz, 18H, $SiCH_2CH_3$), 0.72-0.66 (m, 8H, $CH_2CH_2CH_3$), 0.60-0.52 (m, 18H, $CH_2CH_2CH_3$ and $SiCH_2$); $^{13}C\{^1H\}$ 134.0 (virtual t,[63] $^2J_{CP}$ = 5.4 Hz, *o* to P),

133.0 (m, J = 68.4 Hz, J = 18.4 Hz, *i* to P),[60] 131.0 (s, *p* to P), 128.5 (virtual t,[63] $^3J_{CP}$ = 5.4 Hz, *m* to P), 91.0 (s, PtC≡C),[70] 81.0 (s, PtC≡C),[70] 65.1 (s, PtC≡CC), 57.6 (s, PtC≡CC≡C), 53.4 (s, C≡CSi), 41.4 (s, ≡CSi), 40.6 (t, $^2J_{CP}$ = 6.6 Hz, $C(CH_2)_4$), 34.6 (t, $^1J_{CP}$ = 16.5 Hz, PCH_2),[61] 31.6 (s, $CH_2CH_2CH_2CH_3$), 24.7 (s, $CH_2CH_2CH_3$), 22.6 (s, $CH_2CH_2CH_3$), 13.6 (s, $CH_2CH_2CH_3$), 7.3 (s, $SiCH_2CH_3$), 4.3 (s, $SiCH_2$); $^{31}P\{^1H\}$ –6.2 (s, $^1J_{PPt}$ = 2223 Hz).[67]

IR (cm^{-1}, powder film): 2954 (m), 2870 (m), 2155 (s, $\nu_{C\equiv C}$), 2021 (s, $\nu_{C\equiv C}$), 1435 (m), 1234 (m), 1002 (m), 912 (w), 810 (m), 725 (s), 694 (s).

MS (MALDI$^+$, matrix THAP):[59] 1132 ([**5b** + K]$^+$, 40%), 1116 ([**5b** + Na]$^+$, 40%), 1094 ([**5b** + H]$^+$, 100%).

***trans*-(*p*-tol$_3$P)$_2$Pt(C≡CSiEt$_3$)$_2$ (6).** A Schlenk flask was fitted with a condenser and charged with *cis/trans*-(*p*-tol$_3$P)$_2$PtCl$_2$ (0.9829 g, 1.124 mmol),[44] HC≡CSiEt$_3$ (0.60 mL, 0.47 g, 3.4 mmol), $HNEt_2$ (70 mL), and CuCl (0.0114 g, 0.115 mmol) with stirring. The mixture was refluxed. After 24 h, the solvent was removed and the residue was chromatographed on a silica gel column (30 × 4.5 cm) eluted with 9:1 v/v EtOAc/hexanes. The solvents were removed from the product containing fractions by oil pump vacuum to give **6** as a white solid (1.4167 g, 1.3089 mmol, 52%), which yellowed at 168 °C and liquefied at 202 °C. Anal. Calcd. for $C_{58}H_{72}P_2PtSi_2$ (1082.39 g/mol): C, 64.36; H, 6.70; Found: C, 64.16; H, 6.66.

NMR (δ (ppm), $CDCl_3$): ^1H 7.63 (d, $^3J_{HP}$ = 5.7 Hz, 12H, *o* to P), 7.10 (d, $^2J_{HP}$ = 5.9 Hz, 12H, *m* to P), 2.35 (s, 18H, $C_6H_5CH_3$), 0.49 (t, $^3J_{HH}$ = 7.1 Hz, 18H, CH_2CH_3), 0.01 (q, $^3J_{HH}$ = 7.1 Hz, 12H, CH_2); $^{13}C\{^1H\}$ 139.7 (s, *p* to P), 135.1 (virtual t,[63] $^2J_{CP}$ = 6.4 Hz, *o* to P), 129.0 (virtual t,[63] $^1J_{CP}$ = 30.4 Hz, *i* to P), 128.2 (virtual t,[63] $^3J_{CP}$ = 5.7

Hz, *m* to P), 113.4 (s, Pt*C*≡C), 104.9 (s, PtC≡*C*), 21.3 (s, $C_6H_5CH_3$), 7.4 (s, $SiCH_2CH_3$), 4.7 (s, $SiCH_2$); $^{31}P\{^1H\}$ 17.8 (s, $^1J_{PPt}$ = 2684 Hz).[67]

IR (cm^{-1}, powder film): 2947 (m), 2870 (m), 2029 (s, $\nu_{C\equiv C}$), 1597 (m), 1496 (m), 1450 (w), 1396 (m), 1188 (m), 1095 (s), 1002 (s), 802 (s), 748 (s), 725 (s), 640 (s).

MS (MALDI$^+$):[59] 942 ([**6** – C≡C$SiEt_3$]$^+$, 20%), 803 ([**6** – 2C≡C$SiEt_3$]$^+$), 100%), 304 ([*p*-tol_3P]$^+$, 35%).

(*n*-$Bu_2C(CH_2PPh_2)_2$)Pt(C≡C$SiEt_3$)$_2$ (7). A Schlenk flask was charged with **6** (0.2600 g, 0.2402 mmol), **1c** (0.1250 g, 0.2383 mmol), and CH_2Cl_2 (12 mL) with stirring. After 24 h, the solvent was removed and the residue was chromatographed on a silica gel column (30 × 4.5 cm) eluted with CH_2Cl_2/hexanes (1:1 v/v). The solvents were removed from the product containing fractions by oil pump vacuum to give **7** as a white solid (0.1951 g, 0.1954 mmol, 82%), which yellowed at 158 °C, blackened at 182 °C, and liquefied at 189 °C. Anal. Calcd. for $C_{51}H_{72}P_2PtSi_2$ (998.32 g/mol): C, 61.36; H, 7.27; Found: C, 59.33; H, 6.98.[66]

NMR (δ (ppm), $CDCl_3$): ^1H 7.93-7.83 (m, 8H, *o* to P), 7.34-7.28 (m, 12H, *m* and *p* to P), 2.21 (d, $^2J_{HP}$ = 9.9 Hz, 4H, PCH_2), 1.02-0.96 (m, 4H, $CH_2CH_2CH_2CH_3$), 0.71-0.63 (m, 4H, $CH_2CH_2CH_3$), 0.65-0.49 (m with overlapping t, $^3J_{HH}$ = 7.1 Hz, 22H, $CH_2CH_2CH_3$ and $CH_2CH_2CH_2CH_3$), 0.48 (t, $^3J_{HH}$ = 7.1 Hz, 6H, $SiCH_2CH_3$), 0.19 (q, $^3J_{HH}$ = 7.1 Hz, 12H, $SiCH_2CH_3$); $^{13}C\{^1H\}$ 134.5 (virtual t,[63] $^2J_{CP}$ = 12.1 Hz, *o* to P), 132.6 (m, *J* = 67.4 Hz, *J* = 10.8 Hz, *i* to P),[60] 130.1 (s, *p* to P), 121.8 (virtual t,[63] $^3J_{CP}$ = 12.1 Hz, *m* to P), 123.6 (dd, $^2J_{CP}$ = 133.9, $^2J_{CP}$ = 17.4 Hz, Pt*C*≡C), 110.3 (m, *J* = 14.1 Hz, PtC≡*C*),[69] 41.2 (s, $CH_2CH_2CH_2CH_3$), 40.5 (t, $^2J_{CP}$ = 9.5 Hz, $C(CH_2)_4$), 36.1 (t, $^1J_{CP}$ = 15 Hz, PCH_2),[61] 24.7 (s, $CH_2CH_2CH_3$), 22.7 (s, $CH_2CH_2CH_3$), 13.6 (s, $CH_2CH_2CH_3$), 7.6 (s, $SiCH_2CH_3$), 4.9 (s, $SiCH_2$); $^{31}P\{^1H\}$ –5.9 (s, $^1J_{PPt}$ = 2147 Hz).[67]

IR (cm^{-1}, powder film): 2945 (m), 2870 (m), 2059 (m, $\nu_{C\equiv C}$), 1458 (w), 1435 (m), 1257 (m), 1095 (s), 1010 (s), 763 (s), 725 (s), 694 (s).

MS (MALDI$^+$, matrix DCTB):[59] 998 ([**7** + H]$^+$, 100.

Reaction of 5c and 2c. A. A Schlenk flask was fitted with a condenser and charged with **5c** (0.0626 g, 0.0572 mmol), THF (4 mL), and *n*-Bu_4N^+ F^- (0.114 mL, 0.114 mmol; 1 M THF) with stirring. After 45 min, a solution of **2c** (0.0458 g, 0.0579 mmol) and CuI (0.0018 g, 0.0095 mmol) in $HNEt_2$ (8 mL) was added. Then CH_2Cl_2 (10 mL) was added and the mixture was refluxed. After 3 d, the solvents were removed by rotary evaporation. The residue was washed with Et_2O (100 mL) and hexanes (100 mL) and dried by oil pump vacuum to give a tan solid (0.0881 g).

NMR (δ (ppm), $CDCl_3$): ^{1}H 7.80-7.65 (m, 32H, *o* to P), 7.44-7.27 (m, 48H, *m* and *p* to P), 2.29 (br m, 16H, PCH_2), 1.02-0.86 (m, 16H, $CH_2CH_2CH_2CH_3$), 0.77-0.60 (m, 32H, $CH_2CH_2CH_3$), 0.57-0.49 (m, 24H, CH_3); $^{31}P\{^1H\}$ –6.5, –6.7 (2 s, $^1J_{PPt}$ = 2189 Hz).[67]

B. A Schlenk flask was fitted with a condenser and charged with **5c** (0.0684 g, 0.0625 mmol), THF (35 mL), and *n*-Bu_4N^+ F^- (0.120 mL, 0.120 mmol; 1 M THF) with stirring. After 1 h, a solution of **2c** (0.0491 g, 0.0621 mmol) and CuI (0.0023 g, 0.012 mmol) in $HNEt_2$ (10 mL) was added. Then CH_2Cl_2 (10 mL) was added and the mixture was refluxed. After 2 d, the solvents were removed by rotary evaporation. The residue was washed with Et_2O (100 mL) and dried by oil pump vacuum to give a tan solid (0.0863 g).

NMR (δ (ppm), $CDCl_3$): ^{1}H 7.78-7.66 (m, 32H, *o* to P), 7.42-7.28 (m, 48H, *m* and *p* to P), 2.29 (br m, 16H, PCH_2), 1.01-0.89 (m, 16H, $CH_2CH_2CH_2CH_3$), 0.76-0.61

(m, 32H, $CH_2CH_2CH_3$), 0.59-0.46 (m, 24H, CH_3); $^{31}P\{^1H\}$ –6.3, –6.6 (2 s, $^1J_{PPt}$ = 2218 Hz).[67]

C. A Schlenk flask was fitted with a condenser and charged with **5c** (0.0651 g, 0.0595 mmol), THF (70 mL), and *n*-Bu_4N^+ F^- (0.120 mL, 0.120 mmol; 1 M THF) with stirring. After 1 h, a solution of **2c** (0.0454 g, 0.0571 mmol) and CuI (0.0029 g, 0.015 mmol) in $HNEt_2$ (20 mL) was added. Then CH_2Cl_2 (20 mL) was added and the mixture was refluxed. After 2 d, the solvents were removed by rotary evaporation. The residue was washed with Et_2O (100 mL) and dried by oil pump vacuum to give a tan solid (0.0716 g).

NMR (δ (ppm), $CDCl_3$): $^{31}P\{^1H\}$ –6.4, –6.6 (2 s, $^1J_{PPt}$ = 2214 Hz).[67]

MS (MALDI$^+$, matrix THAP):[59] 3165 ([tetramer]$^+$, 100), 2374 ([trimer]$^+$, 70%).

Homocoupling of 3a. A three necked round bottom flask was fitted with a gas dispersion tube and a condenser, and charged with **3a** (0.4988 g, 0.7066 mmol) and acetone (30 mL) with stirring. Then oxygen was aspirated through the mixture. The mixture was heated to 40 °C and a solution of CuCl (0.3398 g, 3.432 mmol) and TMEDA (0.280 mL, 0.218 mmol, 1.87 mmol) in acetone (70 mL; previously stirred for 30 min) was added. After 6 h, the solvent was removed by rotary evaporation. The residue was dried by oil pump vacuum to give an insoluble tan solid (0.4721 g).

IR (cm^{-1}, powder film): 2962 (m), 2912 (m), 2140 (w, $\nu_{C\equiv C}$), 1600 (w), 1435 (m), 1404 (m), 1257 (s), 1041 (s), 1066 (s), 952 (m), 929 (m), 864 (m).

Homocoupling of 3c. A. A three necked round bottom flask was fitted with a gas dispersion tube and a condenser, and charged with **3c** (0.1466 g, 0.1768 mmol) and acetone (40 mL) with stirring. Then oxygen was aspirated through the mixture. The

mixture was heated to 40 °C and a solution of CuCl (0.1079 g, 1.090 mmol) and TMEDA (0.170 mL, 0.l32 g, 1.14 mmol) in acetone (15 mL; previously stirred for 30 min) was added. After 7 h, the solvent was removed by rotary evaporation and the residue was washed with Et_2O (100 mL) and water (50 mL). The residue was dried by oil pump vacuum to give a tan solid (0.4721 g).

NMR (δ (ppm), $CDCl_3$): $^{31}P\{^1H\}$ –6.2, –6.6 (2 s, $^1J_{PPt}$ = 2206 Hz).[67]

B. A three necked round bottom flask was fitted with a gas dispersion tube and a condenser, and charged with **3c** (0.2017 g, 0.2466 mmol) and acetone (55 mL) with stirring. Then oxygen was aspirated through the mixture. The mixture was heated to 40 °C and a solution of CuCl (0.0962 g, 0.972 mmol) and TMEDA (0.181 mL, 0.140 g, 1.21 mmol) in acetone (13 mL; previously stirred for 30 min) was added. After 6 h, the solvent was removed by rotary evaporation and the residue was washed with Et_2O (100 mL) and water (50 mL). The residue was dried by oil pump vacuum to give a tan solid (0. 1503 g).

NMR (δ (ppm), CD_2Cl_2): ^1H 7.91-7.73 (m, 32H, *o* to P), 7.56-7.40 (m, 48H, *m* and *p* to P), 2.37 (br m, 16H, PCH_2), 1.03-0.89 (m, 16H, $CH_2CH_2CH_2CH_3$), 0.79-0.62 (m, 32H, $CH_2CH_2CH_3$), 0.59-0.50 (m, 24H, CH_3); $^{31}P\{^1H\}$ –5.9, –6.1, –6.3, –6.4 (4 s, $^1J_{PPt}$ = 2206 Hz).[67]

IR (cm^{-1}, powder film): 2924 (m), 2862 (m), 2145 (m, $\nu_{C\equiv C}$), 1257 (s), 1095 (s), 1018 (s), 794 (s).

Homocoupling of 3d. A three necked round bottom flask was fitted with a gas dispersion tube and a condenser, and charged with **3d** (0.3090 g, 0.3133 mmol) and acetone (35 mL) with stirring. Then oxygen was aspirated through the mixture. The mixture was heated to 40 °C and a solution of CuCl (0.1325 g, 1.339 mmol) and

TMEDA (0.120 mL, 0.0930 g, 0.802 mmol) in acetone (30 mL; previously stirred for 30 min) was added. After 5 h, the solvent was removed by rotary evaporation and water (100 mL) was added. The mixture was extracted with CH_2Cl_2 (2 × 20 mL). The solvent was removed from the extracts and the residue was dried by oil pump vacuum to give a tan solid (0. 2703 g).

NMR (δ (ppm), $CDCl_3$): ^{1}H 7.81-7.69 (m, 32H, *o* to P), 7.46-7.32 (m, 48H, *m* and *p* to P), 2.30 (br s, 16H, PCH_2), 1.31-0.80 (m, 168H, $(CH_2)_9CH_3$); $^{31}P\{^1H\}$ –6.2, –6.3, –6.6 (3 s, $^1J_{PPt}$ = 2219 Hz).[67]

IR (cm^{-1}, powder film): 2924 (m), 2846 (m), 2144 (m, $\nu_{C\equiv C}$), 1257 (s), 1095 (s), 1018 (s), 794 (s).

Crystallography. A. A CH_2Cl_2 solution of **3a** was stored at at 3 °C. After 3 d, green plates were obtained. Data were collected as outlined in Table 2.11. Cell parameters were obtained from 180 data frames were taken at widths of 0.5°. Integrated intensity information for each reflection was obtained by reduction of the data frames with the program APEX2.[71] Data were corrected for Lorentz and polarization factors, and using SADABS[72] for absorption and crystal decay effects. The structure was solved by direct methods using SHELXTL (SHELXS).[73] All non-hydrogen atoms were refined with anisotropic thermal parameters. The hydrogen atoms were placed in idealized positions, and refined using a riding model. The parameters were refined by weighted least squares refinement on F^2 to convergence.[73]

B. A DMSO solution of **4a** was layered with EtOAc at 3 °C. After 7 d, yellow-brown crystals were obtained. Data were collected as outlined in Table 2.10. Cell parameters were obtained from 180 data frames taken at widths of 0.5°. Integrated intensity information for each reflection was obtained by reduction of the data frames

with the program SAINTplus.[74] Data were corrected for Lorentz and polarization factors, and using SADABS[72] for absorption and crystal decay effects. The structure was solved by direct methods using SHELXTL (SHELXS).[73] All non-hydrogen atoms were refined with anisotropic thermal parameters. Approximately 14-16 DMSO molecules per asymmetric unit were found from the Fourier difference map. Some of the solvent molecules were disordered. The solvent molecules were removed using the programs SQUEEZE and PLATON.[75] The absence of additional symmetry and twin components were verified using PLATON.[75] The thermal parameters of the disordered solvent molecules were restrained to restrict the carbon and the oxygen atoms from becoming non positive definite. The hydrogen atoms were placed in idealized positions, and refined using a riding model. The parameters were refined by weighted least squares refinement on F^2 to convergence.[76]

C. A CH_2Cl_2 solution of **4b** was layered with toluene and Et_2O was stored at 3 °C. After 8 d, colorless multi-faceted crystals were obtained. Data were collected and outlined in Table 2.12. Several molecules of CH_2Cl_2 and other possible solvents were found, amounting to 1606 electrons per asymmetric unit. Most of them were disordered and removed using the same procedure as in B. The structure solution and refinement were carried out analogously to procedure B.

Table 2.11. Crystallographic data for **3a**·CH_2Cl_2.

Empirical formula	$C_{38}H_{34}Cl_2P_2Pt$
Formula weight	818.58
Temperature	110(2) K
Diffractometer	Bruker GADDS
Wavelength	1.54178 Å
Crystal system	Orthorhombic
Space group	*Pbca*
Unit cell dimensions	
a	17.3247(11) Å
b	16.4634(11) Å
c	24.0781(16) Å
α	90°
β	90°
γ	90°
V	6867.6(8) $Å^3$
Z	8
Density (calculated)	1.583 Mg/m^3
Absorption coefficient	10.144 mm^{-1}
F(000)	3232
Crystal size	0.08 × 0.07 × 0.02 mm^3
Theta range for data collection	3.67 to 60.00°
Index ranges	$-18 \le h \le 19$, $-18 \le k \le 18$, $-27 \le l \le 27$
Reflections collected	91288
Independent reflections	5099 [R(int) = 0.1131]
Completeness to theta = 60.00°	100.0%
Max. and min. transmission	0.8229 and 0.4975
Refinement method	Full-matrix least-squares on F^2
Data / restraints / parameters	5099 / 0 / 390
Goodness-of-fit on F^2	1.083
Final R indices [I>2σ(I)]	*R*1 = 0.0244, *w*R2 = 0.0549
R indices (all data)	*R*1 = 0.0353, *w*R2 = 0.0561
Largest diff. peak and hole	0.879 and –0.614 $eÅ^{-3}$

Table 2.12. Crystallographic data for **4a**.

Empirical formula	$C_{132}H_{111}P_8Pt_4$
Formula weight	2725.33
Temperature	110(2) K
Diffractometer	Bruker GADDS
Wavelength	1.54178 Å
Crystal system	Triclinic
Space group	*P-1*
Unit cell dimensions	
a	13.9731(6) Å
b	19.3822(8) Å
c	32.3857(13) Å
α	90.232(2)°
β	100.137(2)°
γ	94.743(2)°
V	8603.0(6) $Å^3$
Z	2
Density (calculated)	1.052 Mg/m^3
Absorption coefficient	6.895 mm^{-1}
F(000)	2670
Crystal size	0.10 × 0.09 × 0.04 mm^3
Theta range for data collection	2.29 to 60.00°
Index ranges	$-15 \le h \le 4$, $-21 \le k \le 21$, $-36 \le l \le 36$
Reflections collected	73407
Independent reflections	24343 [R(int) = 0.0486]
Completeness to theta = 60.00°	95.3%
Max. and min. transmission	0.7700 and 0.5456
Refinement method	Full-matrix least-squares on F^2
Data / restraints / parameters	24343 / 0 / 1297
Goodness-of-fit on F^2	0.957
Final R indices [I>2σ(I)]	*R*1 = 0.0396, *w*R2 = 0.0998
R indices (all data)	*R*1 = 0.0506, *w*R2 = 0.1033
Largest diff. peak and hole	2.540 and –1.109 $eÅ^{-3}$

Table 2.13. Crystallographic data for **4b**.

Empirical formula	$C_{140}H_{136}P_8Pt_4$
Formula weight	2846.61
Temperature	110(2) K
Diffractometer	Bruker GADDS
Wavelength	1.54178 Å
Crystal system	Triclinic
Space group	*P-1*
Unit cell dimensions	
a	21.448(4) Å
b	22.771(4) Å
c	25.579(5) Å
α	106.392(9)°
β	101.573(9)°
γ	111.947(10)°
V	10438(3) $Å^3$
Z	2
Density (calculated)	0.906 Mg/m^3
Absorption coefficient	5.697 mm^{-1}
F(000)	2816
Crystal size	0.04 × 0.03 × 0.03 mm^3
Theta range for data collection	1.92 to 60.00°
Index ranges	$-24 \leq h \leq 24$, $-25 \leq k \leq 25$, $-28 \leq l \leq 28$
Reflections collected	136751
Independent reflections	29149 [R(int) = 0.0737]
Completeness to theta = 60.00°	94.1%
Max. and min. transmission	0.8477 and 0.8042
Refinement method	Full-matrix least-squares on F^2
Data / restraints / parameters	29149 / 0 / 1233
Goodness-of-fit on F^2	1.180
Final R indices [I>2σ(I)]	*R*1 = 0.0755, *w*R2 = 0.2020
R indices (all data)	*R*1 = 0.1039, *w*R2 = 0.2165
Largest diff. peak and hole	7.086 and –4.104 $eÅ^{-3}$

CHAPTER III

CARBON CHAIN COMPLEXES BEARING HIGHLY FLUOROUS PHOSPHINE LIGANDS

INTRODUCTION

The stabilities of polyynediyl chains are known to decrease with increasing chain lengths.[48,50,77-80] These stabilities can be enhanced with the use of suitable protective endgroups. A diagram classifying several generalized endgroups and their respective stabilizing capabilities is offered in Figure 3.1.

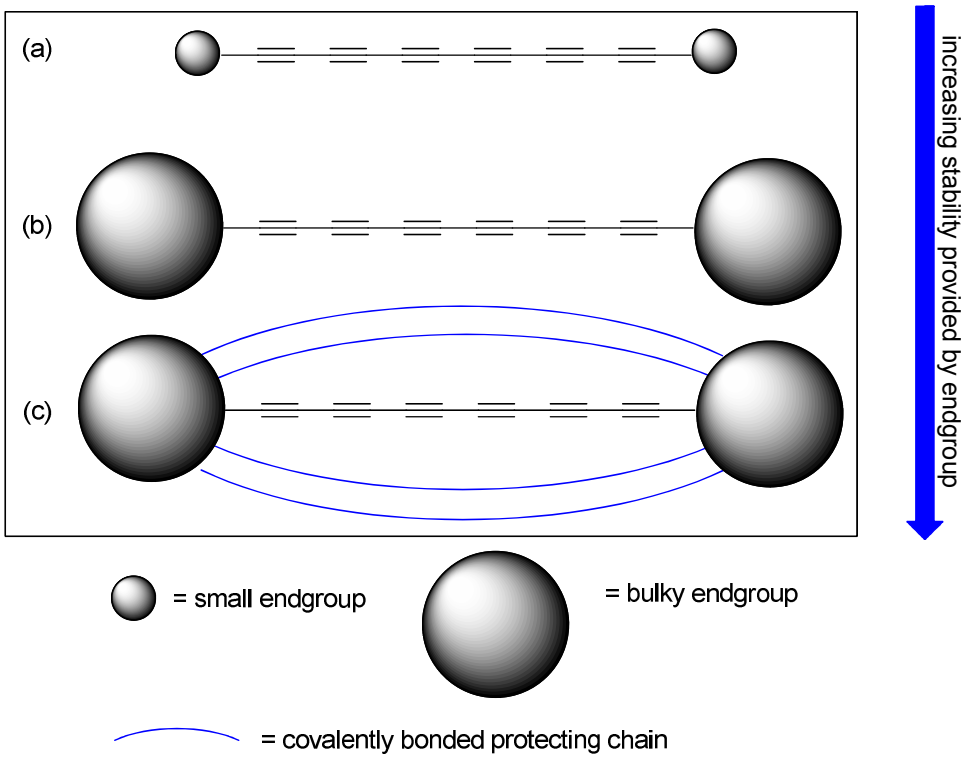

Figure 3.1. Some limiting types of polyynediyl systems and stability generalizations.

Some of the earliest work involving long polyynediyl systems featured tertiary carbon or silicon endgroups. In particular, Walton reported the isolation of a polyyne chain compound with 24 sp carbon atoms capped with *t*-Bu groups, but the highest homolog decomposed within eight min at room temperature. Also synthesized were compounds of the formula $Et_3Si(C{\equiv}C)_nSiEt_3$ with n = 2, 3, 4, and 12 being isolated. For the compound with n = 16, $Et_3Si(C{\equiv}C)_{16}SiEt_3$, trace starting material impurities could not be removed and it was characterized only by UV-vis spectroscopy.[81,82] The longest polyyne chain compounds of these series are depicted in Figure 3.2.

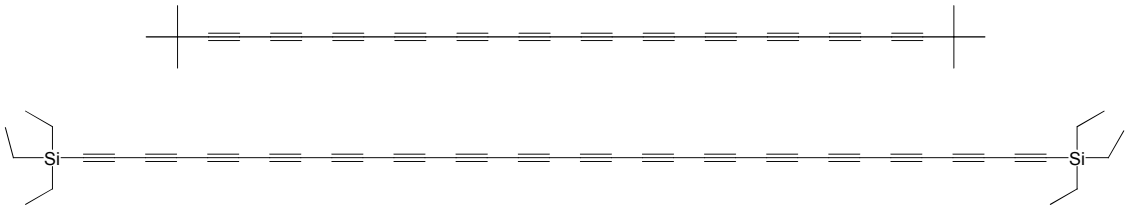

Figure 3.2. Walton's carbon (top) and silicon (bottom) capped polyyne chains with 24 and 32 sp carbon atoms, respectively.

In addition to carbon and silicon based endgroups, a metal endgroup can also serve as a protective moiety for a polyyne carbon chain. The utilization of a transition metal based endgroup in polyyne synthesis has three implications: (1) the metal coordination sphere is typically larger than its carbon or silicon based analogues (represented in going from a to b in Figure 3.1), (2) the metal can serve as a docking point for additional modes of protection for the polyyne chain (represented in going from b to c in Figure 3.1), and (3) the metal is electropositive, possibly providing a better electrostatic match to the electronegative sp carbon atoms.

Some representative metal complexes of polyyne chains are shown in Figure 3.3. These usually represent the longest chain complexes in an extended series and vary in length from 12 to 28 sp carbon atoms.

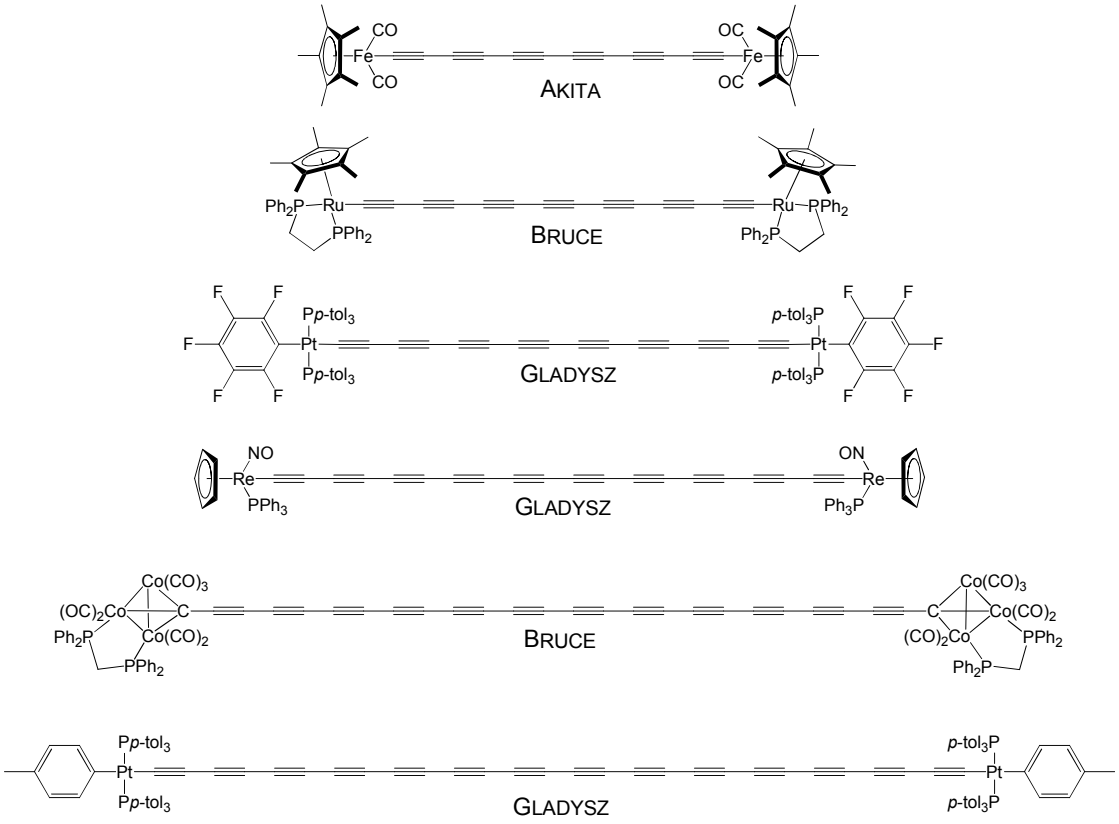

Figure 3.3. Various transition metal capped polyyne chains with 12, 14, 16, 20, 24, and 28 sp carbon atoms.

With respect to (2) above, phosphine ligands on the transition metals can offer versatile platforms for various methods of protection. For instance, long sp^3 carbon chains can be introduced via the phosphine ligands. These long chains have been

engineered to span the endgroups, providing intimate protection. At suitable lengths, they can form helices around the polyyne chain. This type of complex can be synthesized by coordination driven self assembly or metathesis and subsequent hydrogenation (top and bottom, respectively, in Scheme 3.1).

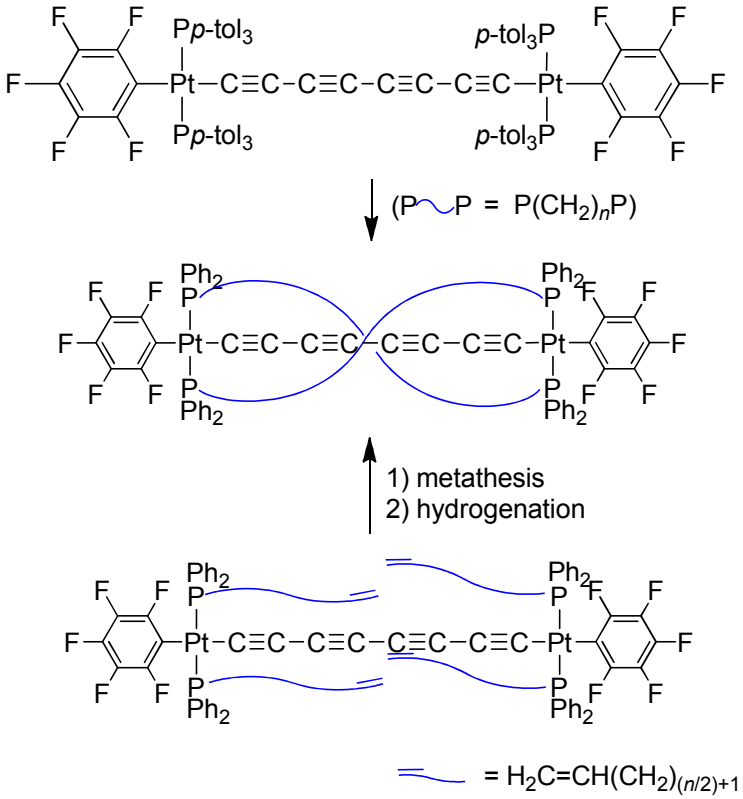

Scheme 3.1. Syntheses of a helically protected polyynediyl complex by coordination driven self assembly (top) and metathesis with subsequent hydrogenation (bottom).

Gladysz has synthesized many examples of polyynediyl complexes with two protective helical sp^3 carbon chains.[83] These methods may allow for the isolation of higher chain length complexes.

Chain protection and insulation can be demonstrated by examining (1) space filling models of protected carbon chain compounds and (2) thermal stabilities of both the parent complex and any accessible oxidized or reduced species. Although the former does not provide a quantitative measurement for the degree of protection, it can give insight into the steric environment around the polyyne chain. An example of this can be seen in the space filling model of a polyyne chain complex shown at the bottom of Figure 3.4, in which a helical chain is deployed via the phosphine ligand.[84]

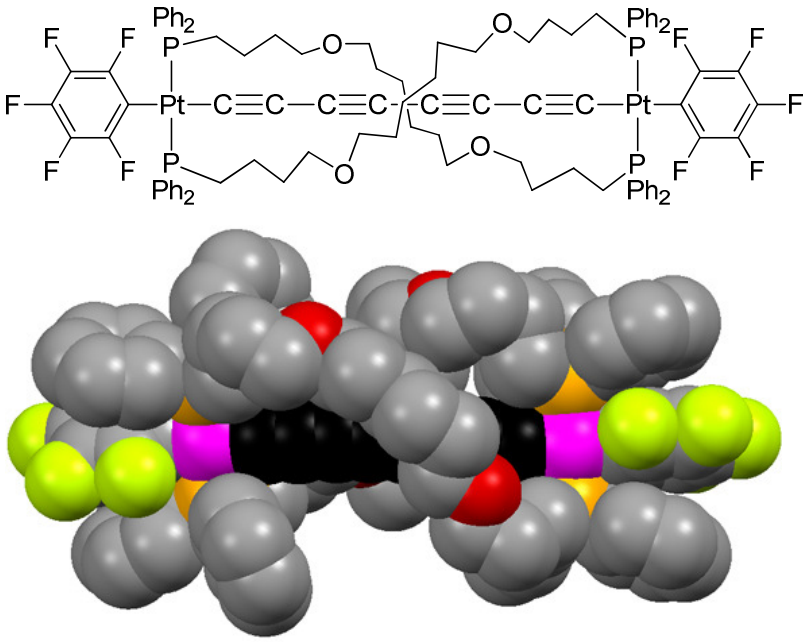

Figure 3.4. A polyyne chain complex employing helical protective alkyl chains (top) and the corresponding space filling model (bottom).

In regard to the latter, polyyne chains with redox active endgroups can undergo one or two electron oxidations to give the corresponding mono or dicationic complexes. The former is always a paramagnetic cation radical, and the latter, depending on the system, may be either a paramagnetic dication diradical or a diamagnetic dication. These have characteristic decomposition pathways involving solvents or other carbon chain complexes. Their stabilities can give insight into the protection offered to the chain. These oxidized species and the corresponding reduced radical anion are depicted in Scheme 3.2.

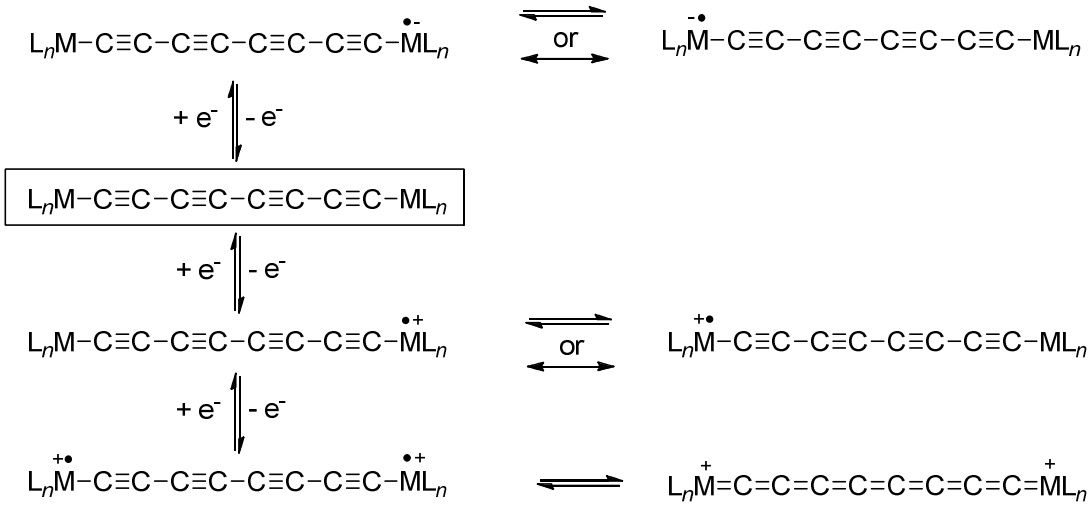

Scheme 3.2. Representation of the one and two electron oxidation and one electron reduction products of $L_nM(C{\equiv}C)_4ML_n$.

Accordingly, cyclic voltammetry provides a measure of the reversibility of a redox couple. Along these lines, a comparison of a series of three octatetraynediyl complexes, one with an unprotected sp carbon chain (**1**),[51] one with an alkyl protected sp carbon chain (**2**),[85] and one with a helically protected sp carbon chain (**3**),[85] as shown

in Figure 3.5, is particularly informative. The cyclic voltammetry traces are given in Figure 3.6 and the corresponding data in Table 3.1. One can see that all three complexes can be oxidized, but those with protected sp carbon chains are more reversibly oxidized.

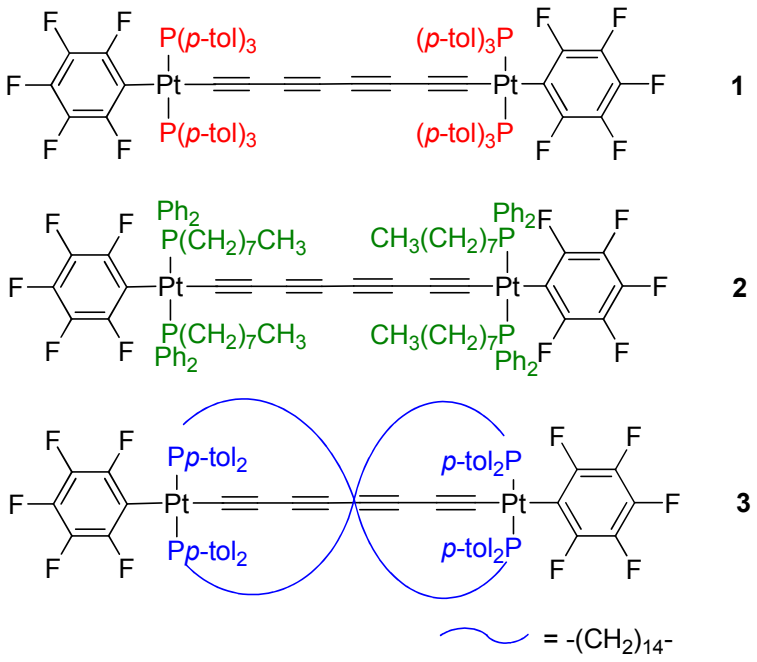

Figure 3.5. Structures of an unprotected carbon chain complex **1** (top), an alkyl protected carbon chain complex **2** (middle), and a helically protected carbon chain complex **3** (bottom).

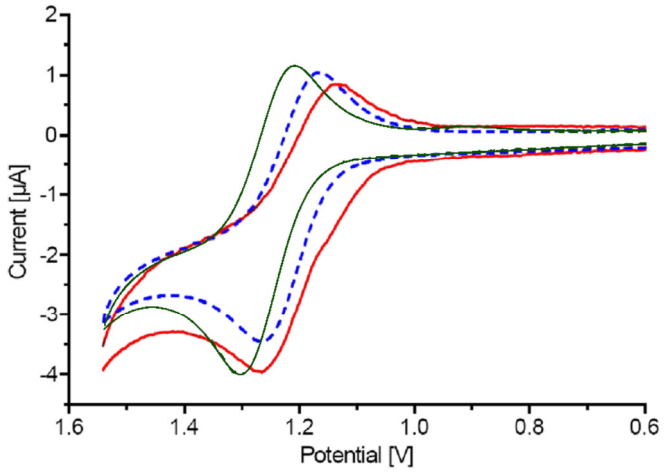

Figure 3.6. Cyclic voltammetry traces of **1** (red), **2** (green), and **3** (blue).

Table 3.1. Cyclic voltammetry data for representative carbon chain complexes.[a]

complex	$E_{p,a}$ (V)	$E_{p,c}$ (V)	E° (V)	ΔE (mV)	$i_{c/a}$
1	1.261	1.143	1.202	118	0.48
2	1.301	1.214	1.258	87	0.68
3	1.259	1.168	1.214	91	0.71

[a] conditions: 7-9 × 10^{-4} M in substrate in CH_2Cl_2, *n*-Bu_4N^+ BF_4^- as the electrolyte; Pt working and counter electrodes, potential vs. Ag wire pseudoreference; scan rate 100 mV/s.

As shown in Table 3.1, the ratio of the cathodic to anodic current ($i_{c/a}$ value) for the unprotected chain **1** is 0.48 while the corresponding value for the alkyl protected carbon chain **2** is 0.68, indicating a higher degree of reversibility,[51] with an $i_{c/a}$ value of 1.00 being consistent with ideal reversible behavior. Furthermore, **3** shows a slightly greater $i_{c/a}$ value of 0.71. The lower degree of reversibility of **1** can theoretically be attributed to radical delocalization onto the polyyne chain and a subsequent

decomposition pathway that may involve chain-solvent, chain-metal, or chain-chain interactions. With this understanding, the data in Table 3.1 support a steric shielding effect.

Although not specific to metal-capped carbon chains, another method of protection involves the use of a macrocycle, which can surround the polyyne chain, ultimately generating a rotaxane.[83,85] In this case, the macrocycle can slide along the polyyne chain in a dynamic process.

The Gladysz group has recently synthesized a polyyne chain complex comprised of eight carbons enclosed by an organic macrocycle. The route used the copper iodide complex **4** shown in Scheme 3.3.[86] The role of the metal is to act both as a template and as a "catalyst" in the homocoupling reaction of the two butadiynyl complexes. The copper iodide adduct effectively forms the topologically complex product by forcing the homocoupling reaction to take place within the center of the macrocycle. As shown in Scheme 3.3, two oxidants were used: molecular oxygen and iodine.

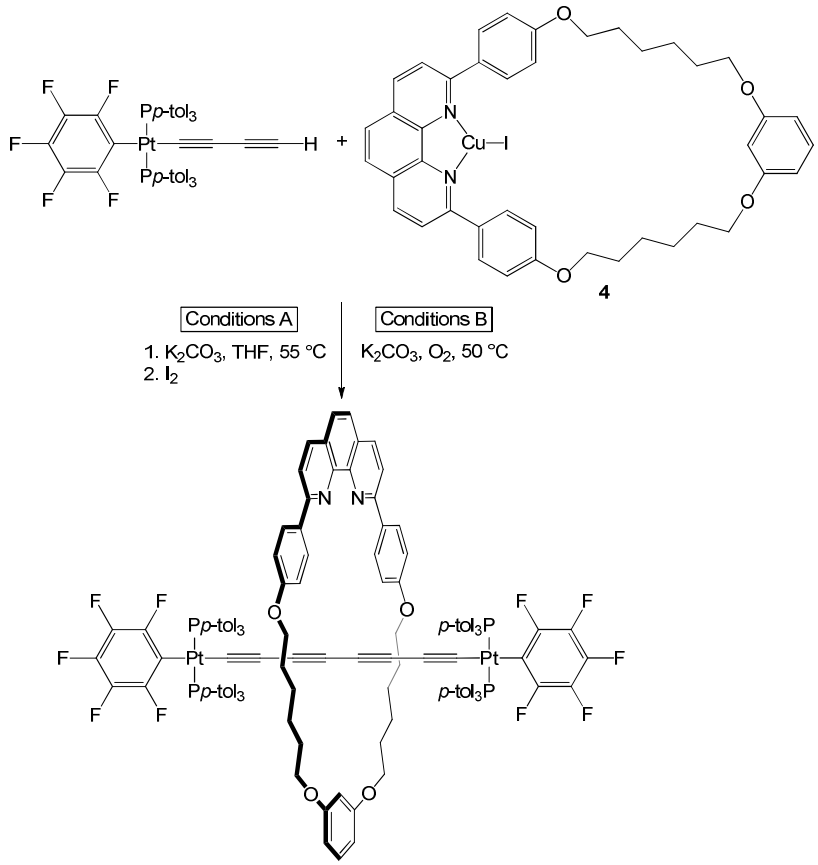

Scheme 3.3. Gladysz's synthesis of a macrocycle protected carbon chain complex with eight sp carbon atoms.

Similarly, Anderson has shown that the non-complexed version of the macrocycle in Scheme 3.3 can be employed in the presence of copper iodide to couple terminal polyynes capped with organic endgroups. As shown in Scheme 3.4, a series of purely organic rotaxanes were realized.[87] Interestingly, a complex with a chain of 20 sp carbon atoms was isolated. In this study, Anderson reports the need for at least eight carbons in the polyyne chain for homocoupling to occur. This is in accord with the space filling model shown at the top of Figure 3.7 (*vide infra*), which suggests it improbable that a shorter chain would effectively accommodate the macrocycle.

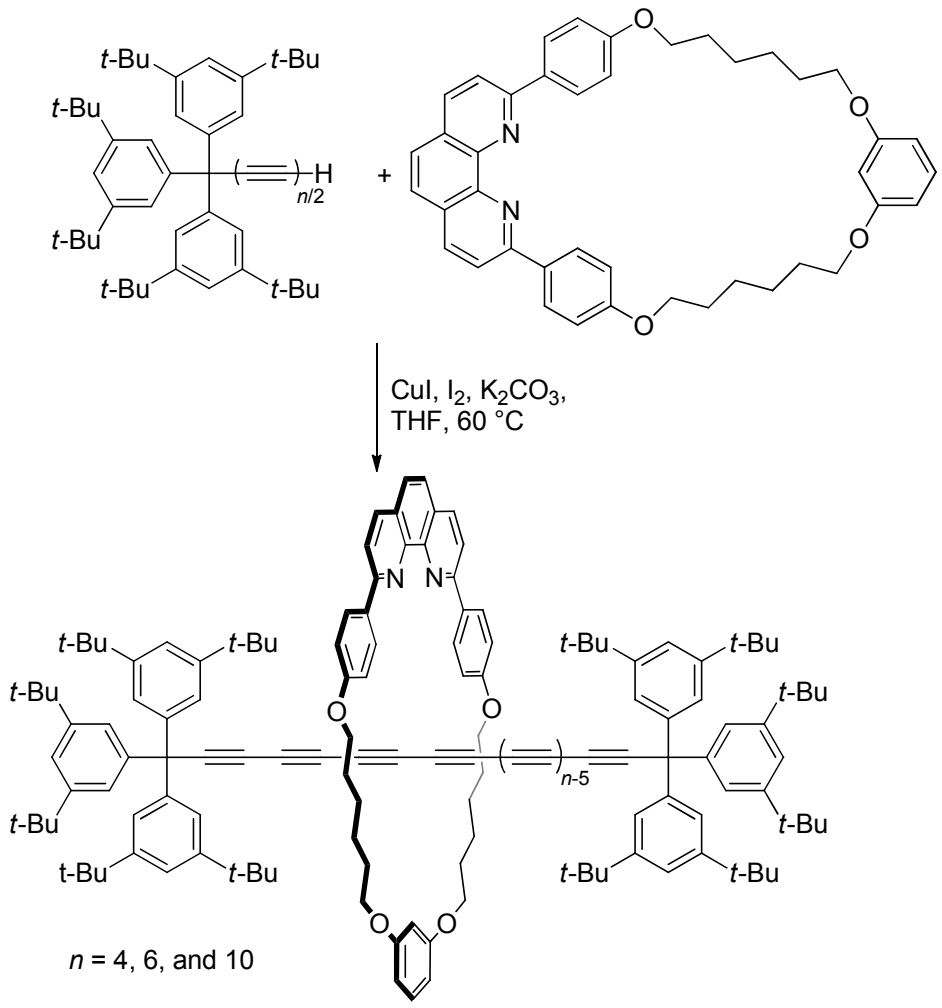

Scheme 3.4. Anderson's syntheses of macrocycle protected carbon chain complexes with up to 20 sp carbon atoms.

As depicted in Figure 3.7, the X-ray crystal structures of the rotaxane in Scheme 3.3 and one of the rotaxanes in Scheme 3.4 show that the sp carbon chains are shielded by their respective macrocycles.

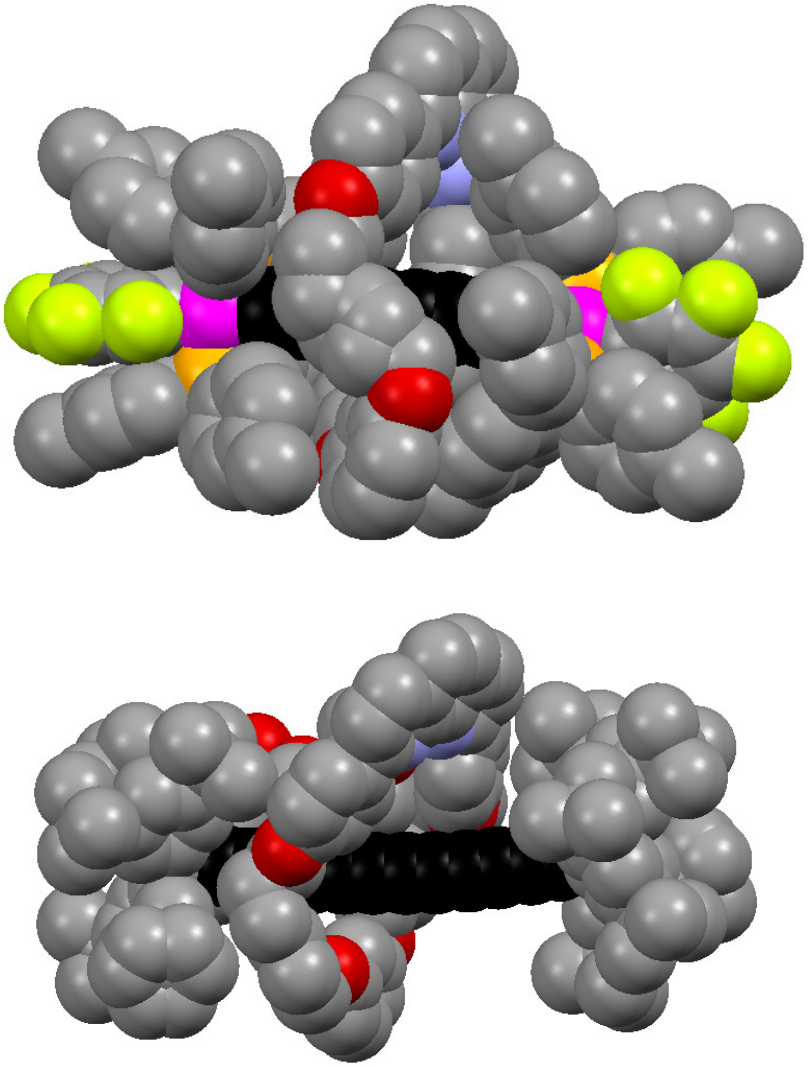

Figure 3.7. Space filling models of Gladysz's (top) and Anderson's (bottom) macrocycle protected polyyne chain complexes.

Figure 3.8 summarizes the three protective methods hitherto discussed (long sp^3 carbon chains (**A**), helical sp^3 carbon chains (**B**), and a macrocycle (**C**)). This provides the framework for the thesis advanced in this dissertation chapter.

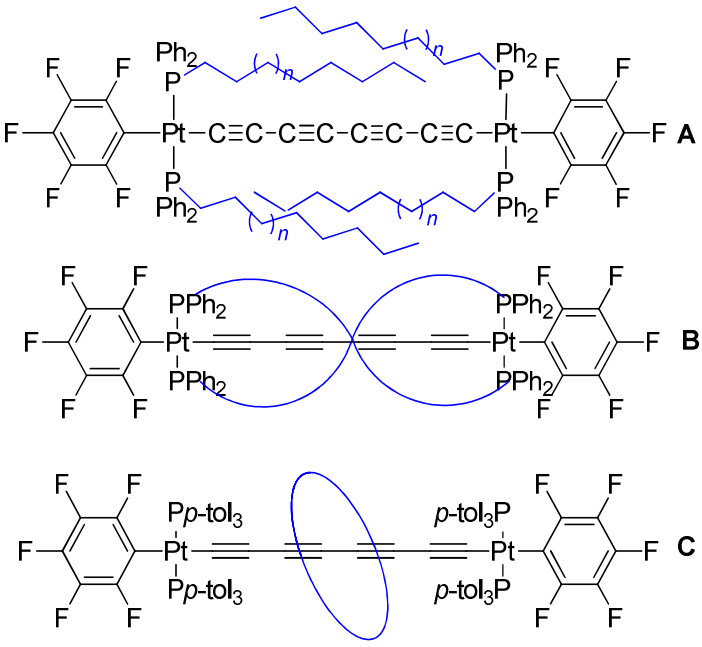

Figure 3.8. Representative polyynediyl complexes employing long sp^3 carbon chains (top), helical sp^3 carbon chains (middle), and a macrocycle (bottom) as protective moieties.

A second generation approach to that represented by **A** or by the specific case of **2** (see Figure 3.5) would be to replace all of the phosphine aryl substituents by long alkyl or similar chains. Furthermore, in one scenario, the alkyl chains can include a fluorous moiety. The term "fluorous" is a relatively new term, only having been introduced in 1994 by Horvath and Rabai.[88] Officially defined in 2002,[89] the term "fluorous" takes on the following meaning: "of, relating to, or having the characteristics of highly fluorinated saturated organic materials, molecules or molecular fragments. Or, more simply (but less precisely), 'highly fluorinated' or 'rich in fluorines' and based upon sp^3 hybridized carbon." Since its introduction, research in the fluorous field has skyrocketed, with applications including facile catalyst separation,[89-95] combinatorial chemistry,[96-98] and reactions in supercritical CO_2[99-102] all spurring further interest.

Fluorous compounds, namely *n*-perfluoroalkanes, often exhibit similar boiling points, enthalpies of vaporization, and molecular polarizabilities as their *n*-alkane analogues.[103] Given the novelty of this project, the differences, rather than similarities, are of great interest. Likely the most striking difference is the behavior of fluorous solvents. They exhibit orthogonality to both the organic and aqueous phases. A graphic illustrating this concept is offered in Figure 3.9, in which representative fluorous solvents are shown on the bottom.

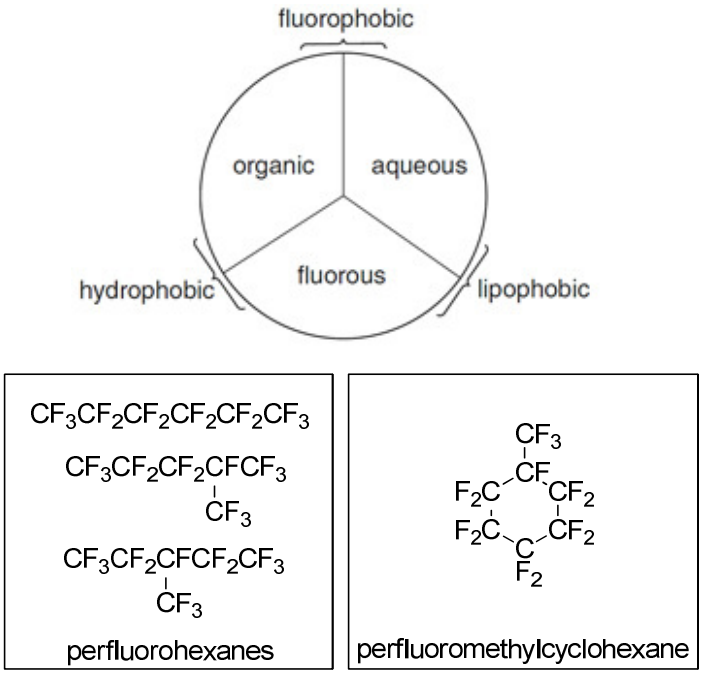

Figure 3.9. Representation of orthogonality between three phases (top) and representative fluorous solvents (bottom).

Furthermore, in X-ray crystal structures of fluorous compounds, the fluorous domains often "phase separate" from the non-fluorous domains. An example of this

phenomenon can be seen in the packing diagram of a fluorous ruthenium salt (**5**), as shown in Figure 3.10. The fluorous domains (yellow-green) are clearly separated from the non-fluorous domains (gray, green, and orange).[104]

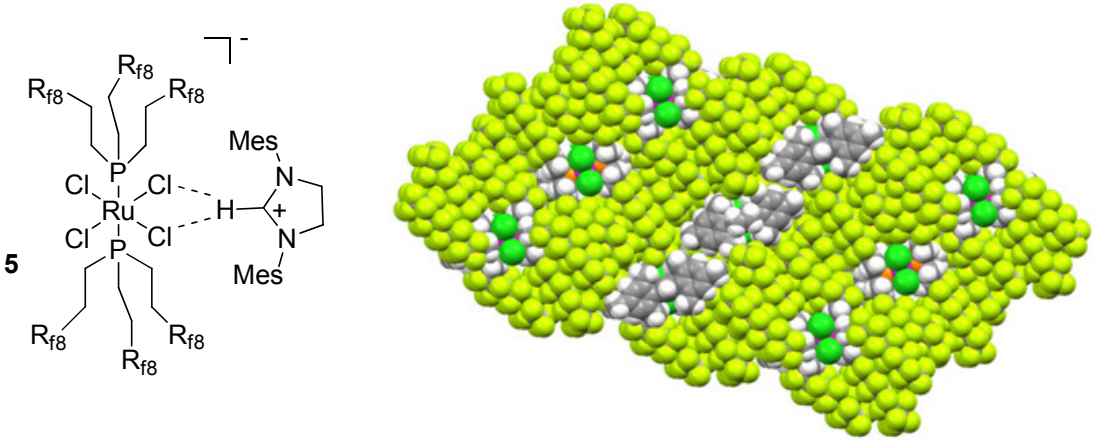

Figure 3.10. Depiction of fluorous ruthenium salt **5** (left) and the corresponding packing diagram (right) with fluorine atoms in yellow-green, chlorine atoms in green, nitrogen atoms in orange, and carbon atoms in gray.

Fluorous compounds exhibit a variety of characteristic spectroscopic properties. For example, the $^{13}C\{^{1}H\}$ NMR spectra will show extensive ^{19}F coupling, with the result that these data are often not reported, or only in abbreviated form. This complication can obviously affect other magnetically active nuclei.

The fluorous moiety is commonly introduced by incorporating fluorous ponytails, which often have the formula $(CH_2)_m(CF_2)_{n-1}CF_3$, with *m* indicating the number of methylene spacers and the perfluoroalkyl moiety abbreviated as R_{fn}. The R_{fn} segment is highly electronegative,[105] and the spacer can be lengthened or shortened to

modulate its electron withdrawing effect. Without spacers, the resulting ligand would have a very low degree of nucleophilicity and basicity.

As evidenced by examples such as **5** in Figure 3.10, the use of methylene spacers is common practice in fluorous ligand design. However, other spacers such as aromatic rings are also employed. As shown in Figure 3.11, a platinum complex synthesized by Koutsantonis features a bidentate fluorous phosphine ligand that incorporates a C_6H_4 spacer.[106]

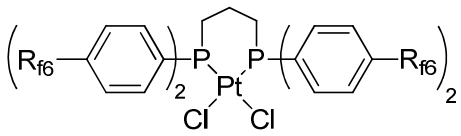

Figure 3.11. Koutsantonis' use of an aromatic moiety as a spacer for a fluorous phosphine ligand.

The effect of the spacer is significant. The influence of methylene groups as spacers was quantified by IR spectroscopy in 2000.[107,108] A study of carbonyl stretching frequencies in the IR spectra of Vaska's complex with various fluorous phosphines proved to be very informative. These data are summarized in Table 3.2, in which the number of methylene groups is increased from two to five. Also included with these data is the corresponding value for a non-fluorous *n*-alkyl analogue.

Table 3.2. IR data for fluorous phosphine analogues of Vaska's complex.

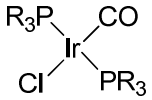

R	IR ν_{CO} (cm^{-1})
$(CH_2)_2R_{f8}$	1973.9
$(CH_2)_3R_{f8}$	1956.7
$(CH_2)_4R_{f8}$	1949.2
$(CH_2)_5R_{f8}$	1946.1
$(CH_2)_7CH_3$	1942.3

As evidenced by the data in Table 3.2, as the number of methylene spacers is increased from two to five, there is more electron donation to the iridium metal center, and ultimately into the antibonding orbital of the carbon-oxygen bond. The spectroscopic result is a lower carbonyl stretching frequency. This is consistent with the expected insulating behavior of the methylene spacers between the transition metal and fluorous moiety. Importantly, the electron withdrawing effects are still felt with up to five methylene spacers, as the analogous non-fluorous phosphine shows an even lower carbonyl stretching frequency of 1942.3 cm^{-1}. A similar conclusion was reached from photoelectron spectra of the fluorous phosphines presented in Table 3.2. This method measures the ease of ionization of the phosphine lone pair. In accord with the data in Table 3.2, the ionizations became easier as the number of methylene spacers was increased.[107]

It should be noted that a $\Delta\nu_{CO}$ value of 17.2 cm^{-1} is observed upon increasing the number of methylene spacers from two to three in Table 3.2, but this decreases to 7.5

cm^{-1} and 3.1 cm^{-1} upon further increase of the number from three to four to five. This indicates that the effect of the fluorous ponytail is in fact decreased upon the addition of an insulating moiety. This also points this chapter in the direction to study the phosphines with the greatest difference in electronics, *i.e.*, the phosphines with two and three methylene spacers.

This chapter aims to answer two fundamental questions. First, do the fluorous phosphine ligands stabilize the polyynediyl chain complexes and/or redox derivatives thereof? In this context, phase separation of the fluorous domain might envelop the polyyne chain, as depicted in Figure 3.12. Second, what effect do the methylene spacers have on the electrochemical properties of the platinum center? In this context, oxidations to mixed-valent radical cations will be studied.

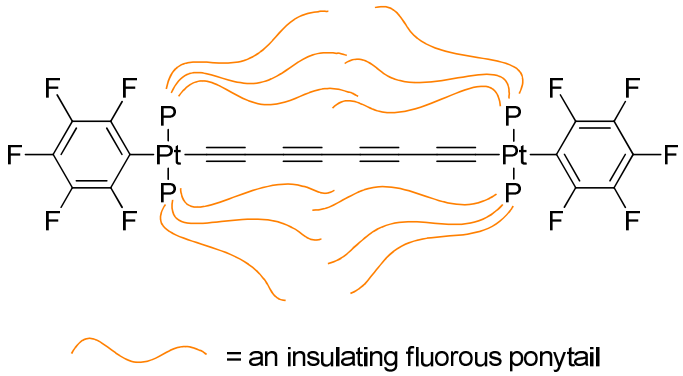

Figure 3.12. Possible enveloping of the polyyne chain by phase separation of fluorous ponytails on the phosphine ligands.

A previous study examined an octatetraynediyl complex of the type **B** (Figure 3.8) in which the helical sp^3 carbon chain incorporated a fluorous segment, as shown in Figure 3.13. Spectroscopic data, which included ^1H and $^{31}P\{^1H\}$ NMR, supported the

proposed structure.[84] However, it could only be characterized in situ, as all workup attempts gave insoluble oligomers. Thus, no crystal structure or electrochemical data were obtained.

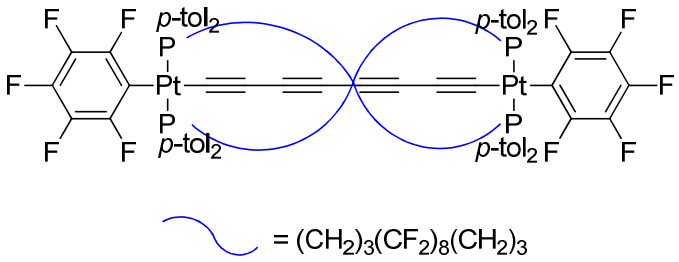

Figure 3.13. Previously reported polyyne chain complex bearing two fluorinated alkyl chain moieties.

The synthetic chemistry needed to access the title compounds involves a chloride bridged platinum dimer (**6**),[109] which is ultimately synthesized from K_2PtCl_4 in a three step process, as shown in Scheme 3.5. Commercially available K_2PtCl_4 and tetrahydrothiophene (THT) are combined in water and acetone to give the resulting yellow solid, $(THT)_2PtCl_2$ as a mixture of *cis* and *trans* isomers. The next step involves the reaction with C_6F_5Li to give a mixture of *cis* and *trans*-$(THT)_2Pt(C_6F_5)_2$. The final step involves a reaction with commercially available $PtCl_2$ to give **6** as a mixture of *syn*- and *anti*- isomers.[109]

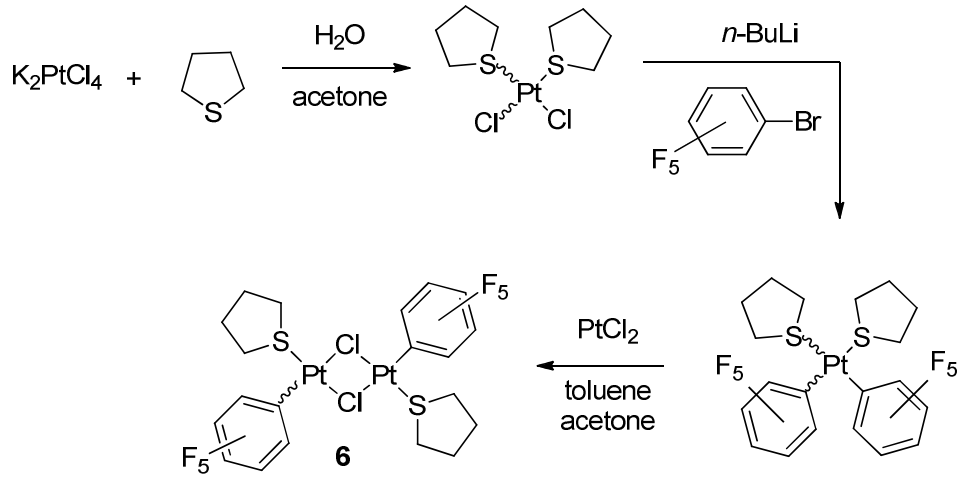

Scheme 3.5. Synthesis of the platinum dimer **6.**

The syntheses of the fluorous phosphines **7a**,[110] **7b**,[111] and **7c**[111] from triethyl phosphite have previously been described and are shown in Scheme 3.6. Upon going from **7a** to **7b**, an extra methylene spacer is added, and upon going from **7b** to **7c**, the R_{fn} moiety is lengthened or made "more fluorous." An alternative synthesis involving PH_3 gas as the starting material is also possible,[112] however this route is willingly avoided to circumvent the complications and dangers encountered with the use of PH_3. Also, neither of these methods can be applied to fluorous phosphines with a single methylene spacer, $(R_{fn}CH_2)_3P$. Hence, there is virtually no coordination chemistry of such ligands known, and they do not play any role in this study.

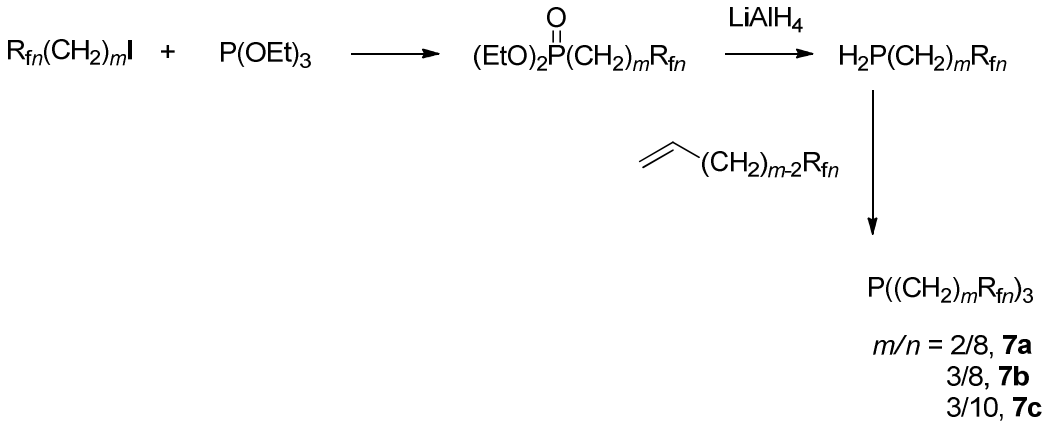

Scheme 3.6. Previously reported syntheses of fluorous phopshines **7a-c.**

RESULTS

1. Fluorous platinum chloride complexes. The fluorous phosphines in Scheme 3.6 are soluble in fluorous solvents and insoluble in most organic solvents with the exception of THF. The phosphines are stable in air as solids but readily oxidize in air when in solution. As shown in Scheme 3.7, the phosphines were combined with **6** in a four to one molar ratio (i.e., two phosphines per platinum atom) in THF. Reflux and workup afforded the platinum chloride complexes **8a-c**.

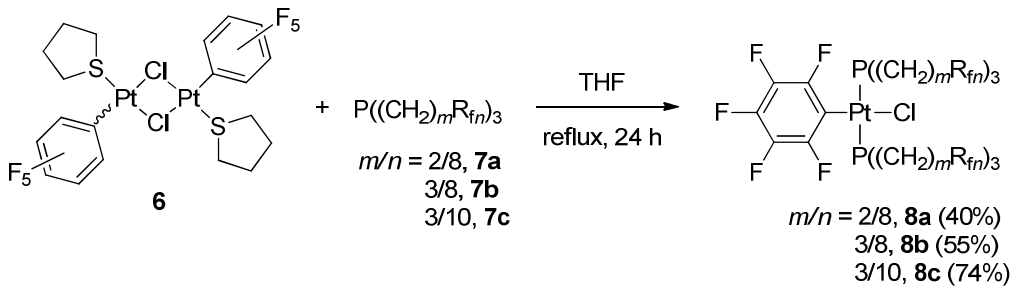

Scheme 3.7. Syntheses of the fluorous platinum chloride complexes **8a-c.**

The platinum chloride complexes **8a-c** are air stable white powders and can be isolated in good yields (40-74%). They are insoluble in organic solvents such as CH_2Cl_2 and acetone. For this reason, perfluorobenzene (C_6F_6) was used as an NMR solvent. A cosolvent ($CDCl_3$) was needed for a deuterium lock. All new complexes were characterized by NMR (^1H, $^{13}C\{^1H\}$, and $^{31}P\{^1H\}$) and IR spectroscopies and microanalyses. The $^{31}P\{^1H\}$ NMR spectra show typical $^1J_{PPt}$ coupling constants, indicating *trans* coordination to the platinum metal center.[113] The $^{31}P\{^1H\}$ NMR data are summarized in Table 3.3.

Table 3.3. $^{31}P\{^1H\}$ data (δ, ppm) for the fluorous platinum chloride complexes.

	$^{31}P\{^1H\}$ NMR ($^1J_{PPt}$, Hz)
8a	11.2 (2628)[a]
8b	9.6 (2550)[a]
8c	10.1 (2324)[b]

[a] in C_6F_6. [b] in $C_6F_6/CDCl_3$.

Single crystals of **8b** were grown, and the X-ray structure determined as described in the experimental section. Three of the six $(CH_2)_3R_{f8}$ chains in **8a** were disordered (chains 2, 3, and 6; see chain designations in Figure 3.14). The dominant conformations are shown in all plots and diagrams. The minor chain conformations are not considered in the analysis. Key crystallographic bond lengths and angles are given in Table 3.4. Thermal ellipsoid diagrams are shown in Figure 3.14, a space filling representation in Figure 3.15, and a packing diagram Figure 3.16. The space filling model in Figure 3.15 illustrates that the fluorous domains and non-fluorous domains phase separate in the crystal lattice.

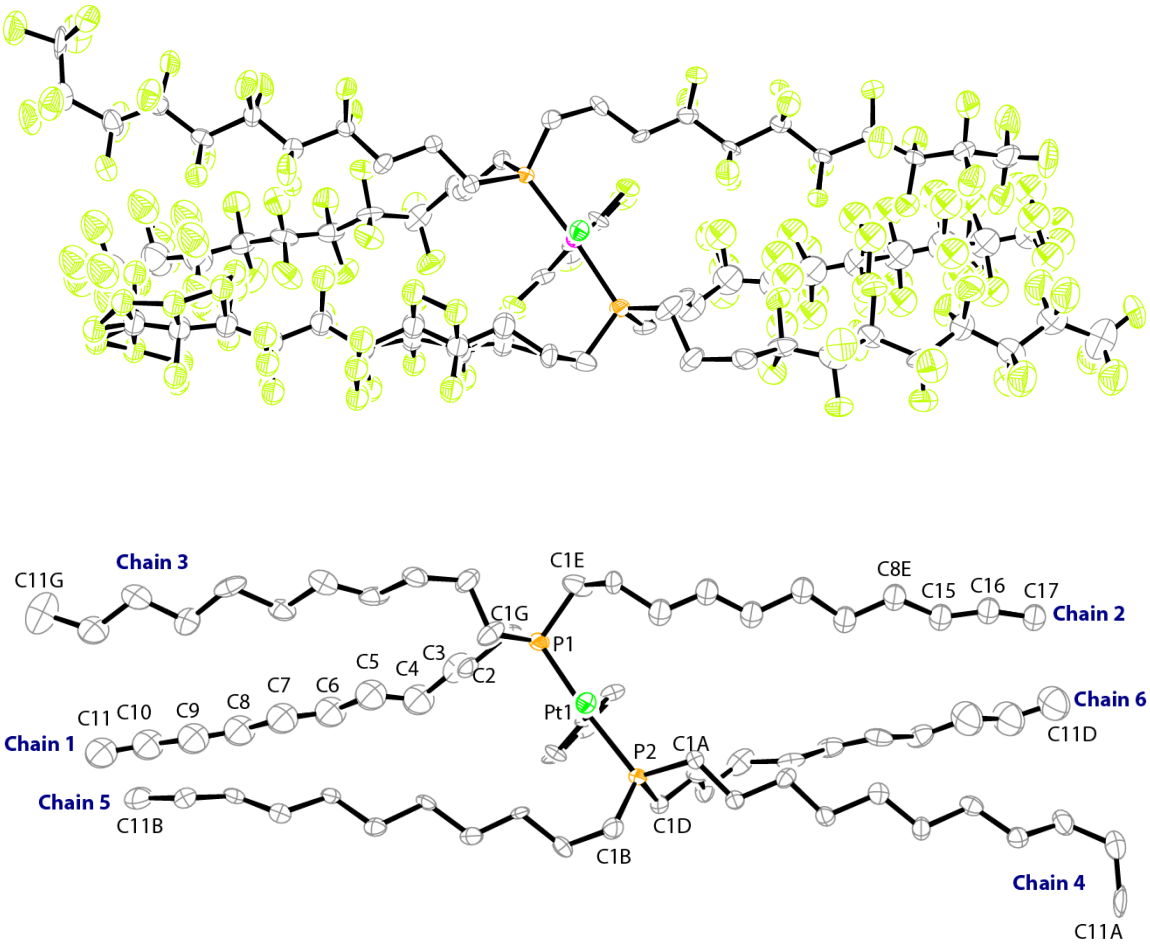

Figure 3.14. Thermal ellipsoid plots (50% probability level) of the dominant configuration of **8b**: view down the Cl-Pt axis (top) and with fluorine atoms omitted for clarity (bottom). Key bond lengths around the phosphorous atoms: Pt1-P2 2.302(4), P2-C1B 1.840(15), P2-C1A 1.833(14), P2-C1D 1.849(15), Pt1-P1 2.312(4), P1-C1 1.772(18), P1-C1G 1.805(17), P1-C13 1.865(17).

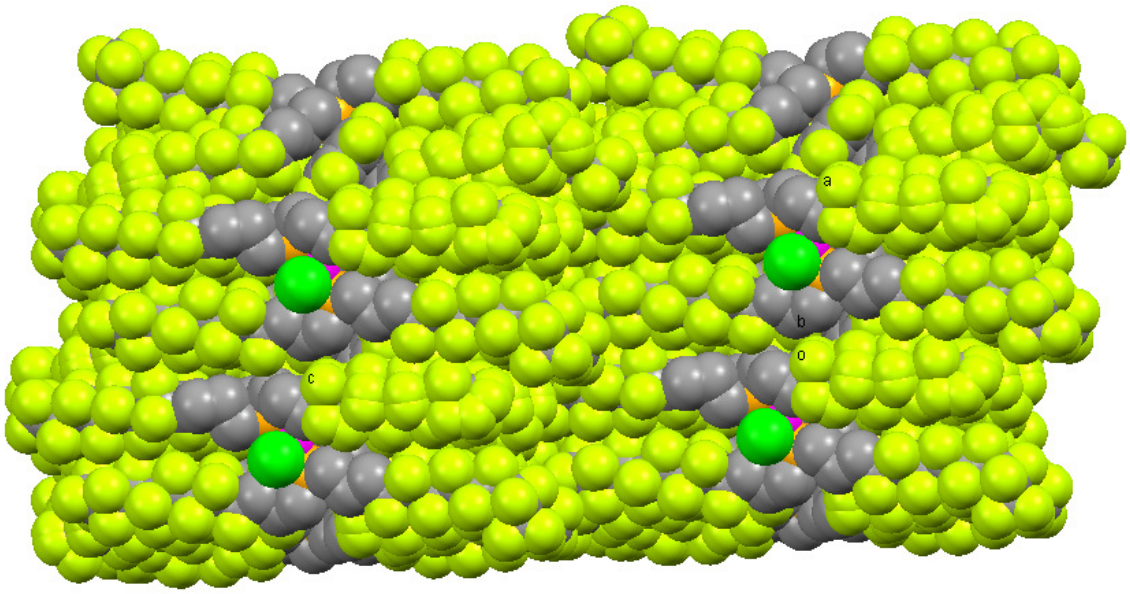

Figure 3.15. Space filling model of the dominant configuration of **8b** with fluorine atoms in yellow-green, chlorine atoms in green, platinum atoms in pink, and carbon atoms in gray.

The packing diagram in Figure 3.16 demonstrates that the C_6F_5 rings of neighboring molecules tend to aggregate in the crystal lattice. The least squares planes defined by the C_6F_5 rings are parallel (0.00°) and separated by a vertical distance of ca. 2.590 Å. A graphic illustrating this phenomenon and these measurements is offered in Figure 3.17.

Key crystallographic torsion angles are presented in Table 3.5. Most of the four-carbon segments of the alkyl chains exhibit approximately *anti* conformations, as quantified by torsion angles in the range of 162 to 175° (absolute values). However, each chain exhibits one four carbon segment that deviates from this trend, adopting an approximately *gauche* conformation, as quantified by torsion angles (absolute values)

ranging from 54(2)° to 95(3)°. The C-C-C-C torsion angles in the R_{f8} chains are slightly less than 180°. This is in accord with studies that have shown that these torsion angles in a perfluorinated chain are less than those in the corresponding *n*-alkane.[114] The torsion angles propagate in the same directional sense to give helical poly(difluoromethylene) segments as observed in the crystal structure.

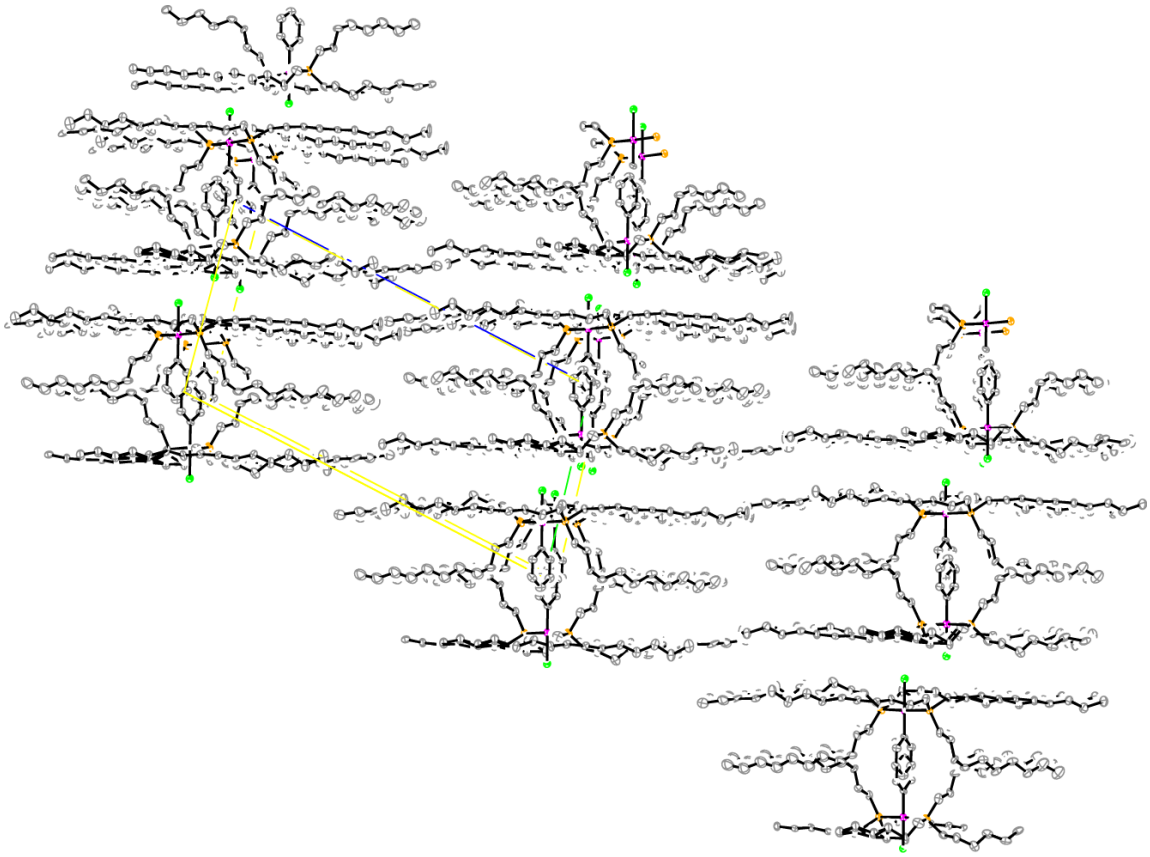

Figure 3.16. Packing diagram of the dominant configuration of **8b** with fluorine atoms omitted for clarity.

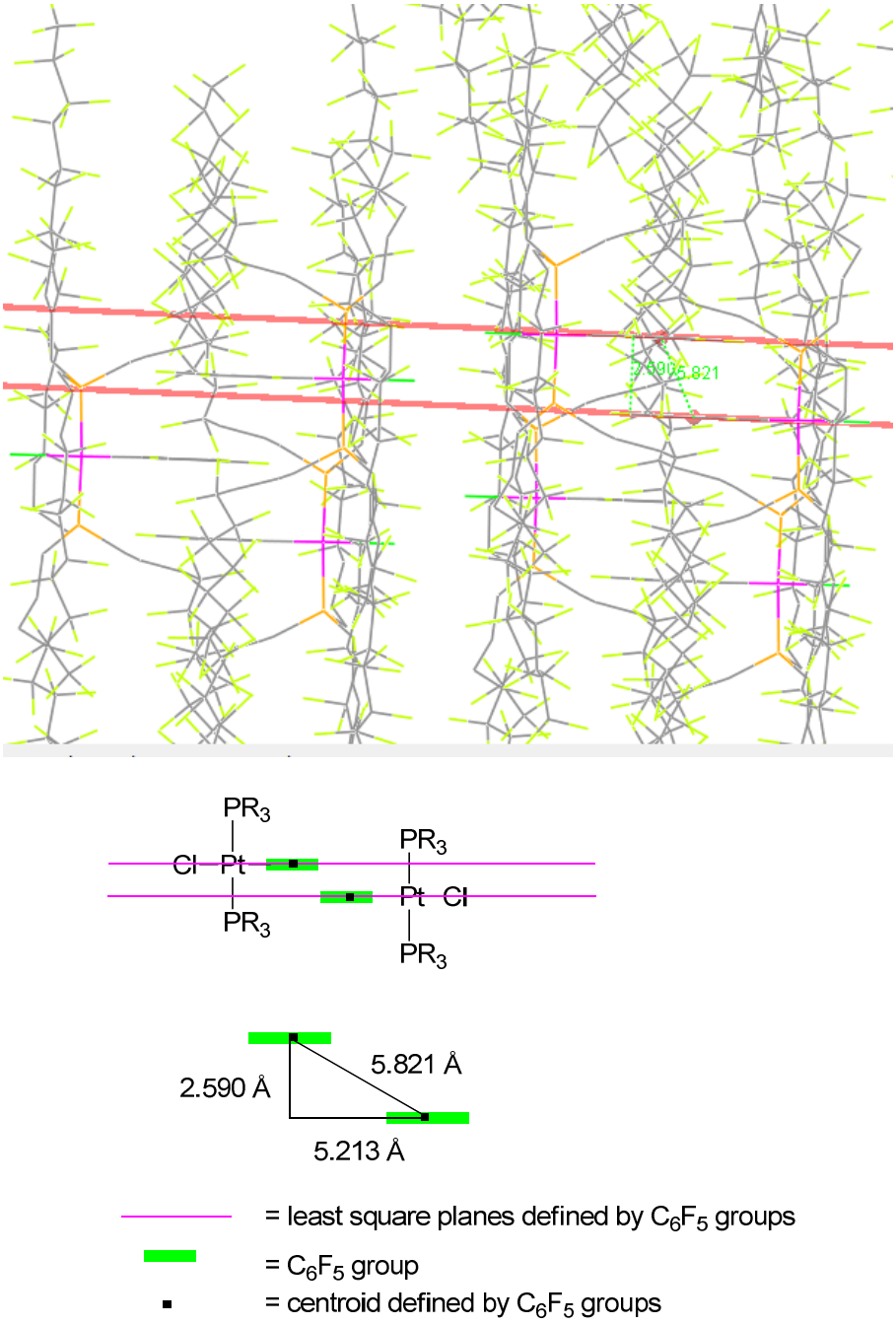

Figure 3.17. Schematic representations of the geometric relationships involving the C_6F_5 rings in **8b**.

Table 3.4. Key crystallographic distances [Å] and angles [°] for **8b**.[a]

Chain 1		Chain 2	
C1–P1	1.772(18)	C1E–P1	1.865(17)
C1–C2	1.57(2)	C1E–C2E	1.51(2)
C2–C3	1.52(2)	C2E–C3E	1.50(3)
C3–C4	1.51(2)	C3E–C4E	1.45(3)
C4–C5	1.47(3)	C4E–C5E	1.50(3)
C5–C6	1.50(2)	C5E–C6E	1.50(3)
C6–C7	1.54(3)	C6E–C7E	1.50(2)
C7–C8	1.54(3)	C7E–C8E	1.49(2)
C8–C9	1.55(3)	C8E–C15	1.42(2)
C9–C10	1.49(3)	C15–C16	1.31(2)
C10–C11	1.54(3)	C16–C17	1.30(2)
C2–C1–P1	112.7(13)	C2E–C1E–P1	114.3(12)
C3–C2–C1	113.9(15)	C3E–C2E–C1E	124.4(18)
C4–C3–C2	117.0(15)	C4E–C3E–C2E	115(2)
C5–C4–C3	116.6(15)	C3E–C4E–C5E	119(2)
C4–C5–C6	117.6(15)	C4E–C5E–C6E	123.8(19)
C5–C6–C7	116.9(14)	C7E–C6E–C5E	120.7(17)
C6–C7–C8	115.4(14)	C8E–C7E–C6E	120.2(16)
C7–C8–C9	116.2(15)	C15–C8E–C7E	129.4(15)
C10–C9–C8	116.5(16)	C16–C15–C8E	145.2(13)
C9–C10–C11	123(2)	C17–C16–C15	159.7(13)
Chain 3		Chain 4	
C1G–P1	1.805(17)	C1A–P2	1.833(14)
C1G–C2G	1.54(2)	C1A–C2A	1.54(2)
C2G–C3G	1.52(2)	C2A–C3A	1.50(2)
C3G–C4G	1.48(3)	C3A–C4A	1.50(2)
C4G–C5G	1.39(3)	C4A–C5A	1.57(2)
C5G–C6G	1.44(3)	C5A–C6A	1.50(2)
C6G–C7G	1.46(3)	C6A–C7A	1.56(2)
C7G–C8G	1.44(3)	C7A–C8A	1.53(2)
C8G–C9G	1.36(3)	C8A–C9A	1.50(2)
C9G–C10G	1.41(3)	C9A–C10A	1.57(3)
C10G–C11G	1.35(3)	C10A–C11A	1.52(3)
C2G–C1G–P1	115.4(11)	C2A–C1A–P2	116.4(1)

[a] chains are numbered as given in Figure 3.14.

Table 3.4 (Continued)

C3G–C2G–C1G	110.7(14)	C3A–C2A–C1A	111.4(12)
C4G–C3G–C2G	113.5(17)	C4A–C3A–C2A	112.4(12)
C5G–C4G–C3G	125.8(18)	C3A–C4A–C5A	113.2(12)
C4G–C5G–C6G	128.7(19)	C6A–C5A–C4A	117.7(13)
C5G–C6G–C7G	128(2)	C5A–C6A–C7A	116.5(13)
C8G–C7G–C6G	131.3(19)	C8A–C7A–C6A	116.4(13)
C9G–C8G–C7G	136.6(19)	C9A–C8A–C7A	117.2(14)
C8G–C9G–C10G	143.4(19)	C8A–C9A–C10A	120.1(16)
C11G–C10G–C9G	148.7(17)	C11A–C10A–C9A	117.9(15)
Chain 5		Chain 6	
C1B–P2	1.840(15)	C1D–P2	1.849(15)
C1B–C2B	1.50(2)	C1D–C2D	1.50(2)
C2B–C3B	1.51(2)	C2D–C3D	1.53(2)
C3B–C4B	1.46(2)	C3D–C4D	1.49(3)
C4B–C5B	1.53(2)	C4D–C5D	1.52(3)
C5B–C6B	1.54(2)	C5D–C6D	1.54(2)
C6B–C7B	1.53(2)	C6D–C7D	1.54(3)
C7B–C8B	1.54(2)	C7D–C8D	1.54(2)
C8B–C9B	1.51(2)	C8D–C9D	1.50(3)
C9B–C10B	1.49(2)	C9D–C10D	1.39(3)
C10B–C11B	1.50(3)	C10D–C11D	1.36(3)
C2B–C1B–P2	117.4(12)	C2D–C1D–P2	112.8(1)
C1B–C2B–C3B	116.0(13)	C1D–C2D–C3D	111.61(2)
C4B–C3B–C2B	114.5(12)	C4D–C3D–C2D	113.91(3)
C3B–C4B–C5B	117.8(12)	C3D–C4D–C5D	118.91(5)
C4B–C5B–C6B	117.4(12)	C4D–C5D–C6D	118.81(4)
C7B–C6B–C5B	115.8(12)	C7D–C6D–C5D	115.31(4)
C6B–C7B–C8B	115.8(12)	C8D–C7D–C6D	116.11(4)
C9B–C8B–C7B	118.6(14)	C9D–C8D–C7D	118.91(6)
C10B–C9B–C8B	118.8(16)	C10D–C9D–C8D	127(2)
C9B–C10B–C11B	120.0(18)	C11D–C10D–C9D	138(2)

Table 3.5. Key torsion angles [°] for **8b**.[a]

Chain 1		Chain 2	
P1–C1–C2–C3	159.2(12)	P1–C1E–C2E–C3E	74(2)
C1–C2–C3–C4	–79(2)	C1E–C2E–C3E–C4E	95(3)
C2–C3–C4–C5	–166.0(15)	C2E–C3E–C4E–C5E	180(2)
C3–C4–C5–C6	–166.2(15)	C3E–C4E–C5E–C6E	–166(2)
C4–C5–C6–C7	–164.0(15)	C4E–C5E–C6E–C7E	–165(2)
C5–C6–C7–C8	–162.4(15)	C5E–C6E–C7E–C8E	–163.8(18)
C6–C7–C8–C9	–166.5(14)	C6E–C7E–C8E–C15	–175.0(17)
C7–C8–C9–C10	–168.2(15)	C7E–C8E–C15–C16	–172(2)
C8–C9–C10–C11	–172.2(17)	C8E–C15–C16–C17	–171(3)
F1–C4–C5–F4	–166.0(13)	F2E–C4E–C5E–F3E	–67(2)
F2–C4–C5–F4	79.1(17)	F1E–C4E–C5E–F3E	–174.1(18)
F1–C4–C5–F3	–50.4(17)	F2E–C4E–C5E–F4E	–168.9(17)
F2–C4–C5–F3	–165.3(13)	F1E–C4E–C5E–F4E	83.7(19)
F4–C5–C6–F6	–49.9(19)	F3E–C5E–C6E–F5E	–155.5(17)
F3–C5–C6–F6	–164.3(13)	F4E–C5E–C6E–F5E	–54(2)
F4–C5–C6–F5	–166.8(14)	F3E–C5E–C6E–F6E	93(2)
F3–C5–C6–F5	78.8(18)	F4E–C5E–C6E–F6E	–165.6(16)
F6–C6–C7–F7	–163.3(14)	F5E–C6E–C7E–F7E	–164.5(16)
F5–C6–C7–F7	–48.1(18)	F6E–C6E–C7E–F7E	–50(2)
F6–C6–C7–F8	80.3(17)	F5E–C6E–C7E–F8E	80.2(19)
F5–C6–C7–F8	–164.5(14)	F6E–C6E–C7E–F8E	–165.6(15)
F7–C7–C8–F9	78.9(17)	F7E–C7E–C8E–F10E	88.7(17)
F8–C7–C8–F9	–165.3(14)	F8E–C7E–C8E–F10E	–156.9(15)
F7–C7–C8–F10	–164.5(13)	F7E–C7E–C8E–F9E	–163.3(14)
F8–C7–C8–F10	–48.6(18)	F8E–C7E–C8E–F9E	–48.9(18)
F9–C8–C9–F12	–165.1(15)	F10E–C8E–C15–F11E	–64.5(15)
F10–C8–C9–F12	78.8(18)	F9E–C8E–C15–F11E	–170.6(12)
F9–C8–C9–F11	–48.7(19)	F10E–C8E–C15–F12E	–162.1(14)
F10–C8–C9–F11	–164.8(13)	F9E–C8E–C15–F12E	91.8(14)
F12–C9–C10–F13	–166.0(17)	F11E–C15–C16–F13E	98.0(11)

[a] chains are numbered as given in Figure 3.14.

Table 3.5. (Continued)

F11–C9–C10–F13	80(2)	F12E–C15–C16–F13E	–166.4(12)
F12–C9–C10–F14	–53(2)	F11E–C15–C16–F14E	–169.5(11)
F11–C9–C10–F14	–167.5(14)	F12E–C15–C16–F14E	–73.9(12)
F13–C10–C11–F17	60(3)	F13E–C16–C17–F15E	44(2)
F14–C10–C11–F17	–49(3)	F14E–C16–C17–F15E	–48(2)
F13–C10–C11–F16	–172.3(19)	F13E–C16–C17–F17E	–80.7(11)
F14–C10–C11–F16	79(2)	F14E–C16–C17–F17E	–173.1(10)
F13–C10–C11–F15	–61(3)	F13E–C16–C17–F16E	175.8(11)
F14–C10–C11–F15	–169.9(18)	F14E–C16–C17–F16E	83.4(11)
Chain 3		Chain 4	
P1–C1G–C2G–C3G	–162.7(12)	P2–C1A–C2A–C3A	151.8(11)
C1G–C2G–C3G–C4G	179.6(15)	C1A–C2A–C3A–C4A	–169.4(12)
C2G–C3G–C4G–C5G	66(3)	C2A–C3A–C4A–C5A	175.1(12)
C3G–C4G–C5G–C6G	154.4(19)	C3A–C4A–C5A–C6A	175.5(13)
C4G–C5G–C6G–C7G	162(2)	C4A–C5A–C6A–C7A	168.7(13)
C5G–C6G–C7G–C8G	173.2(19)	C5A–C6A–C7A–C8A	163.3(13)
C6G–C7G–C8G–C9G	178(2)	C6A–C7A–C8A–C9A	164.5(14)
C7G–C8G–C9G–C10G	169(2)	C7A–C8A–C9A–C10A	165.9(15)
C8G–C9G–C10G–C11G	179(3)	C8A–C9A–C10A–C11A	54(2)
F2G–C4G–C5G–F4G	64(3)	F1A–C4A–C5A–F3A	–71.7(15)
F1G–C4G–C5G–F4G	160(3)	F2A–C4A–C5A–F3A	173.4(11)
F2G–C4G–C5G–F3G	169(2)	F1A–C4A–C5A–F4A	174.8(11)
F1G–C4G–C5G–F3G	–95(3)	F2A–C4A–C5A–F4A	59.9(14)
F4G–C5G–C6G–F6G	–146(3)	F3A–C5A–C6A–F6A	168.3(13)
F3G–C5G–C6G–F6G	116(3)	F4A–C5A–C6A–F6A	–76.5(16)
F4G–C5G–C6G–F5G	122(3)	F3A–C5A–C6A–F5A	51.1(16)
F3G–C5G–C6G–F5G	25(2)	F4A–C5A–C6A–F5A	166.3(12)
F6G–C6G–C7G–F7G	–144(3)	F6A–C6A–C7A–F7A	162.4(12)
F5G–C6G–C7G–F7G	–50(3)	F5A–C6A–C7A–F7A	–83.0(15)
F6G–C6G–C7G–F8G	121(3)	F6A–C6A–C7A–F8A	48.2(16)

Table 3.5. (Continued)

F5G–C6G–C7G–F8G	–146(3)	F5A–C6A–C7A–F8A	162.7(12)
F7G–C7G–C8G–F10G	–178(2)	F7A–C7A–C8A–F10A	166.0(12)
F8G–C7G–C8G–F10G	–86(3)	F8A–C7A–C8A–F10A	–78.4(15)
F7G–C7G–C8G–F9G	75(3)	F7A–C7A–C8A–F9A	50.1(16)
F8G–C7G–C8G–F9G	168(3)	F8A–C7A–C8A–F9A	165.7(12)
F10G–C8G–C9G–F11G	164(2)	F10A–C8A–C9A–F11A	166.4(14)
F9G–C8G–C9G–F11G	–94(2)	F9A–C8A–C9A–F11A	–78.1(17)
F10G–C8G–C9G–F12G	61(2)	F10A–C8A–C9A–F12A	50.3(18)
F9G–C8G–C9G–F12G	163(2)	F9A–C8A–C9A–F12A	165.7(13)
F11G–C9G–C10G–F13G	84.8(19)	F11A–C9A–C10A–F14A	–60.2(19)
F12G–C9G–C10G–F13G	–176.9(16)	F12A–C9A–C10A–F14A	53.3(19)
F11G–C9G–C10G–F14G	–177.5(17)	F11A–C9A–C10A–F13A	55.4(19)
F12G–C9G–C10G–F14G	–79.1(17)	F12A–C9A–C10A–F13A	168.9(14)
F13G–C10G–C11G–F16G	61(3)	F14A–C10A–C11A–F16A	–70.6(19)
F14G–C10G–C11G–F16G	–36(3)	F13A–C10A–C11A–F16A	173.1(14)
F13G–C10G–C11G–F15G	–95.8(18)	F14A–C10A–C11A–F17A	52(2)
F14G–C10G–C11G–F15G	167.4(17)	F13A–C10A–C11A–F17A	–65(2)
F13G–C10G–C11G–F17G	171.3(15)	F14A–C10A–C11A–F15A	169.7(15)
F14G–C10G–C11G–F17G	74.5(15)	F13A–C10A–C11A–F15A	53.4(19)
Chain 5		Chain 6	
P2–C1B–C2B–C3B	–70.1(18)	P2–C1D–C2D–C3D	–165.7(11)
C1B–C2B–C3B–C4B	–166.0(14)	C1D–C2D–C3D–C4D	179.0(14)
C2B–C3B–C4B–C5B	–168.3(13)	C2D–C3D–C4D–C5D	60(2)
C3B–C4B–C5B–C6B	–165.4(13)	C3D–C4D–C5D–C6D	158.7(14)
C4B–C5B–C6B–C7B	–164.2(13)	C4D–C5D–C6D–C7D	168.2(14)
C5B–C6B–C7B–C8B	–163.9(13)	C5D–C6D–C7D–C8D	165.5(13)
C6B–C7B–C8B–C9B	–160.2(14)	C6D–C7D–C8D–C9D	170.0(17)
C7B–C8B–C9B–C10B	–159.9(14)	C7D–C8D–C9D–C10D	174(2)
C8B–C9B–C10B–C11B	–159.1(15)	C8D–C9D–C10D–C11D	176(3)
F2B–C4B–C5B–F3B	–162.6(11)	F1D–C4D–C5D–F4D	159.2(13)

Table 3.5. (Continued)

F1B–C4B–C5B–F3B	–51.7(14)	F2D–C4D–C5D–F4D	47.5(17)
F2B–C4B–C5B–F4B	83.3(13)	F1D–C4D–C5D–F3D	–87.1(17)
F1B–C4B–C5B–F4B	–165.8(11)	F2D–C4D–C5D–F3D	161.2(12)
F3B–C5B–C6B–F5B	86.6(14)	F4D–C5D–C6D–F6D	–80.5(16)
F4B–C5B–C6B–F5B	–159.3(11)	F3D–C5D–C6D–F6D	165.7(13)
F3B–C5B–C6B–F6B	–157.7(11)	F4D–C5D–C6D–F5D	164.0(13)
F4B–C5B–C6B–F6B	–43.6(15)	F3D–C5D–C6D–F5D	50.2(18)
F5B–C6B–C7B–F8B	–164.6(11)	F6D–C6D–C7D–F7D	164.6(13)
F6B–C6B–C7B–F8B	79.9(14)	F5D–C6D–C7D–F7D	–77.2(16)
F5B–C6B–C7B–F7B	–47.1(15)	F6D–C6D–C7D–F8D	47.6(17)
F6B–C6B–C7B–F7B	–162.6(11)	F5D–C6D–C7D–F8D	165.9(13)
F8B–C7B–C8B–F9B	–159.3(13)	F7D–C7D–C8D–F9D	55.9(18)
F7B–C7B–C8B–F9B	83.8(15)	F8D–C7D–C8D–F9D	172.9(15)
F8B–C7B–C8B–F10B	–44.7(16)	F7D–C7D–C8D–F10D	172.7(14)
F7B–C7B–C8B–F10B	–161.6(11)	F8D–C7D–C8D–F10D	–70.3(19)
F9B–C8B–C9B–F12B	–161.5(13)	F9D–C8D–C9D–F12D	–169(2)
F10B–C8B–C9B–F12B	83.7(15)	F10D–C8D–C9D–F12D	77(3)
F9B–C8B–C9B–F11B	–48.1(18)	F9D–C8D–C9D–F11D	–61(2)
F10B–C8B–C9B–F11B	–162.9(12)	F10D–C8D–C9D–F11D	–174.8(18)
F12B–C9B–C10B–F14B	–46.9(19)	F12D–C9D–C10D–F14D	–131(3)
F11B–C9B–C10B–F14B	–160.5(13)	F11D–C9D–C10D–F14D	125(2)
F12B–C9B–C10B–F13B	–161.6(14)	F12D–C9D–C10D–F13D	148(2)
F11B–C9B–C10B–F13B	84.8(17)	F11D–C9D–C10D–F13D	44(3)
F14B–C10B–C11B–F17B	–42(2)	F14D–C10D–C11D–F15D	–2(4)
F13B–C10B–C11B–F17B	69(2)	F13D–C10D–C11D–F15D	74(4)
F14B–C10B–C11B–F15B	–167.5(17)	F14D–C10D–C11D–F17D	145(2)
F13B–C10B–C11B–F15B	–56(2)	F13D–C10D–C11D–F17D	–139(2)
F14B–C10B–C11B–F16B	78(2)	F14D–C10D–C11D–F16D	–110(2)
F13B–C10B–C11B–F16B	–171.1(14)	F13D–C10D–C11D–F16D	–34(2)

2. Fluorous platinum butadiynyl and diplatinum octatetraynediyl complexes. The next step in the syntheses of the target complexes involved

functionalization using butadiyne. As shown in Scheme 3.8, **8a-c** were combined with an excess of butadiyne (ca. 40 equiv.) in the presence of the base $HNEt_2$, trifluorotoluene, and a copper catalyst. The cosolvent trifluorotoluene is regarded as a "hybrid" organic/fluorous solvent,[115] and is often capable of dissolving appreciable concentrations of both fluorous and non-fluorous solutes. The reactants in Scheme 3.8 were poorly soluble in the usual solvent $HNEt_2$, but readily dissolved in the mixture trifluorotoluene/$HNEt_2$.

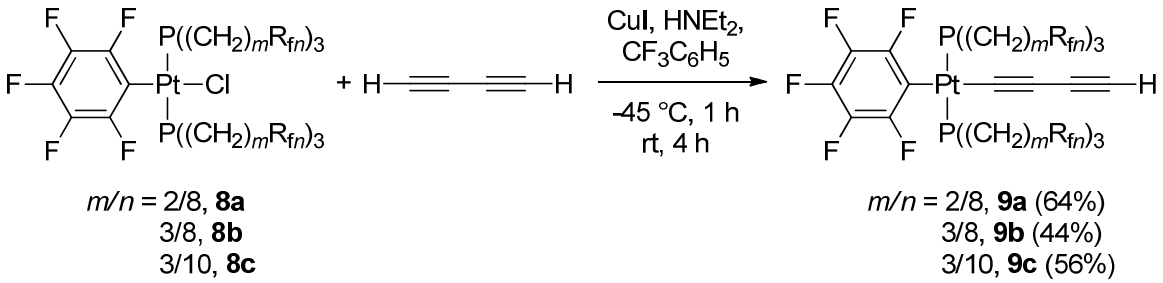

Scheme 3.8. Syntheses of the fluorous platinum butadiynyl complexes **9a-c**.

The resulting platinum butadiynyl complexes **9a-c** are air stable tan powders and were isolated in moderate yields (44-64%). Similar to **8a-c**, the $^{31}P\{^1H\}$ NMR spectra exhibited $^1J_{PPt}$ values typical of *trans* complexes. These data are summarized in Table 3.6. The properties of **9a-c** were similar to those of **8a-c**, but with additional characteristic NMR and IR C≡C signals and NMR ≡CH signals from the butadiyne linkages.

Table 3.6. $^{31}P\{^{1}H\}$ data (δ, ppm; C_6F_6) for the fluorous butadiynyl complexes.

	$^{31}P\{^{1}H\}$ NMR ($^{1}J_{PPt}$, Hz)
9a	9.2 (2535)
9b	8.0 (2470)
9c	9.7 (2520)

To access the title compounds, the butadiynyl complexes **9a-c** were subjected to Hay homocoupling conditions, which involves a copper catalyst in the presence of molecular oxygen. The reactants in Scheme 3.9 readily dissolved in acetone at a slightly elevated temperature (40 °C) so a cosolvent was not required. As shown in Scheme 3.9, the carbon chain complexes **10a-c** were isolated as air stable tan or yellow solids in moderate yields (35-52%) after workup. They were only soluble in fluorous solvents.

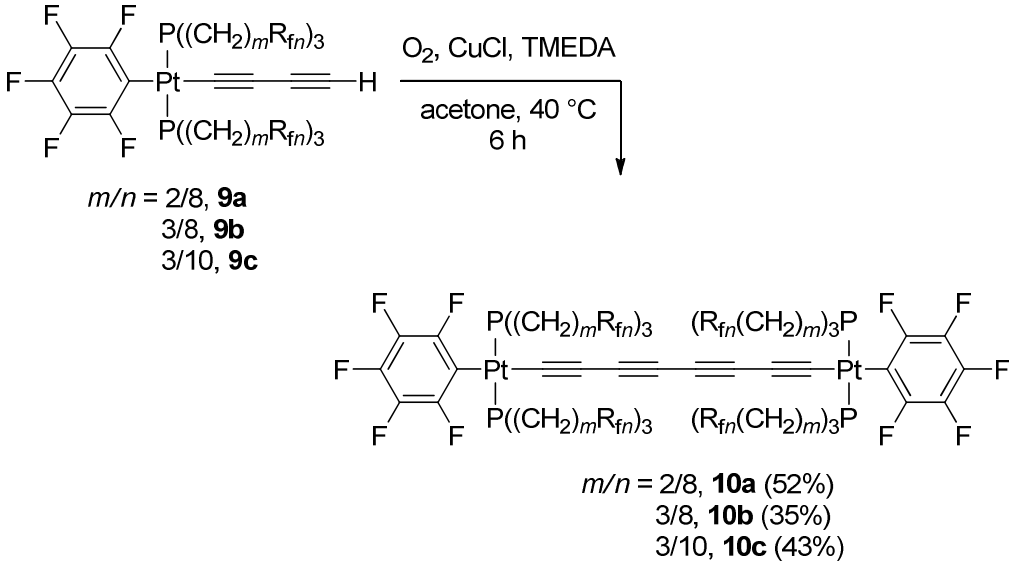

Scheme 3.9. Syntheses of the fluorous diplatinum octatetraynediyl complexes **10a-c**.

As expected, the characteristic ^{1}H NMR signals of **9a-c** disappeared in the octatetraynediyl complexes **10a-c**. The $^{31}P\{^{1}H\}$ NMR data are summarized in Table 3.7. Whereas **9a-c** gave one characteristic $\nu_{C\equiv C}$ band (2153-2152 cm^{-1} (m-w)), **10a-c** exhibited two (2160-2152 cm^{-1} (m-w) and 2029-2037 cm^{-1} (w)).

Table 3.7. $^{31}P\{^{1}H\}$ data (δ, ppm; C_6F_6) for the fluorous diplatinum octatetraynediyl complexes.

	$^{31}P\{^{1}H\}$ NMR ($^{1}J_{PPt}$, Hz)
10a	9.1 (2304)
10b	7.6 (2458)
10c	9.7 (2600)

For all of these complexes, the $^{13}C\{^{1}H\}$ NMR spectra exhibited the expected extended coupling to the ^{19}F nuclei. The $^{13}C\{^{1}H\}$ signals were assigned in accordance with NMR spectra previously reported for fluorous phosphines.[116,117] For instance, the most upfield CH_2 signal was assigned to the P$\underline{C}H_2$ carbon and the most downfield CH_2 signal was assigned to $\underline{C}H_2CF_2$ carbon.[116] Similarly, the most upfield CF_2 signal was assigned to the $\underline{C}F_2CH_2$ carbon.[117]

3. Partition coefficients. The partition coefficients of the free phosphines and complexes **8a-c**, **9a-c**, and **10a-c** were measured as described in the experimental section[118] and are summarized in Table 3.8. The free phosphines show that elongating the R_{fn} moiety slightly increases the relative solubility in the fluorous phase, a trend expected when making the chain more "fluorous." Not surprisingly, the corresponding platinum complexes show similar behavior; *i.e.*, they are preferentially soluble in the fluorous solvent, $CF_3C_6F_{11}$, rather than the non-fluorous solvent, toluene. Although only

slight, the differences in partition coefficients between the free phosphines and the phosphine complexes demonstrate a familiar theme: employing multiple fluorous units in one molecule increases the partition coefficient with respect to a single unit. This phenomenon can be summarized by the phrase "the sum is greater than the parts," which has been previously observed in other metal complexes of fluorous ligands.[119]

Table 3.8 Partition coefficients of fluorous phosphines and complexes.

phosphine	$CF_3C_6F_{11}$:toluene
7a	>99.7:<0.3[108]
7b	98.8:1.2[108]
7c	>99:<1
8a	>99:<1
8b	>99:<1
8c	>99:<1
9a	>99:<1
9b	>99:<1
9c	>99:<1
10a	>99:<1
10b	>99:<1
10c	>99:<1

4. Electrochemistry. Next, the oxidative stabilities of the title compounds were probed. Cyclic voltammograms were recorded under the conditions detailed in the

experimental section and the results are depicted in Figures 3.18-3.20. Measurements were made in a mixture of acetonitrile and trifluorotoluene, with the latter cosolvent needed for solubility purposes. Each complex showed an oxidation or anoidic peak as summarized in Table 3.9, but no follow-up reduction or cathodic peak, for an apparent $i_{c/a}$ value of zero. This indicates a rapid decomposition of the initial oxidation product. Although the apparent oxidation potentials are similar, that of **10b** is less positive than **10a**, suggesting a thermodynamically more favorable oxidation, consistent with the trend expected when an additional methylene spacer is added to each of the twelve ponytails.

To probe whether the solvent mixture might have contributed to the lack of reversibility of these oxidations, the non fluorous analogue **1** (see Figure 3.5) was assayed under identical conditions. The cyclic voltammogram is shown in Figure 3.21 and these data are included in Table 3.9. It can be observed that a reduction peak is apparent with an $i_{c/a}$ value is 0.27, indicating less reversibility than when measured in CH_2Cl_2, which gave an $i_{c/a}$ value of 0.48 (see Table 3.1). Although the reversibility is decreased in the acetonitrile/trifluorotoluene mixture, it is still apparent. However, this indicates that the solvent may play some role in the absence of any reversibility with **10a-c**.

Table 3.9. Cyclic voltammetry data for the fluorous and non-fluorous diplatinum octatetraynediyl complexes.[a]

complex	$E_{p,a}$ (V)	$E_{p,c}$ (V)	E° (V)	ΔE (mV)	$i_{c/a}$
10a	1.148	-	-	-	0
10b	1.019	-	-	-	0
10c	1.144	-	-	-	0
1	1.251	1.207	1.229	44	0.27

[a] conditions: scan rate 100 mV/s in 50:50 v/v acetonitrile/trifluorotoluene under conditions described in the experimental section.

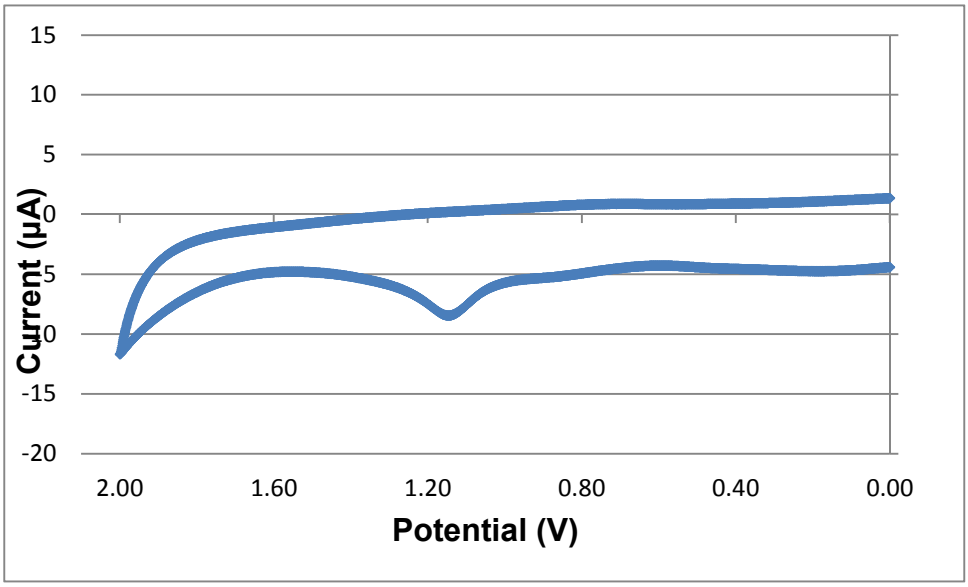

Figure 3.18. Cyclic voltammogram of **10a** under the conditions in Table 3.9.

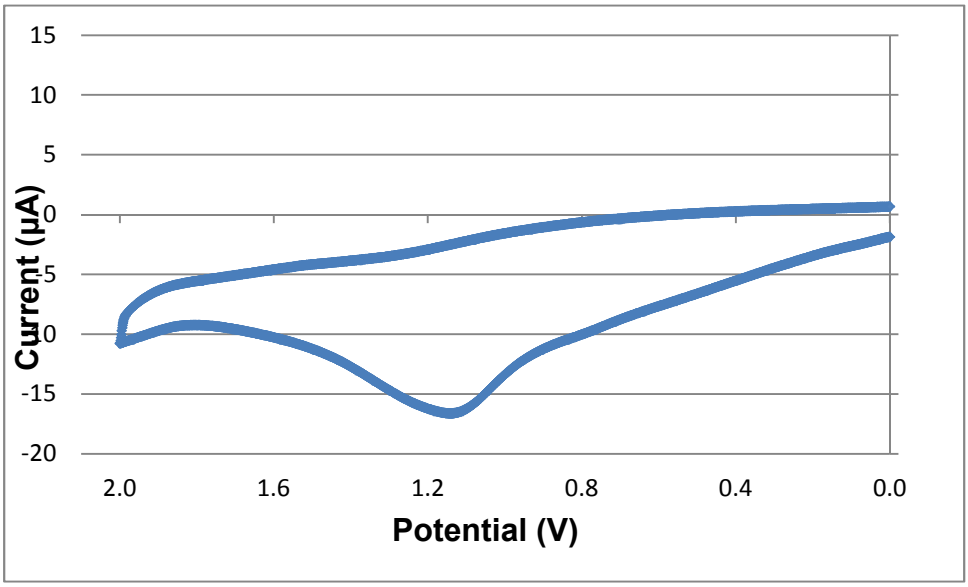

Figure 3.19. Cyclic voltammogram of **10b** under the conditions in Table 3.9.

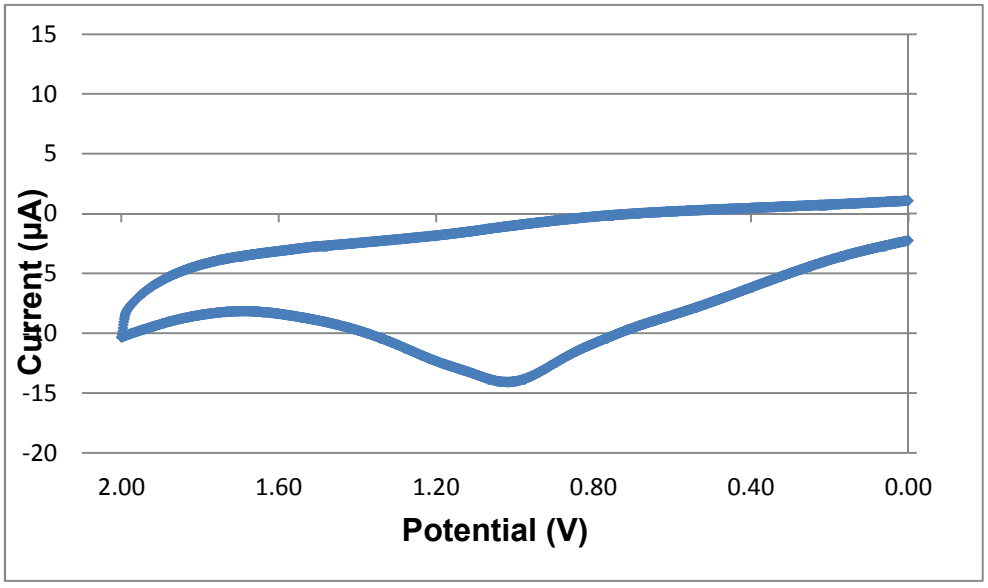

Figure 3.20. Cyclic voltammogram of **10c** under the conditions in Table 3.9.

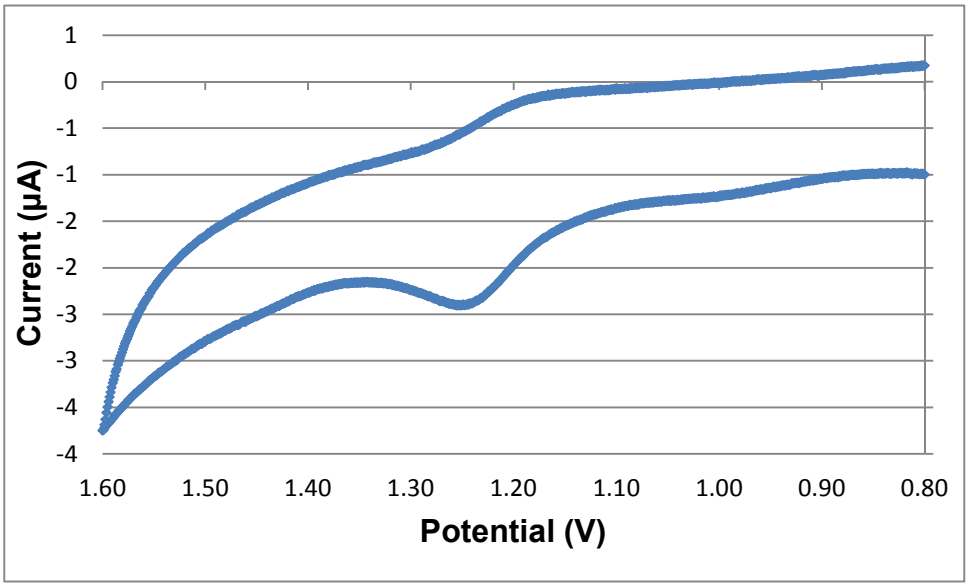

Figure 3.21. Cyclic voltammogram of **1** under the conditions in Table 3.9.

DISCUSSION

1. Biphasic nature of title compounds. The unusual phase properties of fluorous solutes and solvents – and in particular the biphasic mixture commonly obtained with fluorous and organic solvents (see Figure 3.9) – proved to be helpful in the isolation of the fluorous platinum complexes described herein. For both the introduction of the butadiyne ligand and the homocoupling reactions shown in Schemes 3.8 and 3.9, the catalyst mixture can easily be separated from the products by a biphasic extraction. The copper species is preferentially soluble in CH_2Cl_2 and the product in perfluorohexanes. The separation was attempted using toluene, but CH_2Cl_2 proved to be more efficient at removing the catalyst. Figure 3.22 shows the biphasic nature of catalyst removal.

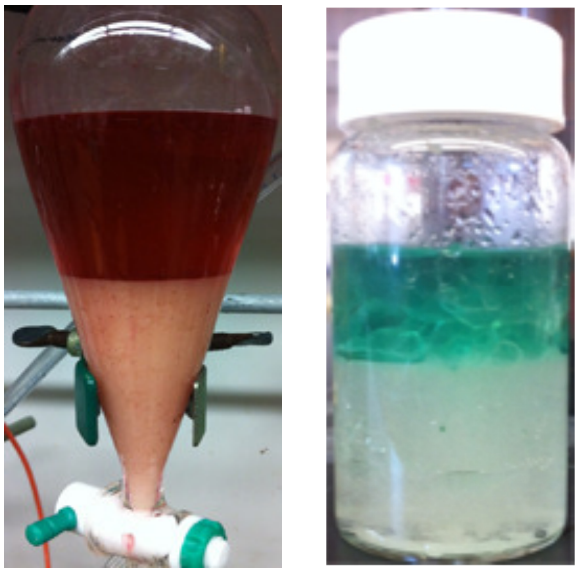

Figure 3.22. Biphasic separation of catalytic species in CH_2Cl_2 (top layers) and fluorous platinum complexes in perfluorohexanes (bottom layers). Left, workup of **9a** in Scheme 3.8. Right, workup of **10a** in Scheme 3.9.

2. Electrochemistry. The cyclic voltammetry data show that the oxidation products of the carbon chain complexes **10a-c** are not inherently stable, since no discernible reduction was observed. A comparison to non-fluorous model complexes **11a** and **11b**, illustrated in Figure 3.23, gives insight into the role of the fluorous ponytails. Complexes **11a** and **11b** feature butadiynediyl and octatetraynediyl chains. The cyclic voltammetry data for these complexes are summarized in Table 3.10.[51] In general, shorter chains are thermodynamically less difficult to oxidize and can exhibit far more reversible couples. The $E_{p,a}$ value of **11a** can be compared to those of the fluorous octatetraynediyl complexes **10a-c**. Surprisingly, the latter appeared to be more readily oxidized thermodynamically, in contrast to the expectations from the IR data in Table 3.2. It is well known that the $E_{p,a}$ values of complexes with highly irreversible couples are not very reliable, and perhaps this accounts for the counterintuitive trend. In any

case, unlike the polyynediyl complexes **11a** and **11b**, the fluorous analogues **10a-c** could not to any extent be reversibly oxidized, indicating an inherent instability introduced by the fluorous moieties. Perhaps the CH_2CF_2 linkages help initiate an ECE process, with one possibility being via HF elimination from an activated CH_2CF_2 moiety.[120]

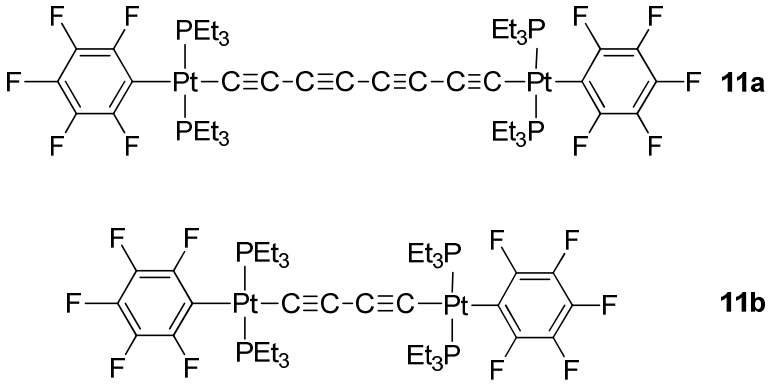

Figure 3.23. Non-fluorous polyynediyl complexes with trialkyl phosphine ligands.

Table 3.10. Cyclic voltammetry data for non-fluorous diplatinum polyynediyl complexes.[a]

complex	$E_{p,a}$ (V)	$E_{p,c}$ (V)	$i_{c/a}$
11a	1.313	1.220	0.42
11b	1.035	0.957	0.91

[a] conditions: 7-9 × 10^{-4} M in substrate in CH_2Cl_2, *n*-Bu_4N^+ BF_4^- as the electrolyte; Pt working and counter electrodes, potential vs. Ag wire pseudoreference; scan rate 100 mV/s.

However, there is precedent for only a modest effect of a fluorous ponytail upon a redox potential of a donor ligand. As shown in Figure 3.24, bipy ligands were functionalized at the 4-positions with fluorous ponytails that incorporated two methylene spacers (**12b-d**). These were compared to non-fluorous analogues bearing hydrogen (**12a**), methyl (**12e**), or *n*-nonyl (**12f**) substituents at the 4-positions. Table 3.11 summarizes the cyclic voltammetry data for these ligands.[121]

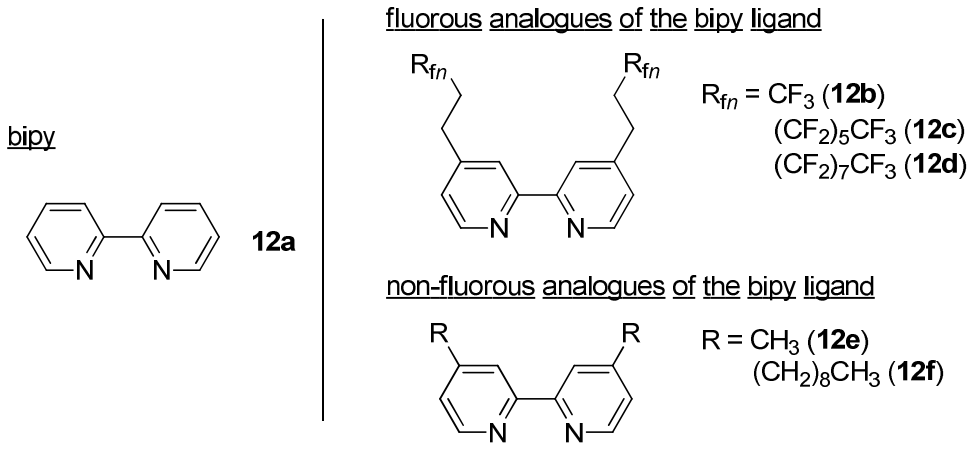

Figure 3.24. Bennett's fluorous (top right) and non-fluorous (bottom right) analogues of the bipy ligand (left).

Table 3.11. Cyclic voltammetry data for disubstituted bipy ligands.[a]

ligand	$E_{1/2}$ (V)	ΔE_p (mV)[b]
12a	–2.405	260
12b	–2.404	239
12c	–2.407	291
12d	–2.405	288
12e	–2.494	253
12f	–2.501	299

[a] conditions: ferrocene/ferrocenium couple as a reference, scan rate 10V/s, *n*-Bu_4N^+ PF_6^- as the electrolyte. [b] separation of cathodic and anodic peaks.

Table 3.11 shows that the half wave potentials of the fluorous bipy ligands are similar to those of the unsubstituted analogue **12a**. Furthermore, lengthening of the fluorous R_{fn} moiety did not have a significant effect upon the half wave potentials, as evidenced by the data for **12b-d**. This would seem to indicate that the inductive effect of a R_{fn} moiety is not very different from that of a CF_3 group. Furthermore, the inductive effects of $CH_2CH_2R_{fn}$ groups at the 4-positions in these compounds are not very different from those of hydrogen atoms, at least with respect to the electroactive center.

3. Crystal structures. Although no crystals were obtained for the title compounds **10a-c**, the crystal structure of **8b** does prove to be very informative, particularly in terms the packing motifs demonstrated in Figure 3.17. A similar platinum complex, synthesized by Gorun in 1999, is shown in Figure 3.25.[122] This complex has the formula *trans*-$((R_{f6}CH_2CH_2)_3P)_2PtCl_2$ and features an analogous fluorous phosphine with a shorter R_{fn} segment and the same number of methylene spacers. Thus, the X-ray crystal structure of **8b** provides a valuable compliment to the growing number of structurally characterized complexes with fluorous phosphine ligands.[104,123-139]

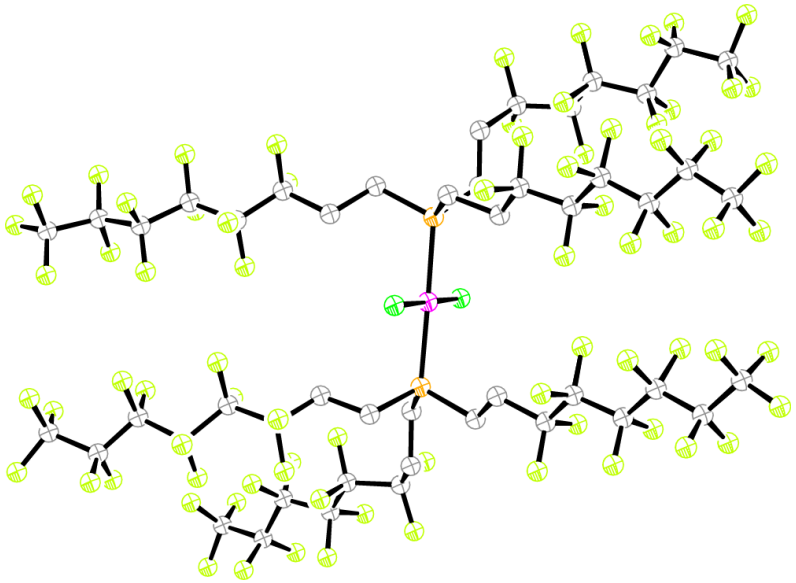

Figure 3.25. Thermal ellipsoid plot (50% probability level) of Gorun's fluorous platinum chloride complex of the formula *trans*-$((R_{f6}CH_2CH_2P)_3)_2PtCl_2$.

A literature search in the Cambridge Structural Database revealed only two complexes of the formula $(C_6F_5)(R_3P)_2PtCl$ where R does not represent an aromatic moiety. In 1978, Randaccio reported the crystal structure of *cis*-$(C_6F_5)(Et_3P)_2PtCl$[140] and in 2004, Hughes described the crystal structure of *cis*-(C_6F_5)(dmpe)PtCl (dmpe = 1,2-dimethylphosphinoethane).[141] Thus, **8b** represents the first *trans*-$(C_6F_5)(PR_3)_2PtCl$ type complex where R does not represent an aromatic moiety to be structurally characterized.

CONCLUSION

In summary, this work has expanded the array of diplatinum polyynediyl sp chain complexes synthesized to date. Previous works featured chain protection via sp^3 carbon double helices, rotaxane-derived macrocycles, and alkyl chains. This has now been extended to fluorous alkyl chains. Schemes 3.8 and 3.9 demonstrate that platinum chloride and platinum butadiynyl complexes bearing highly fluorous phosphine ligands are easily accessible. The homocoupling reactions in Scheme 3.10 illustrate that polyyne chains with eight carbons atoms can be realized. The cyclic voltammetry data show that these complexes are irreversibly oxidized in solution, with the oxidation potentials being comparable to the triethylphosphine analogues in Figure 3.22. Oxidation appears to be thermodynamically more favorable than non-fluorous analogues, but there are a number of caveats, and the resulting radical cations are clearly very unstable. In order to achieve reversible or partially reversible oxidations of diplatinum octatetraynediyl complexes with fluorous phosphines, it may be necessary to employ triarylphosphine derivatives (see Figure 3.11) or trialkylphosphines with $CH_2(C(CH_3)_2)R_{fn}$ or similar substituents that lack CH_2CF_2 junctions.

EXPERIMENTAL

General: All reactions were conducted under inert atmospheres using standard Schlenk and vacuum line techniques. Workups were carried out in air. Chemicals were treated as follows: THF (Fisher Scientific, ACS grade), dried and degassed using a Glass Contour solvent purification system; acetone (BDH, ACS grade), distilled from $CaSO_4$; $CDCl_3$ and C_6D_6 (2 × Cambridge Isotope Laboratories), silica (Acros, 60 Å),

trifluorotoluene (Acros, 99+%), C_6F_6 (Oakwood Products), CuI (Alfa Aesar, 99.999%), CuCl (Alfa Aesar, 99.999%), $HNEt_2$ (99+%, Alfa Aesar), acetonitrile (EMD, ACS grade), CH_2Cl_2 (EMD, ACS grade), toluene (Macron Chemicals, ACS grade), perfluorohexanes (Apollo Scientific, 98% mixed isomers), $CF_3C_6F_{11}$ (ABCR, 90%), *n*-Bu_4N^+ PF_6^- (Oakwood Products), TMEDA (tetramethylethylenediamine, 99%, Acros), and Ph_3PO (Aldrich, 98%), used as received.

NMR spectra were recorded on a Varian NMRS 500 MHz spectrometer at ambient probe temperatures and referenced as follows: ^1H: residual internal $CHCl_3$ (δ, 7.26 ppm), C_6D_5H (δ, 7.16 ppm), ^{13}C: internal $CDCl_3$ (δ, 77.20 ppm), C_6F_6 (δ, 138.80 ppm), ^{31}P: external H_3PO_4 (δ, 0.00 ppm). IR spectra were recorded using a Shimadzu IRAffinity-1 spectrometer with a Pike MIRacle ATR system (diamond/ZnSe crystal). Melting points were recorded with a Stanford Research Systems (SRS) MPA100 (Opti-Melt) automated melting point system. Microanalyses were conducted by Atlantic Microlab.

***trans*-$(C_6F_5)((R_{f8}(CH_2)_2)_3P)_2PtCl$ (8a).** A Schlenk flask was fitted with a condenser and charged with $P(CH_2CH_2R_{f8})_3$ (**7a**;[110] 0.1250 g, 0.1292 mmol), [(THT)Pt(C_6F_5)μ-Cl]$_2$ (THT = tetrahydrothiophene) (**6**;[109] 0.6369 g, 0.4641 mmol), and THF (20 mL) with stirring. The mixture was refluxed. After 24 h, the solvent was removed by rotary evaporation. The residue was recrystallized from trifluorotoluene and washed with cold trifluorotoluene. The solid was dried by oil pump vacuum to give **8a** as a white powder (0.3238 g, 0.1030 mmol, 40%), mp 97-100 °C. Anal. Calcd. for $C_{66}H_{24}ClF_{107}P_2Pt$ (3142.21 g/mol): C, 25.23; H, 0.77. Found: C, 25.29; H, 0.61.

NMR (δ (ppm)): ^1H (C_6F_6 + C_6D_6 capillary) 2.65-2.45 (m, 12H, CF_2CH_2), 2.37-2.26 (m, 12H, PCH_2); ^1H (C_6F_6 + $CDCl_3$) 2.75-2.38 (m, 12H, CF_2CH_2), 2.36-2.20 (m,

12H, PCH_2); $^{13}C\{^1H\}$[142] (C_6F_6 + $CDCl_3$) 146.0 (dd, $^1J_{CF}$ = 218.2 Hz, $^2J_{CF}$ = 18.2 Hz, *o* to Pt), 138.5-137.6 (2 m, *m* and *p* to Pt), 121.1 (t, $^2J_{CF}$ = 33.6 Hz, CH_2CF_2),[117] 118.8 (t, $^2J_{CF}$ = 33.3 Hz, CF_3), 116.5 (t, $^2J_{CF}$ = 33.2 Hz, CF_2), 114.2 (t, $^2J_{CF}$ = 33.3 Hz CF_2), 113.6-112.3 (m, CF_2), 111.6-110.2 (m, CF_2), 109.3-108.2 (m, CF_2), 107.1-106.2 (m, CF_2), 26.0-25.3 (m, CH_2CF_2),[116] 17.1-16.8 (m, PCH_2); $^{31}P\{^1H\}$ (C_6F_6) 11.2 (s, $^1J_{PPt}$ = 2628 Hz);[67] $^{31}P\{^1H\}$ (C_6F_6 + $CDCl_3$) 12.2 (s, $^1J_{PPt}$ = 2632 Hz).[67]

IR (cm^{-1}, powder film): 1512 (w), 1458 (w), 1365 (w), 1195 (s), 1149 (s), 1064 (m), 956 (m), 802 (m), 702 (m).

***trans*-$(C_6F_5)((R_{f8}(CH_2)_3)_3P)_2PtCl$ (8b).** A Schlenk flask was fitted with a condenser and charged with $P(CH_2CH_2CH_2R_{f8})_3$ (**7b**;[111] 0.8120 g, 0.5741 mmol), **6** (0.1394 g, 0.1441 mmol),[109] and THF (30 mL) with stirring. The mixture was refluxed. After 24 h, the solvent was removed by rotary evaporation. Trifluorotoluene (30 mL) was added, and the solution was passed through a silica gel plug. The plug was washed with additional trifluorotoluene (50 mL). The solvent was removed from the combined filtrates by oil pump vacuum to give **8b** as a white solid (0.5115 g, 0.1585 mmol, 55%), mp 107-110 °C. Anal. Calcd. for $C_{72}H_{36}ClF_{107}P_2Pt$ (3226.37 g/mol): C, 26.80; H, 1.12. Found: C, 26.71; H, 1.12.

NMR (δ (ppm)): ^1H (C_6F_6 + $CDCl_3$ capillary) 2.35-2.22 (m, 12H, CH_2CF_2), 2.10-2.00 (m, 24H, PCH_2CH_2); $^{13}C\{^1H\}$[142] (C_6F_6) 145.9 (dd, $^1J_{CF}$ = 240.2 Hz, $^2J_{CF}$ = 22.1 Hz, *o* to Pt), 137.8-136.9 (2 m, *m* and *p* to Pt), 120.4-119.0 (m, CH_2CF_2),[117] 118.1-117.1 (m, CF_3), 116.0-114.9 (m, CF_2), 113.5-111.5 (m, CF_2), 111.1-109.0 (m, 2 CF_2), 108.8-107.0 (m, CF_2), 106.2-105.1 (m, CF_2), 31.4-30.7 (m, CH_2CF_2), 21.0-20.5 (m, PCH_2CH_2),[116] 14.6 (s, PCH_2); $^{31}P\{^1H\}$ (C_6F_6) 9.6 (s, $^1J_{PPt}$ = 2550 Hz).[67]

IR (cm^{-1}, powder film): 1504 (m), 1458 (m), 1334 (m), 1196 (s), 1149 (s), 1111 (s), 1064 (m), 1010 (m), 957 (m), 802 (m), 702 (w).

***trans*-$(C_6F_5)((R_{f10}(CH_2)_3)_3P)_2PtCl$ (8c).** A Schlenk flask was fitted with a condenser and charged with $P(CH_2CH_2CH_2R_{f10})_3$ (**7c**;[111] 1.7026 g, 0.9931 mmol), **6** (0.2474 g, 0.2557 mmol),[143] and THF (40 mL) with stirring. The mixture was refluxed. After 24 h, the solvent was removed by rotary evaporation. The residue was dissolved in warm trifluorotoluene. The solution was kept at 3 °C for 18 h. The precipitate was collected by filtration, washed with cold trifluorotoluene, and dried by oil pump vacuum to give **8c** as a white solid (1.4403 g, 0.3764 mmol, 74%), mp 136-139 °C. Anal. Calcd. for $C_{84}H_{36}ClF_{131}P_2Pt$ (3826.46 g/mol): C, 26.37; H, 0.95; F, 65.04. Found: C, 26.61; H, 0.83; F, 64.97.

NMR (δ (ppm)): ^1H (C_6F_6 + $CDCl_3$) 2.44-2.30 (m, 12H, PCH_2), 2.16-2.09 (m, 24H, C$H_2CH_2CF_2$); $^{13}C\{^1H\}$[142] (C_6F_6 + $CDCl_3$) 144.9 (dd, $^1J_{CF}$ = 229.1 Hz, $^2J_{CF}$ = 20.1 Hz, *o* to Pt), 139.1-137.9 (m, *m* and *p* to Pt), 121.1 (t, $^2J_{CF}$ = 36.9, CH_2CF_2),[117] 118.8 (t, $^2J_{CF}$ = 31.5, CF_3), 116.5 (t, $^2J_{CF}$ = 32.6, CF_2), 114.2 (t, $^2J_{CF}$ = 32.6, CF_2), 113.8-112.7 (m, CF_2), 111.8-110.6 (m, 2 CF_2), 109.7-108.3 (m, CF_2), 107.5-106.4 (m, CF_3), 100.7 (t, $^2J_{CF}$ = 27.5, CF_2), 32.9-32.6 (m, CF_2CH_2),[116] 32.4-29.9 (m, PCH_2CH_2), 16.2-15.7 (m, PCH_2); $^{31}P\{^1H\}$ (C_6F_6 + $CDCl_3$) 10.1 (s, $^1J_{PPt}$ = 2324 Hz).[67]

IR (cm^{-1}, powder film): 1504 (w), 1458 (w), 1342 (w), 1203 (bs), 1149 (s), 1072 (m), 956 (w), 887 (w), 663 (w), 640 (w), 516 (s).

***trans*-$(C_6F_5)((R_{f8}(CH_2)_2)_3P)_2Pt(C{\equiv}C)_2H$ (9a).** A Schlenk flask was charged with **8a** (0.6840 g, 0.2177 mmol), CuI (0.1067 g, 0.5603 mmol), $HNEt_2$ (25 mL), and trifluorotoluene (12 mL) with stirring and cooled to –45 °C (acetonitrile/CO_2). A

solution of $H(C{\equiv}C)_2H$ (0.44 g, 8.7 mmol in 2.7 mL THF)[68] was added. After 1 h, the cold bath was removed. The solution turned reddish-brown. After 4 h, the solvents were removed by rotary evaporation. Toluene (20 mL) and CH_2Cl_2 (20 mL) were added. The mixture was extracted with perfluorohexanes (3 × 20 mL). The solvent was removed from the extracts by oil pump vacuum to give **9a** as a tan solid (0.4366 g, 0.1383 mmol, 64%), which yellowed at 117 °C and liquefied at 141 °C. Anal. Calcd. for $C_{70}H_{25}F_{107}P_2Pt$ (3155.81 g/mol): C, 26.64; H, 0.80; F, 64.42. Found: C, 26.92; H, 0.84; F, 64.12.

NMR (δ (ppm)): ^1H (C_6F_6 + $CDCl_3$) 2.58-2.36 (m, 12H, CF_2CH_2), 2.33-2.19 (m, 12H, PCH_2), 1.70 (s, 1H, ≡C*H*); $^{13}C\{^1H\}$[142] (C_6F_6) 149.3 (dd, $^1J_{CF}$ = 217.2 Hz, $^2J_{CF}$ = 20.3 Hz, *o* to Pt), 140.5-139.4 (m, *m* and *p* to Pt), 122.7-121.9 (m, CH_2CF_2),[117] 119.0-118.2 (m, CF_3), 166.7-116.0 (m, CF_2), 114.7-113.9 (m, CF_2), 113.8-112.7 (m, CF_2), 110.2-109.3 (m, CF_2), 109.2-107.9 (m, CF_2), 107.2-106.1 (m, CF_2), 98.5 (s, Pt*C*≡C), 95.1 (s, PtC≡*C*), 71.2 (s, PtC≡C*C*), 59.0 (s, PtC≡CC≡*C*), 27.0-26.5 (m, CH_2CF_2),[116] 17.9-17.4 (m, PCH_2); $^{31}P\{^1H\}$ (C_6F_6) 9.2 (s, $^1J_{PPt}$ = 2535 Hz).[67]

IR (cm^{-1}, powder film): 3311 (w), 2153 (m, $\nu_{C\equiv C}$), 1505 (m), 1451 (m), 1327 (m), 1196 (s), 1142 (s), 1072 (m), 957 (s), 655 (s).

***trans*-$(C_6F_5)((R_{f8}(CH_2)_3)_3P)_3)_2Pt(C{\equiv}C)_2H$ (9b).** A Schlenk flask was charged with **8b** (0.3225 g, 0.09999 mmol), CuI (0.0285 g, 0.135 mmol), $HNEt_2$ (15 mL), and trifluorotoluene (7 mL) with stirring and cooled to –45 °C (acetonitrile/CO_2). A solution of $H(C{\equiv}C)_2H$ (0.19 g, 3.9 mmol, in 1.2 mL THF)[68] was added. After 1 h, the cold bath was removed. The solution turned reddish-brown. After 4 h, the solvents were removed by rotary evaporation. Toluene (20 mL) and CH_2Cl_2 (20 mL) were added. The mixture was extracted with perfluorohexanes (50 mL). The solvent was removed from the

extracts by rotary evaporation and the solid was dried by oil pump vacuum to give **9b** as a tan solid (0.1411 g, 0.04355 mmol, 44%), which yellowed at 115 °C and liquefied at 129 °C. Anal. Calcd. for $C_{76}H_{37}F_{107}P_2Pt$ (3239.97 g/mol): C, 28.17; H, 1.15; F, 62.74. Found: C, 27.90; H, 1.14.

NMR (δ (ppm)): ^{1}H (C_6F_6 + $CDCl_3$) 2.49-2.28 (m, 12H, CF_2CH_2), 2.26-2.03 (m, 24H, PCH_2CH_2), 1.72 (s, 1H, ≡C*H*); $^{13}C\{^1H\}$[144] (C_6F_6) 150.2 (dd, $^1J_{CF}$ = 214.5 Hz, $^2J_{CF}$ = 20.9 Hz, *o* to Pt), 141.6-140.0 (m, *m* and *p* to Pt), 124.1-122.8 (m, CH_2CF_2),[117] 122.1-120.8 (m, CF_3), 120.0-118.6 (m, CF_2), 117.1-115.5 (m, 2 CF_2), 114.7-113.3 (m, CF_2), 112.1-111.4 (m, CF_2), 109.8-109.0 (m, CF_2), 97.2 (s, PtC≡C), 94.5 (s, PtC≡*C*), 72.4 (s, PtC≡C*C*), 61.6 (s, PtC≡CC≡*C*), 35.6-34.3 (m, CH_2CF_2),[116] 27.4-26.1 (m, $CH_2CH_2CF_2$), 18.8 (s, PCH_2); $^{31}P\{^1H\}$ (C_6F_6) 8.0 (s, $^1J_{PPt}$ = 2470 Hz).[67]

IR (cm^{-1}, powder film): 3309 (w), 2152 (m, $\nu_{C\equiv C}$), 1504 (m), 1458 (m), 1334 (m), 1195 (s), 1149 (s), 1111 (s), 956 (m), 825 (m), 702 (m).

***trans*-$(C_6F_5)((R_{f10}(CH_2)_3)_3P)_2Pt(C\equiv C)_2H$ (9c).** A Schlenk flask was charged with **8c** (0.5569 g, 0.1455 mmol), CuI (0.0364 g, 0.1911 mmol), $HNEt_2$ (20 mL), and trifluorotoluene (10 mL) with stirring and cooled to –45 °C (acetonitrile/CO_2). A solution of $H(C\equiv C)_2H$ (0.29 g, 5.8 mmol, in 1.8 mL THF)[68] was added. After 1 h, the cold bath was removed. The solution turned reddish-brown. After 4 h, the solvents were removed by rotary evaporation. Toluene (20 mL) and CH_2Cl_2 (20 mL) were added. The mixture was extracted with perfluorohexanes (2 × 15 mL). The solvent was removed from the extracts by oil pump vacuum to give **9c** as a cream colored solid (0.3131 mmol, 0.08154 mmol, 56%), which yellowed at 112 °C, browned at 130 °C, and liquefied at 135 °C. Anal. Calcd. for $C_{88}H_{37}F_{131}P_2Pt$ (3840.06 g/mol): C, 27.52; H, 0.97. Found: C, 26.83; H, 0.78.[145]

NMR (δ (ppm)): ^{1}H (C_6F_6 + $CDCl_3$) 2.37-2.23 (m, 12H, CH_2CF_2), 2.19-2.03 (m, 24H, PCH_2CH_2), 1.48 (s, 1H, ≡C*H*); ^{13}C{^{1}H}[142] (C_6F_6) 147.8 (dd, $^{1}J_{CF}$ = 244.8 Hz, $^{2}J_{CF}$ = 20.8 Hz, *o* to Pt), 139.0-138.2 (2 m, *m* and *p* to Pt), 121.0 (t, $^{2}J_{CF}$ = 33.3 Hz, CH_2CF_2),[117] 118.8 (t, $^{2}J_{CF}$ = 31.5 Hz, CF_3), 116.5 (t, $^{2}J_{CF}$ = 33.3 Hz, CF_2), 114.2 (t, $^{2}J_{CF}$ = 33.3 Hz, CF_2), 113.8-112.5 (m, CF_2), 111.7-110.0 (m, 2 CF_2), 109.7-108.2 (m, 2 CF_2), 107.3-106.4 (m, CF_2), 99.8 (s, Pt*C*≡C), 92.8 (s, PtC≡*C*), 70.3 (s. PtC≡C*C*), 58.3 (s, ≡*C*H), 32.7-31.6 (m, CH_2CF_2),[116] 21.8 (t, $^{2}J_{CF}$ = 15.5 Hz, PCH_2CH_2), 15.7 (s, PCH_2); ^{31}P{^{1}H} (C_6F_6) 9.7 (s, $^{1}J_{PPt}$ = 2835 Hz).[67]

IR (cm^{-1}, powder film): 3310 (w), 2924 (w), 2854 (w), 2152 (w, $\nu_{C\equiv C}$), 1743 (w), 1505 (w), 1458 (w), 1373 (w), 1342 (w), 1204 (s), 1150 (s), 1072 (s), 957 (s), 894 (s), 802 (m), 710 (m).

***trans,trans*-(C_6F_5)(($R_{f8}(CH_2)_2)_3P)_2Pt(C≡C)_4(C_6F_5)(P((CH_2)_2R_{f8})_3)_2Pt$ (10a).** A three necked round bottom flask was fitted with a gas dispersion tube and a condenser, and charged with **9a** (0.1021 g, 0.03235 mmol) and acetone (10 mL) with stirring. Then oxygen was aspirated through the mixture. The mixture was heated to 40 °C and a solution of CuCl (0.0140 g, 0.141 mmol) and TMEDA (0.010 mL, 0.0078 g, 0.067 mmol) in acetone (10 mL; previously stirred for 30 min) was added. After 6 h, the solvent was removed by rotary evaporation. Toluene (20 mL) and CH_2Cl_2 (20 mL) were added. The mixture was extracted with perflurohexanes (3 × 15 mL). The solvent was removed from the extracts by oil pump vacuum to give **10a** as a light yellow solid (0.0534 g, 0.00847 mmol, 52%), which yellowed at 120 °C and liquefied at 135 °C. Anal. Calcd. for $C_{140}H_{48}F_{214}P_4Pt_2$ (6309.60 g/mol): C, 26.65; H, 0.77; F, 64.42. Found: C, 26.37; H, 0.72; F, 64.16.

NMR (δ (ppm)): ^{1}H (C_6F_6 + $CDCl_3$) 2.60-2.42 (m, 24H, CF_2CH_2), 2.34-2.21 (m, 48H, PCH_2); $^{13}C\{^{1}H\}$[142] (C_6F_6) 145.6 (dd, $^{1}J_{CF}$ = 221.2 Hz, $^{2}J_{CF}$ = 19.8 Hz, *o* to Pt), 137.8-136.9 (m, *m* and *p* to Pt), 117.7-117.0 (m, CH_2CF_2),[117] 115.3-114.3 (m, CF_3), 112.9-112.2 (m, CF_2), 109.9-108.1 (m, CF_2), 107.9-107.0 (m, 2 CF_2), 105.9-105.1 (m, 2 CF_2), 99.5 (PtC≡C), 88.5 (PtC≡C), 57.5 (s, PtC≡CC), 51.5 (s, PtC≡CC≡C), 25.7-25.1 (m, CH_2CF_2),[116] 14.7-14.3 (m, PCH_2); $^{31}P\{^{1}H\}$ (C_6F_6) 9.1 (s, $^{1}J_{PPt}$ = 2304 Hz).[67]

IR (cm^{-1}, powder film): 2160 (w, $\nu_{C\equiv C}$), 2029 (w, $\nu_{C\equiv C}$), 1975 (w), 1504 (m), 1458 (m), 1195 (s), 1149 (s), 1072 (s), 956 (m), 894 (m), 802 (m), 640 (s).

***trans,trans*-$(C_6F_5)((R_{f8}(CH_2)_3)_3P)_2Pt(C\equiv C)_4(C_6F_5)(P((CH_2)_3R_{f8})_3)_2Pt$ (10b).** A three necked round bottom flask was fitted with a gas dispersion tube and a condenser, and charged with **9b** (0.1037 g, 0.03201 mmol) and acetone (10 mL) with stirring. Then oxygen was aspirated through the mixture. The mixture was heated to 40 °C and a solution of CuCl (0.0145 g, 0.147 mmol) and TMEDA (0.010 mL, 0.0078 g, 0.067 mmol) in acetone (5 mL; previously stirred for 30 min) was added. After 6 h, the solvent was removed by rotary evaporation. Toluene (10 mL) and CH_2Cl_2 (10 mL) were added. The mixture was extracted with perfluorohexanes (2 × 15 mL). The solvent was removed from the extracts by rotary evaporation and the residue washed with toluene (10 mL) and CH_2Cl_2 (10 mL). The solid was dried by oil pump vacuum to give **10b** as a light yellow solid (0.0358 g, 0.00553 mmol, 35%), which darkened at 90 °C, liquefied at 107 °C, and blackened at 175 °C. Anal. Calcd. for $C_{152}H_{72}F_{214}P_4Pt_2$ (6477.92 g/mol): C, 28.18; H, 1.12. Found: C, 28.05; H, 1.17.

NMR (δ (ppm)): ^{1}H (C_6F_6 + $CDCl_3$) 2.45-2.37 (m, 24H, PCH_2), 2.22-2.04 (m, 48H, $CH_2CH_2CF_2$); $^{13}C\{^{1}H\}$[142] (C_6F_6) 147.2 (dd, $^{1}J_{CF}$ = 216.4 Hz, $^{2}J_{CF}$ = 24.1 Hz, *o* to Pt), 138.5-137.5 (m, *m* and *p* to Pt), 121.2-120.1 (m, CH_2CF_2),[117] 118.6-117.9 (m,

CF_3), 116.6-115.5 (m, *C*F_2), 113.7-112.2 (m, *C*F_2), 111.3-110.0 (m, 2 *C*F_2), 109.1-108.0 (m, 2 *C*F_2), 106.9-105.6 (m, *C*F_2), 96.7 (s, Pt*C*≡C), 92.0 (s, PtC≡*C*), 69.4 (s, PtC≡C*C*), 58.5 (s, PtC≡CC≡*C*), 35.6-34.3 (m, *C*H_2CF_2),[116] 27.4-26.1 (m, *C*$H_2CH_2CF_2$), 18.8 (s, P*C*H_2); $^{31}P\{^1H\}$ (C_6F_6) 7.6 (s, $^1J_{PPt}$ = 2458 Hz).[67]

IR (cm^{-1}, powder film): 2152 (m, $\nu_{C\equiv C}$), 2029 (w, $\nu_{C\equiv C}$), 1504 (m), 1458 (m), 1365 (m), 1334 (m), 1195 (s), 1149 (s), 1111 (s), 1064 (m), 1018 (m), 956 (s), 817 (w), 786 (m).

***trans,trans*-$(C_6F_5)((R_{f10}(CH_2)_3)_3P)_2Pt(C\equiv C)_4(C_6F_5)(P((CH_2)_3R_{f10})_3)_2Pt$ (10c).** A three necked round bottom flask was fitted with a gas dispersion tube and a condenser, and charged with **9c** (0.1212 g, 0.03156 mmol) and acetone (10 mL) with stirring. Then oxygen was aspirated through the mixture. The mixture was heated to 40 °C and a solution of CuCl (0.0151 g, 0.154 mmol) and TMEDA (0.010 mL, 0.0078 g, 0.067 mmol) in acetone (5 mL; previously stirred for 1 h) was added. After 6 h, the solvent was removed by rotary evaporation. CH_2Cl_2 (20 mL) was added. The mixture was extracted with perfluorohexanes (3 × 15 mL). The solvent was removed from the extracts by oil pump vacuum to give **10c** as a light yellow solid (0.0520 g, 0.00677 mmol, 43%), which yellowed at 115 °C and liquefied at 133 °C. Anal. Calcd. for $C_{176}H_{72}F_{262}P_4Pt_2$ (7678.10 g/mol): C, 27.53; H, 0.95. Found: C, 26.30; H, 0.73.[145]

NMR (δ (ppm)): ^1H (C_6F_6 + $CDCl_3$) 2.39-2.20 (m, 24H, PCH_2), 2.18-2.01 (m, 48H, CH_2C$H_2$$CF_2$); $^{13}C\{^1H\}$[142] (C_6F_6) 147.0 (dd, $^1J_{CF}$ = 246.1 Hz, $^2J_{CF}$ = 18.9 Hz, *o* to Pt), 138.2-137.5 (2 m, *m* and *p* to Pt), 120.2 (t, $^2J_{CF}$ = 36.0 Hz, CH_2CF_2),[117] 118.0 (t, $^2J_{CF}$ = 27.2 Hz, *C*F_3), 115.7 (t, $^2J_{CF}$ = 27.2 Hz, *C*F_2), 113.9-112.1 (m, 2 *C*F_2), 111.3-109.6 (m, 2 *C*F_2), 108.7-107.9 (m, *C*F_2), 106.5-105.5 (m, *C*F_2), 99.3 (s, Pt*C*≡C), 90.3 (s, PtC≡*C*), 73.7 (s, PtC≡C*C*), 60.3 (s, PtC≡CC≡*C*), 31.7-30.9 (m, *C*H_2CF_2),[116] 21.5-20.6

(m, PCH_2CH_2), 14.9-14.6 (m, PCH_2); $^{31}P\{^1H\}$ ($CF_3C_6F_5$) 10.0 ($^1J_{PPt}$ = 2581 Hz);[67] $^{31}P\{^1H\}$ (C_6F_6) 9.7 ($^1J_{PPt}$ = 2600 Hz).[67]

IR (cm^{-1}, powder film): 2160 (w, $\nu_{C\equiv C}$), 2037 (w, $\nu_{C\equiv C}$), 1975 (w), 1859 (w), 1504 (m), 1458 (m), 1203 (s), 1149 (s), 1072 (m), 979 (m), 956 (m), 894 (m), 802 (m).

Partition Coefficients. A. The following is representative of data in Table 3.4. A vial was charged with the fluorous compound (0.00090-0.00521 mmol), $CF_3C_6F_{11}$ (2.00 mL, delivered by syringe), toluene (2.00 mL, delivered by syringe), and a stir bar. It was tightly sealed and vigorously stirred for 24 h. Stirring was halted. After 10 min, aliquots (1.00 mL) were removed from each phase by syringe. The solvents were removed by rotary evaporation. A standard solution of Ph_3PO in $CDCl_3$ was prepared in a volumetric flask (0.0267 M). To each residue was added C_6F_6 (0.50 mL) and the standard solution (0.50 mL) by syringe. The samples were analyzed by ^1H NMR, integrating the CH_2 signals of the fluorous compound versus the aromatic signals of Ph_3PO.

B. Representative example: The vial was charged with **10c** (0.0069 g, 0.00090 mmol) and $CF_3C_6F_{11}$ (2.00 mL) to give a 4.5×10^{-4} M solution as in A. Addition of toluene (see A) gave a biphase mixture. After stirring and workup, integration indicated 4.43×10^{-4} mmol in the fluorous phase and 8.31×10^{-7} mmol in the toluene phase. After normalization for the aliquot size, this indicated a total mass recovery of 99%.

Cyclic Voltammetry. A BASi Voltammetric Analyzer with the program EpsilonEC (version 2.13.77_USB) was employed. Cells were fitted with a Pt working and counter electrodes, and an Ag/AgCl electrode. All acetonitrile/trifluorotoluene (1:1 v/v) solutions were 1.4-2.5 $\times 10^{-4}$ M in substrate, 0.4 M in *n*-Bu_4N^+ PF_6^-, and prepared under nitrogen.

Crystallography. A C_6F_6 solution of **8b** was layered with toluene and stored at rt. After 12 d, colorless multi-faceted crystals were obtained. Data were collected as outlined in Table 3.11. Cell parameters were obtained from 180 data frames taken at widths of 0.5°. Integrated intensity information for each reflection was obtained by reduction of the data frames with the program APEX2.[71] Data were corrected for Lorentz and polarization factors, and using SADABS[72] for absorption and crystal decay effects. The structure was solved by direct methods using SHELXTL (SHELXS).[73] Three of the six fluorous chains were disordered. The hydrogen atoms were placed in idealized positions and were refined using a riding model. The disorder was successfully modeled using extensive restraints (EADP and EXYZ) to keep the thermal ellipsoids meaningful and for the refinement to converge. The chain with C(E) and C(F) designations was modeled with a 66:34 occupancy ratio. The chain with C(D) and C(I) designations was modeled with a 50:50 occupancy ratio. Part of the chain with C(G) and C(H) designations was modeled with a 69:31 occupancy ratio except C(9)-C(11) of this chain which was modeled with a 53:47 occupancy ratio. All non-hydrogen atoms were refined with anisotropic thermal parameters. The final refinement was restricted to 100 degrees as no reflections were observed above that angle. The parameters were refined by weighted least squares refinement on F^2 to convergence.[73]

Table 3.12. Crystallographic data for **8b**.

Empirical formula	$C_{72}H_{36}ClF_{107}P_2Pt$
Formula weight	3226.49
Temperature	110(2) K
Diffractometer	BRUKER GADDS
Wavelength	1.54178 Å
Crystal system	Triclinic
Space group	*P-1*
Unit cell dimensions	
a	11.4468(16) Å
b	15.504(2) Å
c	30.558(5) Å
α	103.379(16)°
β	95.714(16)°
γ	103.257(11)°
V	5068.2(14) $Å^3$
Z	2
Density (calculated)	2.114 Mg/m^3
Absorption coefficient	5.413 mm^{-1}
F(000)	3112
Crystal size	0.09 x 0.05 x 0.01 mm^3
Theta range for data collection	1.51 to 50.00°
Index ranges	$-11 \le h \le 11, -14 \le k \le 15, -30 \le l \le 30$
Reflections collected	44792
Independent reflections	10107 [R(int) = 0.0830]
Completeness to theta = 50.00°	96.9 %
Max. and min. transmission	0.9479 and 0.6415
Refinement method	Full-matrix least-squares on F^2
Data / restraints / parameters	10107 / 178 / 1413
Goodness-of-fit on F^2	1.045
Final R indices [I>2σ(I)]	*R*1 = 0.0865, *w*R2 = 0.2236
R indices (all data)	*R*1 = 0.1016, *w*R2 = 0.2411
Extinction coefficient	0.00025(6)
Largest diff. peak and hole	2.642 and –1.702 $eÅ^{-3}$

CHAPTER IV

MULTIMETALLIC COMPLEXES ARISING FROM CLICK REACTIONS CONDUCTED IN METAL COORDINATION SPHERES*

INTRODUCTION

The 1,3-dipolar cycloaddition reaction between an azide and an alkyne is widely used in synthetic and medicinal chemistry to produce a 5-membered heterocycle, namely a 1,2,3-triazole.[146-149] This cycloaddition was first described by Huisgen.[150,151] This uncatalyzed reaction is versatile but suffers from some limitations. These include the requirement for temperatures of ca. 80 °C, but most importantly, the production of two regioisomers, both 1,4 and 1,5, as drawn in Scheme 4.1. The isomer ratio is governed by the sterics and electronics of the reaction. This can lower yields and/or introduce challenges in terms of separation and purification.

Click chemistry, coined by Sharpless in 2001,[10] represents a wide range of reactions that are held to certain criteria: they must be wide in scope, involve simple reaction conditions and product isolations, and give high yields, to name a few.[10] The 1,3-dipolar cycloaddition was named the "cream of the crop" of click reactions. Unlike the Huisgen 1,3-dipolar cycloaddition, the click reaction between an azide and an alkyne uses a copper catalyst and produces only one regioisomer of the 1,2,3-triazole.

---

* Part of the data in this chapter is reprinted with permission from Clough, M. C.; Zeits, P. D.; Bhuvanesh, N.; Gladysz, J. A. *Organometallics* **2012**, *31*, 5231-5234. Copyright 2012 American Chemical Society.

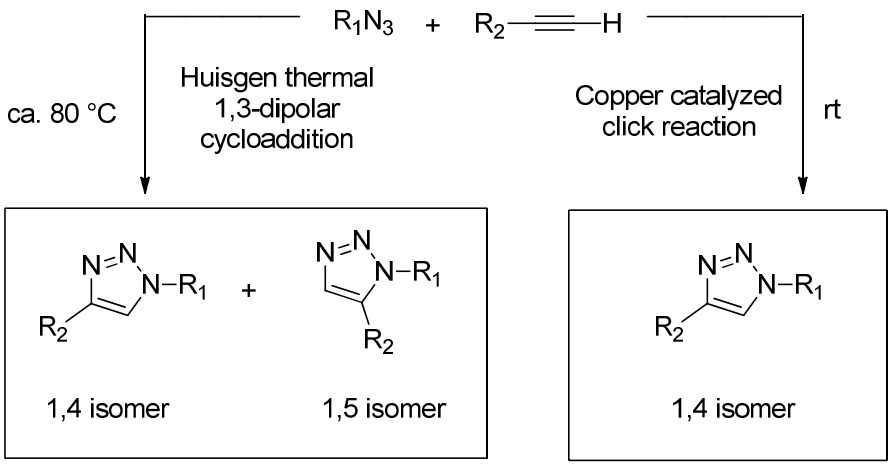

Scheme 4.1. Reaction between an azide and an alkyne by two different pathways: Huisgen thermal 1,3-dipolar cycloaddition (left) and the copper catalyzed click reaction (right).

The click reaction between an azide and an alkyne is a useful tool in producing highly functionizable 1,2,3-triazoles. Unlike the uncatalyzed analogue, this reaction does not require elevated temperatures, which can widen the scope of applicability, and can see a dramatic increase in reaction rate, often 7 to 8 orders of magnitude faster.[152] The mechanism of this transformation involves a Cu(I) catalyst. The catalyst produces a copper acetylide, which is ubiquitous in carbon-carbon bond forming reactions. Next, the electron rich R-N-N≡N nitrogen atom of the azide (*i.e.*, the carbon-bound nitrogen) binds to the copper metal center, which contributes to the regioselectivity of this reaction. Then the distal nitrogen attacks the carbon atom of the alkyne to form an unusual and short-lived six-membered ring transition state. This step is highly endothermic and the barrier is considerably less than that of the uncatalyzed analogue. This is the main contributor to the rate acceleration versus the uncatalyzed version. The following steps in the mechanism involve ring contraction and subsequent protonation to

regioselectively form the 1,2,3-triazole and the free catalyst.[152] This general mechanism involving an alkyne and an azide is summarized in Scheme 4.2.

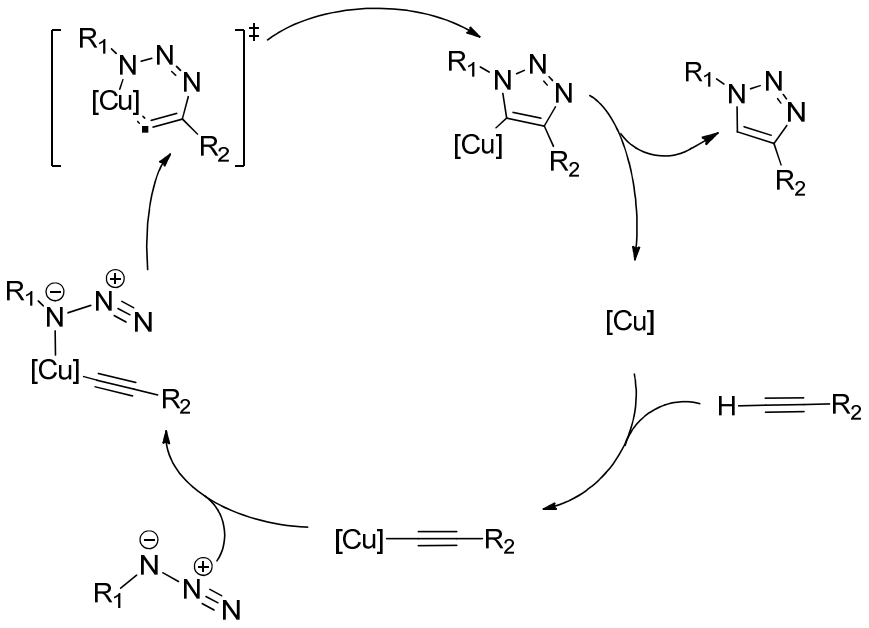

Scheme 4.2. Mechanism of copper catalyzed click reaction.

Of interest to the Gladysz group are click reactions involving organometallic polyyne chains. This theme was initially explored by Tywkinski who used both stable and unstable organic terminal polyynes, with the latter accessed by in-situ deprotection. Tykwinski employed the copper catalyzed click reaction in trapping experiments, in which the resulting triazole serves as method to trap the captured form of an otherwise unstable intermediate.[153] Tykwinski's click reactions were shown to tolerate various functional groups on the substituted terminus of the polyyne chain (R in Scheme 4.3),

such as aromatics, alcohols, silanes, and ketones. Importantly, when terminal 1,3,5,7-tetraynes were employed, there was no evidence of multiple azide additions.[154]

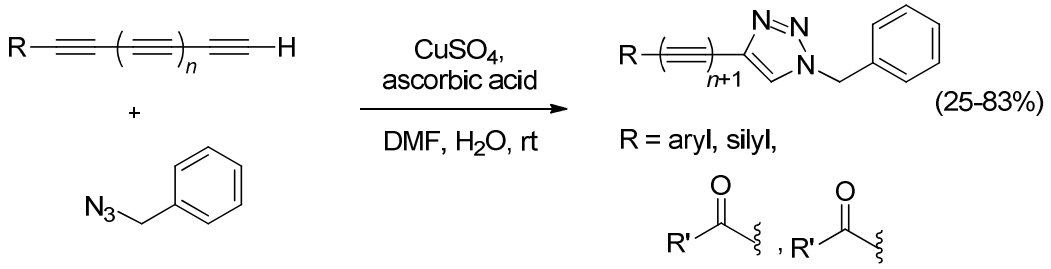

Scheme 4.3. Tykwinski's copper catalyzed click reactions with n = 0 to 3.

Much less explored than their purely organic counterparts are click reactions within a metal coordination sphere. Nevertheless, copper catalyzed click 3 + 2 cycloadditions of terminal alkynes and azides to give 1,2,3-triazoles are seeing ever increasing use in metal coordination spheres.[155-162] Similar reactions without added catalysts have also been reported.[163-166] Researchers have employed ethynyl moieties appended to various metal ligands,[155-161] as well as azido species that incorporate metals.[159,163,164,167] Examples of each of these are further discussed below.

To date, the most explored metal coordination sphere click reactions involve ferrocene, partly due to the ease of functionalization of the cyclopentadienyl ring. Ferrocenyl containing systems can serve as a vehicle for the alkyne and/or azide functionality.[162] A recent example involving click chemistry using a ferrocenyl azide was reported by Molina.[168] As shown in Scheme 4.4, he clicked a ferrocenyl azide and a terminal organic alkyne to produce a functionalized ferrocene in 55% yield after workup,[168] and this study served as the inspiration for a portion of this research.

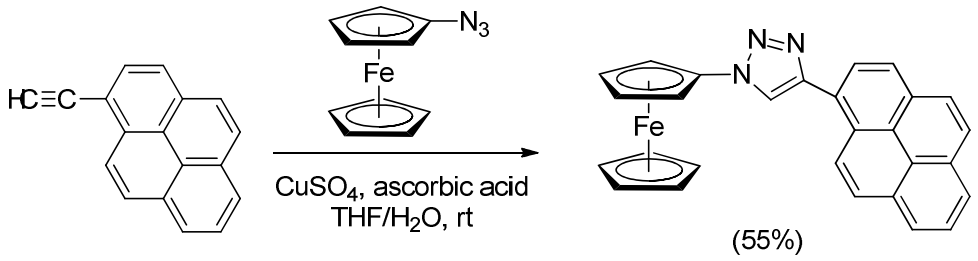

Scheme 4.4. Molina's click reaction within a metal coordination sphere involving a ferrocenyl moiety.

Gladysz has used click chemistry in conjunction with previously synthesized platinum complexes to carry out the described organic azide/terminal alkyne click reactions within metal coordination spheres (Scheme 4.5).[169] The alkyne employed was a platinum-capped carbon chain ranging from four to 12 carbons. Well known in terminal polyyne chain chemistry is the increasing instability of the carbon chain as it is extended, requiring protection by a triethylsilyl (or other) group upon reaching six sp carbon atoms. Thus, the click reaction between the organic azide and stable or unstable alkyne chain complexes proved to be a way to assay for and trap such complexes.

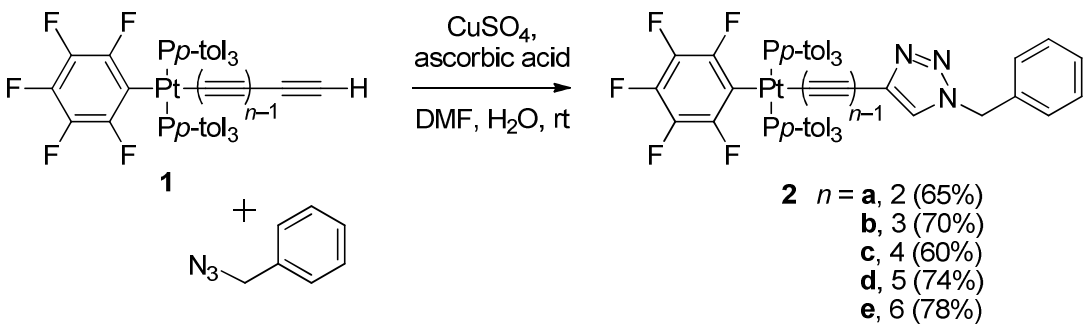

Scheme 4.5. Gladysz's click reactions within metal coordination spheres.

Given the wide range of metal-containing azides and alkynes available, this type of chemistry could lend itself to the synthesis of multimetallic complexes. Molecular frameworks that can incorporate tailor-made heteromultimetallic arrays – to wit, M, M', M'', M''', M'''' … or more ambitiously *a*M, *b*M', *c*M'', *d*M''', *e*M'''' … – might serve as precursors to unusual bulk or nanoscopic species. To date, the most advanced efforts along these lines are those of Lang,[170-172] who has synthesized molecules with three, four, five, and even six different metal atoms. The latter molecule contains one of each of six different metal atoms: iron, ruthenium, rhenium, gold, copper, and titanium (**3**). As shown in Figure 4.1, **3** (bottom) features carbon-rich alkyne and/or arene bridging units. However, certain metal atoms in **3** would be challenging to vary; a number of limitations are obvious. Also shown in Figure 4.1 are complexes that incorporate four (iron, ruthenium, rhenium, and rhodium) and five (iron, ruthenium, gold, copper, and titanium) different transition metals, all prepared by Lang in earlier studies.

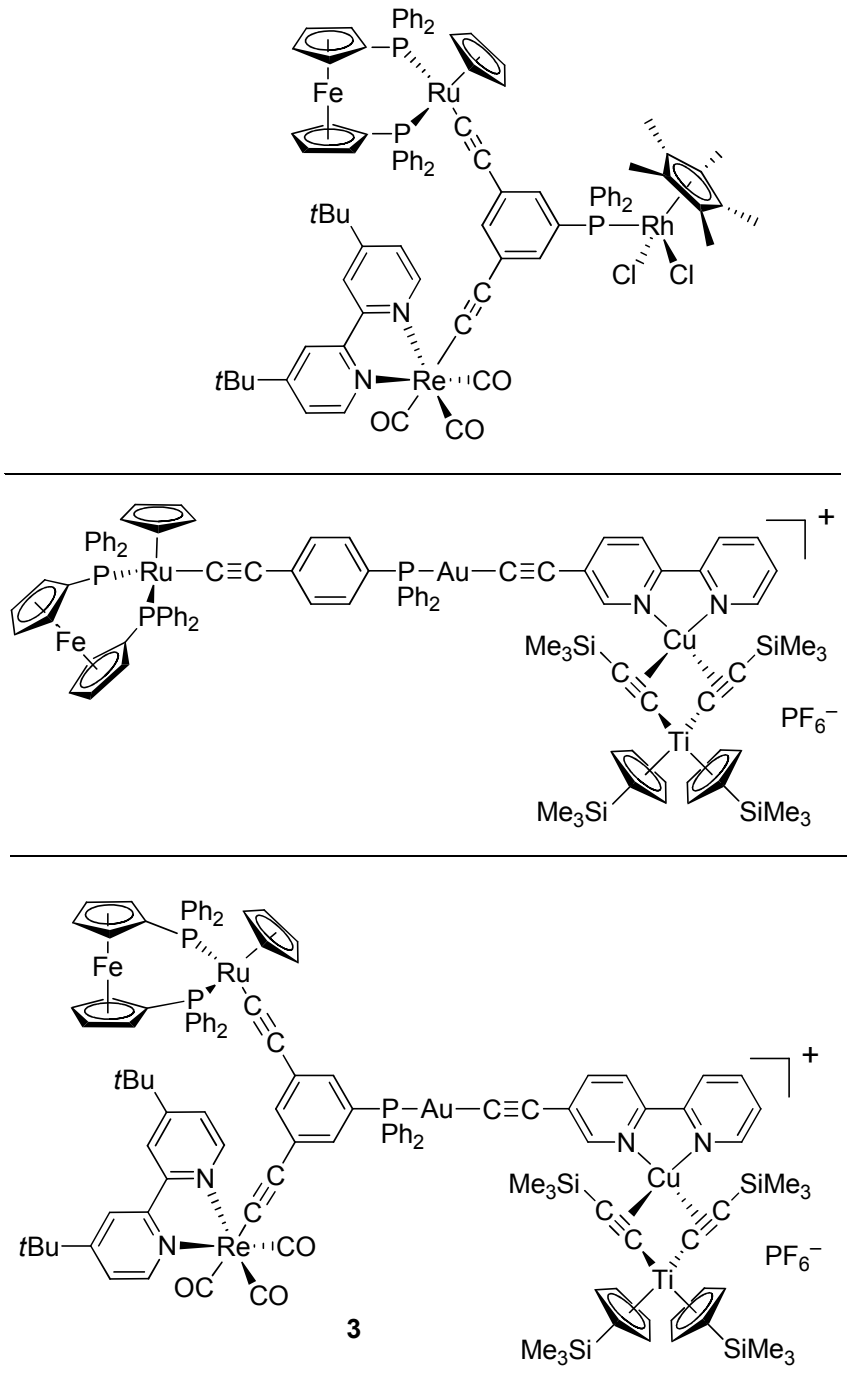

Figure 4.1. Lang's complexes incorporating four (top), five (middle), and six (bottom) different transition metals.

Importantly, the triazoles produced by click reactions have two additional sites, as shown in Figure 4.2, that are amenable to functionalization: (a) the nucleophilic lone pair of the unsubstituted nitrogen atom (N3) that is remote from the substituted nitrogen atom (N1),[173] and (b) the carbon with the moderately acidic proton, or the =CH moiety (C'),[173-186] abstraction of which can lead to an "abnormal" or "mesoionic"[187] N-heterocyclic carbene (NHC).

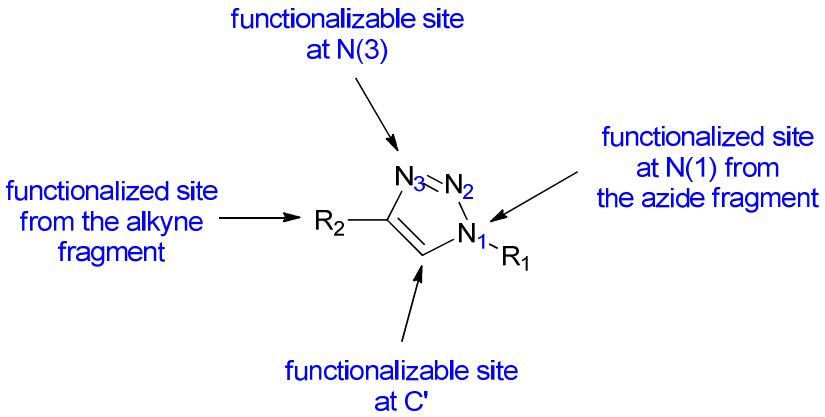

Figure 4.2. Analysis of sites for functionalizations of 1,2,3-triazoles.

Mesoionic NHC's are stronger electron donors than their normal NHC counterparts.[187] Unlike their normal NHC counterparts, no canonical resonance form can be drawn for mesoionic NHC's without additional charges.[187] A schematic representation is provided in Figure 4.3.

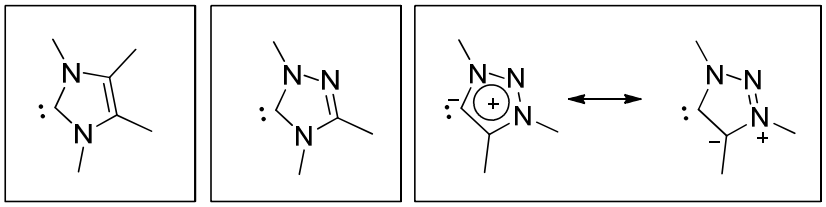

Figure 4.3. Representations of normal (left and middle) and mesoionic (right) carbenes.

Hence, a 1,2,3-triazole core could seemingly serve as a versatile template for assemblies containing four different transition metal atoms, and I set out to explore protocols towards this end.

In recent work, Viege has demonstrated that the gold azide and alkynyl complexes Ph_3PAuN_3 and $PhC{\equiv}CAuPPh_3$ react to give the digold complex shown in Scheme 4.6 in 88% yield after workup. Interestingly, this reaction does not require a catalyst.[167] This indicates that click reactions in metal coordination spheres can take place in the absence of a catalyst by alternative mechanisms. Similar uncatalyzed 3 + 2 cycloaddition reactions involving metal species have also been reported.[164-166]

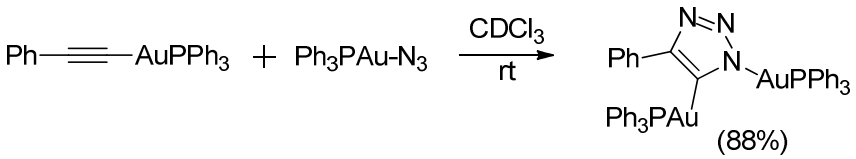

Scheme 4.6. Previously reported 3 + 2 cycloaddition in a metal coordination sphere by Viege.

Considering again the functionalizable sites in Figure 4.2 that are not connected with the alkyne or azide, derivatization at the N(3) position can be considered. Selective

alkylation at the N(3) position has been shown to proceed with ease and with good yields by Albrecht[173] and Huynh.[185] They treated organic 1,2,3-triazoles with organic halides to give the 1,2,3-triazolium salts shown in Scheme 4.7.

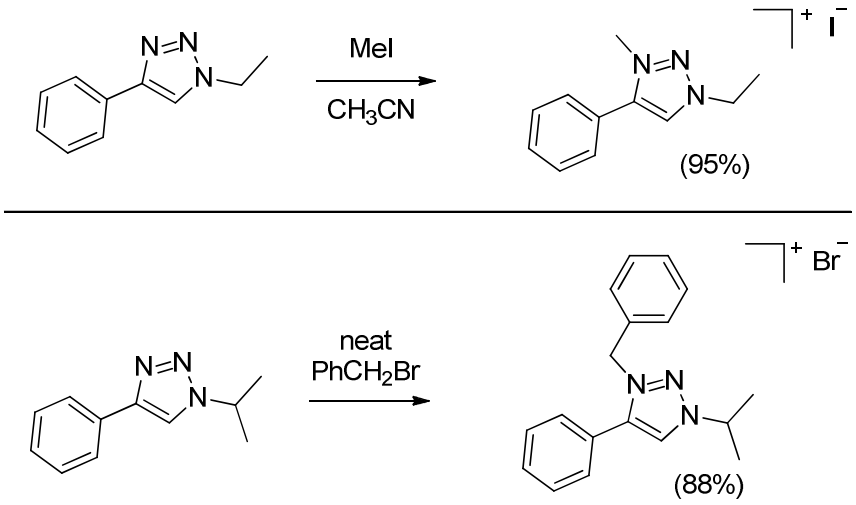

Scheme 4.7. Albrecht's (top) and Huynh's (bottom) method of alkylating N(3) of a 1,2,3-triazole.

Metallation at the carbene-like carbon of a 1,2,3-triazole or the corresponding triazolium salt also has precedent. One of the first examples was shown by Albrecht, in which the metallation of this carbon was achieved directly using a palladium source, as shown in Scheme 4.8. Alternatively, this carbon can be transmetallated using silver oxide and further reacted with the rhodium or iridium dimers $[MCl(cod)]_2$ to give mesoionic carbene complexes.[173]

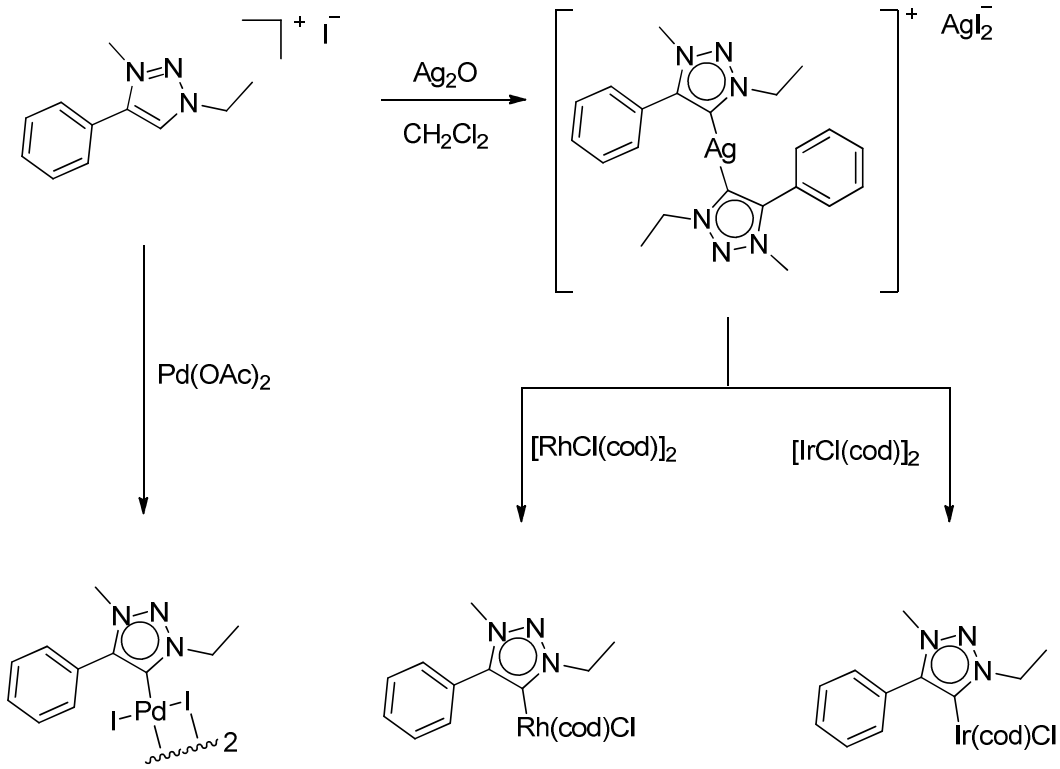

Scheme 4.8. Albrecht's method of metallating the carbene-like carbon on a 1,2,3-triazolium salt by direct and transmetallation routes.

Using much the same precedent, this chemistry can be very easily expanded to heteromultimetallic complexes involving 1,2,3-triazoles. The first two metal fragments in the target complex would arise from alkyne and azide functionality. Thus, the plan for this approach is outlined in Scheme 4.9, in which a bimetallic 1,2,3-triazole is first synthesized from a platinum starting material and an azide containing metal fragment. Metallation at the N(3) position is the next goal, and alkylation methods discussed (*vide supra*) will be employed. Attempts to metallate at the =CH moiety are then discussed by both direct and indirect (transmetallation) routes. To date, there have been no trimetallated or tetrametallated (permetallated) triazoles reported.

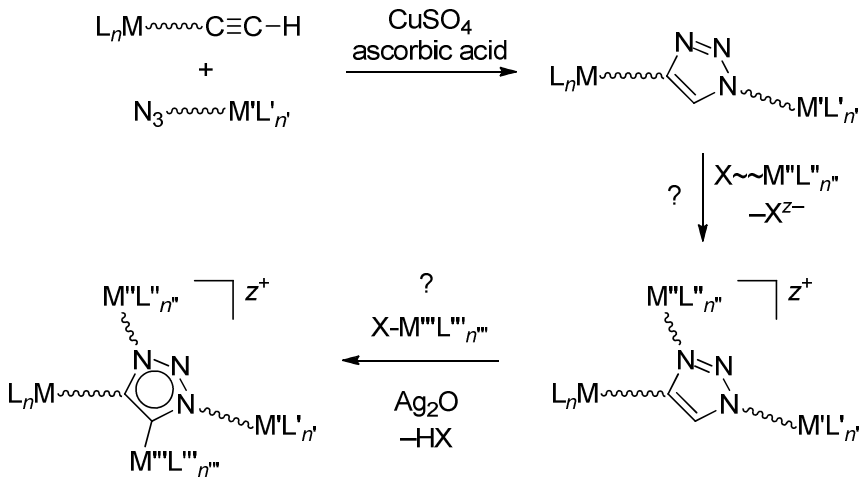

Scheme 4.9. Approach to permetallation of 1,2,3-triazole.

Several possible ways to implement Scheme 4.9 were considered. Given the experience with the platinum polyynyl complexes in Scheme 4.5, complex **1a** was targeted for initial study. The ultimate starting material for this compound is the platinum chloride complex **4**,[50] which is synthesized from a platinum dimer. The necessary C≡CH unit was introduced by a reaction with butadiyne. This reaction is done in the presence of a copper catalyst using diethylamine as the solvent (Scheme 4.10). The platinum butadiynyl complex **1a** can be isolated as a fine off-white powder in 55% yield and is air stable.

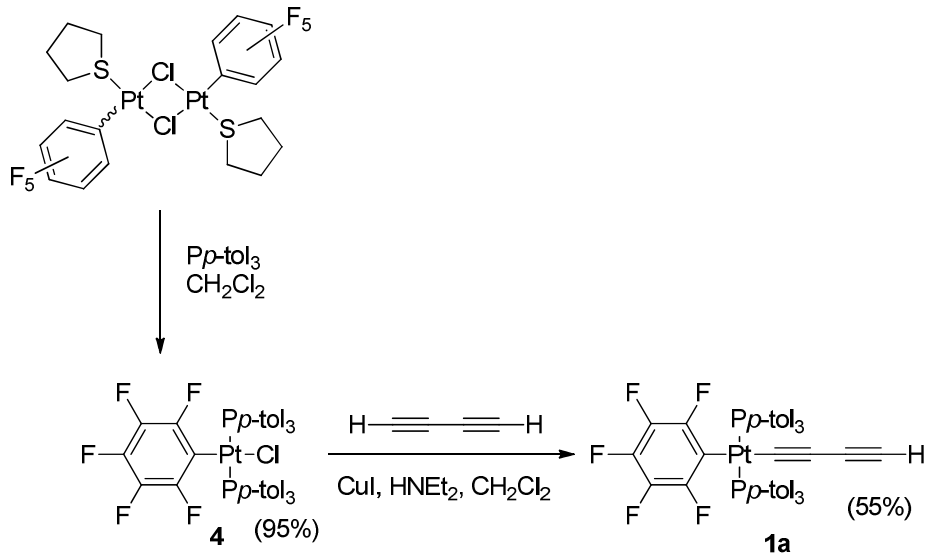

Scheme 4.10. Synthesis of platinum butadiynyl complex **1a**.

In terms of electrophilic metals that might be used to functionalize the N(3) position, my attention was drawn to $Re(CO)_5Br$ (**5**) and $Re(CO)_5OTf$ (**6**), both synthesized from the rhenium dimer $Re_2(CO)_{10}$ as shown in Scheme 4.11.[188,189] The rhenium dimer can be "titrated" with bromine to break the rhenium-rhenium bond and effect conversion to the rhenium bromide complex **5**. This complex is then treated with silver triflate in the dark to achieve conversion to **6**. These have been previously shown to react with N-donor ligands to give substituted products.[190,191]

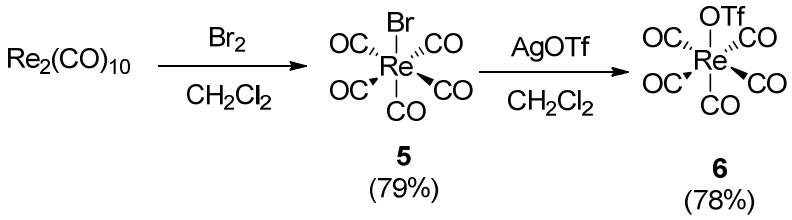

Scheme 4.11. Syntheses of rhenium complexes **5** and **6**.

A similar click reaction will be discussed using ferrocenyl diazide **8**, first described by Molina.[192] This building block is synthesized from ferrocene and triisopropylsulfonyl azide **7**. Complex **8** is light sensitive, but air stable, and can be isolated in 46% yield (Scheme 4.12).

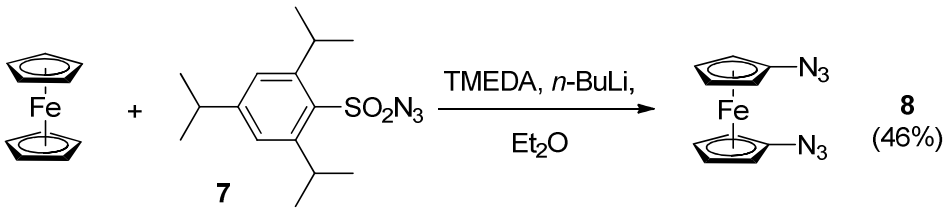

Scheme 4.12. Molina's synthesis of ferrocenyl diazide **8**.

RESULTS

The click reactions investigated in this project utilize the platinum butadiynyl complex **1a** in Scheme 4.10 as the source of terminal alkyne. The second component needed for the click reaction is the azide. In exploratory experiments, several metal-containing azides were initially assayed. The first featured an azide bonded directly to a transition metal, $(\eta^5\text{-}C_5H_5)Re(NO)(PPh_3)(N_3)$,[144] as depicted in Scheme 4.13. This rhenium complex was combined with **1a**, $CuSO_4 \cdot 5H_2O$, ascorbic acid, DMF, and water. Only starting materials were recovered, indicating that no 3 + 2 cycloaddition took place.

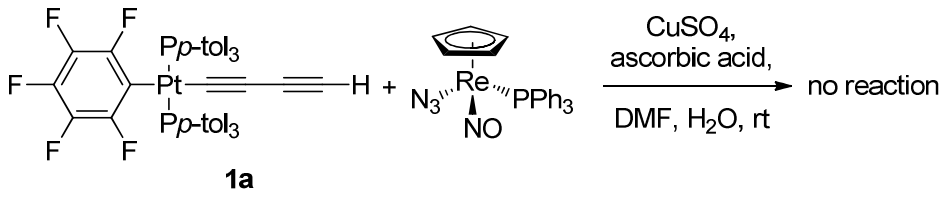

Scheme 4.13. Attempted click reaction with a rhenium complex with an azide directly bonded to the metal center.

A rhenium complex in which the azide was not directly bonded to the metal center was evaluated next. As shown in Scheme 4.14, the cyclopentadienyl azide complex (η^5-$C_5H_4N_3$)$Re(CO)_5$ (**9**) was synthesized. This compound is prepared by first treating (η^5-C_5H_5)$Re(CO)_3$ with *n*-BuLi to generate (η^5-C_5H_4Li)$Re(CO)_3$, followed by subsequent addition of tosyl azide to form the azide adduct. This reaction is done in the dark and the resulting rhenium complex is isolated as a slightly light-sensitive white solid in 68% yield.

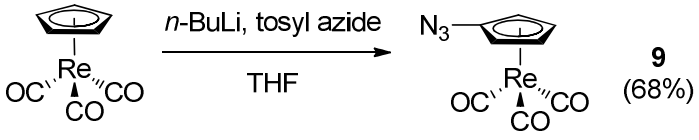

Scheme 4.14. Synthesis of rhenium azide complex **5**.

The click reaction was then carried out with equimolar quantities of **1a** and **9** in DMF. As shown in Scheme 4.15, $CuSO_4 \cdot 5H_2O$ (1.63 mol%), ascorbic acid (2.28 mol%), and water were added. Workup and column chromatography gave the anticipated product, the heterobimetallic cycloadduct **10** as a stable white solid in 54%

yield. The NMR and IR properties of **10** combined features typical for monosubstituted cyclopentadienyl complexes of rhenium tricarbonyl and those observed with adducts of **1a** and organic azides described earlier. Namely, the ^{1}H NMR spectrum showed two signals of the cyclopentadienyl protons for the monosubstituted product (δ ($CDCl_3$) 5.67 and 5.27 ppm) instead of one signal for its unsubstituted counterpart. The terminal ≡CH proton, now incorporated in the heterocycle, underwent the largest ^{1}H NMR chemical shift, going from δ 1.46 to 6.29 (ppm, $CDCl_3$). Additionally, two C≡C ^{13}C NMR signals in **1a** at δ 72.5 and 59.6 (ppm, $CDCl_3$) disappear upon formation of **10**.

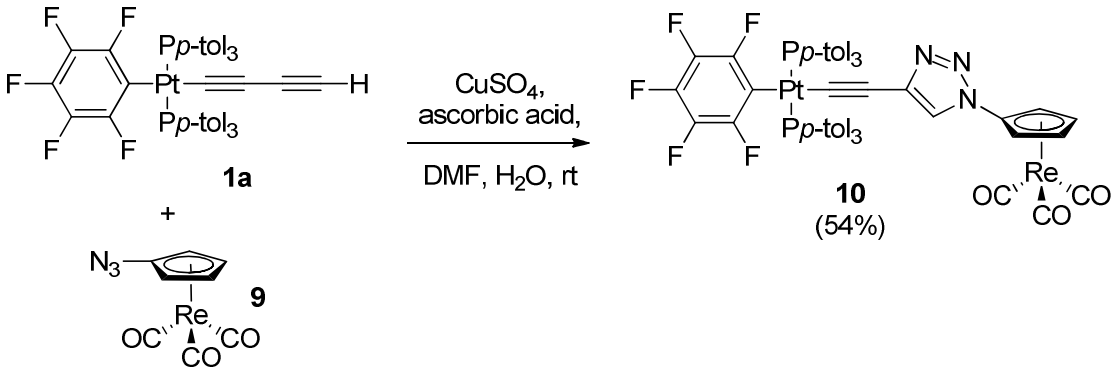

Scheme 4.15. Synthesis of bimetallic triazole **10**.

The introduction of a third metal was sought. Accordingly, **10** was combined with 1.15 equiv. of the rhenium triflate complex **6** in CH_2Cl_2. After 5 d at room temperature, workup gave the salt $\mathbf{11}^{+}$ TfO^{-} as a white solid in 84% yield. The NMR and IR properties of $\mathbf{11}^{+}$ TfO^{-} were similar to those of **10**, but with the characteristic bands of the $Re(CO)_5$ fragment, suggesting the structure with the N(3) functionalized triazole depicted in Scheme 4.16. An analogous but slower reaction with the rhenium

bromide complex **5** appeared to give the neutral carbonyl displacement product **12** as a white solid in 98% yield.

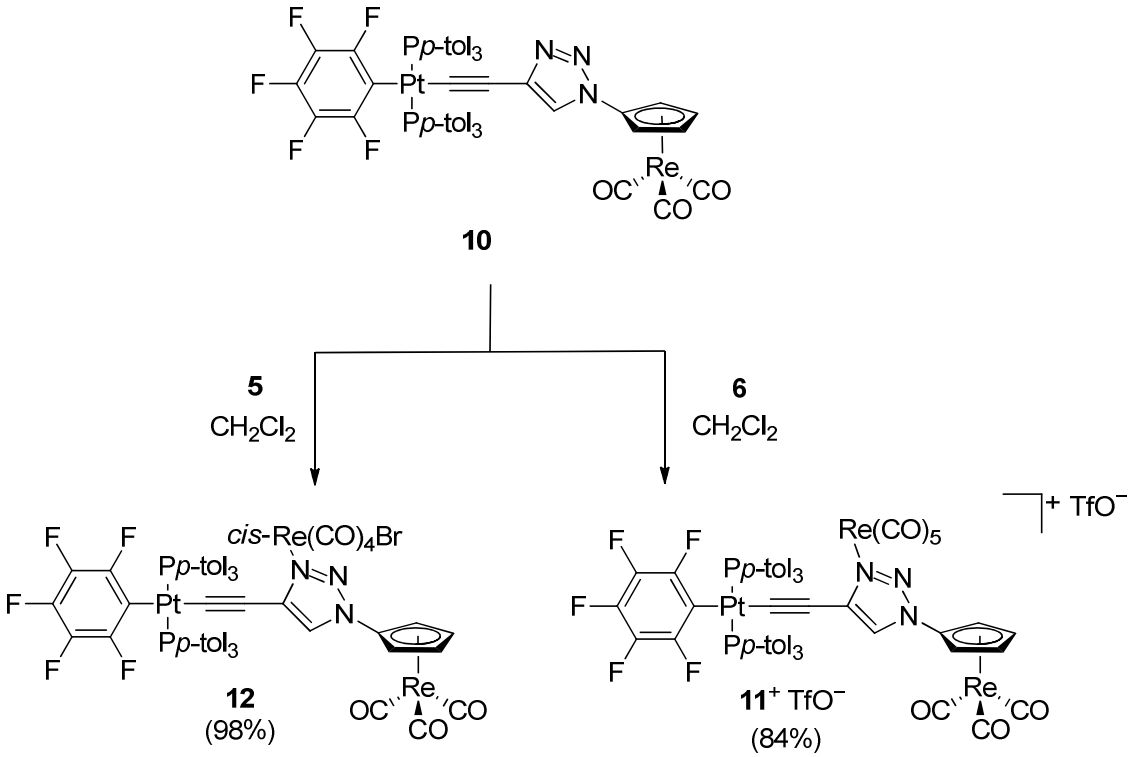

Scheme 4.16. Syntheses of triazolium salts **11**$^{+}$ TfO^{-} and **12.**

This process was monitored by ^{1}H NMR spectroscopy, using the cyclopentadienyl and =CH protons of the educts and products. For the rata data presented in Figure 4.4, the product cyclopentadienyl ^{1}H NMR resonance was integrated versus the total cyclopentadienyl signal. In all cases, no byproducts were apparent and the reaction mixtures remained homogeneous. The slower reaction with **5** required

elevated temperatures (ca. 40 °C) to reach completion within 10 d, whereas the analogous reaction with **6** reached completion at room temperature within 3 d.

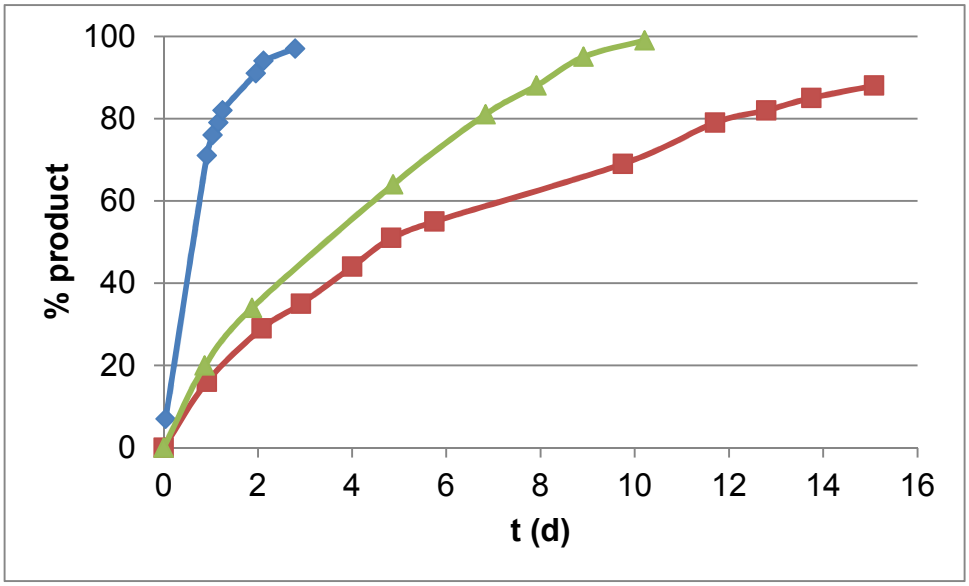

Figure 4.4. Rates of formation of $\mathbf{11}^{+}$ TfO^{-} and **12** in CH_2Cl_2: **12** at 40 °C (green triangle); **12** at rt (red square); $\mathbf{11}^{+}$ TfO^{-} at rt (blue diamond).

The cyclopentadienyl protons of both products were seen to shift downfield, whereas the carbene-type protons were seen to shift upfield. The upfield and downfield shifts are exemplified in Figure 4.5, in which the triazole moiety was functionalized using **5**.

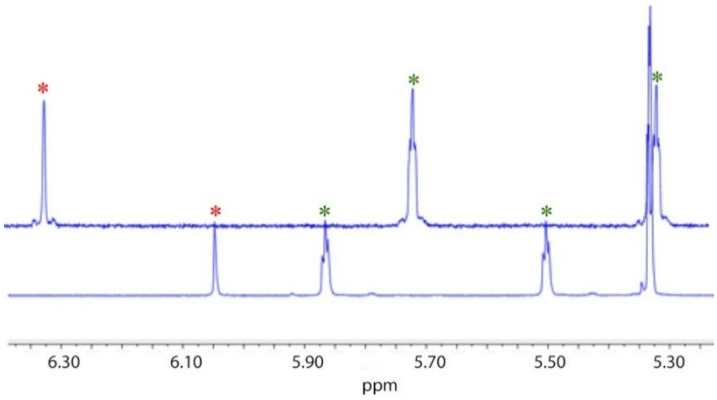

Figure 4.5. ^{1}H NMR spectra (partial, CD_2Cl_2) of **10** (top) and **12** (bottom) (red = =CH signal, green = cyclopentadienyl signals).

The IR band pattern of **12** is further indicative of a *cis*-$Re(CO)_4Br$ complex. The IR spectrum of free $Re(CO)_5Br$ shows three ν_{CO} absorption bands[193] at 2158, 2047, and 1991 cm^{-1} corresponding to a weak a_1 band, an intense e band, and a very weak a_1 band or shoulder, typical for octahedral $M(CO)_5L$ geometries.[194] The carbonyl displacement product **12** shows a band pattern typical for *cis*-$M(CO)_4L_2$ geometries;[194] *i.e.*, the IR-active bands corresponding to a_1, b_1, and b_2 modes, which in the case of **12**, appear at 2013, 1990, and 1936 cm^{-1}.

Single crystals of the solvates **10**·$2CH_2Cl_2$, **11**$^{+}$ TfO^{-}·CH_2Cl_2, and **12**·$2CH_2Cl_2$ were grown, and the X-ray structures determined as described in the experimental section. The thermal ellipsoid diagrams and space filling models are shown in Figures 4.6, 4.7, and 4.8. The space filling models are positioned in such a way as to emphasize the sterics around the N(3) position of the triazole ring. A comparison of the three structures is given in Table 4.1. In **12**·$2CH_2Cl_2$ the bromide ligand of the *cis*-$Re(CO)_4Br$ moiety was disordered over two positions (84:16), *trans* from each other. The dominant conformation is depicted in Figure 4.8.

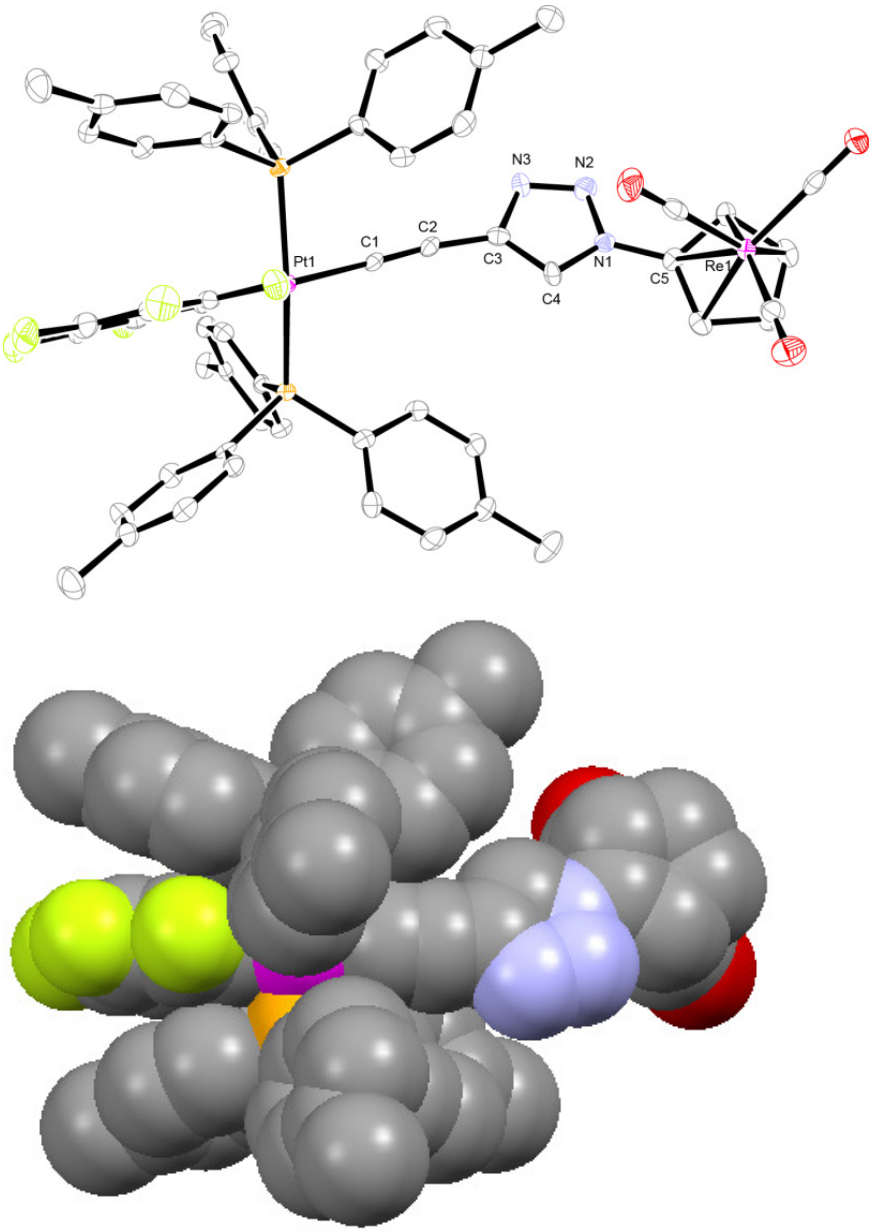

Figure 4.6. Top: thermal ellipsoid plot (50% probability level) of the molecular structure of **10**·2CH_2Cl_2 with the solvate molecules omitted. Key bond lengths and angles: Pt1-C1 1.998(4), C1≡C2 1.210(5), C2-C3 1.422(6), C3=C4 1.368(5), C4-N1 1.345(5), N1-N2 1.348(4), N2=N3 1.317(4), N3-C3 1.380(5), C_{ipso}-Pt1-C1 170.00(15), Pt1-C1-C2 167.7(3), C1-C2-C3 171.8(4); Bottom: corresponding space filling model of **10**·2CH_2Cl_2 with the solvate molecules omitted.

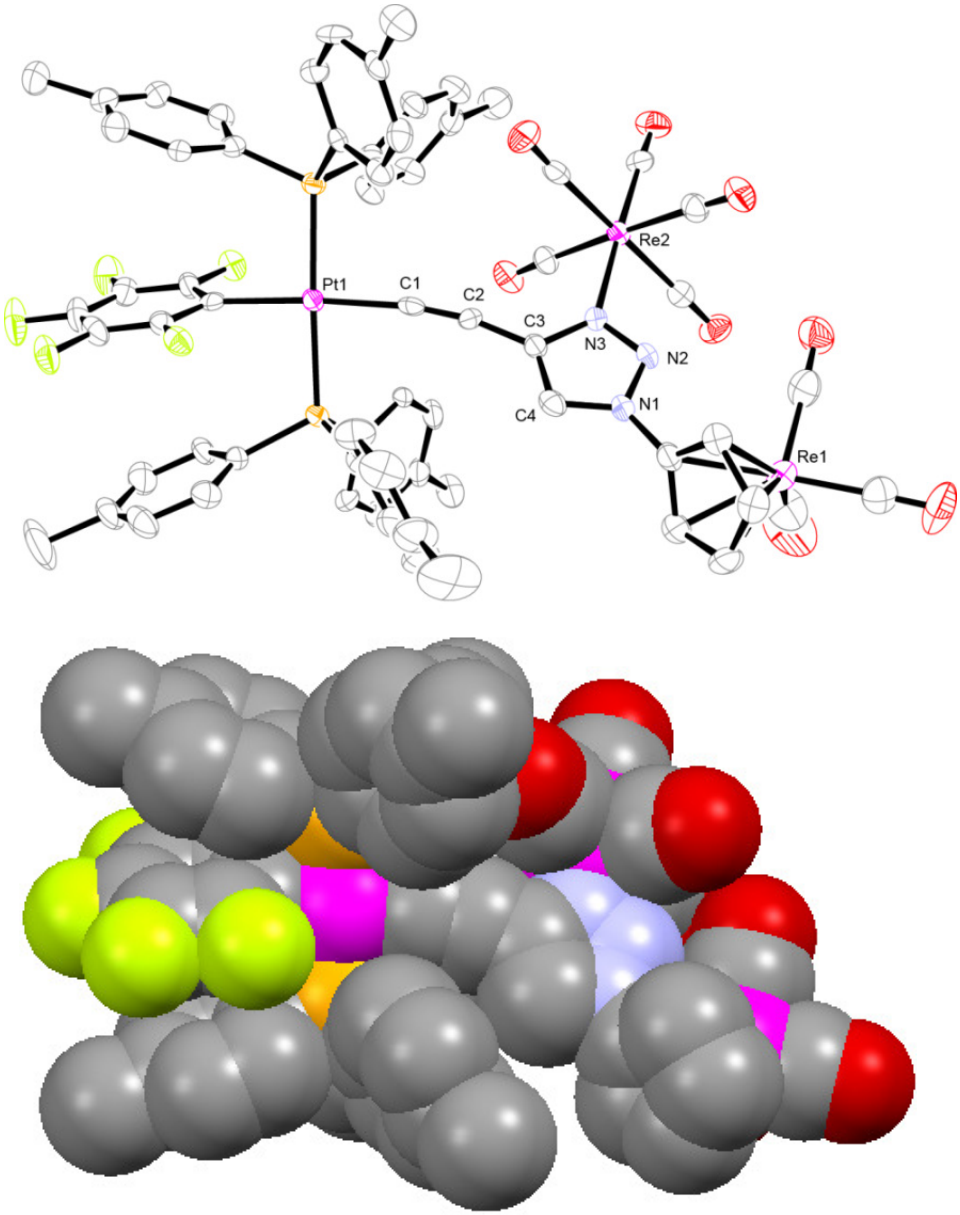

Figure 4.7. Top: thermal ellipsoid plot (50% probability level) of the molecular structure of **11**$^{+}$ $TfO^{-}\cdot CH_2Cl_2$ with the anion and solvate molecule omitted. Key bond lengths and angles: Pt1-C1 2.001(7), C1≡C2 1.202(9), C2-C3 1.414(9), C3=C4 1.352(10), C4-N1 1.351(9), N1-N2 1.316(7), N2=N3 1.288(7), N3-C3 1.373(8), C_{ipso}-Pt1-C1 175.8(3), Pt1-C1-C2 171.7(6), C1-C2-C3 169.4(7); Bottom: corresponding space filling model of the molecular structure of **11**$^{+}$ $TfO^{-}\cdot CH_2Cl_2$ with the anion and solvate molecule omitted.

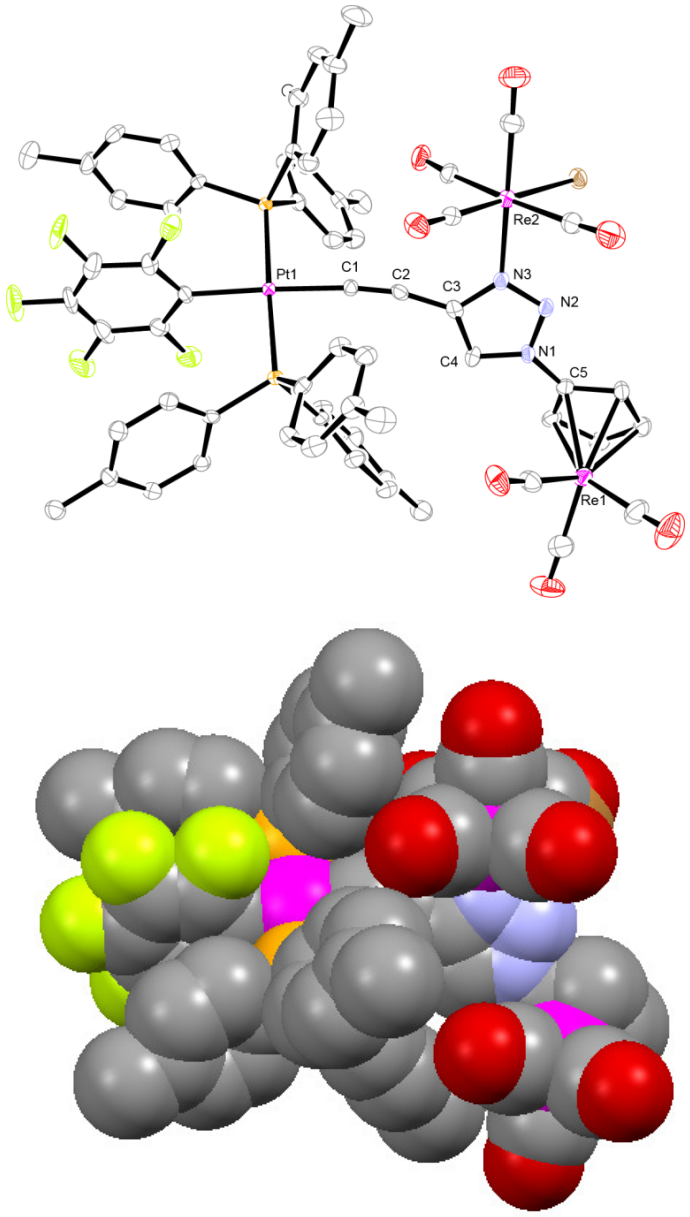

Figure 4.8. Top: thermal ellipsoid plot (50% probability level) of the dominant conformation of the molecular structure of **12**·$2CH_2Cl_2$ with the solvate molecules omitted. Key bond lengths and angles: Pt1-C1 1.995(5), C1≡C2 1.207(7), C2-C3 1.407(7), C3=C4 1.387(8), C4-N1 1.351(6), N1-N2 1.343(6), N2=N3 1.323(6), N3-C3 1.387(7), C_{ipso}-Pt1-C1 177.6(2), Pt1-C1-C2 173.4(4), C1-C2-C3 166.6(5); Bottom: corresponding space filling model of the dominant conformation of the molecular structure of **12**·$2CH_2Cl_2$ with the solvate molecules omitted.

Table 4.1. Key crystallographic distances [Å] and angles [°] for complexes with a single triazole.

	10·2CH_2Cl_2	**11**$^+$ TfO^-·CH_2Cl_2[a]	**12**·2CH_2Cl_2[a]
Pt1-C1	1.998(4)	2.001(7)	1.995(5)
C1≡C2	1.210(5)	1.202(9)	1.207(7)
C2-C3	1.422(6)	1.414(9)	1.407(7)
C3=C4	1.368(5)	1.352(10)	1.387(8)
C4-N1	1.345(5)	1.351(9)	1.351(6)
N1-N2	1.348(4)	1.316(7)	1.343(6)
N2=N3	1.317(4)	1.288(7)	1.323(6)
N3-C3	1.380(5)	1.373(8)	1.387(7)
N-C5	1.419(5)	1.426(9)	1.417(7)
C_{ipso}[b]-Pt1-C1	170.00(15)	175.8(3)	177.6(2)
Pt1-C1-C2	167.7(3)	171.7(6)	173.4(4)
C1-C2-C3	171.8(4)	169.4(7)	166.6(5)
N-Re1	-	2.168(6)	2.174(5)
av. Re1-CO	-	2.004	1.973
av. Re1C≡O	-	1.124	1.149
Re2-C_5H_4 centroid	1.971	1.963	1.967
av. Re2-CO	1.921	1.903	1.917
av. Re2C≡O	1.146	1.153	1.140
angle triazole/ C_6F_5 median planes	60.49	38.16	20.95
angle triazole/ C_5H_4 median planes	20.21	67.59	25.21
av. π stacking[c]	3.738	3.685	3.647
angle stacking[d]	163.1	160.1	166.0

[a] The atomic numbering for **11**$^+$ TfO^- and **12** has been changed from those in the CIF files to facilitate comparison of structural features with the other complexes. [b] C_{ipso} is the platinum bound C_6F_5 carbon atom. [c] Average distance between midpoints of the C_6F_5 and $C_6H_4CH_3$ rings. [d] Angle of midpoints of the three rings in c.

Attempts to metallate at the fourth position of the 1,2,3-triazole, the =CH moiety, were then undertaken and are henceforth discussed. Methodologies similar to those used by Albrecht in Scheme 4.8 were employed.[173] First, **12** was treated with various metal sources with varying temperature and reaction times. These data are summarized in Table 4.2.

Table 4.2. Attempts to metallate the =CH moiety of triazole **12.**

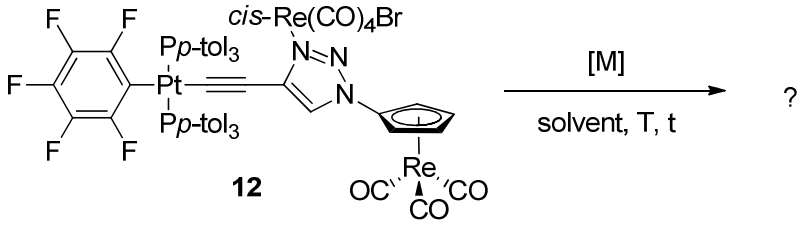

entry	reagent(s)	solvent	T (°C)	t (d)	observation
1	Ag_2O	CH_2Cl_2	40	1	nr
2	Cu_2O	CH_2Cl_2	40	7	nr
3	$Pd(OAc)_2$	CH_2Cl_2	rt	1	nr
4	NEt_3, $Pd(OAc)_2$	CH_2Cl_2	rt	0.05	Pd black, nr
5	Cs_2CO_3, $Pd(OAc)_2$	THF	rt	3	Reaction, no C-H activation
6	Ag_2O / $[RhCl(cod)]_2$	CH_2Cl_2	40	1	nr
7	Ag_2O / $PdCl_2(NCMe)_2$	CH_2Cl_2	rt	1	nr

These reactions were monitored by ^{1}H NMR spectroscopy, specifically for the disappearance of the =CH proton. Like Albrecht, transmetallation was first attempted using either silver(I) or copper(I) oxide in CH_2Cl_2. No C-H activation was seen at 40 °C (entries 1 and 2). Direct metallation was attempted with a palladium source (entry 3; see Scheme 4.8). *In situ* transmetallation was also attempted, hoping that if only small equilibrium quantities of the silver or copper activated complex were present, they could nonetheless be trapped immediately upon reaction with another transition metal (entries 6 and 7). The reaction mixture was monitored by ^{1}H NMR under these conditions. No reaction and importantly no C-H activation was observed. Bases were added in an attempt to abstract the C-H proton or otherwise facilitate metallation (entries 4 and 5). In these cases, the metal either crashed out or a side reaction occurred that did not involve the =CH moiety. In the latter case, a new set of cyclopentadienyl and =CH protons grew in as the starting material was consumed, indicating that a reaction took place that did not involve the =CH moiety. This reaction was not further probed. In any case, no C-H activation was detected in entries 1-7 of Table 4.2.

A similar approach was taken with **11**$^+$ TfO^-. As this complex is cationic, it was thought that deprotonation might be facilitated and would proceed with more ease. The same methodology was employed (*vide supra*). These data are summarized in Table 4.3.

Table 4.3. Attempts to metallate the =CH moiety of triazolium salt **11**$^{+}$ TfO^{-}.

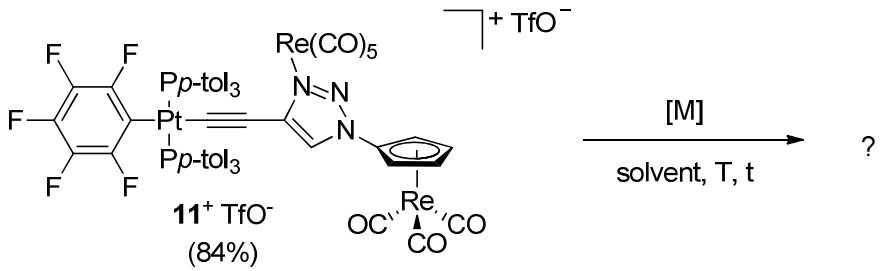

entry	reagent(s)	solvent	T (°C)	t (d)	observation
1	Ag_2O	CH_2Cl_2	rt	0.25	nr
2	Ag_2O	CH_2Cl_2	40	4	nr
3	Cu_2O	CH_2Cl_2	rt	11	nr
4	$[IrCl(cod)]_2$	CH_2Cl_2	40	2	nr
5	KO*t*Bu / $[IrCl(cod)]_2$	CH_2Cl_2	rt	2	nr
6	$[RhCl(cod)]_2$	CH_2Cl_2	40	4	Reaction, no C-H activation

Similarly, these reactions were monitored by ^{1}H NMR spectroscopy, specifically the disappearance of the =CH proton. Transmetallation was first attempted with silver(I) and copper(I) oxide in CH_2Cl_2. No C-H activation was seen with silver(I) oxide at room temperature or 40 °C and with copper(I) oxide at room temperature (entries 1-3). The same sources of rhodium and iridum were used as in Table 4.2 (entries 4-6). In entry 5, a base was added in an attempt to mediate metallation. The use of KO*t*Bu was modeled after a related reaction by Lassaletta, shown in Scheme 4.17, in which proton abstraction from a =CH moiety and treatment with the iridum dimer $[IrCl(cod)]_2$ resulted in an aryl iridium adduct, although in a relatively low yield.[195] When the rhodium dimer

[RhCl(cod)]$_2$ was added (entry 6), a reaction took place; a new set of cyclopentadienyl and =CH protons grew in as the starting material was consumed, indicating that a reaction took place that did not involve the =CH moiety. This reaction was not probed further (entry 6). In any case, no C-H activation was observed in entries 1-6 of Table 4.3.

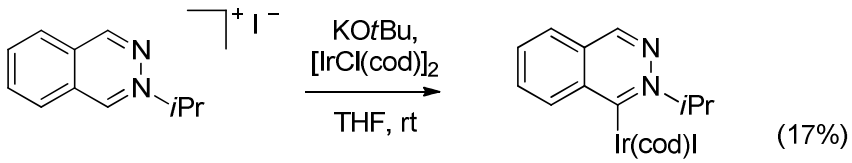

Scheme 4.17. Lassaletta's base mediated metallation of a heterocyclic compound.

Possible steric and electronic effects upon =CH metallation were investigated. First, attempts to metallate at the =CH moiety before derivatizing at N(3) were conducted. For this, the bimetallic complex **10** was used.

Table 4.4. Attempts to metallate the =CH moiety of triazole **10**.

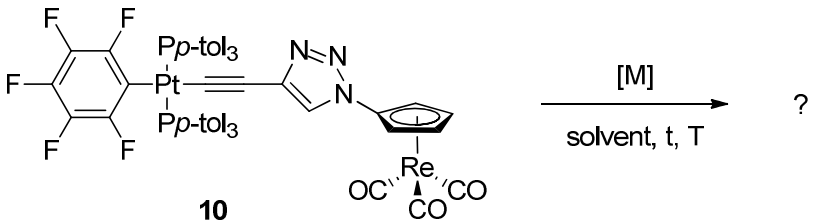

10

entry	reagent	solvent	T (°C)	t (d)	observation
1	Ag_2O	CH_2Cl_2	rt	3	nr
2	Ag_2O	CH_2Cl_2	40	3	nr
3	Cu_2O	CH_2Cl_2	rt	3	nr
4	Cu_2O	CH_2Cl_2	40	3	nr
5	$PhAuPPh_3$	THF	rt	1	nr

These reactions were monitored by ^1H NMR spectroscopy, specifically the disappearance of the =CH proton. Transmetallation was attempted with silver(I) and copper(I) oxide in CH_2Cl_2. No C-H activation was seen with silver(I) and copper(I) oxide at both room temperature and 40 °C (entries 1-4). An attempt to directly metallate using $PhAuPPh_3$ in THF at room temperature also showed no C-H activation (entry 5).

The next investigation focused on answering the following question: Is it possible to metallate at the =CH position when neither the N(1) or C' positions (see Figure 4.2) bear any metal fragment? In all prior attempts (Tables 4.2-4.4), both were metallated. For this, a compound in which the N(1) and C' positions were substituted with purely organic fragments was needed (*i.e.*, a metal-free triazole). Thus, a literature

compound was prepared as a model: a *p*-tol/benzyl substituted 1,2,3-triazole (**13**), which is the click product between benzyl azide and *p*-tolylacetylene.[196] This triazole was then functionalized according to the previously described methods (*vide supra*) using **5** and **6** (Scheme 4.18).

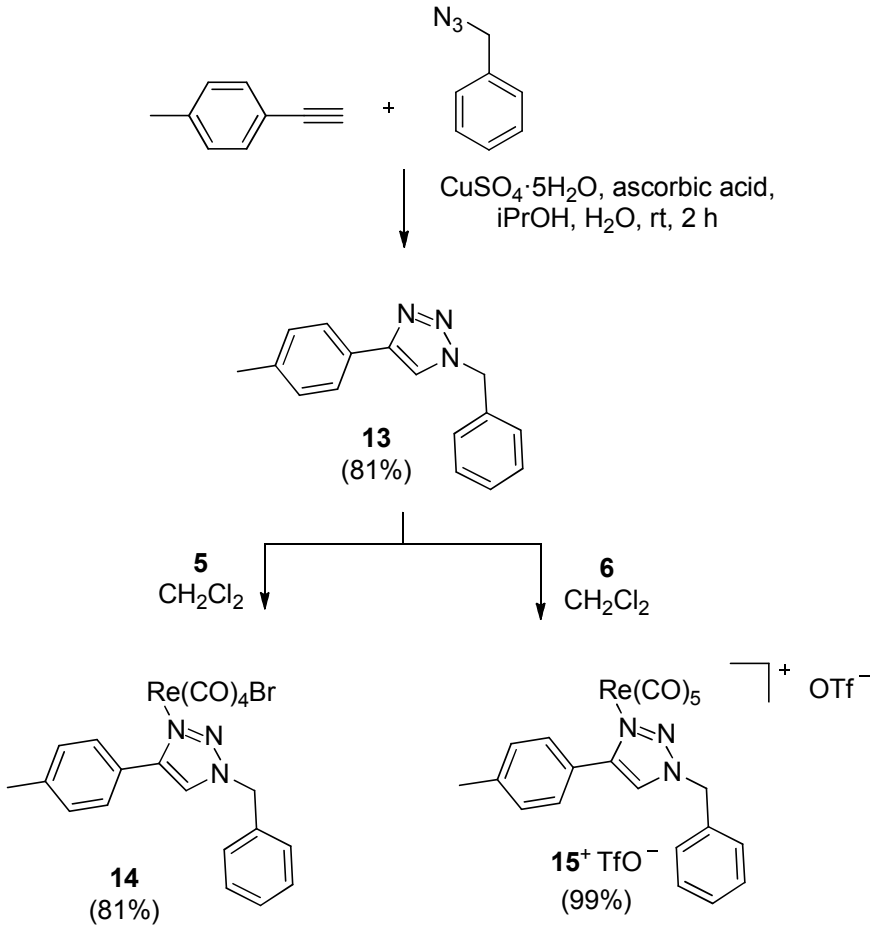

Scheme 4.18. Metallation of **13** to give monometallic complexes **14** and **15**$^{+}$ TfO^{-}.

The substituted triazoles **14** and **15**$^{+}$ TfO^{-} were isolated as off-white powders in good yields (81-99%). The rates of these reactions closely resemble those of the

dimetalated analogues in Scheme 4.16. These data are depicted in Figure 4.9, and were determined analogously to those in Figure 4.4.

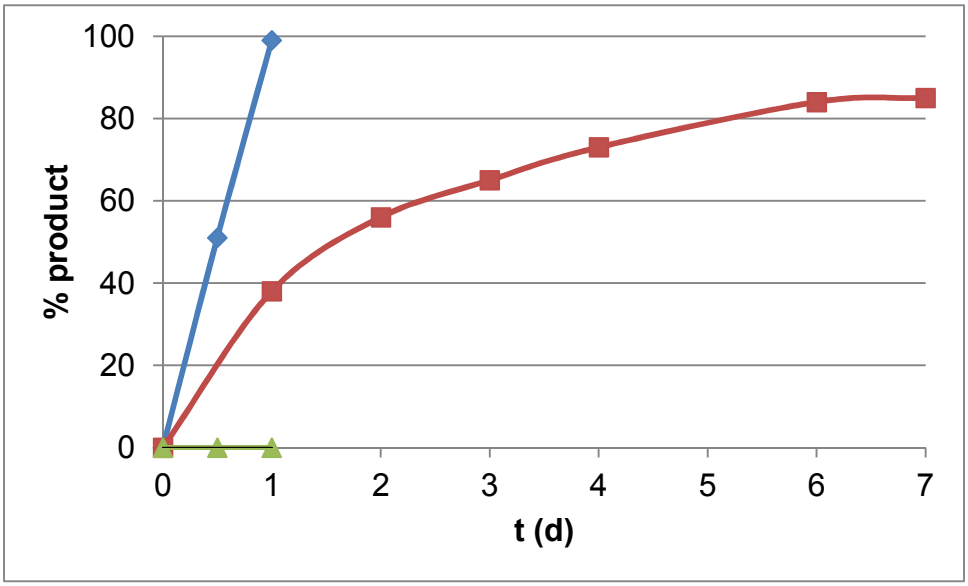

Figure 4.9. Rates of formation of **14** and **15**$^{+}$ TfO^{-} in CH_2Cl_2: **14** at rt (green triangle); **14** at 40 °C (red square); **15**$^{+}$ TfO^{-} at rt (blue diamond).

The triazole **15**$^{+}$ TfO^{-} was then tested for further derivatization using various metal sources. These data are summarized in Table 4.5. As can be observed, **15**$^{+}$ TfO^{-} was not disposed to C-H activation when using silver(I) and copper(I) oxide in CH_2Cl_2 at room temperature or at 40 °C (entries 1-4). An attempt to directly metallate using $PhAuPPh_3$ in THF at room temperature also showed no C-H activation (entry 5).

Table 4.5. Attempts to metallate the =CH moiety of triazolium salt **15**$^{+}$ TfO^{-}.

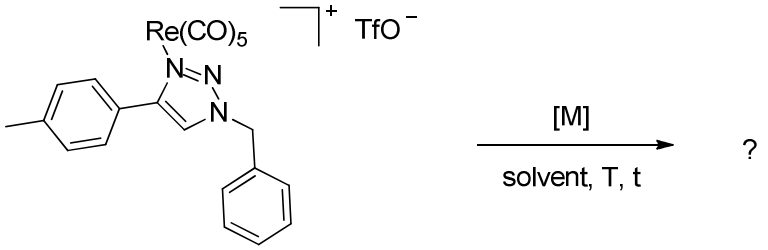

entry	reagent	solvent	T (°C)	t (d)	observation
1	Ag_2O	CH_2Cl_2	rt	3	nr
2	Ag_2O	CH_2Cl_2	40	3	nr
3	Cu_2O	CH_2Cl_2	rt	3	nr
4	Cu_2O	CH_2Cl_2	40	3	nr
5	$PhAuPPh_3$	CH_2Cl_2	rt	3	nr

The possibility that metallating first at the N(3) position might be problematic was considered. To provide a test, the triazole **2a**, previously synthesized from the platinum complex **1a** and benzyl azide,[169] was employed (Scheme 4.20). These data are summarized in Table 4.6.

Table 4.6. Attempts to metallate the =CH moiety of triazole **2a.**

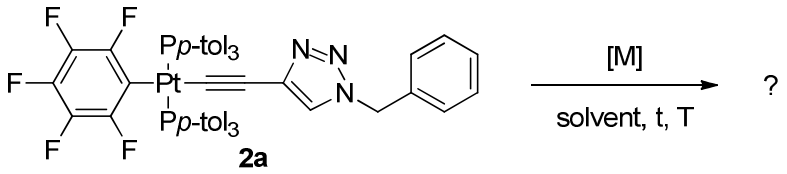

2a

entry	reagent	solvent	T (°C)	t (d)	observation
1	Ag_2O	CH_2Cl_2	rt	3	nr
2	Ag_2O	CH_2Cl_2	40	3	nr
3	Cu_2O	CH_2Cl_2	rt	3	nr
4	Cu_2O	CH_2Cl_2	40	3	nr
5	$PhAuPPh_3$	CH_2Cl_2	rt	3	nr

These reactions were monitored by ^1H NMR spectroscopy, specifically the disappearance of the =CH proton. Transmetallation was first attempted with silver(I) and copper(I) oxide in CH_2Cl_2. No C-H activation was seen with silver(I) oxide and with copper(I) oxide at room temperature and at 40 °C (entries 1-4). An attempt to directly metallate using $PhAuPPh_3$ in THF at room temperature also showed no C-H activation (entry 5). Thus, it can be seen that triazole **2a** was not disposed towards C-H activation using silver, copper, and gold sources. Substituting first at the N(3) position was not an intrinsic source of difficulty for this reaction.

It was next sought to test whether derivatization of triazole **2a** at N(3) with an organic electrophile might promote subsequent C-H activation at the =CH moiety. Accordingly, triazole **2a** was treated with MeI in CH_2Cl_2 at 40 °C for 36 h. The methyl group selectively added to the N(3) position to give a charged monometallated

triazolium salt **16**$^{+}$ I^{-} in 81% yield after workup (Scheme 4.19). The spectroscopic data for **16**$^{+}$ I^{-} were very similar to those of **2a**, with the exception of the ^{1}H NMR chemical shift of the =CH proton, which exhibited a downfield shift from δ 1.75 to 8.01 (ppm, CD_2Cl_2).

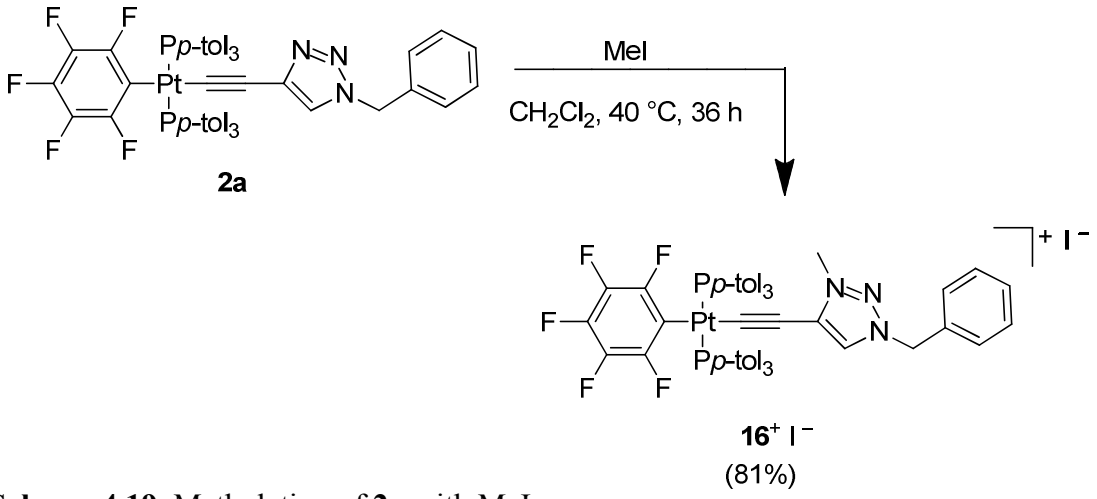

Scheme 4.19. Methylation of **2a** with MeI.

Complex **16**$^{+}$ I^{-} was investigated with respect to C-H activation using the same recipes. These data are described in Table 4.7.

Table 4.7. Attempts to metallate the =CH moiety of triazolium salt $\mathbf{16}^+ \, I^-$.

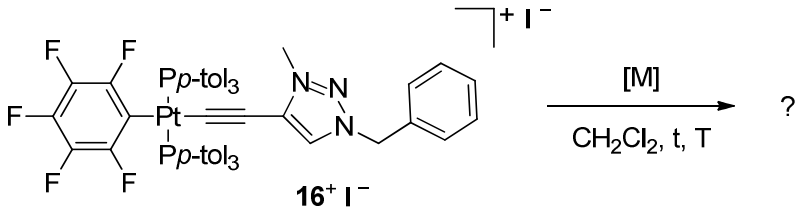

entry	reagent(s)	T (°C)	t (d)	observation
1	Cu_2O	40	6	nr
2	Ag_2O	40	2	nr
3	Cu_2O	40	3	nr
4	Ag_2O / $[RhCl(cod)]_2$	40	3	C-H activation

The =CH moiety was not reactive when using copper(I) and silver(I) oxide alone in CH_2Cl_2 at 40 °C (entries 1-3). However, the =CH bond was activated when using silver oxide and a rhodium dimer *in situ* (entry 4). Clean conversion to the bimetallic N-heterocyclic carbene complex **17** shown in Scheme 4.20 occurred, as assayed by ^1H NMR and evidenced by a characteristic ^{13}C NMR signal at δ 168.6 ppm (d, $^1J_{CRh}$ = 46.9 Hz). For example, the analogous rhodium complex in Scheme 4.8 showed a ^{13}C NMR signal at δ 170.6 ppm (d) with a $^1J_{CRh}$ value of 46.6 Hz.[173,175]

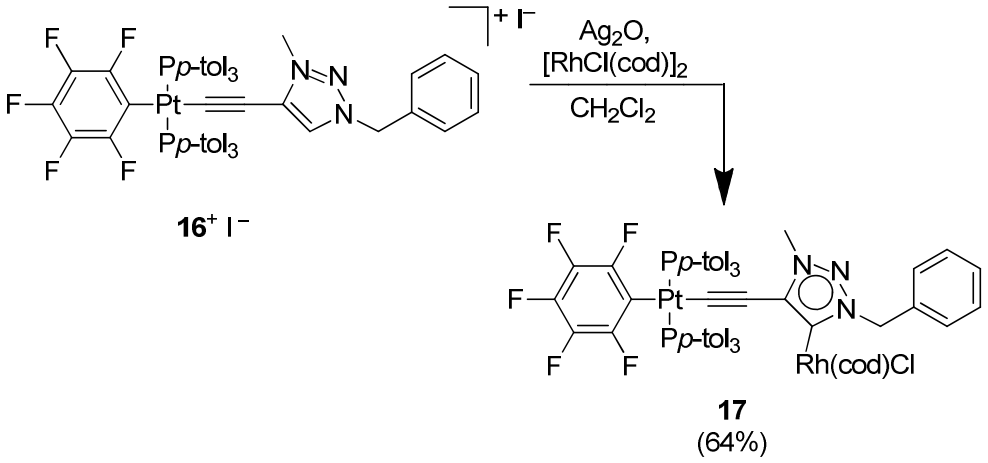

Scheme 4.20. Metallation of monometallic triazole **16**$^{+}$ I^{-}**.**

Scheme 4.20 establishes that bimetallic complexes can be accessed by the final step in Scheme 4.9, but as further analyzed in the discussion section, leave open the issue of tetra- or permetallated systems with M, M', M", M"' arrays. Looking further ahead, the challenge of modulating the stoichiometry – *i.e.* arrays of the type aM, bM', cM", dM"' – remains. Towards this end, one obvious approach is to engineer polytriazole systems. For example, if one metal is equipped with two azide functionalities, it should in principle be possible to access arrays of the type M, 2M', 2M", 2M"'.

To test feasibility, the copper catalyzed click reaction using a ferrocenyl diazide (η^5-$C_5H_4N_3)_2Fe$ (**8**) was utilized. The synthesis of **8** was reported by Molina per Scheme 4.12.[192] This synthesis utilizes triisopropylbenzenesulfonyl azide **7** as the azide source, the preparation of which was adapted from a patent.[197] Since no spectroscopic characterization of **7** was provided in the patent, ^{1}H and ^{13}C NMR data are provided. Compound **7** was obtained from triisopropylbenzenesulfonyl chloride and sodium azide as a stable clear oil in 87% yield. Experiments with the monoazide analogue of **8** were

also contemplated.[168] However, when the literature synthesis was attempted using (η^5-C_5H_4Li)(η^5-C_5H_5)Fe and **7**, difficulties were encountered. Specifically, the monoazide was much less stable on a silica gel column.

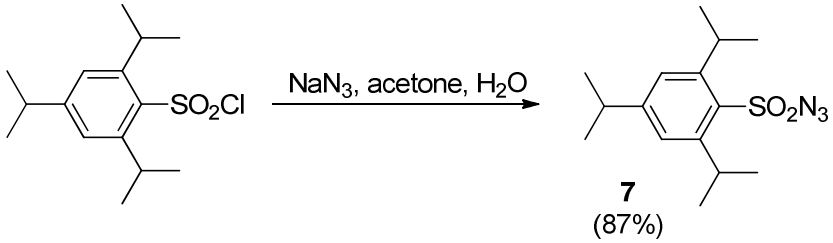

Scheme 4.21. Synthesis of azide **7**.

As shown in Scheme 4.22, the diazide **8** was then treated with two equiv. of **2a** in the presence of $CuSO_4 \cdot 5H_2O$, ascorbic acid, water, and DMF. Workup and column chromatography gave the trimetallic complex **18** in 47% yield, in which two equiv. of the platinum complex **2a** were added to the **8** to form two 1,2,3-triazole rings. Similar to the reaction in Scheme 4.15, the two C≡C ^{13}C NMR signals (δ 72.5 and 59.6 ppm ($CDCl_3$)) disappear during the course of this reaction, and the terminal ≡CH ^{1}H NMR signal of **2a** shifts far downfield as it is converted to the triazole =CH ^{1}H NMR signal of **18** (δ 1.46 to 6.47 ppm ($CDCl_3$)).

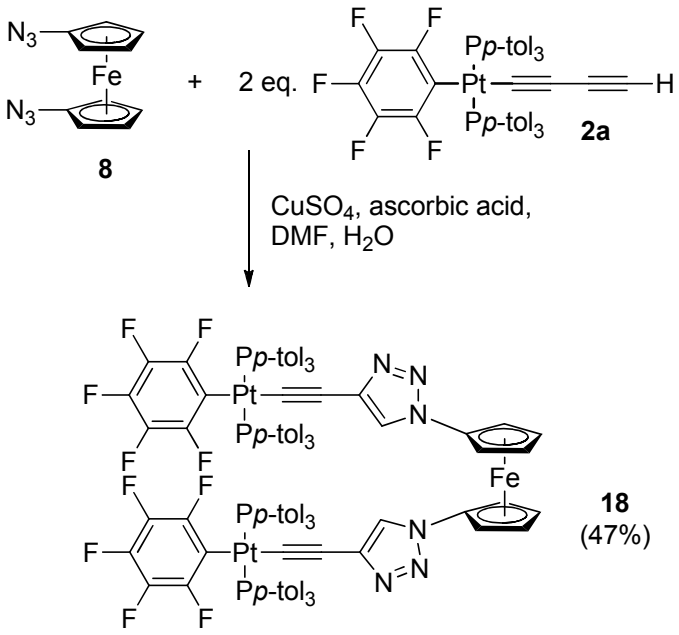

Scheme 4.22. Synthesis of trimetallic complex **18**.

Single crystals of **18** were grown, and the X-ray structure determined. Thermal ellipsoid plots are shown in Figure 4.10. Surprisingly, the cyclopentadienyl substituents exhibited, instead of an approximate anti relationship, an ortho motif with a (N)C-Cp(centroid)-Cp(centroid)-C(N) torsion angle of 78.56°. This can be clearly seen on the top right plot in Figure 4.10, in which the view is along the ferrocene axis. Interestingly, the cyclopentadienyl ligands are essentially eclipsed, as found in ferrocene.[198] Additional crystallographic data of interest is provided in Table 4.8.

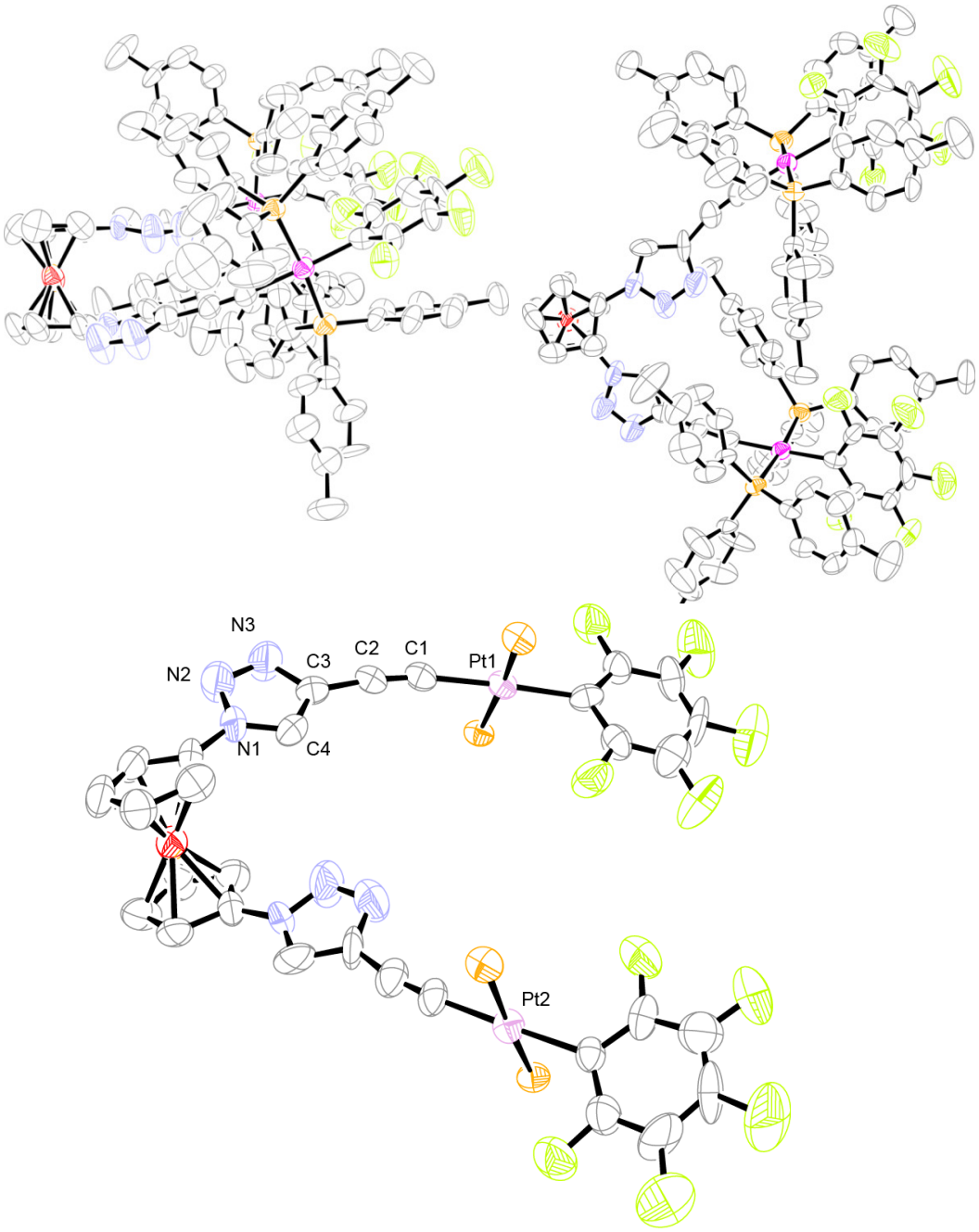

Figure 4.10. Thermal ellipsoid plots (50% probability level) of **18**. Side view (top, left), top view (top, right), and with *p*-tolyl groups omitted for clarity (bottom).

Table 4.8. Key crystallographic distances [Å] and angles [°] for **18**.

	Pt1-chain	Pt2-chain [a]
Pt-C1	1.961(9)	1.980(10)
C1≡C2	1.199(10)	1.183(11)
C2-C3	1.454(12)	1.437(13)
C3=C4	1.346(10)	1.365(10)
C4-N1	1.343(11)	1.348(10)
N1-N2	1.340(9)	1.314(10)
N2=N3	1.313(10)	1.325(10)
N3-C3	1.373(10)	1.370(11)
N-C5	1.412(11)	1.430(11)
C_{ipso}[b]-Pt1-C1	177.3(4)	175.8(3)
Pt1-C1-C2	169.7(8)	171.7(6)
C1-C2-C3	172.3(10)	169.4(7)
angle triazole/ C_6F_5 planes	5.4	21.6
angle triazole/ C_5H_4 planes	29.3	16.5
angle C_5H_4 twist[c]	78.6	---
angle C_5H_4 ring tilt[c]	4.2	---
av. π stacking[d]	3.761	3.631
angle stacking[e]	158.94	162.34

[a] For ease of comparison, the atoms of the two ferrocenyl substituents have been identically numbered. [b] C_{ipso} is the platinum bound C_6F_5 carbon atom. [c] This angle is defined in Figure 4.14. [d] Average distance between midpoints of the C_6F_5 and $C_6H_4CH_3$ rings. [e] Angle of midpoints of the three rings in c.

DISCUSSION

1. Approach to Permetallation. Although a permetallated cycloadduct was not ultimately obtained, the reactions in Schemes 4.15 and 4.16 establish that bi- and trimetallated triazole rings can be accessed by well-known click reaction conditions and subsequent functionalization with rhenium fragments. Furthermore, Scheme 4.20 shows that it is feasible to metallate the fourth site, albeit with fewer metals in the other positions. Upon implementation of these latter reaction conditions and the methodologies described in Scheme 4.22 in which a trimetallic species is accessed by a diazide complex, a complex with up to seven metals –M, 2M', 2M'', and 2M''' – could potentially be realized.

The intrinsic flexibility of this methodology is obvious. For example, other readily available metal butadiynyl complexes encompassing various transition metals include (bipy)$(CO)_3$ReC≡CC≡CH,[143] (p-tolP)AuC≡CC≡CH,[199] and (dppe)(η^7-C_7H_7)MoC≡CC≡CH.[200] Various diazides are readily available, such as the ruthenium analogue of **8**, (η^5-$C_5H_4N_3)_2$Ru.[201] Scheme 4.22 establishes an alternative route to a trimetallated complex involving a two-fold triazole ring formation by a click reaction. The syntheses of organic tetraazides have been reported[202,203] One such tetraazide, whose synthesis is shown in Scheme 4.23,[204] could be adapted to an organometallic analogue with suitable ligand based leaving groups.

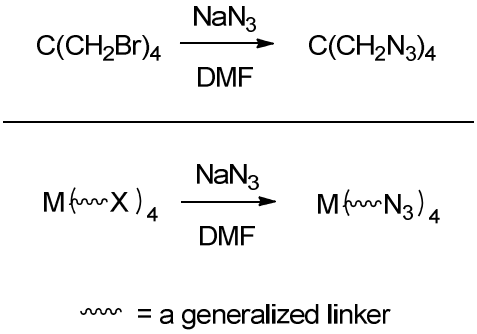

Scheme 4.23. Synthesis of an organic tetraazide by Romagnoli (top) and a possible organometallic analogue (bottom).

In view of the structural data in Figures 4.6-4.8, it is unlikely that the failures described in Tables 4.2-4.6 are due to steric effects. The possibility that electronic effects might underly the recalcitrant C-H activation leading to these failures was considered. The ^{1}H NMR chemical shifts of the triazole or triazolium =CH moieties in the preceding compounds proved to be particularly informative. These are summarized in Table 4.9, together with that of the purely organic salt $C_6H_5\overline{C{=}CHN(Et)N{=}N}(Me)]^+$ I^- (**19**$^+$ I^-), shown in Figure 4.11.[173]

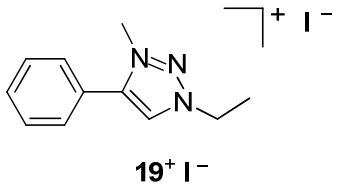

19$^+$ I^-

Figure 4.11. Albrecht's purely organic triazolium salt **19**$^+$ I^-.

As previously shown in Scheme 4.8, compound **19**$^{+}$ I^{-} readily reacts with Ag_2O to give a cationic bis(triazolylidene) silver complex that is easily transmetallated to give rhodium and iridium adducts. Importantly, **19**$^{+}$ I^{-} exhibits the most downfield =CH signal (δ 9.52 ppm, $CDCl_3$), suggestive of the greatest acidity. In the remaining complexes, the =CH signal generally shifts upfield as the number of electropositive metal substituents increases (δ 8.01-6.15 ppm for one metal fragment, δ 6.26 ppm for two, and δ 6.03-5.81 ppm for three). Of all the new complexes in this study, only **16**$^{+}$ I^{-} underwent C-H activation (Scheme 4.20). Accordingly, it exhibits the second most deshielded =CH ^{1}H NMR signal in Table 4.9 (δ 8.01 ppm, CD_2Cl_2). Hence, a chemical shift of ca. δ 7.9 ppm seems to represent an operational cutoff for elaborating this carbon atom to a carbene complex under the conditions investigated.

The chemical shift of the =CH triazole proton of **18** (δ 6.47 ppm, $CDCl_3$) is not significantly different from the rhenium cyclopentadienyl analogue **10** (δ 6.29 ppm, $CDCl_3$), with a Δδ of just 0.18. This would indicate that methodologies for functionalization at the =CH triazole moiety similar to those in Scheme 4.20 would not be successful with **18**.

Table 4.9. =CH ^{1}H NMR data for compounds with the structural unit I.

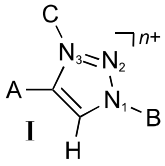 I	*n*	A	B	C	δ, =CH (ppm)
11	0	$ArL_2PtC{\equiv}C^a$	$(C_5H_4)Re(CO)_3$	$Re(CO)_4Br$	5.81[c], 5.73[b]
12$^+$ TfO^-	1	$ArL_2PtC{\equiv}C^a$	$(C_5H_4)Re(CO)_3$	$Re(CO)_5$	6.03[c], 6.09[b]
10	0	$ArL_2PtC{\equiv}C^a$	$(C_5H_4)Re(CO)_3$	---	6.26[b]
18	0	$ArL_2PtC{\equiv}C^a$	$[(\eta^5\text{-}C_5H_4)_2Fe]_{0.5}$	---	6.29 [b]
2a	0	$ArL_2PtC{\equiv}C^a$	CH_2Ph	---	6.15[b]
15$^+$ TfO^-	1	$CH_3C_6H_5$	CH_2Ph	$Re(CO)_5$	7.83[b]
16$^+$ I^-	1	$ArL_2PtC{\equiv}C^a$	CH_2Ph	Me	8.01[c]
19$^+$ I^-	1	Ph	Et	Me	9.52[b]

[a] ArL_2 = *trans*-$(C_6F_5)(p\text{-}tol_3P)_2$. [b] in $CDCl_3$. [c] in CD_2Cl_2.

2. Crystal Structures of Non-Ferrocenyl Complexes. The X-ray crystal structures of **10**·$2CH_2Cl_2$, **11**$^+$ TfO^-·CH_2Cl_2, and **12**·$2CH_2Cl_2$ show very similar features in terms of bond lengths and angles of the triazole and carbon chain moieties. However, the planarity of the units defined by the C_6F_5/triazole/C_5H_4 rings varies greatly. The angles between the individual rings are summarized in Table 4.1. For instance, **10**·$2CH_2Cl_2$ exhibits the lowest degree of planarity between the triazole and C_6F_5 rings, with a median plane/plane angle of 60.49°, whereas analogous measurements for **11**$^+$ TfO^-·CH_2Cl_2 and **12**·$2CH_2Cl_2$ show angles of only 38.16° and 20.95°, respectively. However, when examining the planarity of the units defined by the triazole and C_5H_4 rings, **10**·$2CH_2Cl_2$ shows the highest degree of planarity with a median plane angle of 20.21°, whereas **11**$^+$ TfO^-·CH_2Cl_2 shows the lowest degree of

planarity with a median plane angle of 67.59°. In all cases, stacking of the $C_6H_4CH_3/C_6F_5/C_6H_4CH_3$ moieties was observed, with an average π stacking distance of 3.690 Å. This type of stacking has been seen before in similar platinum complexes and the π stacking distances are comparable.[169]

In **12**·$2CH_2Cl_2$, the bromide ligand of the *cis*-$Re(CO)_4Br$ moiety was disordered over two positions (84:16), *trans* to each other. The bond lengths within the trinitrogen heterocycles also showed various trends. For example, with the cationic complex $\mathbf{11}^+$ $TfO^-\cdot CH_2Cl_2$, the N1-N2 and N2=N3 bond lengths (1.316(7) and 1.288(7) Å) were slightly shorter than those in the others (1.343(6)-1.348(4) and 1.323(6)-1.317(4) Å). Although the N2=N3 bond lengths do not follow suit, analogous N1-N2 contractions have been observed upon alkylations of 1-aminotriazoles previously studied by Hawkins.[205] Hawkins' unsubstituted triazole has an N1-N2 bond length of 1.345(2) Å. The data in Table 4.10 show that an average shortening of ca. 0.030 Å is observed upon alkylation at the N(3) position, which is consistent with the N1-N2 bond shortening found in $\mathbf{11}^+$ $TfO^-\cdot CH_2Cl_2$.

Table 4.10. Bond lengths in Hawkins' 1-aminotriazoles and corresponding triazolium salts.

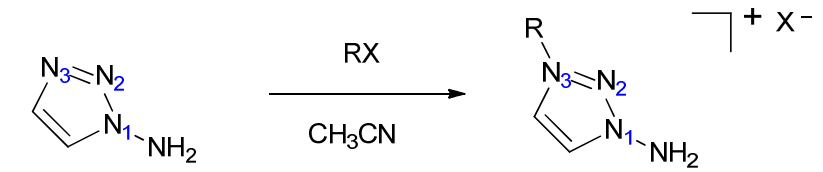

N1-N2 = 1.345(2) Å

RX	N1-N2, Å
MeI	1.314(2)
EtBr	1.322(3)
PrBr	1.307(8)
BuBr	1.318(2)

The crystal lattices were also examined for special features. Interestingly, the triazole ends of **10** aggregate together in the crystal structure, to effect a "tail to tail" packing in which the triazole rings are oppositely stacked between opposing layers, as depicted in Figure 4.12.

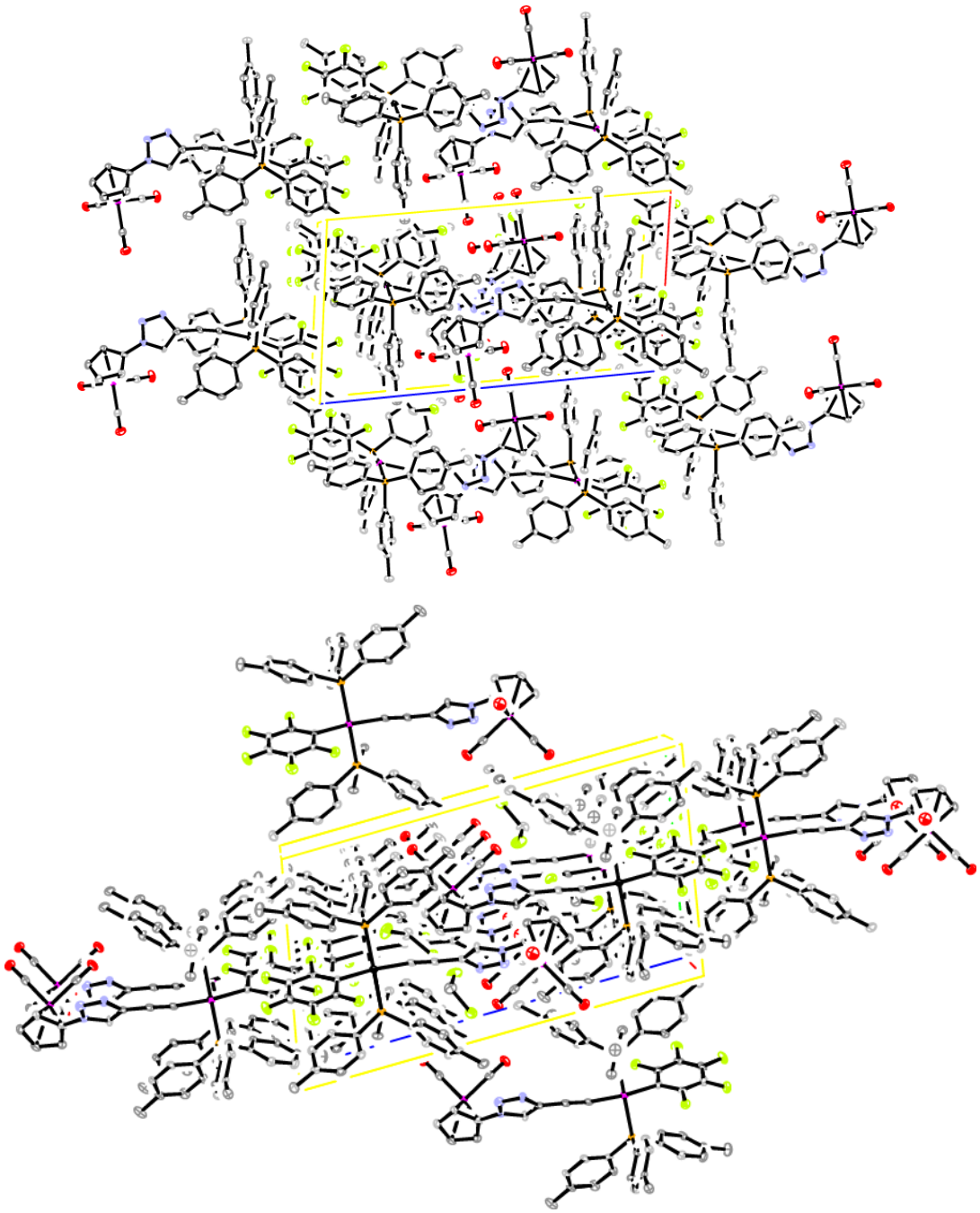

Figure 4.12. Thermal ellipsoid plots (50% probability level) of the crystal packing in **10**·2CH_2Cl_2: view down the triazole rings (top) and side view (bottom). The solvent molecules have been removed for clarity.

3. Crystal Structure of Ferrocenyl Complexes. Although the reaction in Scheme 4.22 is not the first click reaction involving **8**,[206] it is the first click reaction involving **8** and a terminal alkyne attached to a transition metal. The crystal structure of **18** is similar to a complex reported by Molina, in which the same ferrocenyl diazide (**8**) was clicked with 2-ethynylpyridine.[206] The resulting complex **20** displays similar quasi eclipsed cyclopentadienyl substituents, which are twisted from the eclipsed conformation by 18.1°, as shown in Figure 4.13. As mentioned before, the cyclopentadienyl rings in **18** are twisted from an eclipsed conformation by 78.6° (about one fifth of a turn), which can be seen in Figure 4.10, demonstrating the greater steric bulk on the triazole in **18** versus that in **20**.

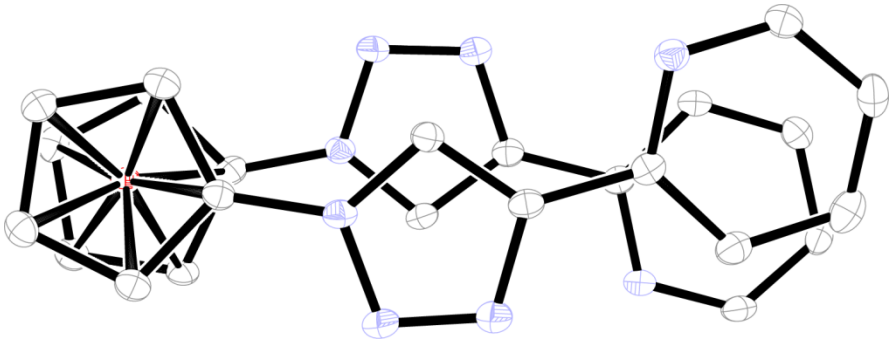

Figure 4.13. Thermal ellipsoid plot (50% probability level) of Molina's ferrocene-based ditriazole complex (**20**) with a cyclopentadienyl substituent twist of 18.1°.

The angle between the cyclopentadienyl rings in **18** is given in Table 4.8. The low value, 1.4°, indicates a nearly parallel relationship. The corresponding angle in **20** is 4.2°. This larger value may be due to the smaller cyclopentadienyl twist angle, which

forces the organic substituents to have more interaction. How these angles are defined and measured is depicted in Figure 4.14.

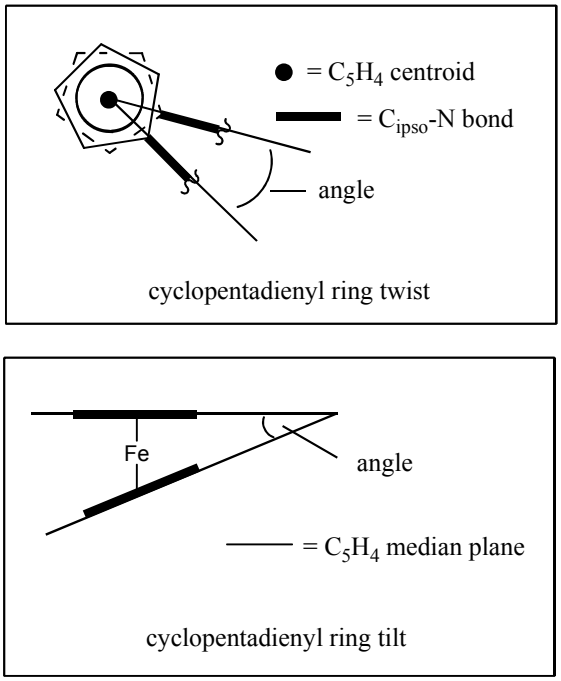

Figure 4.14. Schematic representation of the cyclopentadienyl ring tilt and twist angles measured in **18** and **20**.

The two triazole/carbon chains of **18** exhibit very different packing features. The chain of Pt1 shows almost planar behavior between the triazole and C_6F_5 rings, with an angle of only 5.4°, whereas the analogous angle of the Pt2 chain is 21.6°. The difference in the two chains is further emphasized when comparing the angle between the triazole and C_5H_4 rings. In the Pt1 chain, the two rings deviate further from planarity than in the Pt2 chain (29.3° vs. 16.5°). Not surprisingly, this is strikingly different from the two

triazole rings on **20**, which are perfectly planar with respect to the cyclopentadienyl rings.

CONCLUSION

In summary, this work has significantly expanded the scope of click chemistry in metal coordination spheres. Given that alkynyl, azide, and electrophilic derivatives of every transition metal are known, this methodology should allow the facile assembly of virtually any hetereotrimetallic combination. Furthermore, there are several means by which the stoichiometry of the metals may be varied. However, a comparatively versatile introduction of a fourth metal onto the triazole or triazolium core must await one of two developments. The most desirable would be the discovery of new =CH functionalization methodologies that are not as sensitive to proton acidity. Alternatively, more electronegative metal fragments could be employed, possibly in conjunction with spacers that would enhance insulation from the heterocycle core.

EXPERIMENTAL

General: All reactions were conducted under inert atmospheres using standard Schlenk and vacuum line techniques unless otherwise noted. Workups were carried out in air. Chemicals were treated as follows: CH_2Cl_2 (ACS grade, Fisher Scientific; reaction solvent) and THF (Fisher Scientific; reaction solvent), dried and degassed using a Glass Contour solvent purification system; acetone (ACS grade, BDH), distilled from $CaSO_4$; CH_2Cl_2 (ACS grade, EMD Chemicals; chromatography/workups), hexanes (ACS grade, Macron Chemicals; chromatography/workups), DMF (ACS grade, Fisher

Scientific), EtOH (Koptec), $CDCl_3$ and CD_2Cl_2 (2 × Cambridge Isotope Laboratories), silica (Acros, 60 Å), alumina (neutral, Brockmann I, 50-200 μm), $CuSO_4 \cdot 5H_2O$ (98+%, BDH), ascorbic acid (99.7%, EMD Chemicals), triisopropylbenzenesulfonyl chloride (98%, Alfa Aesar), MeI (98%, Alfa Aesar), NaN_3 (99.0%, Aldrich), *n*-BuLi (Alfa Aesar, 2.73 M in hexanes), $[RhCl(cod)]_2$ (Pressure Chemical), and Ag_2O (99+%, Acros), used as received.

NMR spectra were recorded on a Varian NMRS 500 MHz spectrometer at ambient probe temperatures and referenced as follows: ^1H: residual internal $CHCl_3$ (δ, 7.26 ppm), $CHDCl_2$ (δ, 5.32 ppm), ^{13}C: internal $CDCl_3$ (δ, 77.20 ppm), CD_2Cl_2 (δ, 54.00 ppm), ^{31}P external H_3PO_4 (δ, 0.00 ppm). IR spectra were recorded using a Shimadzu IRAffinity-1 spectrometer with a Pike MIRacle ATR system (diamond/ZnSe crystal). Melting points were recorded with a Stanford Research Systems (SRS) MPA100 (Opti-Melt) automated melting point system. Microanalyses were conducted by Atlantic Microlab.

Triisopropylbenzenesulfonyl azide (7).[197] A round bottom flask was charged with acetone (40 mL) and triisopropylbenzenesulfonyl chloride (4.3426 g, 14.335 mmol) and cooled to 0 °C. Then NaN_3 (1.4430 g, 22.197 mmol) was added with stirring and the cold bath was removed. After 5 h, the solvent was removed by rotary evaporation and H_2O (50 mL) was added. The mixture was extracted with CH_2Cl_2 (3 × 50 mL) and the extract was dried ($MgSO_4$). The solvent was removed by rotary evaporation and the residue was dried by oil pump vacuum to give **7** as a clear oil (3.8506 g, 12.444 mmol, 89%).

NMR (δ (ppm): ^1H ($CDCl_3$): 7.22 (s, 2H, *m* to S), 4.05 (sept, 2H, $^3J_{HH}$ = 6.5 Hz, *i*-C*H*$(CH_3)_2$), 2.93 (sept, 1H, $^3J_{HH}$ = 6.9 Hz, *p*-C*H*$(CH_3)_2$), 1.28 (d, 12H, $^3J_{HH}$ = 6.8

Hz, *i*-CH(CH_3)$_2$), 1.26 (d, 6H, $^3J_{HH}$ = 6.9 Hz, *p*-CH(CH_3)$_2$); ^{13}C{^{1}H} 155.0 (s, *p* to S), 151.1 (s, *o* to S), 133.2 (s, *i* to S), 124.3 (s, *m* to S), 34.6 (s, *p*-*C*H(CH$_3$)$_2$), 30.0 (s, *i*-*C*H(CH$_3$)$_2$), 25.0 (s, *i*-CH(*C*H$_3$)$_2$), 23.7 (s, *p*-CH(*C*H$_3$)$_2$).

(η^5-$C_5H_4N_3$)Re(CO)$_3$ (9). A round bottom flask was charged with (η^5-C_5H_5)Re(CO)$_3$ (0.7711 g, 2.299 mmol)[207] and THF (30 mL) and cooled to −78 °C. A solution of *n*-BuLi (0.93 mL, 2.73 M in hexanes, 2.5 mmol) was added with stirring. After 1 h, a solution of tosyl azide (0.9635 g, 4.885 mmol)[208] in THF (20 mL) was added, and the assembly was wrapped in foil. After 14 h, the solvent was removed by oil pump vacuum and the residue was chromatographed on a silica gel column (40 × 3 cm) using 2:3 v/v CH_2Cl_2/hexanes. Some (η^5-C_5H_5)Re(CO)$_3$ eluted first, followed by **9**, and then excess tosyl azide. The solvent was removed from the middle fractions by oil pump vacuum to give **9** as an off-white solid (0.5726 g, 1.521 mmol, 68%). This complex has been previously characterized in situ by ^{1}H NMR spectroscopy.[209]

NMR (δ (ppm), $CDCl_3$): ^{1}H 5.32 (t, 2H, $^3J_{HH}$ = 2.3 Hz, NCC*H*), 5.23 (t, 2H, $^3J_{HH}$ = 2.3 Hz, NCCHC*H*); ^{13}C{^{1}H}[210] 193.0 (*C*O), 119.4 (*C*N$_3$), 81.8 (2C of C_5H_4N), 73.5 (2C of C_5H_4N).

IR (ATR, cm^{-1}): 2122 (s, ν_{NNN}), 2021 (s, ν_{CO}), 1913 (s, ν_{CO}), 1470 (m), 1385 (w), 1280 (m), 1153 (w), 1022 (w), 821 (w), 744 (w).

***trans*-(C_6F_5)(*p*-tol$_3$P)$_2$PtC≡CC=CHN((η^5-C_5H_4)Re(CO)$_3$)N=N (10).** A round bottom flask was charged in the dark with *trans*-(C_6F_5)(*p*-tol$_3$P)$_2$PtC≡CC≡CH (**1a**;[50] 0.0987 g, 0.0968 mmol), **9** (0.0367 g, 0.0975 mmol), DMF (5 mL), $CuSO_4 \cdot 5H_2O$ (0.0394 g, 0.158 mmol), ascorbic acid (0.0390 g, 0.221 mmol), and water (1 mL) with stirring. After 15 h, the solvent was removed by oil pump vacuum. Water (10 mL) was

added, and the mixture was extracted with CH_2Cl_2 (3 × 15 mL) and the extract was dried ($MgSO_4$). The solvent was removed by rotary evaporation and the residue was chromatographed on a silica gel column (30 × 4.5 cm) with CH_2Cl_2. The excess **9** eluted first. The solvent was removed from the next band by oil pump vacuum to give **10** as a white solid (0.0731 g, 0.0524 mmol, 54%), which yellowed at 162 °C, blackened at 194 °C and liquefied at 208 °C. Anal. Calcd. for $C_{60}H_{47}F_5N_3O_3P_2PtRe$ (1396.26 g/mol): C, 51.50; H, 3.60; N, 3.00. Found: C, 51.69; H, 3.46; N, 3.01.

NMR (δ (ppm), $CDCl_3$): ^{1}H 7.57-7.48 (m, 12H, *o* to P), 7.13-7.06 (m, 12H, *m* to P), 6.29 (s, 1H, C=C*H*N), 5.67 (t, 2H, $^3J_{HH}$ = 2.3 Hz, C_5H_4N), 5.27 (t, 2H, $^3J_{HH}$ = 2.3 Hz, C_5H_4N), 2.35 (s, 18H, CH_3); $^{13}C\{^1H\}$[210] 192.4 (s, Re(*C*O)$_3$), 146.1 (dd, $^1J_{CF}$ = 220 Hz, $^2J_{CF}$ = 23 Hz, *o* to Pt), 140.8 (s, *p* to P), 137.7 (m, *p* to Pt), 136.2 (s, PtC≡C*C*), 135.8 (m, *m* to Pt), 134.6 (virtual t,[63] $^2J_{CP}$ = 12.7 Hz, *o* to P), 128.7 (virtual t,[63] $^3J_{CP}$ = 11.0 Hz, *m* to P), 127.8 (virtual t,[63] $^1J_{CP}$ = 60 Hz, *i* to P), 123.0 (s, C=*C*HN), 111.0 (s, Pt*C*≡C), 100.7 (s, PtC≡*C*), 82.1 and 76.1 (2 s, C_5H_4N), 21.6 (s, CH_3); $^{31}P\{^1H\}$ 17.94 (s, $^1J_{PPt}$ = 2700 Hz).[67]

IR (ATR, cm^{-1}): 2129 (m, $\nu_{C\equiv C}$), 2021 (s, ν_{CO}), 1921 (s, ν_{CO}), 1496 (m), 1450 (m), 1095 (m), 948 (s), 802 (s).

MS (ESI^+):[59] 1397 ([**10**+H]$^+$, 100%).

[*trans*-(C$_6$F$_5$)(*p*-tol$_3$P)$_2$PtC≡CC=CHN((η^5-C$_5$H$_4$)Re(CO)$_3$)N=N(Re(CO)$_5$)]$^+$ TfO$^-$ (11$^+$ TfO$^-$). A Schlenk flask was charged with **10** (0.1010 g, 0.07239 mmol), $Re(CO)_5OTf$ (**6**;[188] 0.0398 g, 0.08373 mmol) and CH_2Cl_2 (15 mL) with stirring. After 5 d, the solvent was removed by rotary evaporation. The residue was washed with Et_2O (10 mL) and dried by oil pump vacuum to give **11**$^+$ TfO^- as a white solid (0.1133 g, 0.06054 mmol, 84%), which slightly darkened at 125 °C and liquefied at 200 °C. Anal.

Calcd. for $C_{66}H_{47}F_8N_3O_{11}P_2PtRe_2S$ (1871.59 g/mol): C, 42.35; H, 2.53; N, 2.25. Found: C, 42.00; H, 2.57; N, 2.12.

NMR (δ (ppm), CD_2Cl_2): ^{1}H 7.55-7.47 (m, 12H, *o* to P), 7.23-7.17 (m, 12H, *m* to P), 6.03 (s, 1H, C=C*H*N), 5.85 (t, $^3J_{HH}$ = 2.4 Hz, 2H, C_5H_4N), 5.50 (t, $^3J_{HH}$ = 2.4 Hz, 2H, C_5H_4N), 2.39 (s, 18H, CH_3); $^{13}C\{^1H\}$[210] 192.1 (s, Re(*C*O)$_3$), 180.1 (s, *C*O), 178.7 (s, *C*O), 142.2 (s, *p* to P), 141.1 (s, PtC≡C*C*), 134.9 (m, *o* to P), 129.5 (virtual t,[63] $^3J_{CP}$ = 8.9 Hz, *m* to P), 128.1 (s, CC=*C*H), 127.6 (virtual t,[63] $^1J_{CP}$ = 60.3 Hz, *i* to P), 106.4 (s, Pt*C*≡C), 98.7 (s, PtC≡*C*), 84.0 and 80.3 (2 s, C_5H_4N), 21.7 (s, CH_3); $^{31}P\{^1H\}$ 17.6 (s, $^1J_{PPt}$ = 2623 Hz).[67]

NMR (δ (ppm), $CDCl_3$): 7.54-7.47 (m, 12H, *o* to P), 7.22-7.12 (m, 12H, *m* to P), 6.09 (s, 1H, C=C*H*N), 5.92 (t, $^3J_{HH}$ = 2.4 Hz, 2H, C_5H_4N), 5.39 (t, $^3J_{HH}$ = 2.4 Hz, 2H, C_5H_4N), 2.38 (s, 18H, CH_3); $^{31}P\{^1H\}$ 17.6 (s, $^1J_{PPt}$ = 2621 Hz).[67]

IR (ATR, cm^{-1}): 2106 (m, $\nu_{C\equiv C}$), 2044 (s, ν_{CO}), 2029 (s, ν_{CO}), 1921 (br s, ν_{CO}), 1496 (m), 1458 (m), 1257 (s), 1157 (w), 1095 (m), 1026 (s), 948 (m), 802 (s).

MS (ESI^+):[59] 1723 ([**11**]$^+$, 100%).

***trans*-(C_6F_5)(*p*-$tol_3P)_2$PtC≡CC=CHN((η^5-C_5H_4)Re$(CO)_3$)N=N(*cis*-Re$(CO)_4$-Br)·$2CH_2Cl_2$ (12·$2CH_2Cl_2$)**. A Schlenk flask was charged with **10** (0.0411 g, 0.0316 mmol), $Re(CO)_5Br$ (**5**;[189] 0.0149 g, 0.0367 mmol) and CH_2Cl_2 (6 mL) with stirring. After 10 d, the solvent was removed by rotary evaporation. The residue was washed with EtOH (20 mL) and dried under oil pump vacuum to give **12**·$2CH_2Cl_2$ as a white solid (0.0560 g, 0.0311 mmol, 98%), which yellowed at 160 °C and blackened at 228 °C. Anal. Calcd. for $C_{64}H_{47}BrF_5N_3O_7P_2PtRe_2 \cdot 2CH_2Cl_2$ (1944.28 g/mol): C, 40.77; H, 2.64; N, 2.16. Found: C, 40.73; H, 2.58; N, 2.33.

NMR (δ (ppm), CD_2Cl_2): ^{1}H 7.59-7.49 (m, 12H, *o* to P), 7.22-7.13 (m, 12H, *m* to P), 5.81 (s, 1H, C=C*H*N), 5.71 (t, $^3J_{HH}$ = 2.3 Hz, 2H, C_5H_4N), 5.41 (t, $^3J_{HH}$ = 2.3 Hz, 2H, C_5H_4N), 5.32 (s, 4H, CH_2Cl_2), 2.38 (s, 18H, CH_3); $^{13}C\{^1H\}$[210] 192.3 (s, Re(*C*O)$_3$), 180.1 (s, *C*O), 179.7 (s, *C*O), 178.7 (s, *C*O), 141.8 (s, *p* to P), 141.1 (s, PtC≡C*C*), 135.0 (virtual t,[63] $^2J_{CP}$ = 13.4 Hz, *o* to P), 129.3 (virtual t,[63] $^3J_{CP}$ = 11.4 Hz, *m* to P), 127.9 (virtual t,[63] $^1J_{CP}$ = 60.8 Hz, *i* to P), 126.0 (s, CC=*C*H), 108.6 (s, Pt*C*≡C), 99.7 (s, PtC≡*C*), 83.5 and 78.0 (2 s, C_5H_4N), 22.2 (s, CH_3); $^{31}P\{^1H\}$ 17.7 (s, $^1J_{PPt}$ = 2653 Hz).[67]

NMR (δ (ppm), $CDCl_3$): ^{1}H 7.56-7.48 (m, 12H, *o* to P), 7.17-7.11 (m, 12H, *m* to P), 5.73 (s, 1H, C=C*H*N), 5.66 (t, $^3J_{HH}$ = 2.3 Hz, 2H, C_5H_4N), 5.35 (t, $^3J_{HH}$ = 2.3 Hz, 2H, C_5H_4N), 5.30 (s, 4H, CH_2Cl_2), 2.38 (s, 18H, CH_3).

IR (ATR, cm^{-1}): 2113 (m, $\nu_{C\equiv C}$), 2029 (s, ν_{CO}), 2013 (s, ν_{CO}), 1990 (s, ν_{CO}), 1936 (br s, ν_{CO}), 1921 (s, ν_{CO}), 1597 (w), 1496 (w), 1458 (w), 1188 (w), 1095 (m), 948 (s).

MS (ESI$^+$):[59] 1774 ([**12**]$^+$, 100%).

***p*-$CH_3C_6H_4$C=CHN($CH_2C_6H_5$)N=N(*cis*-$Re(CO)_4Br$) (14).** A round bottom flask was fitted with a condenser and charged with *p*-$CH_3C_6H_4$C=CHN($CH_2C_6H_5$)N=N (**13**;[196] 0.3037 g, 1.291 mmol), **5** (0.5279 g, 1.300 mmol)[189] and CH_2Cl_2 (40 mL) with stirring. The mixture was refluxed. After 10 d, the solvent was removed by rotary evaporation. The residue was washed with EtOH (50 mL) to give **14** as a tan solid (0.6588 g, 1.050 mmol, 81%), which liquefied at 127-130 °C.

NMR (δ (ppm), $CDCl_3$): ^{1}H 7.61 (s, 1H, C=C*H*N), 7.51-7.29 (m, 9H, C_6H_4 and C_6H_5), 5.52 (s, 2H, CH_2), 2.28 (s, 3H, CH_3); $^{13}C\{^1H\}$ 189.2 (s, *C*O), 189.1 (s, *C*O), 182.8 (s, *C*O), 154.9 (s, N*C*=C), 141.7 (s, *i* to CH_2), 131.2 (s, *i* to CH_3), 130.7 (s, *o* to

CH_3), 130.5 (s, *m* to CH_2), 130.4 (s, *o* to CH_2), 129.7 (s, *p* to CH_3), 129.4 (s, *p* to CH_2), 127.4 (s, *m* to CH_3), 123.6 (s, C=*C*HN), 59.7 (s, *C*H_2), 21.7 (s, *C*H_3).

IR (ATR, cm^{-1}): 2029 (s, ν_{CO}), 1982 (s, ν_{CO}), 1937 (s, ν_{CO}), 1898 (s, ν_{CO}), 717 (m).

[*p*-$CH_3C_6H_4$C=CHN($CH_2C_6H_5$)N=N($Re(CO)_5$)]$^+$ TfO^- ($\mathbf{15}^+$ $\mathbf{TfO^-}$**)**. A round bottom flask was charged with **13** (0.1012 g, 0.4301 mmol),[196] **6** (0.2056 g, 0.4325 mmol),[188] and CH_2Cl_2 (20 mL) with stirring. After 4 d, the solvent was removed by rotary evaporation. The residue was washed with EtOH (20 mL) to give $\mathbf{15}^+$ TfO^- as a cream colored sticky solid (0.3027 g, 0.4260 mmol, 99%). Anal. Calcd. for $C_{22}H_{15}F_3N_3O_8ReS$ (724.64 g/mol): C, 36.46; H, 2.09; N, 5.80. Found: C, 36.94; H, 2.07; N, 6.04.

NMR (δ (ppm), $CDCl_3$): ^{1}H 7.83 (s, 1H, C=C*H*N), 7.53-7.26 (m, 9H, C_6H_4 and C_6H_5), 5.71 (s, 2H, CH_2), 2.39 (s, 3H, CH_3); $^{13}C\{^1H\}$ 178.7 (s, *C*O), 178.5 (s, *C*O), 152.9 (s, N*C*=C), 142.0 (s, *i* to CH_2), 132.6 (s, *i* to CH_3), 130.1 (s, *o* to CH_3), 129.6 (s, *m* to CH_2), 129.5 (s, *o* to CH_2), 129.4 (s, *p* to CH_3), 125.9 (s, *p* to CH_2), 124.9 6 (s, m to CH_3), 122.1 (s, C=*C*HN), 56.2 (s, *C*H_2), 21.6 (s, *C*H_3).

IR (ATR, cm^{-1}): 2099 (w, ν_{CO}), 2014 (br s, ν_{CO}), 1936 (s, ν_{CO}), 1906 (br s, ν_{CO}), 1257 (s), 1157 (s), 1026 (s).

MS (MALDI$^+$):[59] 576 ([**15**]$^+$, 100%), 548 ([**15** – CO]$^+$, 88%), 520 ([**15** – 2CO]$^+$, 90%).

[*trans*-(C_6F_5)(*p*-tol_3P)$_2$PtC≡CC=CHN($CH_2C_6H_5$)N=N(Me)]$^+$ I^- ($\mathbf{16}^+$ $\mathbf{I^-}$**)**. A Schlenk flask was charged with *trans*-(C_6F_5)(*p*-tol_3P)$_2$PtC≡CC=CHN($CH_2C_6H_5$)N=N (**2a**;[169] 0.1035 g, 0.08970 mmol), MeI (0.0664 mL, 0.151 g, 1.07 mmol), and CH_2Cl_2

(10 mL), and fitted with a condenser. The mixture was kept at 40 °C for 4 d. The solvent was removed by rotary evaporation. The residue was washed with hexanes (50 mL) and dried by oil pump vacuum to give **16**$^+$ I$^-$ as a yellow solid (0.0940 g, 0.0726 mmol, 81%), which darkened at 141 °C, browned at 158 °C and liquefied at 164 °C. Anal. calcd. for $C_{60}H_{53}F_5IN_3P_2Pt$ (1295.01 g/mol): C, 55.65; H, 4.13; N, 3.24. Found: C, 55.21; H, 4.30; N, 3.26.[211]

NMR (δ (ppm)): ^{1}H (CD_2Cl_2) 8.01 (s, 1H, C=C*H*N), 7.58-7.36 (m, 17H, *o* to P and C_6H_5), 7.24-7.17 (d, 12H, *m* to P), 5.91 (s, 2H, CH_2), 2.97 (s, 3H, NCH_3), 2.36 (s, 18H, $C_6H_4CH_3$); ^{13}C{^{1}H} ($CDCl_3$)[212] 146.7 (m, *o* to Pt), 141.7 (s, *p* to P), 134.3 (virtual t,[63] $^2J_{CP}$ = 13.0 Hz, *o* to P), 132.3 and 130.0 (s, PtC≡C*C* and *i* to CH_2), 129.8 (s, *m* to Pt), 129.3 (s, *m* or *o* to CH_2), 129.2 (virtual t,[63] $^3J_{CP}$ = 11.2 Hz, *m* to P), 128.4 (s, *m* or *o* to CH_2), 126.7 (virtual t,[63] $^1J_{CP}$ = 60.8 Hz, *i* to P), 121.0 (s, =*C*H), 106.8 (s, Pt*C*≡C), 102.4 (PtC≡*C*), 57.6 (s, *C*H_2), 36.2 (s, N*C*H_3), 21.6 (s, C_6H_4*C*H_3); ^{31}P{^{1}H} (CD_2Cl_2) 17.9 (s, $^1J_{PPt}$ = 2614 Hz).[67]

IR (ATR, cm^{-1}): 3016 (w), 2924 (w), 2862 (w), 2121 (m, $\nu_{C\equiv C}$), 1597 (m), 1558 (m), 1496 (s), 1450 (s), 1396 (w), 1188 (m), 1095 (s), 1049 (m), 948 (s), 802 (s), 709 (s).

MS (ESI$^+$):[59] 1167 ([**16**]$^+$, 100%).

***trans*-(C_6F_5)(*p*-tol_3P)$_2$PtC≡CC=C(RhCl(cod))N($CH_2C_6H_5$)N=N(Me) (17)**. A Schlenk flask was fitted with a condenser and charged with **16**$^+$ I$^-$ (0.2504 g, 0.1934 mmol), [RhCl(cod)]$_2$ (0.1250 g, 0.2535 mmol), Ag_2O (0.0781 g, 0.3371 mmol), and CH_2Cl_2 (45 mL). The mixture was refluxed. After 2 d, the solvent was removed by rotary evaporation. The residue was washed with pentane (100 mL). The gray solid was filtered through a plug of alumina with CH_2Cl_2. The solvent was removed from the filtrate by oil pump vacuum to give **17** as a yellow solid (0.1763 g, 0.1247 mmol, 64%),

which browned at 182 °C, blackened at 201 °C and liquefied at 224 °C. Anal. calcd. for $C_{68}H_{64}ClF_5N_3P_2PtRh$ (1413.64 g/mol): C, 57.77; H, 4.56; N, 2.97. Found: C, 58.49; H, 5.04; N, 2.76.[211]

NMR (δ (ppm): ^{1}H (CD_2Cl_2) 7.61-7.55 (m, 12H, *o* to P), 7.51-7.46 (m, 2H, *o* to CH_2), 7.36-7.27 (m, 3H, *m* and *p* to CH_2), 7.19-7.13 (m, 12H, *m* to P), 5.94 (br s, 2H, CH_2C$_6$H$_5$), 4.69 (m, 2H, CH_{cod}), 3.78 (s, 1H, CH_{cod}), 2.79 (s, 3H, NCH_3), 2.63 (s, 2H, CH_{cod}), 2.34 (s, 18H, C$_6$H$_4$CH_3), 2.18 (s, 2H, CH_{cod}), 1.91 (s, 1H, CH_{cod}), 1.73 (s, 1H, CH_{cod}), 1.59 (m, 3H, CH_{cod}); ^{13}C ($CDCl_3$)[212] 168.6 (d, $^1J_{RhC}$ = 46.9 Hz, N*C*Rh), 145.7 (m, *o* to P), 141.1 (s, *p* to P), 136.4 (s, PtC≡C*C* or *i* to CH_2), 134.6 (virtual t,[63] $^2J_{CP}$ = 12.6 Hz, *o* to P), 132.9 (s, *m* to Pt), 129.1 (s, PtC≡C*C* or *i* to CH_2), 128.9 (virtual t,[63] $^3J_{CP}$ = 11.8 Hz, *m* to P), 128.8 (s, *m* to P), 128.5 and 128.1 (2s, *m* or *o* to CH_2), 127.7 (virtual t,[63] $^1J_{CP}$ = 59.0 Hz, *i* to P), 119.1 (s, Pt*C*≡C), 100.2 (s, PtC≡*C*), 95.4 (s, *C*H$_{cod}$), 69.7 (s, *C*H$_{cod}$), 58.3 (s, *C*H$_2$C$_6$H$_5$), 34.9 (s, N*C*H$_3$), 32.5 (s, *C*H$_{2cod}$), 31.9 (s, *C*H$_{2cod}$), 29.6 (s, *C*H$_{2cod}$), 29.4 (s, *C*H$_{2cod}$), 21.5 (s, C$_6$H$_4$*C*H$_3$); ^{31}P{^{1}H} (CD_2Cl_2) 16.7 (s, $^1J_{PPt}$ = 2665 Hz).[67]

IR (ATR, cm^{-1}): 3032 (m), 2954 (m), 2916 (m), 2870 (m), 2823 (m), 2106 (m, $\nu_{C\equiv C}$), 1705 (w), 1597 (m), 1496 (s), 1450 (s), 1396 (m), 1188 (s), 1095 (s), 1049 (s), 948 (s), 801 (s), 709 (s).

MS (ESI$^+$):[59] 1377 ([**17** – Cl]$^+$, 100%).

(η^5-C$_5$H$_4$NN=N-C(*trans*-(C≡C)Pt(P*p*-tol$_3$)$_2$(C$_6$F$_5$)=CH)$_2$Fe (18). A Schlenk flask was charged with **1a** (0.1406 g, 0.1379 mmol),[50] DMF (2.8 mL), (η^5-$C_5H_4N_3$)$_2$Fe (**8**;[192] 0.0350 g, 0.130 mmol), $CuSO_4 \cdot 5H_2O$ (0.0307 g, 0.123 mmol), ascorbic acid (0.0334 g, 0.190 mmol), and water (0.56 mL) with stirring. After 16 h, the solvents were removed by rotary evaporation, and water (10 mL) was added. The aqueous phase was

extracted with CH_2Cl_2 (3 × 20 mL). The combined CH_2Cl_2 layers were dried ($MgSO_4$). The solvent was removed by rotary evaporation and the residue was chromatographed on a silica gel column (30 × 4.5 cm) with CH_2Cl_2. The solvent was removed from the product containing fractions by rotary evaporation to give **18** as a yellow solid (0.1400 g, 0.06066 mmol, 47%), mp 187-190 °C. Anal. calcd. for $C_{114}H_{94}F_{10}FeN_6P_4Pt$ (2307.90 g/mol): C, 59.33; H, 4.11. Found: C, 58.11; H, 4.01.[211]

NMR (δ (ppm), $CDCl_3$): ^{1}H 7.57 (m, 24H, *o* to P), 7.11 (d, $^3J_{HH}$ = 7.3 Hz, 24H, *m* to P), 6.47 (s, 2H, =C*H*), 4.49 (t, $^3J_{HH}$ = 3.4 Hz, 4H, C_5H_4N), 4.04 (t, $^3J_{HH}$ = 3.4 Hz, 4H, C_5H_4N), 2.31 (s, 36H, CH_3); $^{13}C\{^1H\}$ 146.0 (dd, $^1J_{CF}$ = 222.6 Hz, $^2J_{CF}$ = 21.2 Hz, *o* to Pt), 140.7 (s, *p* to P), 137.6 (m, *p* to Pt), 135.6 (m, *m* to Pt), 135.6 (s, PtC≡C*C*), 134.6 (virtual t,[63] $^2J_{CP}$ = 11.9 Hz, *o* to Pt), 128.7 (virtual t,[63] $^3J_{CP}$ = 11.4 Hz, *m* to P), 127.9 (virtual t,[63] $^1J_{CP}$ = 60.1 Hz, *i* to P), 123.8 (s, =*C*H), 110.3 (s, Pt*C*≡C), 101.6 (s, PtC≡*C*C), 95.0 (s, C_5H_4N), 69.0 (s, C_5H_4N), 63.7 (s, C_5H_4N), 21.5 (s, CH_3); $^{31}P\{^1H\}$ 17.2 (s, $^1J_{PPt}$ = 2666 Hz).[67]

IR (ATR, cm^{-1}): 2122 (m, $\nu_{C\equiv C}$), 1599 (m), 1498 (s), 1453 (s), 1190 (m), 1098 (s), 952 (s), 804 (s), 731 (s), 707 (s).

Crystallography. **A**. A CH_2Cl_2 solution of **10** was stored at –20 °C. Green plates were obtained. Data were collected as outlined in Table 4.8. Cell parameters were obtained from 180 data frames were taken at widths of 0.5°. Integrated intensity information for each reflection was obtained by reduction of the data frames with the program APEX2.[71] Data were corrected for Lorentz and polarization factors, and using SADABS[72] absorption and crystal decay effects. The structure was solved by direct methods using SHELXTL (SHELXS).[73] All non-hydrogen atoms were refined with anisotropic thermal parameters. The hydrogen atoms were placed in idealized positions,

and refined using a riding model. The parameters were refined by weighted least squares refinement on F^2 to convergence.[73]

B. A CH_2Cl_2 solution of **11**$^+$ TfO^- was stored at room temperature. Colorless crystals were obtained. Data were collected as outlined in Table 4.9. Structure solution and refinement were carried out analogously to procedure A.

C. A CH_2Cl_2 solution of **12** was stored at –20 °C. Colorless multi-faceted crystals were obtained. Data were collected as outlined in Table 4.10. Cell parameters were obtained from 60 data frames taken at widths of 0.5°. Integrated intensity information for each reflection was obtained by reduction of the data frames with the program APEX2.[71] Data were corrected for Lorentz and polarization factors. Face-indexing was also carried out with APEX2 software. SADABS[72] was employed to correct the data for absorption effects including face information. The structure was solved by direct methods using SHELXTL (SHELXS).[73] All non-hydrogen atoms were refined with anisotropic thermal parameters. Hydrogen atoms were placed in idealized positions, and refined using a riding model. The thermal ellipsoids for one CO ligand were elongated, and Br(1) refined to an occupancy of *ca*. 0.84, suggesting disorder. This was successfully modeled (84:16 occupancy ratio) using restraints to keep the bond distances and thermal ellipsoids meaningful. The parameters were refined by weighted least squares refinement on F^2 to convergence.[73]

D. A CH_2Cl_2 solution of **18** was stored at room temperature. Yellow crystals were obtained. Data were collected as outlined in Table 4.11. Structure solution and refinement were carried out analogously to procedure A.

Table 4.8. Crystallographic Data for **10**·$2CH_2Cl_2$.

Empirical formula	$C_{62}H_{51}Cl_4F_5N_3O_3P_2PtRe$
Formula weight	1566.09
Temperature	110(2) K
Diffractometer	BRUKER GADDS
Wavelength	1.54178 Å
Crystal system	Triclinic
Space group	*P-1*
Unit cell dimensions	
a	11.5032(17) Å
b	12.3428(18) Å
c	21.855(3) Å
α	100.450(7)°
β	93.729(7)°
γ	104.277(7)°
V	2937.6(7) $Å^3$
Z	2
Density (calculated)	1.771 Mg/m^3
Absorption coefficient	11.087 mm^{-1}
F(000)	1528
Crystal size	0.03 × 0.02 × 0.02 mm^3
Theta range for data collection	2.07 to 59.99°
Index ranges	$-12 \le h \le 12$, $-13 \le k \le 13$, $-23 \le l \le 20$
Reflections collected	39214
Independent reflections	8148 [R(int) = 0.0436]
Completeness to theta = 59.99°	93.5%
Max. and min. transmission	0.2152 and 0.1255
Refinement method	Full-matrix least-squares on F^2
Data / restraints / parameters	8148 / 0 / 736
Goodness-of-fit on F^2	1.045
Final R indices [I>2σ(I)]	$R1$ = 0.0225, $wR2$ = 0.0471
R indices (all data)	$R1$ = 0.0310, $wR2$ = 0.0484
Largest diff. peak and hole	0.673 and –0.645 $eÅ^{-3}$

Table 4.9. Crystallographic Data for $\mathbf{11}^{+}$ $TfO^{-}\cdot CH_2Cl_2$**.**

Empirical formula	$C_{67}H_{50}Cl_2F_8N_3O_{11}P_2PtRe_2S$
Formula weight	1957.49
Temperature	296(2) K
Diffractometer	Bruker GADDS
Wavelength	0.71073 Å
Crystal system	Monoclinic
Space group	*P2(1)/n*
Unit cell dimensions	
a	12.815(3) Å
b	24.031(6) Å
c	24.532(6) Å
α	90°
β	102.149(12)°
γ	90°
V	7386(3) $Å^3$
Z	4
Density (calculated)	1.760 Mg/m^3
Absorption coefficient	5.380 mm^{-1}
F(000)	3764
Crystal size	0.10 × 0.08 × 0.08 mm^3
Theta range for data collection	1.67 to 25.00°
Index ranges	$-14\leq h\leq 15$, $-28\leq k\leq 28$, $-29\leq l\leq 29$
Reflections collected	119252
Independent reflections	12983 [R(int) = 0.0823]
Completeness to theta = 25.00°	99.7%
Max. and min. transmission	0.6728 and 0.6152
Refinement method	Full-matrix least-squares on F^2
Data / restraints / parameters	12983 / 0 / 880
Goodness-of-fit on F^2	1.050
Final R indices [I>2σ(I)]	*R*1 = 0.0429, *w*R2 = 0.0971
R indices (all data)	*R*1 = 0.0615, *w*R2 = 0.1023
Largest diff. peak and hole	3.145 and –1.447 $eÅ^{-3}$

Table 4.10. Crystallographic Data for **12**·$2CH_2Cl_2$.

Empirical formula	$C_{66}H_{51}BrCl_4F_5N_3O_7P_2PtRe_2$
Formula weight	1944.24
Temperature	110(2) K
Diffractometer	Bruker APEX 2
Wavelength	0.71073 Å
Crystal system	Orthorhombic
Space group	*P2(1)2(1)2*
Unit cell dimensions	
a	12.1623(16) Å
b	46.074(6) Å
c	11.9613(16) Å
α	90°
β	90°
γ	90°
V	6702.7(15) $Å^3$
Z	4
Density (calculated)	1.927 Mg/m^3
Absorption coefficient	6.557 mm^{-1}
F(000)	3720
Crystal size	0.50 × 0.14 × 0.07 mm^3
Theta range for data collection	1.70 to 27.49°
Index ranges	$-15 \le h \le 15$, $-59 \le k \le 59$, $-15 \le l \le 15$
Reflections collected	134479
Independent reflections	15360 [R(int) = 0.0455]
Completeness to theta = 27.49°	99.8%
Max. and min. transmission	0.6568 and 0.1381
Refinement method	Full-matrix least-squares on F^2
Data / restraints / parameters	15360 / 5 / 836
Goodness-of-fit on F^2	1.043
Final R indices [I>2σ (I)]	*R*1 = 0.0264, *w*R2 = 0.0668
R indices (all data)	*R*1 = 0.0290, *w*R2 = 0.0678
Largest diff. peak and hole	0.949 and –1.088 $eÅ^{-3}$

Table 4.11. Crystallographic Data for **18.**

Empirical formula	$C_{114}H_{94}F_{10}FeN_6P_4Pt_2$
Formula weight	2307.86
Temperature	296(2) K
Diffractometer	Bruker GADDS
Wavelength	0.71073 Å
Crystal system	Triclinic
Space group	*P-1*
Unit cell dimensions	
a	12.4921(18) Å
b	19.290(3) Å
c	23.157(4) Å
α	84.348(9)°
β	86.221(9)°
γ	87.507(8)°
V	5537.0(15) $Å^3$
Z	2
Density (calculated)	1.384 Mg/m^3
Absorption coefficient	2.772 mm^{-1}
F(000)	2304
Crystal size	0.11 × 0.11 × 0.05 mm^3
Theta range for data collection	0.89 to 17.73°
Index ranges	$-10 \leq h \leq 10$, $-16 \leq k \leq 16$, $-19 \leq l \leq 19$
Reflections collected	30813
Independent reflections	7210 [R(int) = 0.0473]
Completeness to theta = 17.73°	98.7%
Max. and min. transmission	0.8854 and 0.7502
Refinement method	Full-matrix least-squares on F^2
Data / restraints / parameters	7210 / 0 / 1246
Goodness-of-fit on F^2	1.013
Final R indices [I>2σ (I)]	*R*1 = 0.0281, *w*R2 = 0.0613
R indices (all data)	*R*1 = 0.0372, *w*R2 = 0.0644
Largest diff. peak and hole	0.375 and –0.306 $eÅ^{-3}$

CHAPTER V

SUMMARY AND CONCLUSIONS

After a brief overview of carbon allotropes and copper catalyzed reactions involving terminal polyynes, chapter II first detailed the syntheses and characterization of 2,2-geminally substituted bidentate diphosphines. The development of platinum-based square corners employing these diphosphines was presented, including both the dichloride and bis(butadiynyl) derivatives. Six new C_4-sided molecular squares were realized via heterocoupling reactions between the corresponding dichloride and bis(butadiynyl) platinum complexes under Sonogashira type conditions. Structural features of two new molecular squares were presented and compared. The solubilities of the resulting squares were tabulated and it was noted that the more lipophilic diphosphines imparted a much higher degree of solubility in solvents such as CH_2Cl_2. Attempts to access higher homologues, i.e. C_6 and C_8-sided squares, by both heterocoupling and oxidative homocoupling reactions were presented, with none leading to a singular self assembly product. Evidence for multiple polygons via mass spectrometry suggested selectivity issues using the chosen square building blocks. Further research efforts are directed towards suitable building blocks for larger polygons.

Chapter III detailed a series of diplatinum octatetraynediyl complexes bearing highly fluorous phosphine ligands. These complexes have added to the diversity of protected octatetraynediyl compounds bearing transition metal endgroups reported to date. The interesting phase behaviors of these complexes and their precursors were presented, and were exploited during workup procedures. The X-ray structure of a fluorous platinum chloride complex added to the relatively scarce sampling of

structurally characterized fluorous phosphine metal complexes. Electrochemistry of the octatetraynediyl complexes was presented. The title compounds were found to exhibit irreversible oxidations. Reasons for the absence of reversibility were postulated, which included solvent effects and/or ECE processes. Recommended future research efforts in this field would involve fluorous phosphine ligands that do not bear CH_2CF_2 junctions.

Chapter IV described the development of click reactions conducted in metal coordination spheres. Although a click reaction using a metal bound azide could not be effected, the use of an azide containing ligand on both rhenium and iron complexes was successful. Further metallations of the functionalized 1,2,3-triazole rings were realized using electrophilic rhenium complexes. The resulting adducts represent the first trimetallated triazoles reported to date. Methods to metallate at the fourth (=CH) position on the triazole ring were extensively explored. Variables included the use of different transition metals, solvents, temperatures, and the addition of bases. An electronic parameter based on the ^{1}H NMR chemical shift of the =CH group of the triazole was established. A signal at δ 7.9 ppm seemed to be the downfield limit for substrates amenable to functionalization. One dimetallated complex and three trimetallated complexes were structurally characterized and compared.

The studies in this dissertation have greatly expanded the scope of reactions available to terminal alkynes and polyynes, particularly those with metal endgroups. Copper catalyzed transformations allow for a wide range of target compounds to be realized, which can incorporate themes such as novel phosphines, scaffolds for future functionalizations, or supramolecular architectures.

REFERENCES

(1) Kroto, H. W.; Heath, J. R.; Obrien, S. C.; Curl, R. F.; Smalley, R. E. *Nature* **1985**, *318*, 162-163.

(2) Diederich, F. *Nature* **1994**, *369*, 199-207.

(3) Smith, P. P. K.; Buseck, P. R. *Science* **1982**, *216*, 984-986.

(4) Hu, Y. H. *Phys. Lett. A* **2009**, *373*, 3554-3557.

(5) Chinchilla, R.; Najera, C. *Chem. Rev.* **2007**, *107*, 874-922.

(6) Sonogashira, K. *J. Organomet. Chem.* **2002**, *653*, 46-49.

(7) Hay, A. S. *J. Org. Chem.* **1962**, *27*, 3320-3321.

(8) Glaser, C. *Ber. Dtsch. Chem. Ges*. **1869**, *2*, 422-424.

(9) Eglinton, G.; Galbraith, A. R. *J. Chem. Soc.* **1959**, 889-896.

(10) Kolb, H. C.; Finn, M. G.; Sharpless, K. B. *Angew. Chem., Int. Ed.* **2001**, *40,* 2004-2021; *Angew. Chem.*, **2001**, *113*, 2056-2075.

(11) Leininger, S.; Olenyuk, B.; Stang, P. J. *Chem. Rev.* **2000**, *100*, 853-907.

(12) Fujita, M. *Chem. Soc. Rev.* **1998**, *27*, 417-425.

(13) Stang, P. J.; Olenyuk, B. *Acc. Chem. Res.* **1997**, *30*, 502-518.

(14) Holliday, B. J.; Mirkin, C. A. *Angew. Chem., Int. Ed.* **2001**, *40,* 2022-2043; *Angew. Chem.* **2001**, *11*, 2076-2097.

(15) Whitesides, G. M.; Boncheva, M. *Proc. Natl. Acad. Sci. U. S. A.* **2002**, *99*, 4769-4774.

(16) Galstyan, A.; Miguel, P. J. S.; Lippert, B. *Inorg. Chim. Acta* **2011**, *374*, 453-460.

(17) Lopez-Vidal, E. M.; Blanco, V.; Garcia, M. D.; Peinador, C.; Quintela, J. M. *Org. Lett.* **2012**, *14*, 580-583.

(18) Olive, A. G. L.; Parkan, K.; Givelet, C.; Michl, J. *J. Am. Chem. Soc.* **2011**, *133*, 20108-20111.

(19) Northrop, B. H.; Zheng, Y. R.; Chi, K. W.; Stang, P. J. *Acc. Chem. Res.* **2009**, *42*, 1554-1563.

(20) Fujita, M.; Yazaki, J.; Ogura, K. *J. Am. Chem. Soc.* **1990**, *112*, 5645-5647.

(21) Fujita, M.; Yazaki, J.; Ogura, K. *Tetrahedron Lett.* **1991**, *32*, 5589-5592.

(22) Mishra, A.; Jung, H.; Park, J. W.; Kim, H. K.; Kim, H.; Stang, P. J.; Chi, K. W. *Organometallics* **2012**, *31*, 3519-3526.

(23) Vajpayee, V.; Kim, H.; Mishra, A.; Mukherjee, P. S.; Stang, P. J.; Lee, M. H.; Kim, H. K.; Chi, K. W. *Dalton Trans.* **2011**, *40*, 3112-3115.

(24) Kawase, T.; Kurata, H. *Chem. Rev.* **2006**, *106*, 5250-5273.

(25) Shanmugaraju, S.; Vajpayee, V.; Lee, S.; Chi, K.-W.; Stang, P. J.; Mukherjee, P. S. *Inorg. Chem.* **2012**, *51*, 4817-4823.

(26) Dinolfo, P. H.; Hupp, J. T.; Sun, S. S. In *Encyclopedia of Supramolecular Chemistry*.; Atwood, J. L., Ed.; Marcel Dekker: New York, 2004; Vol. 1; p 909-916.

(27) Fujita, M.; Nagao, S.; Iida, M.; Ogata, K.; Ogura, K. *J. Am. Chem. Soc.* **1993**, *115*, 1574-1576.

(28) Beer, P. D.; Szemes, F.; Balzani, V.; Sala, C. M.; Drew, M. G. B.; Dent, S. W.; Maestri, M. *J. Am. Chem. Soc.* **1997**, *119*, 11864-11875.

(29) Slone, R. V.; Yoon, D. I.; Calhoun, R. M.; Hupp, J. T. *J. Am. Chem. Soc.* **1995**, *117*, 11813-11814.

(30) Slone, R. V.; Hupp, J. T.; Stern, C. L.; Albrecht-Schmitt, T. E. *Inorg. Chem.* **1996**, *35*, 4096-4097.

(31) Belanger, S.; Hupp, J. T.; Stern, C. L.; Slone, R. V.; Watson, D. F.; Carrell, T. G. *J. Am. Chem. Soc.* **1999**, *121*, 557-563.

(32) Alqaisi, S. M.; Galat, K. J.; Chai, M. H.; Ray, D. G.; Rinaldi, P. L.; Tessier, C. A.; Youngs, W. J. *J. Am. Chem. Soc.* **1998**, *120*, 12149-12150.

(33) Diederich, F.; Rubin, Y.; Knobler, C. B.; Whetten, R. L.; Schriver, K. E.; Houk, K. N.; Li, Y. *Science* **1989**, *245*, 1088-1090.

(34) Diederich, F.; Rubin, Y. *Angew. Chem., Int. Ed. Engl.* **1992**, *31,* 1101-1123; *Angew. Chem.* **1992**, *104*, 1123-1146.

(35) McElvany, S. W.; Ross, M. M.; Goroff, N. S.; Diederich, F. *Science* **1993**, *259*, 1594-1596.

(36) Yamago, S.; Watanabe, Y.; Iwamoto, T. *Angew. Chem., Int. Ed.* **2010**, *49,* 757-759; *Angew. Chem.*, **2010**, *122*, 769-771.

(37) Dewhurst, R. D.; Hill, A. F.; Willis, A. C. *Organometallics* **2009**, *28*, 4735-4740.

(38) Fuhrmann, G.; Debaerdemaeker, T.; Bauerle, P. *Chem. Commun.* **2003**, 948-949.

(39) Weisbach, N. Doctoral Thesis, Friedrich-Alexander-Universität Erlangen-Nürnberg, Erlangen, Germany, 2011.

(40) Owen, G. final research report, Friedrich-Alexander-Universität Erlangen-Nürnberg, Germany, 2004, unpublished results.

(41) Kraihanzel, C. S.; Ressner, J. M.; Gray, G. M. *Inorg. Chem.* **1982**, *21*, 879-887.

(42) Bianchini, C.; Lee, H. M.; Meli, A.; Moneti, S.; Vizza, F.; Fontani, M.; Zanello, P. *Macromolecules* **1999**, *32*, 4183-4193.

(43) Alt, H. G.; Baumgartner, R.; Brune, H. A. *Chem. Ber.* **1986**, *119*, 1694-1703.

(44) Matern, E.; Pikies, J.; Fritz, G. *Z. Anorg. Allg. Chem.* **2000**, *626*, 2136-2142.

(45) Zheng, Q. L.; Hampel, F.; Gladysz, J. A. *Organometallics* **2004**, *23*, 5896-5899.

(46) van Rijn, J. A.; Siegler, M. A.; Spek, A. L.; Bouwman, E.; Drent, E. *Organometallics* **2009**, *28*, 7006-7014.

(47) Zheng, Q. L. Doctoral Thesis, Friedrich-Alexander-Universität Erlangen-Nürnberg, Erlangen, Germany, 2003.

(48) Zheng, Q. L.; Bohling, J. C.; Peters, T. B.; Frisch, A. C.; Hampel, F.; Gladysz, J. A. *Chem.–Eur. J.* **2006**, *12*, 6486-6505.

(49) Janosi, L.; Kollar, L.; Macchi, P.; Sironi, A. *Transit. Met. Chem.* **2007**, *32*, 746-752.

(50) Mohr, W.; Stahl, J.; Hampel, F.; Gladysz, J. A. *Chem.–Eur. J.* **2003**, *9*, 3324-3340.

(51) Stahl, J. Doctoral Thesis, Friedrich-Alexander-Universität Erlangen-Nürnberg, Erlangen, Germany, 2003.

(52) Owen, G. R.; Stahl, J.; Hampel, F.; Gladysz, J. A. *Chem.–Eur. J.* **2008**, *14*, 73-87.

(53) Sautter, A.; Schmid, D. G.; Jung, G.; Würthner, F. *J. Am. Chem. Soc.* **2001**, *123*, 5424-5430.

(54) Lang, H.; George, D. S. A.; Rheinwald, G. *Coord. Chem. Rev.* **2000**, *206*, 101-197.

(55) Janssen, M. D.; Herres, M.; Zsolnai, L.; Spek, A. L.; Grove, D. M.; Lang, H.; vanKoten, G. *Inorg. Chem.* **1996**, *35*, 2476-2483.

(56) Lang, H.; Herres, M.; Zsolnai, L. *Organometallics* **1993**, *12*, 5008-5011.

(57) Bruce, M. I.; Costuas, K.; Halet, J. F.; Hall, B. C.; Low, P. J.; Nicholson, B. K.; Skelton, B. E.; White, A. H. *J. Chem. Soc., Dalton Trans.* **2002**, 383-398.

(58) Janka, M.; Anderson, G. K.; Rath, N. P. *Organometallics* **2004**, *23*, 4382-4390.

(59) *m/z*, most intense peak of isotope envelope.

(60) This signal is part of a complex spin system and the coupling constants were assigned by a simulation. See Weisbach, N. Doctoral Thesis, Friedrich-Alexander-Universität Erlangen-Nürnberg, Erlangen, Germany, 2011.

(61) This signal is part of a complex spin system and appears as a triplet superimposed upon a broad hump. The coupling constant was assigned by a simulation. See Weisbach, N. Doctoral Thesis, Friedrich-Alexander-Universität Erlangen-Nürnberg, Erlangen, Germany, 2011.

(62) Buwalda, R. T.; Wagenaar, A.; Engberts, J. *Liebigs Ann. Recl.* **1997**, 1745-1753.

(63) The *J* values given for virtual triplets represent the apparent couplings between adjacent peaks and not the mathematically rigorously coupling constants. See Hersh, W. H. *J. Chem. Educ.* **1997**, *74*, 1485-1488.

(64) Ohkita, T.; Tsuchiya, Y.; Togo, H. *Tetrahedron* **2008**, *64*, 7247-7251.

(65) The $^{13}C\{^{1}H\}$ NMR signal with the chemical shift closest to benzene (128.4 ppm) is usually assigned to the meta aryl carbon: Mann, B. E. *J. Chem. Soc. Perkin Trans. 2* **1972**, *30*.

(66) The ^{1}H, $^{31}P\{^{1}H\}$, and $^{13}C\{^{1}H\}$ spectra are shown in Appendix A.

(67) This coupling represents a satellite (d, ^{195}Pt = 33.8%), and is not reflected in the peak multiplicity given.

(68) Verkruijsse, H. D.; Brandsma, L. *Synth. Commun.* **1991**, *21*, 657-659.

(69) Multiplet, including t with apparent *J* values indicated. The coupling constant was assigned by a simulation. See Weisbach, N. Doctoral Thesis, Friedrich-Alexander-Universität Erlangen-Nürnberg, Erlangen, Germany, 2011.

(70) The coupling to phosphorous was not observed.

(71) APEX2, "Program for Data Collection on Area Detectors" BRUKER AXS Inc., 5465 East Cheryl Parkway, Madison, WI 53711-5373 USA.; p

(72) Sheldrick, G. M. *SADABS*, *Program for Absorption Correction of Area Detector Frames*, BRUKER AXS Inc., 5465 East Cheryl Parkway, Madison, WI 53711-5373, USA.

(73) Sheldrick, G. *Acta Crystallogr.* **2008**, *A64*, 112-122.

(74) SAINT (Version 7), 2007. "Program for Data Integration from Area Detector Frames", B. N. I., 5465 East Cheryl Parkway, Madison, WI 53711-5373 USA.

(75) Spek, A. L. *J. Appl. Cryst*. **2003**, *36*, 7-13.

(76) Sheldrick, G. M. "SADABS (version 2008/1): Program for Absorption Correction for Data from Area Detector Frames", University of Göttingen, 2008.

(77) Akita, M.; Sakurai, A.; Chung, M. C.; Moro-oka, Y. *J. Organomet. Chem.* **2003**, *670*, 2-10.

(78) Antonova, A. B.; Bruce, M. I.; Elis, B. G.; Gaudio, M.; Humphrey, P. A.; Jevric, M.; Melino, G.; Nicholson, B. K.; Perkins, G. J.; Skelton, B. W.; Stapleton, B.; White, A. H.; Zaitseva, N. N. *Chem. Commun.* **2004**, 960-961.

(79) Bruce, M. I.; Zaitseva, N. N.; Nicholson, B. K.; Skelton, B. W.; White, A. H. *J. Organomet. Chem.* **2008**, *693*, 2887-2897.

(80) Zheng, Q. L.; Gladysz, J. A. *J. Am. Chem. Soc.* **2005**, *127*, 10508-10509.

(81) Eastmond, R.; Walton, D. R. M.; Johnson, T. R. *Tetrahedron* **1972**, *28*, 4601-4616.

(82) Johnson, T. R.; Walton, D. R. M. *Tetrahedron* **1972**, *28*, 5221-5236.

(83) de Quadras, L.; Bauer, E. B.; Mohr, W.; Bohling, J. C.; Peters, T. B.; Martin-Alvarez, J. M.; Hampel, F.; Gladysz, J. A. *J. Am. Chem. Soc.* **2007**, *129*, 8296-8309.

(84) de Quadras, L.; Bauer, E. B.; Stahl, J.; Zhuravlev, F.; Hampel, F.; Gladysz, J. A. *New J. Chem.* **2007**, *31*, 1594-1604.

(85) Stahl, J.; Mohr, W.; de Quadras, L.; Peters, T. B.; Bohling, J. C.; Martin-Alvarez, J. M.; Owen, G. R.; Hampel, F.; Gladysz, J. A. *J. Am. Chem. Soc.* **2007**, *129*, 8282-8295.

(86) Weisbach, N.; Baranova, Z.; Gauthier, S.; Reibenspies, J. H.; Gladysz, J. A. *Chem. Commun.* **2012**, *48*, 7562-7564.

(87) Movsisyan, L. D.; Kondratuk, D. V.; Franz, M.; Thompson, A. L.; Tykwinski, R. R.; Anderson, H. L. *Org. Lett.* **2012**, *14*, 3424-3426.

(88) Horvath, I. T.; Rabai, J. *Science* **1994**, *266*, 72-75.

(89) Gladysz, J. A.; Curran, D. P. *Tetrahedron* **2002**, *58*, 3823-3825.

(90) de Wolf, E.; van Koten, G.; Deelman, B. J. *Chem. Soc. Rev.* **1999**, *28*, 37-41.

(91) Dobbs, A. P.; Kimberley, M. R. *J. Fluor. Chem.* **2002**, *118*, 3-17.

(92) Fish, R. H. *Chem.–Eur. J.* **1999**, *5*, 1677-1680.

(93) Richter, B.; Spek, A. L.; van Koten, G.; Deelman, B. J. *J. Am. Chem. Soc.* **2000**, *122*, 3945-3951.

(94) Vincent, J. M.; Rabion, A.; Yachandra, V. K.; Fish, R. H. *Angew. Chem., Int. Ed. Engl.* **1997**, *36,* 2346-2349; *Angew. Chem.*, **1997**, *109*, 2438-2440.

(95) Zhang, Q. S.; Luo, Z. Y.; Curran, D. P. *J. Org. Chem.* **2000**, *65*, 8866-8873.

(96) Curran, D. P.; Sui, B. *J. Am. Chem. Soc.* **2009**, *131*, 5411-5413.

(97) Lu, Y. M.; Geib, S. J.; Damodaran, K.; Sui, B.; Zhang, Z. J.; Curran, D. P.; Zhang, W. *Chem. Commun.* **2010**, *46*, 7578-7580.

(98) Zhang, K.; Curran, D. P. *Synlett* **2010**, 667-671.

(99) Chen, W. P.; Xu, L. J.; Hu, Y. L.; Osuna, A. M. B.; Xiao, J. L. *Tetrahedron* **2002**, *58*, 3889-3899.

(100) Hadida, S.; Super, M. S.; Beckman, E. J.; Curran, D. P. *J. Am. Chem. Soc.* **1997**, *119*, 7406-7407.

(101) Osuna, A. M. B.; Chen, W. P.; Hope, E. G.; Kemmitt, R. D. W.; Paige, D. R.; Stuart, A. M.; Xiao, J. L.; Xu, L. J. *J. Chem. Soc., Dalton Trans.* **2000**, 4052-4055.

(102) Zhu, J.; Robertson, A.; Tsang, S. C. *Chem. Commun.* **2002**, 2044-2045.

(103) Gladysz, J. A.; Jurisch, M. *Topics in Current Chemistry* **2012**, *308*, 1-23.

(104) da Costa, R. C.; Hampel, F.; Gladysz, J. A. *Polyhedron* **2007**, *26*, 581-588.

(105) Exner, O. In *Correlation Analysis in Chemistry*; Chapman, N. B.; Shorter, J. Eds.; Plenum Press: New York, 1978; ch 10.

(106) Berven, B. M.; Koutsantonis, G. A.; Skelton, B. W.; Trengove, R. D.; White, A. H. *Dalton Trans.* **2011**, *40*, 4167-4174.

(107) Jiao, H. J.; Le Stang, S.; Soos, T.; Meier, R.; Kowski, K.; Rademacher, P.; Jafarpour, L.; Hamard, J. B.; Nolan, S. P.; Gladysz, J. A. *J. Am. Chem. Soc.* **2002**, *124*, 1516-1523.

(108) Alvey, L. J.; Meier, R.; Soos, T.; Bernatis, P.; Gladysz, J. A. *Eur. J. Inorg. Chem.* **2000**, 1975-1983.

(109) Uson, R.; Fornies, J.; Espinet, P.; Alfranca, G. *Synth. React. Inorganic Met.-Org. Chem.* **1980**, *10*, 579-590.

(110) Emnet, C.; Weber, K. M.; Vidal, J. A.; Consorti, C. S.; Stuart, A. M.; Gladysz, J. A. *Adv. Synth. Catal.* **2006**, *348*, 1625-1634.

(111) Gimbert, C.; Vallribera, A.; Gladysz, J. A.; Jurisch, M. *Tetrahedron Lett.* **2010**, *51*, 4662-4665.

(112) Alvey, L. J.; Rutherford, D.; Juliette, J. J. J.; Gladysz, J. A. *J. Org. Chem.* **1998**, *63*, 6302-6308.

(113) Kamienska-Trela, K.; Wojcik, J. *Nucl. Magn. Reson.* **2011**, *40*, 162-204.

(114) Dunitz, J. D.; Gavezzotti, A.; Schweizer, W. B. *Helv. Chim. Acta* **2003**, *86*, 4073-4092.

(115) Gladysz, J. A.; Emnet, C. In *Handbook of Fluorous Chemistry*; Gladysz, J. A., Curran, D. P., Horvath, I. T., Eds.; Wiley/VCH: Weinheim, 2004, p 11-23.

(116) The most upfield CH_2 signal is assigned to P$\underline{C}H_2$ and the most downfield CH_2 signal is assigned to $\underline{C}H_2CF_2$. See Tuba, R.; Tesevic, V.; Dinh, L. V.; Hampel, F.; Gladysz, J. A. *Dalton Trans*. **2005**, 2275-2283.

(117) The most upfield CF_2 signal is assigned to the $\underline{C}F_2CH_2$ carbon. See Gladysz, J. A.; Jurisch, M. In *Fluorous Chemistry*; Horvath, I. T., Ed.; Springer-Verlag Berlin: Berlin, 2012; Vol. 308, p 1-23.

(118) Gladysz, J. A.; Emnet, C.; Rabai, J. In *Handbook of Fluorous Chemistry*; Gladysz, J. A., Curran, D. P., Horvath, I. T., Eds.; Wiley/VCH: Weinheim, 2004, p 56-100.

(119) Gladysz, J. A.; Jurisch, M. *Topics in Current Chemistry* **2012**, *308*, 1-23.

(120) Clough, P. N.; Polanyi, J. C.; Taguchi, R. T. *Can. J. Chem.* **1970**, *48*, 2919-2930.

(121) Bennett, B. L.; Robins, K. A.; Tennant, R.; Elwell, K.; Ferri, F.; Bashta, I.; Aguinaldo, G. *J. Fluor. Chem.* **2006**, *127*, 140-145.

(122) Stibrany, R. T.; Gorun, S. M. *J. Organomet. Chem.* **1999**, *579*, 217-221.

(123) Kromm, P.; Bideau, J. P.; Cotrait, M.; Destrade, C.; Nguyen, H. *Acta Crystallogr.* **1994**, *C50*, 112-115.

(124) Jablonski, C. R.; Zhou, Z. X. *Can. J. Chem.* **1992**, *70*, 2544-2551.

(125) Guillevic, M. A.; Arif, A. M.; Horvath, I. T.; Gladysz, J. A. *Angew. Chem., Int. Ed. Engl.* **1997**, *36,* 1612-1615; *Angew. Chem*. **1997**, *109*, 1685−1687.

(126) Guillevic, M. A.; Rocaboy, C.; Arif, A. M.; Horvath, I. T.; Gladysz, J. A. *Organometallics* **1998**, *17*, 707-717.

(127) Fawcett, J.; Hope, E. G.; Kemmitt, R. D. W.; Paige, D. R.; Russell, D. R.; Stuart, A. M.; ColeHamilton, D. J.; Payne, M. J. *Chem. Commun.* **1997**, 1127-1128.

(128) Haar, C. M.; Huang, J.; Nolan, S. P.; Petersen, J. L. *Organometallics* **1998**, *17*, 5018-5024.

(129) Fawcett, J.; Hope, E. G.; Kemmitt, R. D. W.; Paige, D. R.; Russell, D. R.; Stuart, A. M. *J. Chem. Soc., Dalton Trans.* **1998**, 3751-3763.

(130) Smith, D. C.; Stevens, E. D.; Nolan, S. P. *Inorg. Chem.* **1999**, *38*, 5277-5281.

(131) Fawcett, J.; Hope, E. G.; Russell, D. R.; Stuart, A. M.; Wood, D. R. W. *Polyhedron* **2001**, *20*, 321-326.

(132) Croxtall, B.; Fawcett, J.; Hope, E. G.; Stuart, A. M. *J. Chem. Soc., Dalton Trans.* **2002**, 491-499.

(133) Adams, D. J.; Gudmunsen, D.; Fawcett, J.; Hope, E. G.; Stuart, A. M. *Tetrahedron* **2002**, *58*, 3827-3834.

(134) de Wolf, E.; Spek, A. L.; Kuipers, B. W. M.; Philipse, A. P.; Meeldijk, J. D.; Bomans, P. H. H.; Frederik, P. M.; Deelman, B. J.; van Koten, G. *Tetrahedron* **2002**, *58*, 3911-3922.

(135) Malosh, T. J.; Wilson, S. R.; Shapley, J. R. *Inorg. Chim. Acta* **2009**, *362*, 2849-2855.

(136) Malosh, T. J.; Wilson, S. R.; Shapley, J. R. *J. Organomet. Chem.* **2009**, *694*, 3331-3337.

(137) Tuba, R.; Tesevic, V.; Dinh, L. V.; Hampel, F.; Gladysz, J. A. *Dalton Trans.* **2005**, 2275-2283.

(138) Consorti, C. S.; Hampel, F.; Gladysz, J. A. *Inorg. Chim. Acta* **2006**, *359*, 4874-4884.

(139) Tuba, R.; Brothers, E. N.; Reibenspies, J. H.; Bazzi, H. S.; Gladysz, J. A. *Inorg. Chem.* **2012**, *51*, 9943-9949.

(140) Bresciani-Pahor, N.; Plazzotta, M.; Randaccio, L.; Bruno, G.; Ricevuto, V.; Romeo, R.; Belluco, U. *Inorg. Chim. Acta* **1978**, *31*, 171-175.

(141) Hughes, R. P.; Ward, A. J.; Golen, J. A.; Incarvito, C. D.; Rheingold, A. L.; Zakharov, L. N. *Dalton Trans.* **2004**, 2720-2727.

(142) The *ipso* C_6F_5 signal was not observed.

(143) Chong, S. H. F.; Lam, S. C. F.; Ko, C. C.; Yam, V. W. W. *J. Clust. Sci.* **2004**, *15*, 301-314.

(144) Dewey, M. A.; Knight, D. A.; Klein, D. P.; Arif, A. M.; Gladysz, J. A. *Inorg. Chem.* **1991**, *30*, 4995-5002.

(145) The ^{1}H, $^{31}P\{^{1}H\}$, and $^{13}C\{^{1}H\}$ spectra are shown in Appendix B.

(146) Tornoe, C. W.; Christensen, C.; Meldal, M. *J. Org. Chem.* **2002**, *67*, 3057-3064.

(147) Rostovtsev, V. V.; Green, L. G.; Fokin, V. V.; Sharpless, K. B. *Angew. Chem., Int. Ed.* **2002**, *41,* 2596-2599; *Angew. Chem.*, **2002**, *114*, 2708-2711.

(148) Hein, J. E.; Fokin, V. V. *Chem. Soc. Rev.* **2010**, *39*, 1302-1315.

(149) Meldal, M.; Tornoe, C. W. *Chem. Rev.* **2008**, *108*, 2952-3015.

(150) Huisgen, R. In *1,3-Dipolar Cycloaddition Chem.*; Padwa, A., Ed.; Wiley: New York, 1984; Vol. 1; p 1-176.

(151) Huisgen, R. *Pure Appl. Chem.* **1989**, *61*, 613-628.

(152) Himo, F.; Lovell, T.; Hilgraf, R.; Rostovtsev, V. V.; Noodleman, L.; Sharpless, K. B.; Fokin, V. V. *J. Am. Chem. Soc.* **2005**, *127*, 210-216.

(153) Luu, T.; McDonald, R.; Tykwinski, R. R. *Org. Lett.* **2006**, *8*, 6035-6038.

(154) Luu, T.; Medos, B. J.; Graham, E. R.; Vallee, D. M.; McDonald, R.; Ferguson, M. J.; Tykwinski, R. R. *J. Org. Chem.* **2010**, *75*, 8498-8507.

(155) Decreau, R. A.; Collman, J. P.; Yang, Y.; Yan, Y. L.; Devaraj, N. K. *J. Org. Chem.* **2007**, *72*, 2794-2802.

(156) McDonald, A. R.; Dijkstra, H. P.; Suijkerbuijk, B.; van Klink, G. P. M.; van Koten, G. *Organometallics* **2009**, *28*, 4689-4699.

(157) Partyka, D. V.; Gao, L.; Teets, T. S.; Updegraff, J. B.; Deligonul, N.; Gray, T. G. *Organometallics* **2009**, *28*, 6171-6182.

(158) Zhou, Y. H.; Lecourt, T.; Micouin, L. *Angew. Chem., Int. Ed.* **2010**, *49,* 2607-2610; *Angew. Chem.*, **2010**, *122*, 2661-2664.

(159) Hanni, K. D.; Leigh, D. A. *Chem. Soc. Rev*. **2010**, *39*, 1240-1251 (see Schemes 5, 6, 13, and 19 and associated references therein).

(160) Forrest, W. P.; Cao, Z.; Chen, W. Z.; Hassell, K. M.; Kharlamova, A.; Jakstonyte, G.; Ren, T. *Inorg. Chem.* **2011**, *50*, 9345-9353.

(161) Joosten, A.; Trolez, Y.; Collin, J. P.; Heitz, V.; Sauvage, J. P. *J. Am. Chem. Soc.* **2012**, *134*, 1802-1809.

(162) Ganesh, V.; Sudhir, V. S.; Kundu, T.; Chandrasekaran, S. *Chem.–Asian J.* **2011**, *6*, 2670-2694.

(163) Liu, F. C.; Lin, Y. L.; Yang, P. S.; Lee, G. H.; Peng, S. M. *Organometallics* **2010**, *29*, 4282-4290.

(164) Partyka, D. V.; Updegraff, J. B.; Zeller, M.; Hunter, A. D.; Gray, T. G. *Organometallics* **2007**, *26*, 183-186.

(165) Robilotto, T. J.; Alt, D. S.; von Recum, H. A.; Gray, T. G. *Dalton Trans.* **2011**, *40*, 8083-8085.

(166) Gao, L.; Niedzwiecki, D. S.; Deligonul, N.; Zeller, M.; Hunter, A. D.; Gray, T. G. *Chem.–Eur. J.* **2012**, *18*, 6316-6327.

(167) Del Castillo, T. J.; Sarkar, S.; Abboud, K. A.; Veige, A. S. *Dalton Trans.* **2011**, *40*, 8140-8144.

(168) Romero, T.; Caballero, A.; Tarraga, A.; Molina, P. *Org. Lett.* **2009**, *11*, 3466-3469.

(169) Gauthier, S.; Weisbach, N.; Bhuvanesh, N.; Gladysz, J. A. *Organometallics* **2009**, *28*, 5597-5599.

(170) Packheiser, R.; Lang, H. *Eur. J. Inorg. Chem.* **2007**, 3786-3788.

(171) Packheiser, R.; Ecorchard, P.; Rueffer, T.; Lang, H. *Chem.–Eur. J.* **2008**, *14*, 4948-4960.

(172) Lang, H.; Packheiser, R. *Collect. Czech. Chem. Commun.* **2007**, *72*, 435-452.

(173) Mathew, P.; Neels, A.; Albrecht, M. *J. Am. Chem. Soc.* **2008**, *130*, 13534-13535.

(174) Karthikeyan, T.; Sankararaman, S. *Tetrahedron Lett.* **2009**, *50*, 5834-5837.

(175) Poulain, A.; Canseco-Gonzalez, D.; Hynes-Roche, R.; Muller-Bunz, H.; Schuster, O.; Stoeckli-Evans, H.; Neels, A.; Albrecht, M. *Organometallics* **2011**, *30*, 1021-1029.

(176) Nakamura, T.; Terashima, T.; Ogata, K.; Fukuzawa, S. *Org. Lett.* **2011**, *13*, 620-623.

(177) Kilpin, K. J.; Paul, U. S. D.; Lee, A. L.; Crowley, J. D. *Chem. Commun.* **2011**, *47*, 328-330.

(178) Nakamura, T.; Ogata, K.; Fukuzawa, S. *Chem. Lett.* **2010**, *39*, 920-922.

(179) Cai, J. J.; Yang, X. P.; Arumugam, K.; Bielawski, C. W.; Sessler, J. L. *Organometallics* **2011**, *30*, 5033-5037.

(180) Saravanakumar, R.; Ramkumar, V.; Sankararaman, S. *Organometallics* **2011**, *30*, 1689-1694.

(181) Prades, A.; Peris, E.; Albrecht, M. *Organometallics* **2011**, *30*, 1162-1167.

(182) Bernet, L.; Lalrempuia, R.; Ghattas, W.; Mueller-Bunz, H.; Vigara, L.; Llobet, A.; Albrecht, M. *Chem. Commun.* **2011**, *47*, 8058-8060.

(183) Hohloch, S.; Su, C. Y.; Sarkar, B. *Eur. J. Inorg. Chem.* **2011**, 3067-3075.

(184) Schulze, B.; Escudero, D.; Friebe, C.; Siebert, R.; Gorls, H.; Kohn, U.; Altuntas, E.; Baumgaertel, A.; Hager, M. D.; Winter, A.; Dietzek, B.; Popp, J.; Gonzalez, L.; Schubert, U. S. *Chem.–Eur. J.* **2011**, *17*, 5494-5498.

(185) Yuan, D.; Huynh, H. V. *Organometallics* **2012**, *31*, 405-412.

(186) Keske, E. C.; Zenkina, O. V.; Wang, R. Y.; Crudden, C. M. *Organometallics* **2012**, *31*, 456-461.

(187) Guisado-Barrios, G.; Bouffard, J.; Donnadieu, B.; Bertrand, G. *Organometallics* **2011**, *30*, 6017-6021.

(188) Schmidt, S. P.; Nitschke, J.; Trogler, W. C.; Huckett, S. I.; Angelici, R. J. *Inorg. Synth.* **1989**, *26*, 113-117.

(189) Schmidt, S. P.; Trogler, W. C.; Basolo, F. *Inorg. Synth.* **1990**, *28*, 160-165.

(190) Sert, S.; Sentürk, O. S.; Özdemir, Ü.; Karacan, N.; Ugur, F. *J. Coord. Chem.* **2004**, *57*, 183-188.

(191) Nieto, S.; Perez, J.; Riera, L.; Riera, V.; Miguel, D.; Golen, J. A.; Rheingold, A. L.; Rheingold, L. *Inorg. Chem.* **2007**, *46*, 3407-3418.

(192) Oton, F.; Espinosa, A.; Tarraga, A.; de Arellano, C. R.; Molina, P. *Chem.–Eur. J.* **2007**, *13*, 5742-5752.

(193) Sazonov, P. K.; Artamkina, G. A.; Khrustalev, V. N.; Antipin, M. Y.; Beletskaya, I. P. *J. Organomet. Chem.* **2003**, *681*, 59-69.

(194) Adams, D. M. *Metal-Ligand and Related Vibrations*; St. Martin's Press: New York, 1968; p 94-106.

(195) Magriz, A.; Gomez-Bujedo, S.; Alvarez, E.; Fernandez, R.; Lassaletta, J. M. *Organometallics* **2010**, *29*, 5941-5945.

(196) Shao, C. W.; Wang, X. Y.; Xu, J. M.; Zhao, J. C.; Zhang, Q.; Hu, Y. F. *J. Org. Chem.* **2010**, *75*, 7002-7005.

(197) Link, J. O.; Graupe, M. PCT Int. Pat. Appl. WO 2005/074904 A2 (filed August 18, 2005); *Chem. Abstr.* **2005**, *143*, 229992.

(198) Bohn, R. K.; Haaland, A. *J. Organomet. Chem.* **1966**, *5*, 470-476.

(199) Bruce, M. I.; Jevric, M.; Skelton, B. W.; Smith, M. E.; White, A. H.; Zaitseva, N. N. *J. Organomet. Chem.* **2006**, *691*, 361-370.

(200) Brown, N. J.; Collison, D.; Edge, R.; Fitzgerald, E. C.; Low, P. J.; Helliwell, M.; Ta, Y. T.; Whiteley, M. W. *Chem. Commun.* **2010**, *46*, 2253-2255.

(201) Oton, F.; Espinosa, A.; Tarraga, A.; Molina, P. *Organometallics* **2007**, *26*, 6234-6242.

(202) Han, T.; Chen, C. F. *J. Org. Chem.* **2008**, *73*, 7735-7742.

(203) Lyssenko, K. A.; Nelubina, Y. V.; Safronov, D. V.; Haustova, O. I.; Kostyanovsky, R. G.; Lenev, D. A.; Antipin, M. Y. *Mendeleev Commun.* **2005**, 232-234.

(204) Hayes, W.; Osborn, H. M. I.; Osborne, S. D.; Rastall, R. A.; Romagnoli, B. *Tetrahedron* **2003**, *59*, 7983-7996.

(205) Kaplan, G.; Drake, G.; Tollison, K.; Hall, L.; Hawkins, T. *J. Heterocycl. Chem.* **2005**, *42*, 19-27.

(206) Otón, F.; González, M. d. C.; Espinosa, A.; Tárraga, A.; Molina, P. *Organometallics* **2012**, *31*, 2085-2096.

(207) Agbossou, F.; O'Connor, E. J.; Garner, C. M.; Quirós Méndez, N.; Fernández, J. M.; Patton, A. T.; Ramsden, J. A.; Gladysz, J. A. *Inorg. Synth.* **1992**, *29*, 211-225.

(208) Ruppel, J. V.; Jones, J. E.; Huff, C. A.; Kamble, R. M.; Chen, Y.; Zhang, X. P. *Org. Lett.* **2008**, *10*, 1995-1998.

(209) Dr. Paul Zeits developed this synthesis; see also Chong, D.; Laws, D. R.; Nafady, A.; Costa, P. J.; Rheingold, A. L.; Calhorda, M. J.; Geiger, W. E. *J. Am. Chem. Soc*. **2008**, *130*, 2692-2703.

(210) The signal for the nitrogen-bound cyclopentadienyl carbon was not observed.

(211) The ^{1}H, $^{31}P\{^{1}H\}$, and $^{13}C\{^{1}H\}$ spectra are shown in Appendix C.

(212) The *ipso* and *para* C_6F_5 and *para* $CH_2C_6H_5$ signals were not observed.

APPENDIX A

NMR SPECTRA AND CHECKCIF REPORTS FOR CHAPTER II

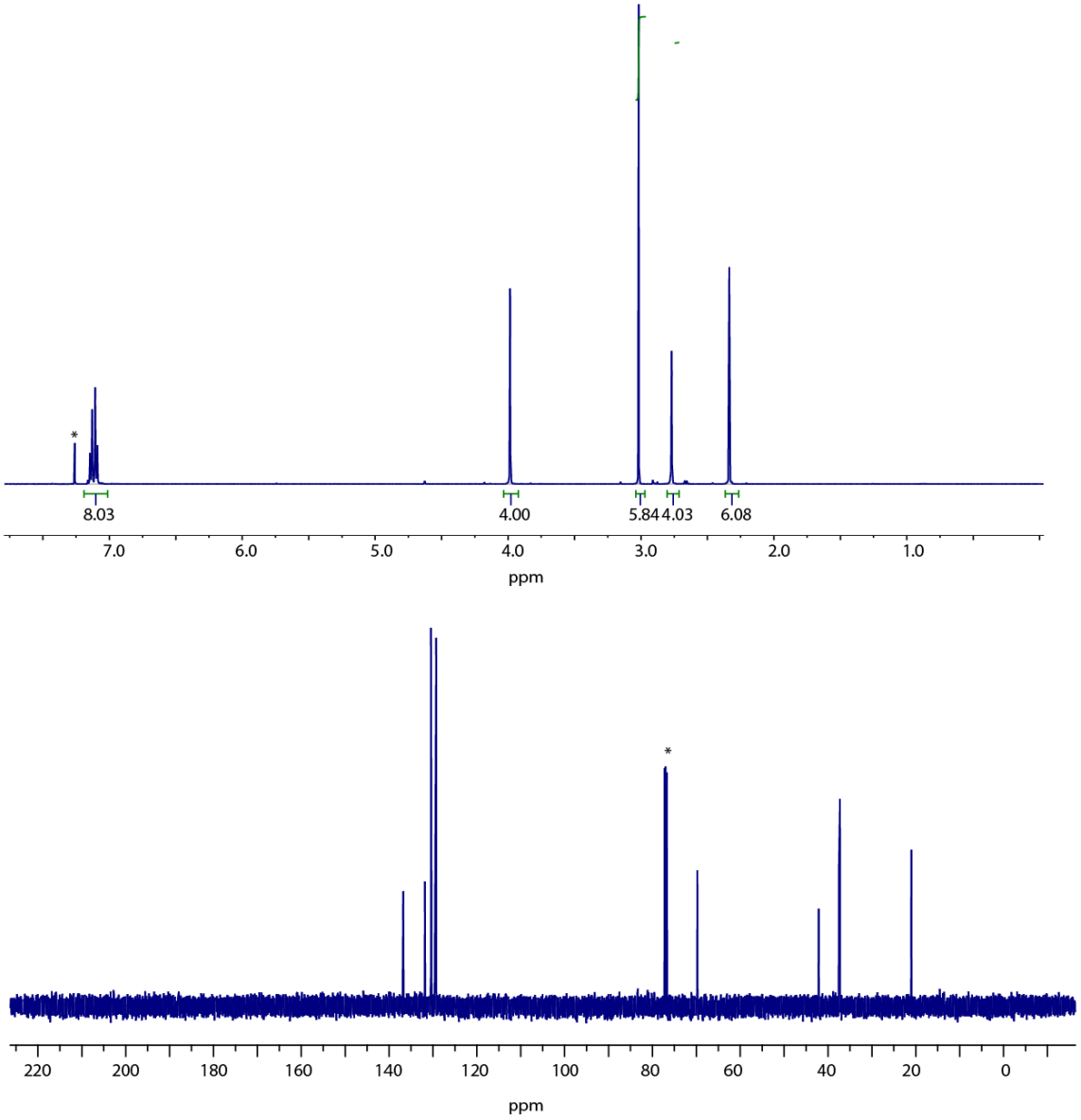

Figure a1. NMR spectra of $(p\text{-tolCH}_2)_2C(CH_2OMs)_2$ ($CDCl_3$): ^1H (top) and $^{13}C\{^1H\}$ (bottom). (* = solvent peak or impurity).

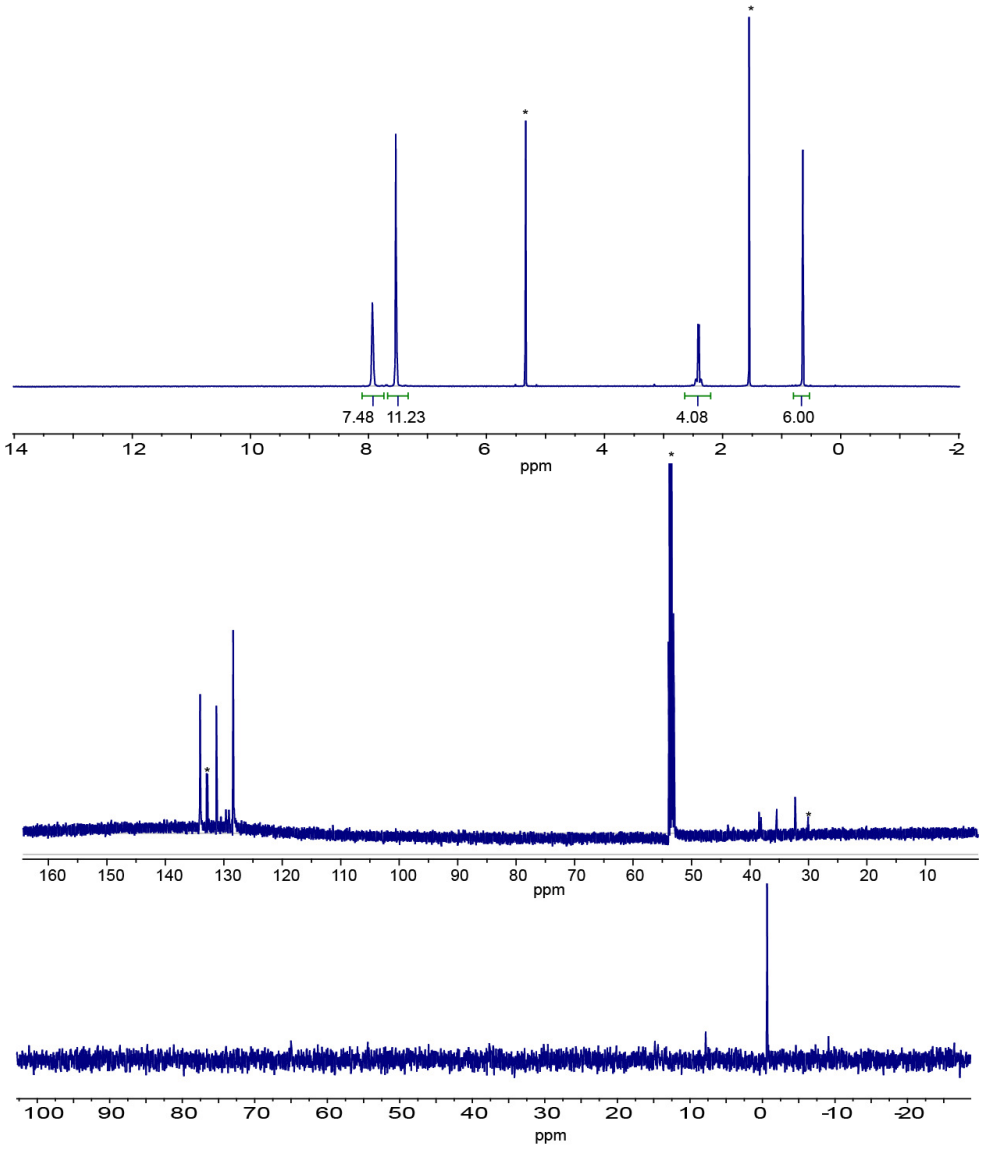

Figure a2. NMR spectra of **2a** (CD_2Cl_2): ^{1}H (top), $^{13}C\{^{1}H\}$ (middle) and $^{31}P\{^{1}H\}$ (bottom) (* = solvent peak or impurity).

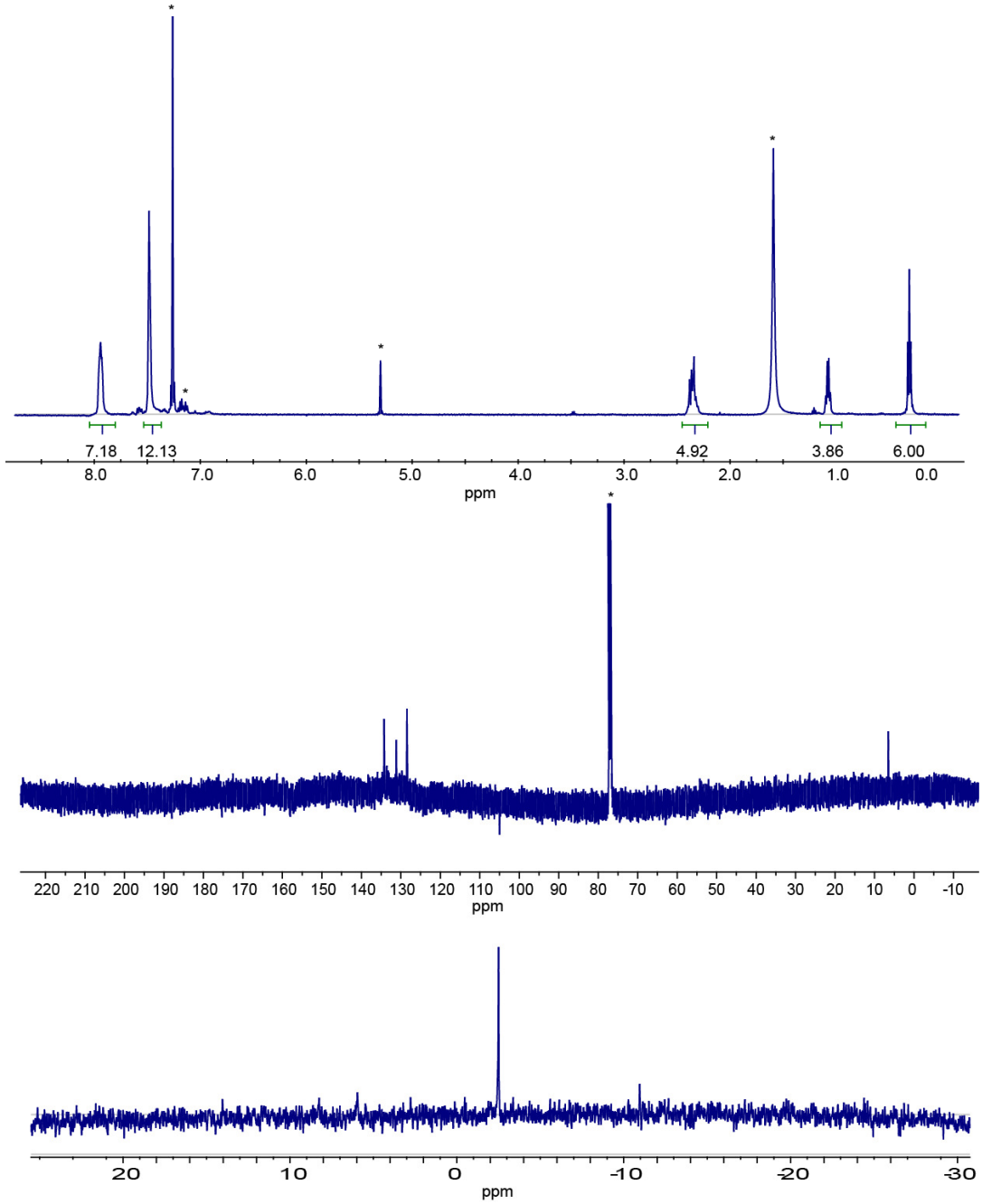

Figure a3. NMR spectra of **2b** ($CDCl_3$): ^{1}H (top), $^{13}C\{^{1}H\}$ (middle) and $^{31}P\{^{1}H\}$ (bottom) (* = solvent peak or impurity).

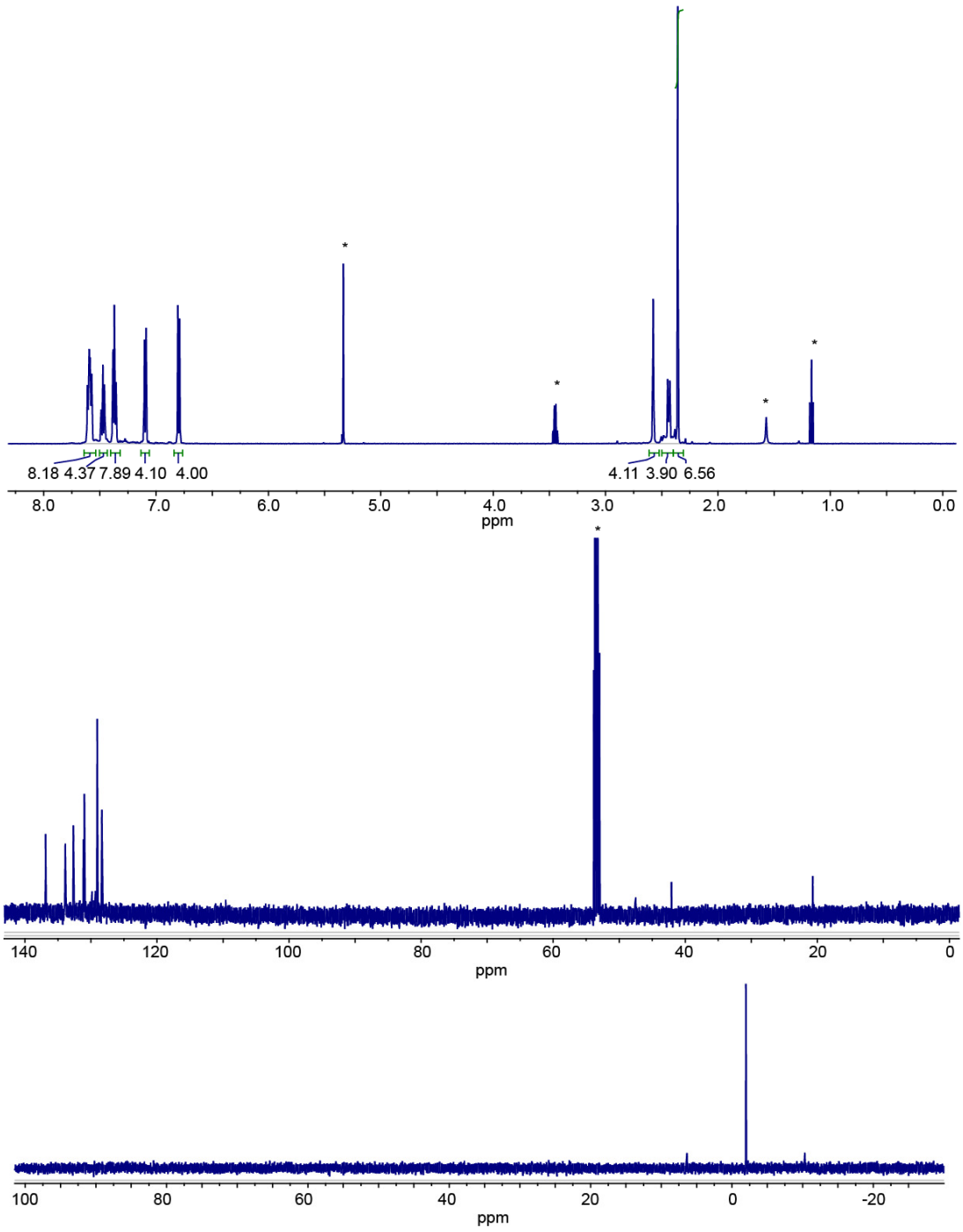

Figure a4. NMR spectra of **2f** (CD_2Cl_2): ^{1}H (top), $^{13}C\{^{1}H\}$ (middle) and $^{31}P\{^{1}H\}$ (bottom) (* = solvent peak or impurity).

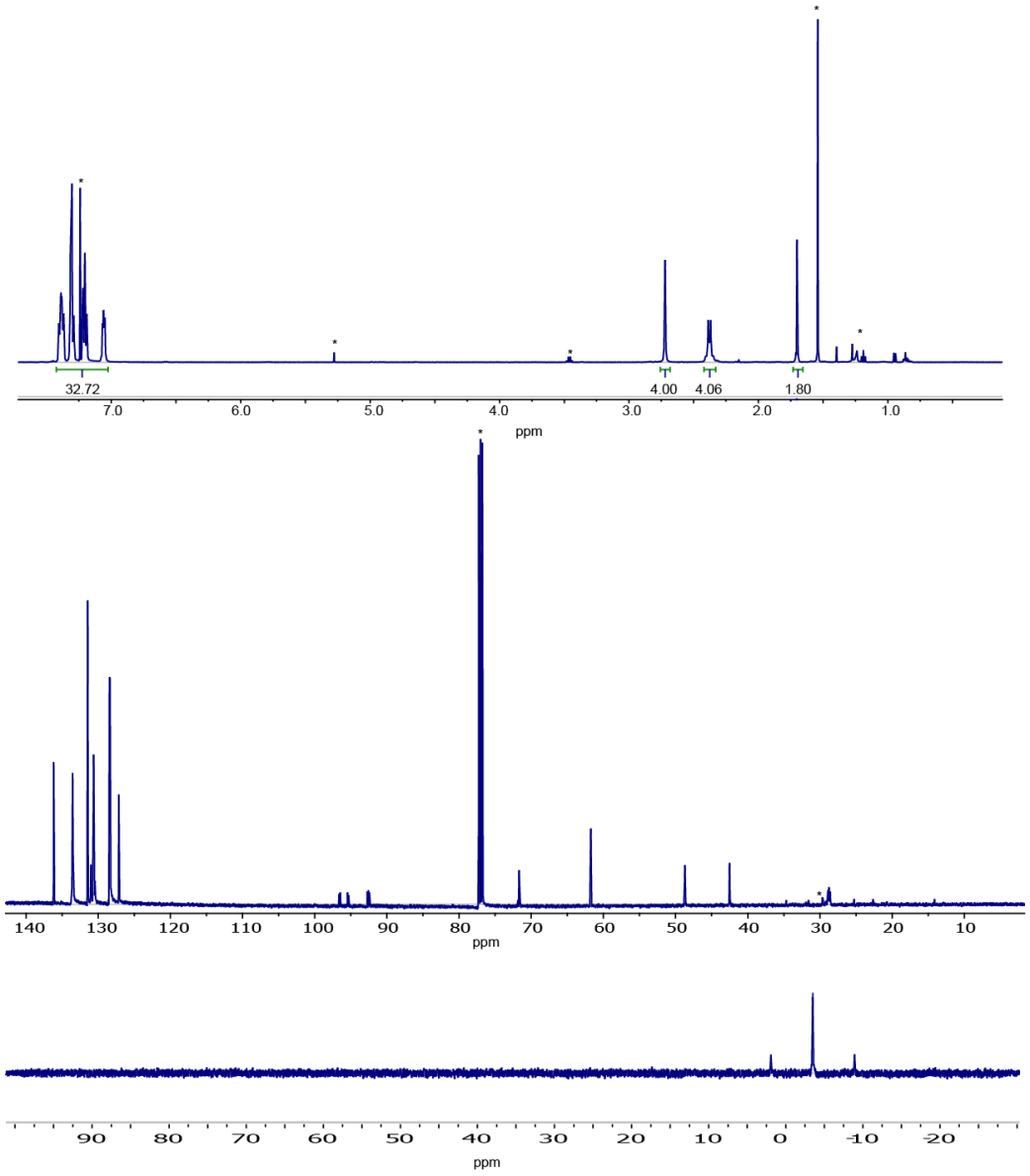

Figure a5. NMR spectra of **3e** (CD_2Cl_3): ^{1}H (top), $^{13}C\{^{1}H\}$ (middle) and $^{31}P\{^{1}H\}$ (bottom) (* = solvent peak or impurity).

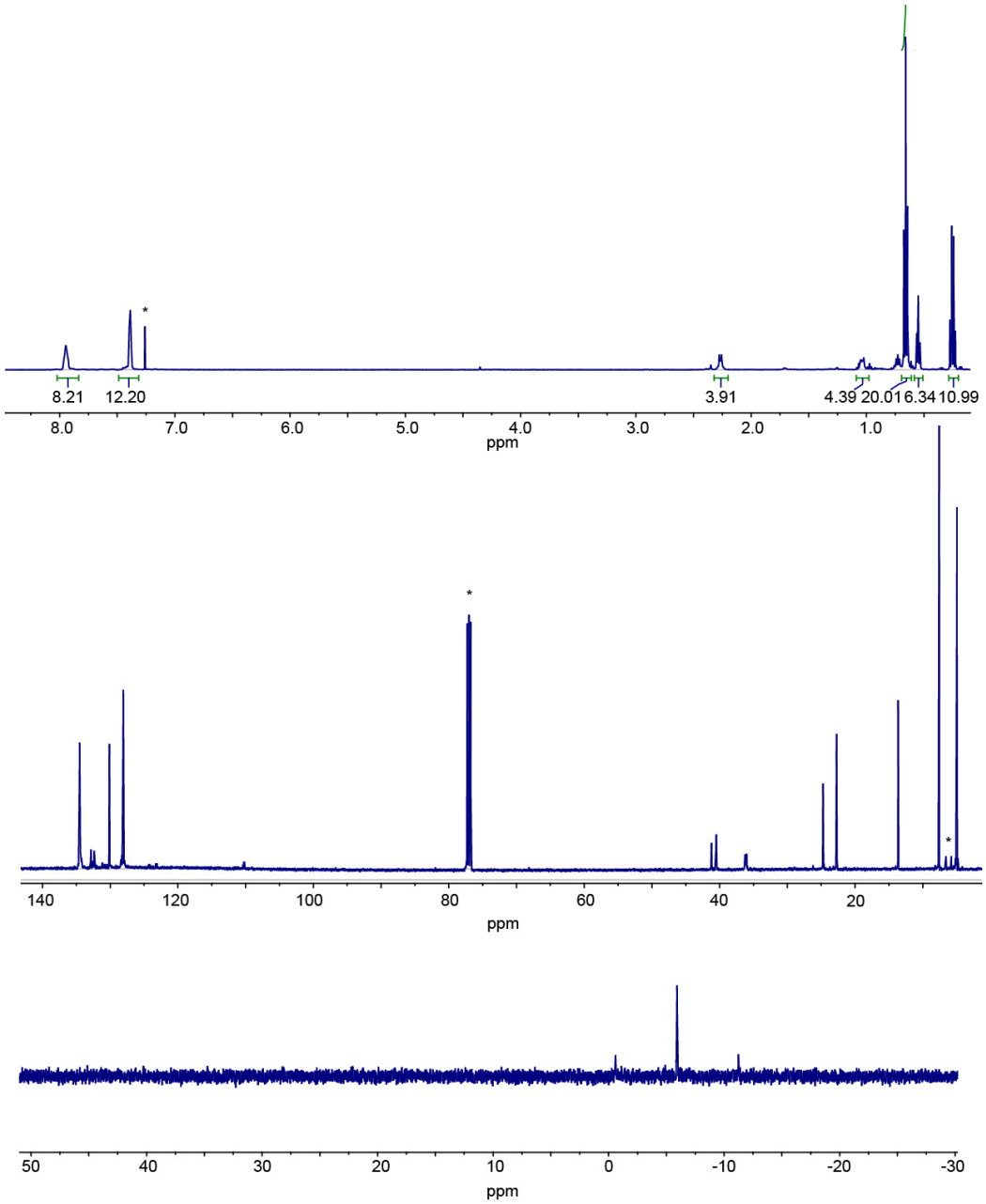

Figure a6. NMR spectra of **7** ($CDCl_3$): ^{1}H (top), $^{13}C\{^{1}H\}$ (middle) and $^{31}P\{^{1}H\}$ (bottom) (* = solvent peak or impurity).

CheckCIF report for **3a**

Bond precision: C-C = 0.0062 A Wavelength=1.54178
Cell: a=17.3247(11) b=16.4634(11) c=24.0781(16)
alpha=90 beta=90 gamma=90
Temperature: 110 K

	Calculated	Reported
Volume	6867.6(8)	6867.6(8)
Space group	P b c a	Pbca
Hall group	-P 2ac 2ab	?
Moiety formula	$C_{37}H_{32}P_2Pt,CH_2Cl_2$	?
Sum formula	$C_{38}H_{34}Cl_2P_2Pt$	$C_{38}H_{34}Cl_2P_2Pt$
Mr	818.57	818.58
Dx,g cm^{-3}	1.583	1.583
Z	8	8
Mu (mm^{-1})	10.144	10.144
F000	3232.0	3232.0
F000’	3211.60	
h,k,lmax	19,18,27	19,18,27
Nref	5100	5099
Tmin,Tmax	0.466,0.816	0.498,0.823
Tmin’	0.423	

Correction method= MULTI-SCAN
Data completeness= 1.000 Theta(max)= 60.000
R(reflections)= 0.0244(3814) wR2(reflections)= 0.0561(5099)
S = 1.083 Npar= 390
The following ALERTS were generated. Each ALERT has the format
test-name_ALERT_alert-type_alert-level.
Alert level B
THETM01_ALERT_3_B The value of sine(theta_max)/wavelength is less than 0.575
Calculated sin(theta_max)/wavelength = 0.5617
Alert level C
PLAT373_ALERT_2_C Long C(sp)-C(sp) Bond C5 - C6 ... 1.38 Ang.
PLAT373_ALERT_2_C Long C(sp)-C(sp) Bond C9 - C10 ... 1.37 Ang.

Alert level G
PLAT005_ALERT_5_G No _iucr_refine_instructions_details in CIF .... ?
PLAT232_ALERT_2_G Hirshfeld Test Diff (M-X) Pt1 -- C8 .. 5.5 su
PLAT710_ALERT_4_G Delete 1-2-3 or 2-3-4 Linear Torsion Angle ... # 2
C8 -PT1 -P2 -C12 -125.90 1.20 1.555 1.555 1.555 1.555
PLAT710_ALERT_4_G Delete 1-2-3 or 2-3-4 Linear Torsion Angle ... # 5
C8 -PT1 -P2 -C18 -9.00 1.20 1.555 1.555 1.555 1.555
PLAT710_ALERT_4_G Delete 1-2-3 or 2-3-4 Linear Torsion Angle ... # 8
C8 -PT1 -P2 -C24 110.50 1.20 1.555 1.555 1.555 1.555
PLAT710_ALERT_4_G Delete 1-2-3 or 2-3-4 Linear Torsion Angle ... # 10
C4 -PT1 -P3 -C29 -113.30 1.10 1.555 1.555 1.555 1.555
PLAT710_ALERT_4_G Delete 1-2-3 or 2-3-4 Linear Torsion Angle ... # 13
C4 -PT1 -P3 -C35 3.80 1.10 1.555 1.555 1.555 1.555
PLAT710_ALERT_4_G Delete 1-2-3 or 2-3-4 Linear Torsion Angle ... # 16
C4 -PT1 -P3 -C28 127.00 1.10 1.555 1.555 1.555 1.555
PLAT710_ALERT_4_G Delete 1-2-3 or 2-3-4 Linear Torsion Angle ... # 19
C8 -PT1 -C4 -C5 -152.00 4.00 1.555 1.555 1.555 1.555
PLAT710_ALERT_4_G Delete 1-2-3 or 2-3-4 Linear Torsion Angle ... # 20
P3 -PT1 -C4 -C5 -86.00 4.00 1.555 1.555 1.555 1.555
PLAT710_ALERT_4_G Delete 1-2-3 or 2-3-4 Linear Torsion Angle ... # 21
P2 -PT1 -C4 -C5 33.00 4.00 1.555 1.555 1.555 1.555
PLAT710_ALERT_4_G Delete 1-2-3 or 2-3-4 Linear Torsion Angle ... # 22
PT1 -C4 -C5 -C6 -39.00 8.00 1.555 1.555 1.555 1.555
PLAT710_ALERT_4_G Delete 1-2-3 or 2-3-4 Linear Torsion Angle ... # 23
C4 -C5 -C6 -C7 4.00 0.00 1.555 1.555 1.555 1.555
PLAT710_ALERT_4_G Delete 1-2-3 or 2-3-4 Linear Torsion Angle ... # 24
C4 -PT1 -C8 -C9 -108.00 5.00 1.555 1.555 1.555 1.555
PLAT710_ALERT_4_G Delete 1-2-3 or 2-3-4 Linear Torsion Angle ... # 25
P3 -PT1 -C8 -C9 77.00 5.00 1.555 1.555 1.555 1.555
PLAT710_ALERT_4_G Delete 1-2-3 or 2-3-4 Linear Torsion Angle ... # 26
P2 -PT1 -C8 -C9 -45.00 6.00 1.555 1.555 1.555 1.555
PLAT710_ALERT_4_G Delete 1-2-3 or 2-3-4 Linear Torsion Angle ... # 27
PT1 -C8 -C9 -C10 63.00 15.00 1.555 1.555 1.555 1.555
PLAT710_ALERT_4_G Delete 1-2-3 or 2-3-4 Linear Torsion Angle ... # 28

C8 -C9 -C10 -C11 82.00 31.00 1.555 1.555 1.555 1.555
PLAT809_ALERT_1_G Can not Parse the SHELXL Weighting Scheme String !

CheckCIF report for **4a**

Bond precision: C-C = 0.0097 A Wavelength=1.54178
Cell: a=13.9731(6) b=19.3822(8) c=32.3857(13)
alpha=90.232(2) beta=100.137(2) gamma=94.743(2)
Temperature: 110 K

	Calculated	Reported
Volume	8603.0(6)	8603.0(6)
Space group	P -1	P-1
Hall group	-P 1	?
Moiety formula	$C_{132}H_{111}P_8Pt_4$	?
Sum formula	$C_{132}H_{111}P_8Pt_4$	$C_{132}H_{111}O_0P_8Pt_4S_0$
Mr	2725.30	2725.33
Dx,g cm^{-3}	1.052	1.052
Z	2	2
Mu (mm^{-1})	6.895	6.895
F000	2670.0	2670.0
F000'	2642.96	
h,k,lmax	15,21,36	15,21,36
Nref	25553	24343
Tmin,Tmax	0.527,0.759	0.546,0.770
Tmin'	0.478	

Correction method= MULTI-SCAN
Data completeness= 0.953 Theta(max)= 60.000
R(reflections)= 0.0396(18977) wR2(reflections)= 0.1033(24343)
S = 0.957 Npar= 1297
The following ALERTS were generated. Each ALERT has the format
test-name_ALERT_alert-type_alert-level.
Alert level B
THETM01_ALERT_3_B The value of sine(theta_max)/wavelength is less than 0.575

Calculated sin(theta_max)/wavelength = 0.5617
PLAT029_ALERT_3_B _diffrn_measured_fraction_theta_full Low 0.953
Alert level C
PLAT041_ALERT_1_C Calc. and Reported SumFormula Strings Differ ?
PLAT094_ALERT_2_C Ratio of Maximum / Minimum Residual Density 2.29
PLAT220_ALERT_2_C Large Non-Solvent C Ueq(max)/Ueq(min) ... 3.5 Ratio
PLAT230_ALERT_2_C Hirshfeld Test Diff for C13 -- C14 .. 6.5 su
PLAT234_ALERT_4_C Large Hirshfeld Difference C72 -- C73 .. 0.18 Ang.
PLAT234_ALERT_4_C Large Hirshfeld Difference C78 -- C79 .. 0.18 Ang.
PLAT241_ALERT_2_C Check High Ueq as Compared to Neighbors for C72
PLAT342_ALERT_3_C Low Bond Precision on C-C Bonds ..... 0.0097 Ang
PLAT366_ALERT_2_C Short? C(sp?)-C(sp?) Bond C102 - C103 ... 1.38 Ang.
PLAT373_ALERT_2_C Long C(sp)-C(sp) Bond C2 - C3 ... 1.38 Ang.
PLAT373_ALERT_2_C Long C(sp)-C(sp) Bond C6 - C7 ... 1.41 Ang.
PLAT373_ALERT_2_C Long C(sp)-C(sp) Bond C10 - C11 ... 1.38 Ang.
PLAT373_ALERT_2_C Long C(sp)-C(sp) Bond C14 - C15 ... 1.37 Ang.
PLAT411_ALERT_2_C Short Inter H...H Contact H91A .. H99A .. 2.11 Ang.
Alert level G
CELLZ01_ALERT_1_G Difference between formula and atom_site contents detected.
CELLZ01_ALERT_1_G ALERT: Large difference may be due to a
symmetry error - see SYMMG tests
From the CIF: _cell_formula_units_Z 2
From the CIF: _chemical_formula_sum C132 H111 O0 P8 Pt4 S0
TEST: Compare cell contents of formula and atom_site data
atom Z*formula cif sites diff
C 264.00 264.00 0.00
H 222.00 222.00 0.00
O 2.00 0.00 2.00
P 16.00 16.00 0.00
Pt 8.00 8.00 0.00
S 2.00 0.00 2.00
PLAT005_ALERT_5_G No _iucr_refine_instructions_details in CIF .... ?
PLAT154_ALERT_1_G The su’s on the Cell Angles are Equal ..... 0.00200 Deg.
PLAT232_ALERT_2_G Hirshfeld Test Diff (M-X) Pt1 -- C16 .. 8.7 su

PLAT232_ALERT_2_G Hirshfeld Test Diff (M-X) Pt4 -- C13 .. 8.3 su
PLAT343_ALERT_2_G Check sp? Angle Range in Main Residue for .. C103
PLAT606_ALERT_4_G VERY LARGE Solvent Accessible VOID(S) in Structure !
PLAT710_ALERT_4_G Delete 1-2-3 or 2-3-4 Linear Torsion Angle ... # 2
C1 -PT1 -P1 -C17 -77.00 2.00 1.555 1.555 1.555 1.555
PLAT710_ALERT_4_G Delete 1-2-3 or 2-3-4 Linear Torsion Angle ... # 5
C1 -PT1 -P1 -C23 41.00 2.00 1.555 1.555 1.555 1.555
PLAT710_ALERT_4_G Delete 1-2-3 or 2-3-4 Linear Torsion Angle ... # 8
C1 -PT1 -P1 -C29 162.00 2.00 1.555 1.555 1.555 1.555
PLAT710_ALERT_4_G Delete 1-2-3 or 2-3-4 Linear Torsion Angle ... # 10
C16 -PT1 -P2 -C34 71.00 1.90 1.555 1.555 1.555 1.555
PLAT710_ALERT_4_G Delete 1-2-3 or 2-3-4 Linear Torsion Angle ... # 13
C16 -PT1 -P2 -C40 -46.60 1.90 1.555 1.555 1.555 1.555
PLAT710_ALERT_4_G Delete 1-2-3 or 2-3-4 Linear Torsion Angle ... # 16
C16 -PT1 -P2 -C33 -168.70 1.90 1.555 1.555 1.555 1.555
PLAT710_ALERT_4_G Delete 1-2-3 or 2-3-4 Linear Torsion Angle ... # 20
C5 -PT2 -P3 -C52 -77.00 3.00 1.555 1.555 1.555 1.555
PLAT710_ALERT_4_G Delete 1-2-3 or 2-3-4 Linear Torsion Angle ... # 23
C5 -PT2 -P3 -C46 41.00 3.00 1.555 1.555 1.555 1.555
PLAT710_ALERT_4_G Delete 1-2-3 or 2-3-4 Linear Torsion Angle ... # 26
C5 -PT2 -P3 -C58 163.00 3.00 1.555 1.555 1.555 1.555
PLAT710_ALERT_4_G Delete 1-2-3 or 2-3-4 Linear Torsion Angle ... # 28
C4 -PT2 -P4 -C62 167.00 3.00 1.555 1.555 1.555 1.555
PLAT710_ALERT_4_G Delete 1-2-3 or 2-3-4 Linear Torsion Angle ... # 31
C4 -PT2 -P4 -C69 47.00 3.00 1.555 1.555 1.555 1.555
PLAT710_ALERT_4_G Delete 1-2-3 or 2-3-4 Linear Torsion Angle ... # 34
C4 -PT2 -P4 -C63 -70.00 3.00 1.555 1.555 1.555 1.555
PLAT710_ALERT_4_G Delete 1-2-3 or 2-3-4 Linear Torsion Angle ... # 38
C9 -PT3 -P5 -C81 84.10 1.80 1.555 1.555 1.555 1.555
PLAT710_ALERT_4_G Delete 1-2-3 or 2-3-4 Linear Torsion Angle ... # 41
C9 -PT3 -P5 -C75 -32.70 1.80 1.555 1.555 1.555 1.555
PLAT710_ALERT_4_G Delete 1-2-3 or 2-3-4 Linear Torsion Angle ... # 44
C9 -PT3 -P5 -C87 -151.50 1.80 1.555 1.555 1.555 1.555
PLAT710_ALERT_4_G Delete 1-2-3 or 2-3-4 Linear Torsion Angle ... # 46

C8 -PT3 -P6 -C92 76.00 2.00 1.555 1.555 1.555 1.555
PLAT710_ALERT_4_G Delete 1-2-3 or 2-3-4 Linear Torsion Angle ... # 49
C8 -PT3 -P6 -C91 -162.00 2.00 1.555 1.555 1.555 1.555
PLAT710_ALERT_4_G Delete 1-2-3 or 2-3-4 Linear Torsion Angle ... # 52
C8 -PT3 -P6 -C98 -40.00 2.00 1.555 1.555 1.555 1.555
PLAT710_ALERT_4_G Delete 1-2-3 or 2-3-4 Linear Torsion Angle ... # 55
C13 -PT4 -P7 -C116 173.00 3.00 1.555 1.555 1.555 1.555
PLAT710_ALERT_4_G Delete 1-2-3 or 2-3-4 Linear Torsion Angle ... # 58
C13 -PT4 -P7 -C110 50.00 3.00 1.555 1.555 1.555 1.555
PLAT710_ALERT_4_G Delete 1-2-3 or 2-3-4 Linear Torsion Angle ... # 61
C13 -PT4 -P7 -C104 -66.00 3.00 1.555 1.555 1.555 1.555
PLAT710_ALERT_4_G Delete 1-2-3 or 2-3-4 Linear Torsion Angle ... # 65
C12 -PT4 -P8 -C121 94.00 1.40 1.555 1.555 1.555 1.555
PLAT710_ALERT_4_G Delete 1-2-3 or 2-3-4 Linear Torsion Angle ... # 68
C12 -PT4 -P8 -C127 -24.30 1.50 1.555 1.555 1.555 1.555
PLAT710_ALERT_4_G Delete 1-2-3 or 2-3-4 Linear Torsion Angle ... # 71
C12 -PT4 -P8 -C120 -146.50 1.40 1.555 1.555 1.555 1.555
PLAT710_ALERT_4_G Delete 1-2-3 or 2-3-4 Linear Torsion Angle ... # 73
C16 -PT1 -C1 -C2 13.00 9.00 1.555 1.555 1.555 1.555
PLAT710_ALERT_4_G Delete 1-2-3 or 2-3-4 Linear Torsion Angle ... # 74
P2 -PT1 -C1 -C2 -169.00 9.00 1.555 1.555 1.555 1.555
PLAT710_ALERT_4_G Delete 1-2-3 or 2-3-4 Linear Torsion Angle ... # 75
P1 -PT1 -C1 -C2 45.00 10.00 1.555 1.555 1.555 1.555
PLAT710_ALERT_4_G Delete 1-2-3 or 2-3-4 Linear Torsion Angle ... # 76
PT1 -C1 -C2 -C3 -64.00 20.00 1.555 1.555 1.555 1.555
PLAT710_ALERT_4_G Delete 1-2-3 or 2-3-4 Linear Torsion Angle ... # 77
C1 -C2 -C3 -C4 69.00 27.00 1.555 1.555 1.555 1.555
PLAT710_ALERT_4_G Delete 1-2-3 or 2-3-4 Linear Torsion Angle ... # 78
C2 -C3 -C4 -PT2 42.00 27.00 1.555 1.555 1.555 1.555
PLAT710_ALERT_4_G Delete 1-2-3 or 2-3-4 Linear Torsion Angle ... # 79
C5 -PT2 -C4 -C3 -16.00 10.00 1.555 1.555 1.555 1.555
PLAT710_ALERT_4_G Delete 1-2-3 or 2-3-4 Linear Torsion Angle ... # 80
P4 -PT2 -C4 -C3 -20.00 12.00 1.555 1.555 1.555 1.555
PLAT710_ALERT_4_G Delete 1-2-3 or 2-3-4 Linear Torsion Angle ... # 81

P3 -PT2 -C4 -C3 166.00 10.00 1.555 1.555 1.555 1.555
PLAT710_ALERT_4_G Delete 1-2-3 or 2-3-4 Linear Torsion Angle ... # 82
C4 -PT2 -C5 -C6 8.00 0.00 1.555 1.555 1.555 1.555
PLAT710_ALERT_4_G Delete 1-2-3 or 2-3-4 Linear Torsion Angle ... # 83
P4 -PT2 -C5 -C6 10.00 0.00 1.555 1.555 1.555 1.555
PLAT710_ALERT_4_G Delete 1-2-3 or 2-3-4 Linear Torsion Angle ... # 84
P3 -PT2 -C5 -C6 12.00 0.00 1.555 1.555 1.555 1.555
PLAT710_ALERT_4_G Delete 1-2-3 or 2-3-4 Linear Torsion Angle ... # 85
PT2 -C5 -C6 -C7 14.00 0.00 1.555 1.555 1.555 1.555
PLAT710_ALERT_4_G Delete 1-2-3 or 2-3-4 Linear Torsion Angle ... # 86
C5 -C6 -C7 -C8 86.00 25.00 1.555 1.555 1.555 1.555
PLAT710_ALERT_4_G Delete 1-2-3 or 2-3-4 Linear Torsion Angle ... # 87
C6 -C7 -C8 -PT3 -53.00 17.00 1.555 1.555 1.555 1.555
PLAT710_ALERT_4_G Delete 1-2-3 or 2-3-4 Linear Torsion Angle ... # 88
C9 -PT3 -C8 -C7 -26.00 5.00 1.555 1.555 1.555 1.555
PLAT710_ALERT_4_G Delete 1-2-3 or 2-3-4 Linear Torsion Angle ... # 89
P5 -PT3 -C8 -C7 153.00 5.00 1.555 1.555 1.555 1.555
PLAT710_ALERT_4_G Delete 1-2-3 or 2-3-4 Linear Torsion Angle ... # 90
P6 -PT3 -C8 -C7 -61.00 7.00 1.555 1.555 1.555 1.555
PLAT710_ALERT_4_G Delete 1-2-3 or 2-3-4 Linear Torsion Angle ... # 91
C8 -PT3 -C9 -C10 64.00 6.00 1.555 1.555 1.555 1.555
PLAT710_ALERT_4_G Delete 1-2-3 or 2-3-4 Linear Torsion Angle ... # 92
P5 -PT3 -C9 -C10 49.00 7.00 1.555 1.555 1.555 1.555
PLAT710_ALERT_4_G Delete 1-2-3 or 2-3-4 Linear Torsion Angle ... # 93
P6 -PT3 -C9 -C10 -119.00 6.00 1.555 1.555 1.555 1.555
PLAT710_ALERT_4_G Delete 1-2-3 or 2-3-4 Linear Torsion Angle ... # 94
PT3 -C9 -C10 -C11 23.00 22.00 1.555 1.555 1.555 1.555
PLAT710_ALERT_4_G Delete 1-2-3 or 2-3-4 Linear Torsion Angle ... # 95
C9 -C10 -C11 -C12 13.00 0.00 1.555 1.555 1.555 1.555
PLAT710_ALERT_4_G Delete 1-2-3 or 2-3-4 Linear Torsion Angle ... # 96
C10 -C11 -C12 -PT4 5.00 0.00 1.555 1.555 1.555 1.555
PLAT710_ALERT_4_G Delete 1-2-3 or 2-3-4 Linear Torsion Angle ... # 97
C13 -PT4 -C12 -C11 51.00 5.00 1.555 1.555 1.555 1.555
PLAT710_ALERT_4_G Delete 1-2-3 or 2-3-4 Linear Torsion Angle ... # 98

P7 -PT4 -C12 -C11 -127.00 5.00 1.555 1.555 1.555 1.555
PLAT710_ALERT_4_G Delete 1-2-3 or 2-3-4 Linear Torsion Angle ... # 99
P8 -PT4 -C12 -C11 1.00 6.00 1.555 1.555 1.555 1.555
PLAT710_ALERT_4_G Delete 1-2-3 or 2-3-4 Linear Torsion Angle ... # 100
C12 -PT4 -C13 -C14 -32.00 10.00 1.555 1.555 1.555 1.555
PLAT710_ALERT_4_G Delete 1-2-3 or 2-3-4 Linear Torsion Angle ... # 101
P7 -PT4 -C13 -C14 -12.00 12.00 1.555 1.555 1.555 1.555
PLAT710_ALERT_4_G Delete 1-2-3 or 2-3-4 Linear Torsion Angle ... # 102
P8 -PT4 -C13 -C14 142.00 10.00 1.555 1.555 1.555 1.555
PLAT710_ALERT_4_G Delete 1-2-3 or 2-3-4 Linear Torsion Angle ... # 103
PT4 -C13 -C14 -C15 -76.00 22.00 1.555 1.555 1.555 1.555
PLAT710_ALERT_4_G Delete 1-2-3 or 2-3-4 Linear Torsion Angle ... # 104
C13 -C14 -C15 -C16 38.00 31.00 1.555 1.555 1.555 1.555
PLAT710_ALERT_4_G Delete 1-2-3 or 2-3-4 Linear Torsion Angle ... # 105
C14 -C15 -C16 -PT1 -22.00 26.00 1.555 1.555 1.555 1.555
PLAT710_ALERT_4_G Delete 1-2-3 or 2-3-4 Linear Torsion Angle ... # 106
C1 -PT1 -C16 -C15 42.00 10.00 1.555 1.555 1.555 1.555
PLAT710_ALERT_4_G Delete 1-2-3 or 2-3-4 Linear Torsion Angle ... # 107
P2 -PT1 -C16 -C15 18.00 12.00 1.555 1.555 1.555 1.555
PLAT710_ALERT_4_G Delete 1-2-3 or 2-3-4 Linear Torsion Angle ... # 108
P1 -PT1 -C16 -C15 -135.00 10.00 1.555 1.555 1.555 1.555
PLAT793_ALERT_4_G The Model has Chirality at P6 (Verify) .... S
PLAT869_ALERT_4_G ALERTS Related to the use of SQUEEZE Suppressed !

CheckCIF report for **4b**

Bond precision: C-C = 0.0195 A Wavelength=1.54178
Cell: a=21.448(4) b=22.771(4) c=25.579(5)
alpha=101.573(9) beta=106.392(9) gamma=111.947(10)
Temperature: 110 K

	Calculated	Reported
Volume	10438(4)	10438(3)
Space group	P -1	P-1

Hall group	-P 1	?
Moiety formula	$C_{140}H_{136}P_8Pt_4$	?
Sum formula	$C_{140}H_{136}P_8Pt_4$	$C_{140}H_{136}P_8Pt_4$
Mr	2846.58	2846.61
Dx,g cm^{-3}	0.906	0.906
Z	2	2
Mu (mm^{-1})	5.697	5.697
F000	2816.0	2816.0
F000’	2789.20	
h,k,lmax	24,25,28	24,25,28
Nref	30990	29149
Tmin,Tmax	0.815,0.843	0.804,0.848
Tmin’	0.796	

Correction method= MULTI-SCAN

Data completeness= 0.941 Theta(max)= 60.000

R(reflections)= 0.0755(19376) wR2(reflections)= 0.2165(29149)

S = 1.180 Npar= 1233

The following ALERTS were generated. Each ALERT has the format
test-name_ALERT_alert-type_alert-level.

Alert level B

THETM01_ALERT_3_B The value of sine(theta_max)/wavelength is less than 0.575
Calculated sin(theta_max)/wavelength = 0.5617

PLAT029_ALERT_3_B _diffrn_measured_fraction_theta_full Low 0.941

PLAT213_ALERT_2_B Atom C36A has ADP max/min Ratio ..... 5.0 oblatPLAT213_ALERT_2_B Atom C52 has ADP max/min Ratio ..... 4.1 prola

Alert level C

DIFMX01_ALERT_2_C The maximum difference density is > 0.1*ZMAX*0.75
_refine_diff_density_max given = 7.086
Test value = 5.850

DIFMX02_ALERT_1_C The maximum difference density is > 0.1*ZMAX*0.75
The relevant atom site should be identified.

REFLT03_ALERT_3_C Reflection count < 95% complete
From the CIF: _diffrn_reflns_theta_max 60.00
From the CIF: _diffrn_reflns_theta_full 60.00

From the CIF: _reflns_number_total 29149

TEST2: Reflns within _diffrn_reflns_theta_max

Count of symmetry unique reflns 30990

Completeness (_total/calc) 94.06%

PLAT022_ALERT_3_C Ratio Unique / Expected Reflections (too) Low .. 0.941

PLAT097_ALERT_2_C Large Reported Max. (Positive) Residual Density 7.09 eA-3

PLAT213_ALERT_2_C Atom C27A has ADP max/min Ratio ..... 3.4 prola

PLAT213_ALERT_2_C Atom C33B has ADP max/min Ratio ..... 3.9 prola

PLAT213_ALERT_2_C Atom C34A has ADP max/min Ratio ..... 3.8 prola

PLAT230_ALERT_2_C Hirshfeld Test Diff for C33B -- C34B .. 5.5 su

PLAT234_ALERT_4_C Large Hirshfeld Difference P20A -- C21A .. 0.16 Ang.

PLAT234_ALERT_4_C Large Hirshfeld Difference P40B -- C47B .. 0.17 Ang.

PLAT234_ALERT_4_C Large Hirshfeld Difference C21B -- C26B .. 0.16 Ang.

PLAT234_ALERT_4_C Large Hirshfeld Difference C21C -- C26C .. 0.17 Ang.

PLAT234_ALERT_4_C Large Hirshfeld Difference C24 -- C25 .. 0.20 Ang.

PLAT234_ALERT_4_C Large Hirshfeld Difference C25A -- C26A .. 0.20 Ang.

PLAT234_ALERT_4_C Large Hirshfeld Difference C27A -- C28A .. 0.19 Ang.

PLAT234_ALERT_4_C Large Hirshfeld Difference C29A -- C30A .. 0.21 Ang.

PLAT234_ALERT_4_C Large Hirshfeld Difference C31 -- C32 .. 0.16 Ang.

PLAT234_ALERT_4_C Large Hirshfeld Difference C31A -- C32A .. 0.20 Ang.

PLAT234_ALERT_4_C Large Hirshfeld Difference C31C -- C32C .. 0.16 Ang.

PLAT234_ALERT_4_C Large Hirshfeld Difference C34B -- C36B .. 0.16 Ang.

PLAT234_ALERT_4_C Large Hirshfeld Difference C34C -- C38C .. 0.16 Ang.

PLAT234_ALERT_4_C Large Hirshfeld Difference C41 -- C46 .. 0.18 Ang.

PLAT234_ALERT_4_C Large Hirshfeld Difference C43 -- C44 .. 0.19 Ang.

PLAT234_ALERT_4_C Large Hirshfeld Difference C45 -- C46 .. 0.18 Ang.

PLAT234_ALERT_4_C Large Hirshfeld Difference C47 -- C48 .. 0.17 Ang.

PLAT234_ALERT_4_C Large Hirshfeld Difference C47A -- C48A .. 0.20 Ang.

PLAT234_ALERT_4_C Large Hirshfeld Difference C47B -- C48B .. 0.17 Ang.

PLAT234_ALERT_4_C Large Hirshfeld Difference C47C -- C52C .. 0.18 Ang.

PLAT234_ALERT_4_C Large Hirshfeld Difference C51 -- C52 .. 0.20 Ang.

PLAT241_ALERT_2_C Check High Ueq as Compared to Neighbors for C25

PLAT241_ALERT_2_C Check High Ueq as Compared to Neighbors for C50B

PLAT330_ALERT_2_C Large Average Phenyl C-C Dist. C27A -C32A 1.42 Ang.
PLAT342_ALERT_3_C Low Bond Precision on C-C Bonds ..... 0.0195 Ang
PLAT373_ALERT_2_C Long C(sp)-C(sp) Bond C2 - C3 ... 1.36 Ang.
PLAT373_ALERT_2_C Long C(sp)-C(sp) Bond C6 - C7 ... 1.36 Ang.
PLAT373_ALERT_2_C Long C(sp)-C(sp) Bond C10 - C11 ... 1.39 Ang.
PLAT373_ALERT_2_C Long C(sp)-C(sp) Bond C14 - C15 ... 1.37 Ang.
Alert level G
PLAT005_ALERT_5_G No _iucr_refine_instructions_details in CIF .... ?
PLAT072_ALERT_2_G SHELXL First Parameter in WGHT Unusually Large. 0.12
PLAT232_ALERT_2_G Hirshfeld Test Diff (M-X) Pt2 -- P40A .. 6.8 su
PLAT232_ALERT_2_G Hirshfeld Test Diff (M-X) Pt3 -- P20B .. 7.4 su
PLAT232_ALERT_2_G Hirshfeld Test Diff (M-X) Pt4 -- P40C .. 5.9 su
PLAT606_ALERT_4_G VERY LARGE Solvent Accessible VOID(S) in Structure !
PLAT710_ALERT_4_G Delete 1-2-3 or 2-3-4 Linear Torsion Angle ... # 1
PT1 -C1 -C2 -C3 30.00 37.00 1.555 1.555 1.555 1.555
PLAT710_ALERT_4_G Delete 1-2-3 or 2-3-4 Linear Torsion Angle ... # 2
C1 -C2 -C3 -C4 3.00 0.00 1.555 1.555 1.555 1.555
PLAT710_ALERT_4_G Delete 1-2-3 or 2-3-4 Linear Torsion Angle ... # 3
C2 -C3 -C4 -PT2 161.00 24.00 1.555 1.555 1.555 1.555
PLAT710_ALERT_4_G Delete 1-2-3 or 2-3-4 Linear Torsion Angle ... # 4
PT2 -C5 -C6 -C7 3.00 0.00 1.555 1.555 1.555 1.555
PLAT710_ALERT_4_G Delete 1-2-3 or 2-3-4 Linear Torsion Angle ... # 5
C5 -C6 -C7 -C8 15.00 0.00 1.555 1.555 1.555 1.555
PLAT710_ALERT_4_G Delete 1-2-3 or 2-3-4 Linear Torsion Angle ... # 6
C6 -C7 -C8 -PT3 1.00 0.00 1.555 1.555 1.555 1.555
PLAT710_ALERT_4_G Delete 1-2-3 or 2-3-4 Linear Torsion Angle ... # 7
PT3 -C9 -C10 -C11 15.00 0.00 1.555 1.555 1.555 1.555
PLAT710_ALERT_4_G Delete 1-2-3 or 2-3-4 Linear Torsion Angle ... # 8
C9 -C10 -C11 -C12 6.00 0.00 1.555 1.555 1.555 1.555
PLAT710_ALERT_4_G Delete 1-2-3 or 2-3-4 Linear Torsion Angle ... # 9
C10 -C11 -C12 -PT4 5.00 0.00 1.555 1.555 1.555 1.555
PLAT710_ALERT_4_G Delete 1-2-3 or 2-3-4 Linear Torsion Angle ... # 10
PT4 -C13 -C14 -C15 4.00 0.00 1.555 1.555 1.555 1.555

PLAT710_ALERT_4_G Delete 1-2-3 or 2-3-4 Linear Torsion Angle ... # 11
C13 -C14 -C15 -C16 17.00 0.00 1.555 1.555 1.555 1.555
PLAT710_ALERT_4_G Delete 1-2-3 or 2-3-4 Linear Torsion Angle ... # 12
C14 -C15 -C16 -PT1 6.00 0.00 1.555 1.555 1.555 1.555
PLAT710_ALERT_4_G Delete 1-2-3 or 2-3-4 Linear Torsion Angle ... # 309
C15 -C16 -PT1 -C1 40.00 16.00 1.555 1.555 1.555 1.555
PLAT710_ALERT_4_G Delete 1-2-3 or 2-3-4 Linear Torsion Angle ... # 310
C15 -C16 -PT1 -P20 -145.00 16.00 1.555 1.555 1.555 1.555
PLAT710_ALERT_4_G Delete 1-2-3 or 2-3-4 Linear Torsion Angle ... # 311
C15 -C16 -PT1 -P40 -3.00 20.00 1.555 1.555 1.555 1.555
PLAT710_ALERT_4_G Delete 1-2-3 or 2-3-4 Linear Torsion Angle ... # 312
C2 -C1 -PT1 -C16 98.00 7.00 1.555 1.555 1.555 1.555
PLAT710_ALERT_4_G Delete 1-2-3 or 2-3-4 Linear Torsion Angle ... # 313
C2 -C1 -PT1 -P20 43.00 9.00 1.555 1.555 1.555 1.555
PLAT710_ALERT_4_G Delete 1-2-3 or 2-3-4 Linear Torsion Angle ... # 314
C2 -C1 -PT1 -P40 -85.00 7.00 1.555 1.555 1.555 1.555
PLAT710_ALERT_4_G Delete 1-2-3 or 2-3-4 Linear Torsion Angle ... # 318
C27 -P20 -PT1 -C1 105.00 2.00 1.555 1.555 1.555 1.555
PLAT710_ALERT_4_G Delete 1-2-3 or 2-3-4 Linear Torsion Angle ... # 319
C21 -P20 -PT1 -C1 -12.00 3.00 1.555 1.555 1.555 1.555
PLAT710_ALERT_4_G Delete 1-2-3 or 2-3-4 Linear Torsion Angle ... # 320
C33 -P20 -PT1 -C1 -134.00 2.00 1.555 1.555 1.555 1.555
PLAT710_ALERT_4_G Delete 1-2-3 or 2-3-4 Linear Torsion Angle ... # 324
C41 -P40 -PT1 -C16 -17.00 4.00 1.555 1.555 1.555 1.555
PLAT710_ALERT_4_G Delete 1-2-3 or 2-3-4 Linear Torsion Angle ... # 325
C35 -P40 -PT1 -C16 -137.00 4.00 1.555 1.555 1.555 1.555
PLAT710_ALERT_4_G Delete 1-2-3 or 2-3-4 Linear Torsion Angle ... # 326
C47 -P40 -PT1 -C16 98.00 4.00 1.555 1.555 1.555 1.555
PLAT710_ALERT_4_G Delete 1-2-3 or 2-3-4 Linear Torsion Angle ... # 333
C6 -C5 -PT2 -C4 -40.00 16.00 1.555 1.555 1.555 1.555
PLAT710_ALERT_4_G Delete 1-2-3 or 2-3-4 Linear Torsion Angle ... # 334
C6 -C5 -PT2 -P40A 137.00 16.00 1.555 1.555 1.555 1.555
PLAT710_ALERT_4_G Delete 1-2-3 or 2-3-4 Linear Torsion Angle ... # 335
C6 -C5 -PT2 -P20A -51.00 18.00 1.555 1.555 1.555 1.555

PLAT710_ALERT_4_G Delete 1-2-3 or 2-3-4 Linear Torsion Angle ... # 336
C3 -C4 -PT2 -C5 10.00 10.00 1.555 1.555 1.555 1.555
PLAT710_ALERT_4_G Delete 1-2-3 or 2-3-4 Linear Torsion Angle ... # 337
C3 -C4 -PT2 -P40A -27.00 13.00 1.555 1.555 1.555 1.555
PLAT710_ALERT_4_G Delete 1-2-3 or 2-3-4 Linear Torsion Angle ... # 338
C3 -C4 -PT2 -P20A -170.00 10.00 1.555 1.555 1.555 1.555
PLAT710_ALERT_4_G Delete 1-2-3 or 2-3-4 Linear Torsion Angle ... # 342
C47A-P40A-PT2 -C4 93.00 4.00 1.555 1.555 1.555 1.555
PLAT710_ALERT_4_G Delete 1-2-3 or 2-3-4 Linear Torsion Angle # 343
C41A-P40A-PT2 -C4 -25.00 4.00 1.555 1.555 1.555 1.555
PLAT710_ALERT_4_G Delete 1-2-3 or 2-3-4 Linear Torsion Angle ... # 344
C35A-P40A-PT2 -C4 -144.00 4.00 1.555 1.555 1.555 1.555
PLAT710_ALERT_4_G Delete 1-2-3 or 2-3-4 Linear Torsion Angle ... # 348
C27A-P20A-PT2 -C5 73.00 4.00 1.555 1.555 1.555 1.555
PLAT710_ALERT_4_G Delete 1-2-3 or 2-3-4 Linear Torsion Angle ... # 349
C33A-P20A-PT2 -C5 -167.00 4.00 1.555 1.555 1.555 1.555
PLAT710_ALERT_4_G Delete 1-2-3 or 2-3-4 Linear Torsion Angle ... # 350
C21A-P20A-PT2 -C5 -46.00 4.00 1.555 1.555 1.555 1.555
PLAT710_ALERT_4_G Delete 1-2-3 or 2-3-4 Linear Torsion Angle ... # 357
C10 -C9 -PT3 -C8 39.00 15.00 1.555 1.555 1.555 1.555
PLAT710_ALERT_4_G Delete 1-2-3 or 2-3-4 Linear Torsion Angle ... # 358
C10 -C9 -PT3 -P20B 0.00 18.00 1.555 1.555 1.555 1.555
PLAT710_ALERT_4_G Delete 1-2-3 or 2-3-4 Linear Torsion Angle ... # 359
C10 -C9 -PT3 -P40B -140.00 15.00 1.555 1.555 1.555 1.555
PLAT710_ALERT_4_G Delete 1-2-3 or 2-3-4 Linear Torsion Angle ... # 360
C7 -C8 -PT3 -C9 -97.00 25.00 1.555 1.555 1.555 1.555
PLAT710_ALERT_4_G Delete 1-2-3 or 2-3-4 Linear Torsion Angle ... # 361
C7 -C8 -PT3 -P20B 80.00 25.00 1.555 1.555 1.555 1.555
PLAT710_ALERT_4_G Delete 1-2-3 or 2-3-4 Linear Torsion Angle ... # 362
C7 -C8 -PT3 -P40B -87.00 26.00 1.555 1.555 1.555 1.555
PLAT710_ALERT_4_G Delete 1-2-3 or 2-3-4 Linear Torsion Angle ... # 363
C33B-P20B-PT3 -C9 -143.00 4.00 1.555 1.555 1.555 1.555
PLAT710_ALERT_4_G Delete 1-2-3 or 2-3-4 Linear Torsion Angle ... # 364
C21B-P20B-PT3 -C9 94.00 4.00 1.555 1.555 1.555 1.555

PLAT710_ALERT_4_G Delete 1-2-3 or 2-3-4 Linear Torsion Angle ... # 365
C27B-P20B-PT3 -C9 -24.00 4.00 1.555 1.555 1.555 1.555
PLAT710_ALERT_4_G Delete 1-2-3 or 2-3-4 Linear Torsion Angle ... # 375
C47B-P40B-PT3 -C8 -66.00 4.00 1.555 1.555 1.555 1.555
PLAT710_ALERT_4_G Delete 1-2-3 or 2-3-4 Linear Torsion Angle ... # 376
C41B-P40B-PT3 -C8 53.00 4.00 1.555 1.555 1.555 1.555
PLAT710_ALERT_4_G Delete 1-2-3 or 2-3-4 Linear Torsion Angle ... # 377
C35B-P40B-PT3 -C8 173.00 4.00 1.555 1.555 1.555 1.555
PLAT710_ALERT_4_G Delete 1-2-3 or 2-3-4 Linear Torsion Angle ... # 381
C14 -C13 -PT4 -C12 45.00 12.00 1.555 1.555 1.555 1.555
PLAT710_ALERT_4_G Delete 1-2-3 or 2-3-4 Linear Torsion Angle ... # 382
C14 -C13 -PT4 -P40C -140.00 12.00 1.555 1.555 1.555 1.555
PLAT710_ALERT_4_G Delete 1-2-3 or 2-3-4 Linear Torsion Angle ... # 383
C14 -C13 -PT4 -P20C 5.00 14.00 1.555 1.555 1.555 1.555
PLAT710_ALERT_4_G Delete 1-2-3 or 2-3-4 Linear Torsion Angle ... # 384
C11 -C12 -PT4 -C13 91.00 7.00 1.555 1.555 1.555 1.555
PLAT710_ALERT_4_G Delete 1-2-3 or 2-3-4 Linear Torsion Angle ... # 385
C11 -C12 -PT4 -P40C 38.00 9.00 1.555 1.555 1.555 1.555
PLAT710_ALERT_4_G Delete 1-2-3 or 2-3-4 Linear Torsion Angle ... # 386
C11 -C12 -PT4 -P20C -93.00 7.00 1.555 1.555 1.555 1.555
PLAT710_ALERT_4_G Delete 1-2-3 or 2-3-4 Linear Torsion Angle ... # 390
C41C-P40C-PT4 -C12 105.00 3.00 1.555 1.555 1.555 1.555
PLAT710_ALERT_4_G Delete 1-2-3 or 2-3-4 Linear Torsion Angle ... # 391
C47C-P40C-PT4 -C12 -14.00 3.00 1.555 1.555 1.555 1.555
PLAT710_ALERT_4_G Delete 1-2-3 or 2-3-4 Linear Torsion Angle ... # 392
C35C-P40C-PT4 -C12 -135.00 3.00 1.555 1.555 1.555 1.555
PLAT710_ALERT_4_G Delete 1-2-3 or 2-3-4 Linear Torsion Angle ... # 396
C21C-P20C-PT4 -C13 94.00 3.00 1.555 1.555 1.555 1.555
PLAT710_ALERT_4_G Delete 1-2-3 or 2-3-4 Linear Torsion Angle ... # 397
C27C-P20C-PT4 -C13 -20.00 3.00 1.555 1.555 1.555 1.555
PLAT710_ALERT_4_G Delete 1-2-3 or 2-3-4 Linear Torsion Angle ... # 398
C33C-P20C-PT4 -C13 -142.00 3.00 1.555 1.555 1.555 1.555
PLAT793_ALERT_4_G The Model has Chirality at P20A (Verify) .... R
PLAT869_ALERT_4_G ALERTS Related to the use of SQUEEZE Suppressed !

APPENDIX B

NMR SPECTRA AND CHECKCIF REPORT FOR CHAPTER III

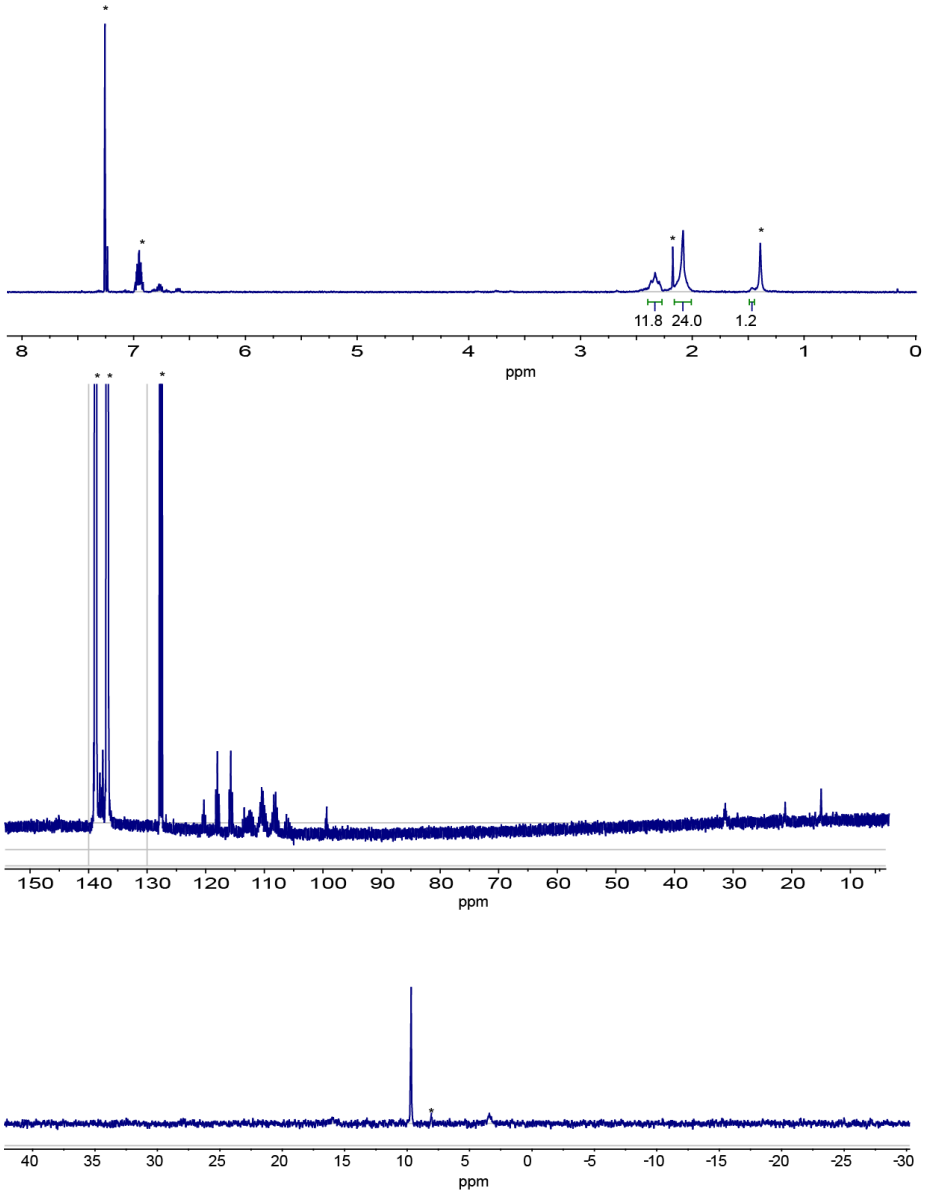

Figure b1. NMR spectra of **9c**: ^{1}H (C_6F_6 + $CDCl_3$; top), $^{13}C\{^{1}H\}$ (C_6F_6 + C_6D_6 capillary; middle) and $^{31}P\{^{1}H\}$ (C_6F_6; bottom) (* = solvent peak or impurity).

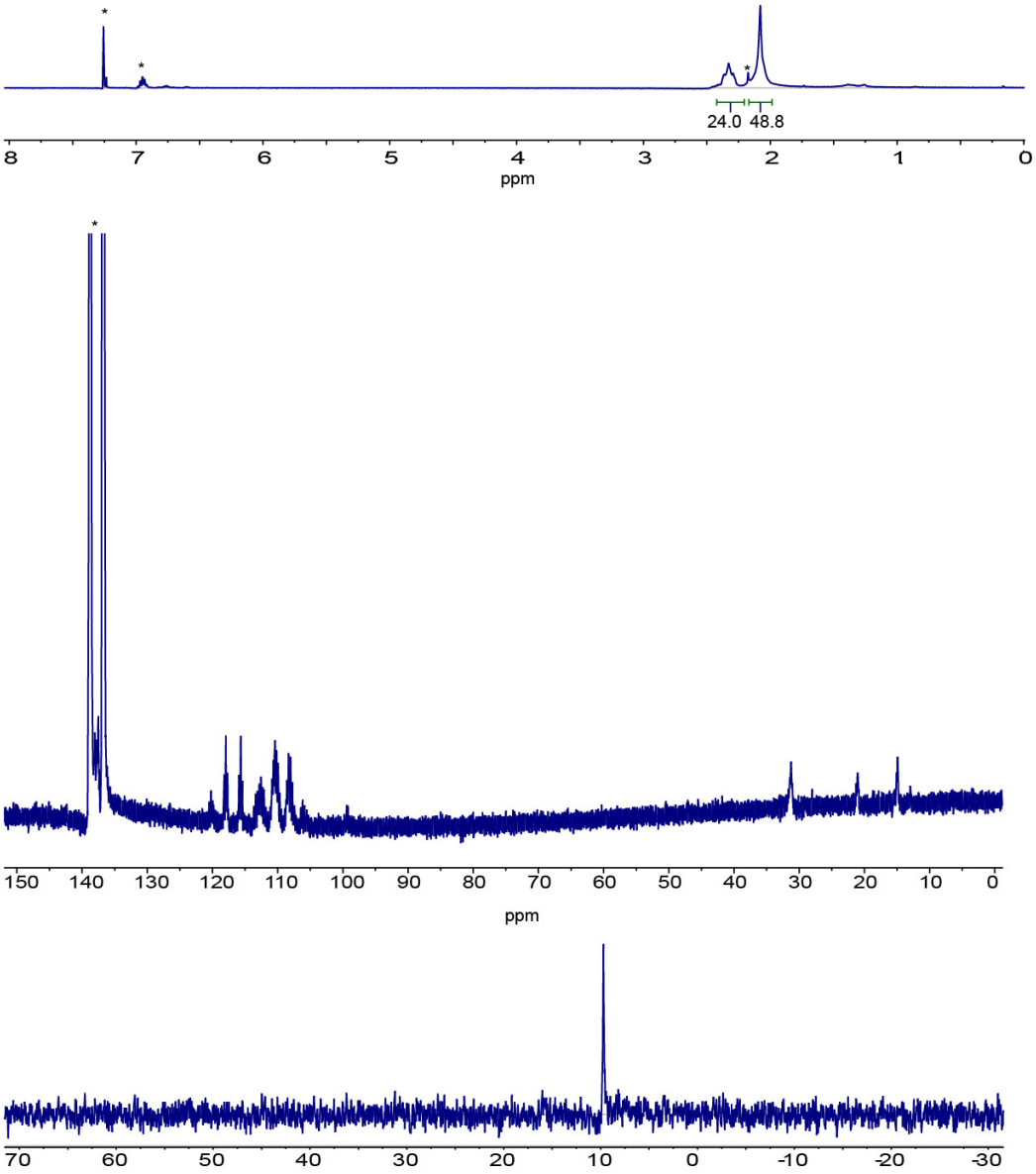

Figure b2. NMR spectra of **10c**: ^{1}H (C_6F_6 + $CDCl_3$; top), $^{13}C\{^{1}H\}$ (C_6F_6; middle) and $^{31}P\{^{1}H\}$ (C_6F_6; bottom) (* = solvent peak or impurity).

CheckCIF report for **8b**.

Bond precision: C-C = 0.0239 A Wavelength=1.54178
Cell: a=11.4468(16) b=15.504(2) c=30.558(5)
alpha=103.379(16) beta=95.714(16) gamma=103.257(11)
Temperature: 110 K

	Calculated	Reported
Volume	5068.2(14)	5068.2(14)
Space group	P -1	P-1
Hall group	-P 1	?
Moiety formula	$C_{69}H_{36}ClF_{100}P_2Pt,C_3F_7$	?
Sum formula	$C_{72}H_{36}ClF_{107}P_2Pt$	$C_{72}H_{36}ClF_{107}P_2Pt$
Mr	3226.48	3226.49
Dx,g cm^{-3}	2.114	2.114
Z	2	2
Mu (mm^{-1})	5.413	5.413
F000	3112.0	3112.0
F000'	3122.67	
h,k,lmax	11,15,30	11,15,30
Nref	10425	10107
Tmin,Tmax	0.759,0.947	0.641,0.948
Tmin'	0.585	

Correction method= MULTI-SCAN
Data completeness= 0.969 Theta(max)= 50.000
R(reflections)= 0.0865(8397) wR2(reflections)= 0.2411(10107)
S = 1.045 Npar= 1413
The following ALERTS were generated. Each ALERT has the format
test-name_ALERT_alert-type_alert-level.
Alert level A
THETM01_ALERT_3_A The value of sine(theta_max)/wavelength is less than 0.550
Calculated sin(theta_max)/wavelength = 0.4969
Author Response: No reflections were observed above 100 degree two theta, even with a 40 second frame on GADDS instrument fitted with Cu (sealed tube) source and a

MWPC areadetector. The refinement was restricted to 100 degrees. This could be attibuted to the the extent of disorder of the long chain hydroflourous chain.
PLAT023_ALERT_3_A Resolution (too) Low [sin(theta)/Lambda < 0.6].. 50.00 Deg.
Author Response: No reflections were observed above 100 degree two theta, even with a 40 second frame on GADDS instrument fitted with Cu (sealed tube) source and a WPC area detector. This could be attributed to the the extent of disorder of the long chain hydroflourous chain.The refinement was restricted to 100 degrees.
Alert level B
REFNR01_ALERT_3_B Ratio of reflections to parameters is < 8 for a centrosymmetric structure
sine(theta)/lambda 0.4969
Proportion of unique data used 1.0000
Ratio reflections to parameters 7.1529
PLAT088_ALERT_3_B Poor Data / Parameter Ratio 7.15
PLAT234_ALERT_4_B Large Hirshfeld Difference F15 -- C11 .. 0.27 Ang.
PLAT342_ALERT_3_B Low Bond Precision on C-C Bonds ..... 0.0239 Ang
PLAT434_ALERT_2_B Short Inter HL..HL Contact F9D .. F12H . 2.57 Ang.
Alert level C
PLAT029_ALERT_3_C _diffrn_measured_fraction_theta_full Low 0.969
PLAT048_ALERT_1_C MoietyFormula Not Given ..... ?
PLAT125_ALERT_4_C No '_symmetry_space_group_name_Hall' Given ..... ?
PLAT213_ALERT_2_C Atom F6 has ADP max/min Ratio ..... 3.2 prola
PLAT213_ALERT_2_C Atom C5P has ADP max/min Ratio ..... 4.0 prola
PLAT213_ALERT_2_C Atom C9 has ADP max/min Ratio ..... 3.1 prola
PLAT213_ALERT_2_C Atom C11A has ADP max/min Ratio ..... 3.4 prola
PLAT220_ALERT_2_C Large Non-Solvent C Ueq(max)/Ueq(min) ... 3.9 Ratio
PLAT230_ALERT_2_C Hirshfeld Test Diff for F12 -- C9 .. 5.6 su
PLAT230_ALERT_2_C Hirshfeld Test Diff for F14 -- C10 .. 5.1 su
PLAT230_ALERT_2_C Hirshfeld Test Diff for F17 -- C11 .. 5.2 su
PLAT234_ALERT_4_C Large Hirshfeld Difference F5P -- C6P .. 0.17 Ang.
PLAT234_ALERT_4_C Large Hirshfeld Difference F10B -- C8B .. 0.16 Ang.
PLAT234_ALERT_4_C Large Hirshfeld Difference F13 -- C10 .. 0.21 Ang.
PLAT234_ALERT_4_C Large Hirshfeld Difference C3D -- C4D .. 0.22 Ang.
PLAT234_ALERT_4_C Large Hirshfeld Difference C7 -- C8 .. 0.18 Ang.

PLAT234_ALERT_4_C Large Hirshfeld Difference C8 -- C9 .. 0.20 Ang.
PLAT242_ALERT_2_C Check Low Ueq as Compared to Neighbors for C6
PLAT242_ALERT_2_C Check Low Ueq as Compared to Neighbors for C6A
PLAT242_ALERT_2_C Check Low Ueq as Compared to Neighbors for C8D
PLAT242_ALERT_2_C Check Low Ueq as Compared to Neighbors for C10
PLAT242_ALERT_2_C Check Low Ueq as Compared to Neighbors for C11A
PLAT722_ALERT_1_C Angle Calc 106.00, Rep 107.20 Dev... 1.20 Deg.
H3FA -C3F -H3FB 1.555 1.555 1.555 # 351
Alert level G
PLAT002_ALERT_2_G Number of Distance or Angle Restraints on AtSite 122
PLAT003_ALERT_2_G Number of Uiso or Uij Restrained Atom Sites 3
PLAT005_ALERT_5_G No _iucr_refine_instructions_details in CIF .... ?
PLAT072_ALERT_2_G SHELXL First Parameter in WGHT Unusually Large. 0.12
PLAT083_ALERT_2_G SHELXL Second Parameter in WGHT Unusually Large. 94.37
PLAT301_ALERT_3_G Note: Main Residue Disorder ..... 33 Perc.
PLAT434_ALERT_2_G Short Inter HL..HL Contact F3 .. F13B . 2.77 Ang.
PLAT434_ALERT_2_G Short Inter HL..HL Contact F3D .. F5H . 2.79 Ang.
PLAT434_ALERT_2_G Short Inter HL..HL Contact F3D .. F10G . 2.81 Ang.
PLAT434_ALERT_2_G Short Inter HL..HL Contact F4 .. F5A . 2.65 Ang.
PLAT434_ALERT_2_G Short Inter HL..HL Contact F4 .. F14F . 2.80 Ang.
PLAT434_ALERT_2_G Short Inter HL..HL Contact F5D .. F11B . 2.80 Ang.
PLAT434_ALERT_2_G Short Inter HL..HL Contact F7A .. F10B . 2.77 Ang.
PLAT434_ALERT_2_G Short Inter HL..HL Contact F8D .. F3G . 2.82 Ang.
PLAT434_ALERT_2_G Short Inter HL..HL Contact F9 .. F11H . 2.78 Ang.
PLAT434_ALERT_2_G Short Inter HL..HL Contact F9D .. F12G . 2.84 Ang.
PLAT434_ALERT_2_G Short Inter HL..HL Contact F12 .. F12 . 2.78 Ang.
PLAT434_ALERT_2_G Short Inter HL..HL Contact F14 .. F17B . 2.82 Ang.
PLAT434_ALERT_2_G Short Inter HL..HL Contact F14A .. F15H . 2.73 Ang.
PLAT710_ALERT_4_G Delete 1-2-3 or 2-3-4 Linear Torsion Angle ... # 462
C6P -C1P -PT1 -CL1 28.00 14.00 1.555 1.555 1.555 1.555
PLAT710_ALERT_4_G Delete 1-2-3 or 2-3-4 Linear Torsion Angle ... # 463
C2P -C1P -PT1 -CL1 -155.00 12.00 1.555 1.555 1.555 1.555
PLAT710_ALERT_4_G Delete 1-2-3 or 2-3-4 Linear Torsion Angle ... # 474
P2 -PT1 -P1 -C1 -99.30 1.70 1.555 1.555 1.555 1.555

PLAT710_ALERT_4_G Delete 1-2-3 or 2-3-4 Linear Torsion Angle ... # 477
P2 -PT1 -P1 -C1G 138.00 1.60 1.555 1.555 1.555 1.555
PLAT710_ALERT_4_G Delete 1-2-3 or 2-3-4 Linear Torsion Angle ... # 480
P2 -PT1 -P1 -C1E 25.40 1.90 1.555 1.555 1.555 1.555
PLAT710_ALERT_4_G Delete 1-2-3 or 2-3-4 Linear Torsion Angle ... # 492
P1 -PT1 -P2 -C1A -0.10 1.80 1.555 1.555 1.555 1.555
PLAT710_ALERT_4_G Delete 1-2-3 or 2-3-4 Linear Torsion Angle ... # 495
P1 -PT1 -P2 -C1B 118.80 1.70 1.555 1.555 1.555 1.555
PLAT710_ALERT_4_G Delete 1-2-3 or 2-3-4 Linear Torsion Angle ... # 498
P1 -PT1 -P2 -C1D -117.70 1.70 1.555 1.555 1.555 1.555
PLAT720_ALERT_4_G Number of Unusual/Non-Standard Labels 36
PLAT779_ALERT_4_G Suspect or Irrelevant (Bond) Angle in CIF .... # 272
C3E -C2E -C3F 1.555 1.555 1.555 34.00 Deg.
PLAT779_ALERT_4_G Suspect or Irrelevant (Bond) Angle in CIF .... # 285
H2EB -C2E -H2EC 1.555 1.555 1.555 28.90 Deg.
PLAT779_ALERT_4_G Suspect or Irrelevant (Bond) Angle in CIF .... # 289
(IUCr) Crystal Structure Communications Online author services
H2EA -C2E -H2ED 1.555 1.555 1.555 19.30 Deg.
PLAT779_ALERT_4_G Suspect or Irrelevant (Bond) Angle in CIF .... # 384
H3GA -C3G -H3GC 1.555 1.555 1.555 0.00 Deg.
PLAT779_ALERT_4_G Suspect or Irrelevant (Bond) Angle in CIF .... # 389
H3GB -C3G -H3GD 1.555 1.555 1.555 0.00 Deg.
PLAT790_ALERT_4_G Centre of Gravity not Within Unit Cell: Resd. # 2
C3 F7
PLAT790_ALERT_4_G Centre of Gravity not Within Unit Cell: Resd. # 3
C3 F7
PLAT811_ALERT_5_G No ADDSYM Analysis: Too Many Excluded Atoms .... !
PLAT860_ALERT_3_G Note: Number of Least-Squares Restraints 178

APPENDIX C

NMR SPECTRA AND CHECKCIF REPORTS FOR CHAPTER IV

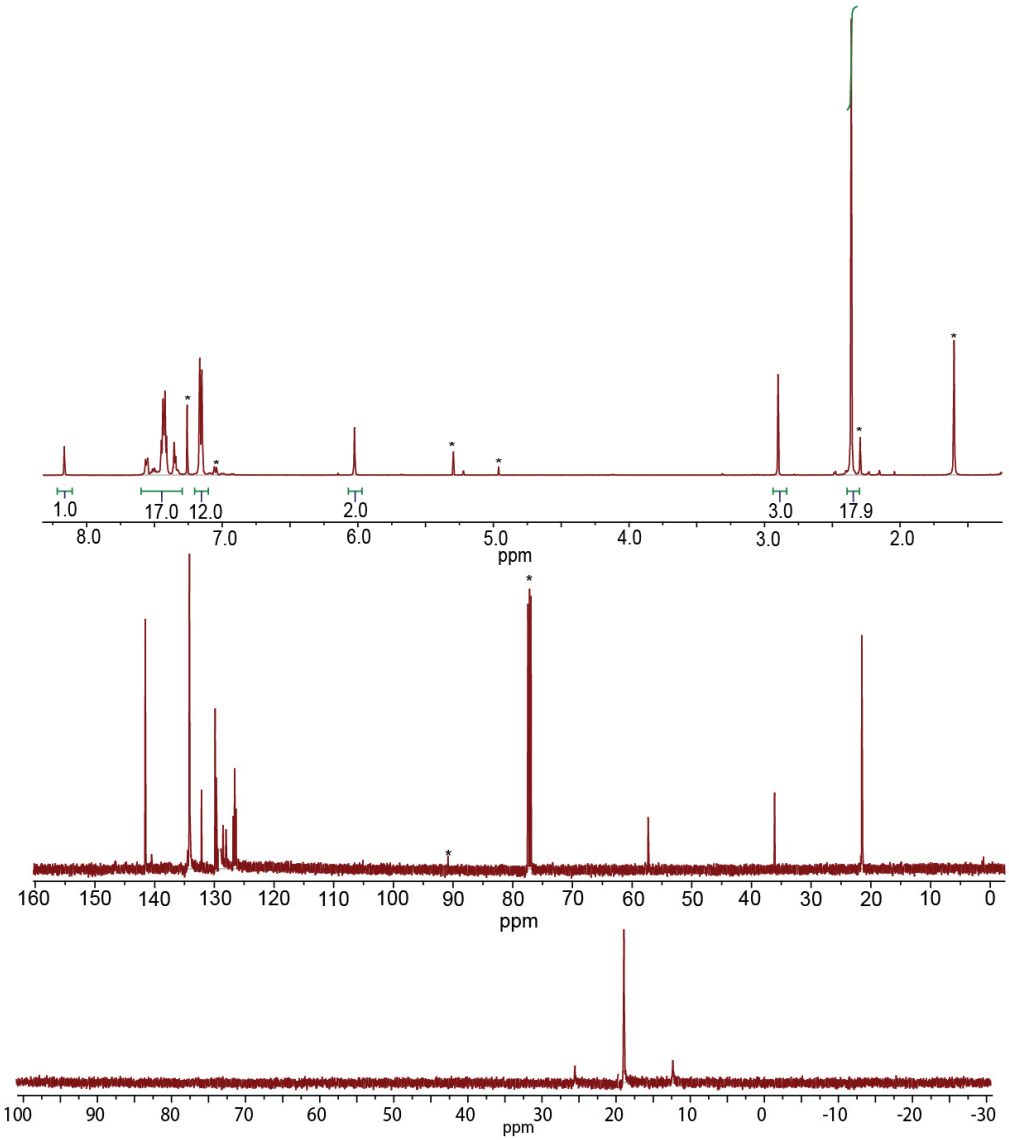

Figure c1. NMR spectra of $\mathbf{16}^{+}$ I^{-} ($CDCl_3$): ^{1}H (top), $^{13}C\{^{1}H\}$ (middle) and $^{31}P\{^{1}H\}$ (bottom) (* = solvent peak or impurity).

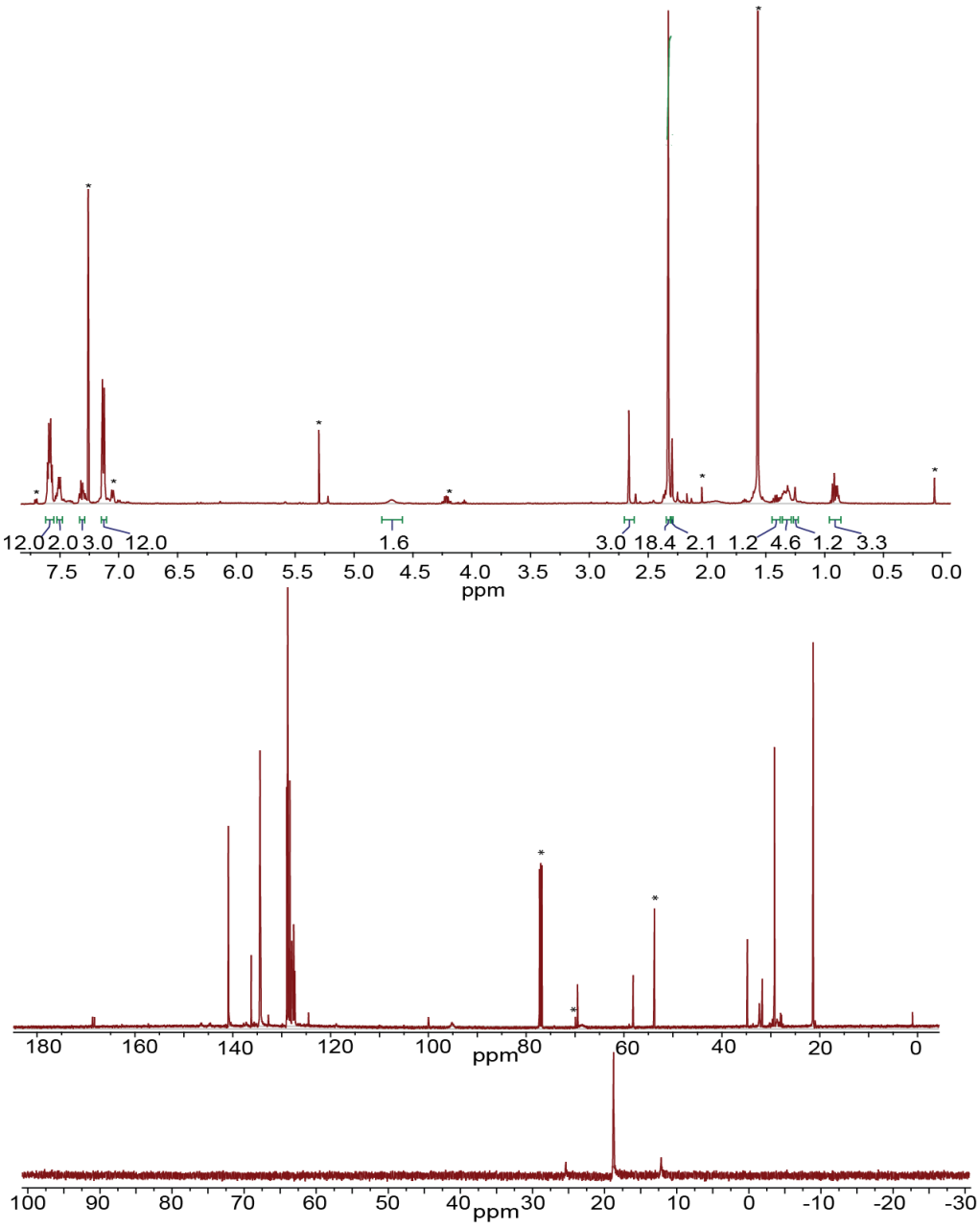

Figure c2. NMR spectra of **17** ($CDCl_3$): ^{1}H (top), $^{13}C\{^{1}H\}$ (middle) and $^{31}P\{^{1}H\}$ (bottom) (* = solvent peak or impurity).

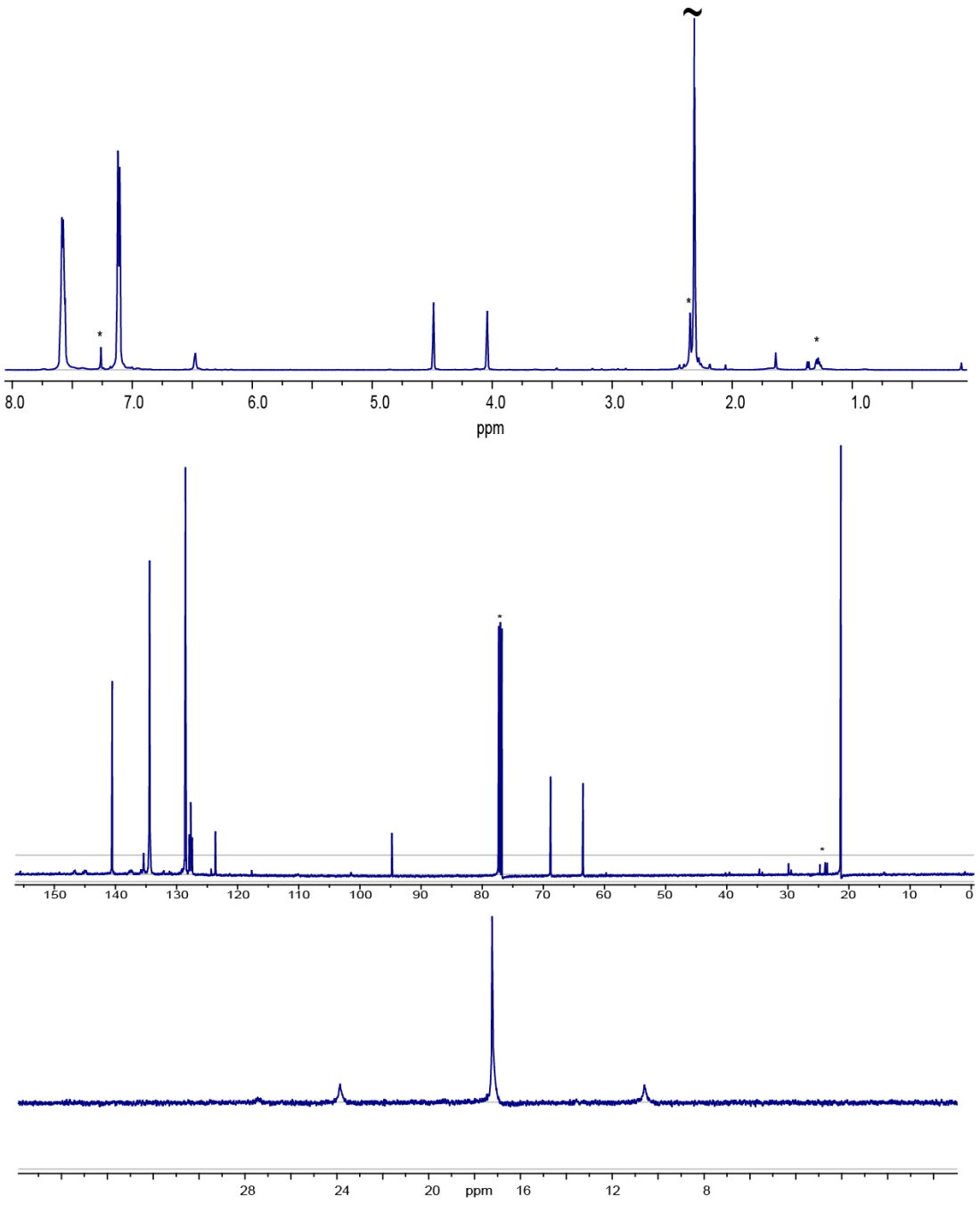

Figure c3. NMR spectra of **18** ($CDCl_3$): ^{1}H (top), $^{13}C\{^{1}H\}$ (middle) and $^{31}P\{^{1}H\}$ (bottom) (* = solvent peak or impurity).

CheckCIF report for **10**

Bond precision: C-C = 0.0059 A Wavelength=1.54178
Cell: a=11.5032(17) b=12.3428(18) c=21.855(3)
alpha=100.450(7) beta=93.729(7) gamma=104.277(7)
Temperature: 110 K

	Calculated	Reported
Volume	2937.6(7)	2937.6(7)
Space group	P -1	P-1
Hall group	-P 1	?
Moiety formula	$C_{60}H_{47}F_5N_3O_3P_2PtRe_2(CH_2Cl_2)$	?
Sum formula	$C_{62}H_{51}Cl_4F_5N_3O_3P_2PtRe$	$C_{62}H_{51}Cl_4F_5N_3O_3P_2PtRe$
Mr	1566.09	1566.09
Dx,g cm^{-3}	1.770	1.771
Z	2	2
Mu (mm^{-1})	11.087	11.087
F000	1528.0	1528.0
F000’	1516.01	
h,k,lmax	12,13,24	12,13,23
Nref	8711	8148
Tmin,Tmax	0.766,0.801	0.125,0.215
Tmin’	0.717	

Correction method= MULTI-SCAN
Data completeness= 0.935 Theta(max)= 59.990
R(reflections)= 0.0225(6643) wR2(reflections)= 0.0484(8148)
S = 1.045 Npar= 736
The following ALERTS were generated. Each ALERT has the format
test-name_ALERT_alert-type_alert-level.
Alert level A
PLAT029_ALERT_3_A _diffrn_measured_fraction_theta_full Low 0.935
Author response: Data was collected on a very small crystal using Cu-source and a multiwire Hi-star detector. Under these condition given a triclinic cell, we could collect only to a completeness of 94 percent. No efforts were made to reorient the crystal to collect the data to increase the coverage.

Alert level B
THETM01_ALERT_3_B The value of sine(theta_max)/wavelength is less than 0.575
Calculated sin(theta_max)/wavelength = 0.5616
Alert level C
REFLT03_ALERT_3_C Reflection count < 95% complete
From the CIF: _diffrn_reflns_theta_max 59.99
From the CIF: _diffrn_reflns_theta_full 59.99
From the CIF: _reflns_number_total 8148
TEST2: Reflns within _diffrn_reflns_theta_max
Count of symmetry unique reflns 8711
Completeness (_total/calc) 93.54%
PLAT022_ALERT_3_C Ratio Unique / Expected Reflections (too) Low .. 0.935
PLAT230_ALERT_2_C Hirshfeld Test Diff for O1 -- C10 .. 6.7 su
Alert level G
PLAT005_ALERT_5_G No _iucr_refine_instructions_details in CIF .... ?
PLAT154_ALERT_1_G The su's on the Cell Angles are Equal ..... 0.00700 Deg.
PLAT232_ALERT_2_G Hirshfeld Test Diff (M-X) Re1 -- C10 .. 6.7 su
PLAT232_ALERT_2_G Hirshfeld Test Diff (M-X) Re1 -- C11 .. 8.0 su
PLAT232_ALERT_2_G Hirshfeld Test Diff (M-X) Re1 -- C12 .. 5.5 su
PLAT371_ALERT_2_G Long C(sp2)-C(sp1) Bond C2 - C3 ... 1.42 Ang.
PLAT710_ALERT_4_G Delete 1-2-3 or 2-3-4 Linear Torsion Angle ... # 19
C13 -PT1 -C1 -C2 -2.00 2.00 1.555 1.555 1.555 1.555
PLAT710_ALERT_4_G Delete 1-2-3 or 2-3-4 Linear Torsion Angle ... # 22
PT1 -C1 -C2 -C3 55.00 4.00 1.555 1.555 1.555 1.555
PLAT710_ALERT_4_G Delete 1-2-3 or 2-3-4 Linear Torsion Angle ... # 23
C1 -C2 -C3 -C4 8.00 3.00 1.555 1.555 1.555 1.555
PLAT710_ALERT_4_G Delete 1-2-3 or 2-3-4 Linear Torsion Angle ... # 24
C1 -C2 -C3 -N3 -172.00 3.00 1.555 1.555 1.555 1.555
PLAT710_ALERT_4_G Delete 1-2-3 or 2-3-4 Linear Torsion Angle ... # 113
C12 -RE1 -C10 -O1 -136.00 8.00 1.555 1.555 1.555 1.555
PLAT710_ALERT_4_G Delete 1-2-3 or 2-3-4 Linear Torsion Angle ... # 114
C11 -RE1 -C10 -O1 135.00 8.00 1.555 1.555 1.555 1.555
PLAT710_ALERT_4_G Delete 1-2-3 or 2-3-4 Linear Torsion Angle ... # 115
C8 -RE1 -C10 -O1 36.00 8.00 1.555 1.555 1.555 1.555

PLAT710_ALERT_4_G Delete 1-2-3 or 2-3-4 Linear Torsion Angle ... # 116
C7 -RE1 -C10 -O1 -30.00 8.00 1.555 1.555 1.555 1.555
PLAT710_ALERT_4_G Delete 1-2-3 or 2-3-4 Linear Torsion Angle ... # 117
C9 -RE1 -C10 -O1 32.00 8.00 1.555 1.555 1.555 1.555
PLAT710_ALERT_4_G Delete 1-2-3 or 2-3-4 Linear Torsion Angle ... # 118
C6 -RE1 -C10 -O1 -33.00 8.00 1.555 1.555 1.555 1.555
PLAT710_ALERT_4_G Delete 1-2-3 or 2-3-4 Linear Torsion Angle ... # 119
C5 -RE1 -C10 -O1 -2.00 8.00 1.555 1.555 1.555 1.555
PLAT710_ALERT_4_G Delete 1-2-3 or 2-3-4 Linear Torsion Angle ... # 120
C12 -RE1 -C11 -O2 141.00 7.00 1.555 1.555 1.555 1.555
PLAT710_ALERT_4_G Delete 1-2-3 or 2-3-4 Linear Torsion Angle ... # 121
C10 -RE1 -C11 -O2 -131.00 7.00 1.555 1.555 1.555 1.555
PLAT710_ALERT_4_G Delete 1-2-3 or 2-3-4 Linear Torsion Angle ... # 122
C8 -RE1 -C11 -O2 14.00 7.00 1.555 1.555 1.555 1.555
PLAT710_ALERT_4_G Delete 1-2-3 or 2-3-4 Linear Torsion Angle ... # 123
C7 -RE1 -C11 -O2 40.00 7.00 1.555 1.555 1.555 1.555
PLAT710_ALERT_4_G Delete 1-2-3 or 2-3-4 Linear Torsion Angle ... # 124
C9 -RE1 -C11 -O2 -22.00 7.00 1.555 1.555 1.555 1.555
PLAT710_ALERT_4_G Delete 1-2-3 or 2-3-4 Linear Torsion Angle ... # 125
C6 -RE1 -C11 -O2 21.00 7.00 1.555 1.555 1.555 1.555
PLAT710_ALERT_4_G Delete 1-2-3 or 2-3-4 Linear Torsion Angle ... # 126
C5 -RE1 -C11 -O2 -35.00 7.00 1.555 1.555 1.555 1.555
PLAT710_ALERT_4_G Delete 1-2-3 or 2-3-4 Linear Torsion Angle ... # 127
C11 -RE1 -C12 -O3 -153.00 13.00 1.555 1.555 1.555 1.555
PLAT710_ALERT_4_G Delete 1-2-3 or 2-3-4 Linear Torsion Angle ... # 128
C10 -RE1 -C12 -O3 117.00 13.00 1.555 1.555 1.555 1.555
PLAT710_ALERT_4_G Delete 1-2-3 or 2-3-4 Linear Torsion Angle ... # 129
C8 -RE1 -C12 -O3 -57.00 13.00 1.555 1.555 1.555 1.555
PLAT710_ALERT_4_G Delete 1-2-3 or 2-3-4 Linear Torsion Angle ... # 130
C7 -RE1 -C12 -O3 -32.00 13.00 1.555 1.555 1.555 1.555
PLAT710_ALERT_4_G Delete 1-2-3 or 2-3-4 Linear Torsion Angle ... # 131
C9 -RE1 -C12 -O3 -27.00 13.00 1.555 1.555 1.555 1.555
PLAT710_ALERT_4_G Delete 1-2-3 or 2-3-4 Linear Torsion Angle ... # 132
C6 -RE1 -C12 -O3 5.00 13.00 1.555 1.555 1.555 1.555

PLAT710_ALERT_4_G Delete 1-2-3 or 2-3-4 Linear Torsion Angle ... # 133
C5 -RE1 -C12 -O3 24.00 13.00 1.555 1.555 1.555 1.555
PLAT710_ALERT_4_G Delete 1-2-3 or 2-3-4 Linear Torsion Angle ... # 134
C1 -PT1 -C13 -C18 176.10 0.70 1.555 1.555 1.555 1.555
PLAT710_ALERT_4_G Delete 1-2-3 or 2-3-4 Linear Torsion Angle ... # 137
C1 -PT1 -C13 -C14 -1.70 1.00 1.555 1.555 1.555 1.555
PLAT790_ALERT_4_G Centre of Gravity not Within Unit Cell: Resd. # 2
C H2 Cl2
PLAT809_ALERT_1_G Can not Parse the SHELXL Weighting Scheme String !

CheckCIF report for **12**·2CH_2Cl_2

Bond precision: C-C = 0.0082 A Wavelength=0.71073
Cell: a=12.1623(16) b=46.074(6) c=11.9613(16)
alpha=90 beta=90 gamma=90
Temperature: 110 K

	Calculated	Reported
Volume	6702.7(15)	6702.7(15)
Space group	P 21 21 2	P2(1)2(1)2
Hall group	P 2 2ab	?
Moiety formula	$C_{64}H_{47}BrF_5N_3O_7P_2PtRe_2$,2($CH_2Cl_2$)	?
Sum formula	$C_{66}H_{51}BrCl_4F_5N_3O_7P_2PtRe_2$	$C_{66}H_{51}BrCl_4F_5N_3O_7P_2PtRe_2$
Mr	1944.24	1944.24
Dx,g cm^{-3}	1.927	1.927
Z	4	4
Mu (mm^{-1})	6.557	6.557
F000	3720.0	3720.0
F000’	3709.24	
h,k,lmax	15,59,15	15,59,15
Nref	8509[15394]	15360
Tmin,Tmax	0.346,0.632	0.138,0.657
Tmin’	0.036	

Correction method= MULTI-SCAN

Data completeness= 1.81/1.00 Theta(max)= 27.490
R(reflections)= 0.0264(14832) wR2(reflections)= 0.0678(15360)
S = 1.043 Npar= 836
The following ALERTS were generated. Each ALERT has the format
test-name_ALERT_alert-type_alert-level.
Alert level C
PLAT220_ALERT_2_C Large Non-Solvent C Ueq(max)/Ueq(min) ... 3.2 Ratio
PLAT244_ALERT_4_C Low 'Solvent' Ueq as Compared to Neighbors of C85D
PLAT334_ALERT_2_C Small Average Benzene C-C Dist. C59 -C64 1.37 Ang.
PLAT342_ALERT_3_C Low Bond Precision on C-C Bonds ..... 0.0082 Ang
Alert level G
REFLT03_ALERT_4_G Please check that the estimate of the number of Friedel pairs is correct. If it is not, please give the correct count in the
_publ_section_exptl_refinement section of the submitted CIF.
From the CIF: _diffrn_reflns_theta_max 27.49
From the CIF: _reflns_number_total 15360
Count of symmetry unique reflns 8509
Completeness (_total/calc) 180.51%
TEST3: Check Friedels for noncentro structure
Estimate of Friedel pairs measured 6851
Fraction of Friedel pairs measured 0.805
Are heavy atom types Z>Si present yes
PLAT002_ALERT_2_G Number of Distance or Angle Restraints on AtSite 7
PLAT005_ALERT_5_G No _iucr_refine_instructions_details in CIF .... ?
PLAT301_ALERT_3_G Note: Main Residue Disorder ..... 4 Perc.
PLAT434_ALERT_2_G Short Inter HL..HL Contact Cl82 .. F1 . 3.09 Ang.
PLAT710_ALERT_4_G Delete 1-2-3 or 2-3-4 Linear Torsion Angle ... # 3
P2 -PT1 -P1 -C24 -114.20 0.80 1.555 1.555 1.555 1.555
PLAT710_ALERT_4_G Delete 1-2-3 or 2-3-4 Linear Torsion Angle ... # 6
P2 -PT1 -P1 -C31 127.50 0.80 1.555 1.555 1.555 1.555
PLAT710_ALERT_4_G Delete 1-2-3 or 2-3-4 Linear Torsion Angle ... # 9
P2 -PT1 -P1 -C17 11.10 0.90 1.555 1.555 1.555 1.555
PLAT710_ALERT_4_G Delete 1-2-3 or 2-3-4 Linear Torsion Angle ... # 12
P1 -PT1 -P2 -C52 -122.10 0.80 1.555 1.555 1.555 1.555

PLAT710_ALERT_4_G Delete 1-2-3 or 2-3-4 Linear Torsion Angle ... # 15
P1 -PT1 -P2 -C45 -2.10 0.90 1.555 1.555 1.555 1.555
PLAT710_ALERT_4_G Delete 1-2-3 or 2-3-4 Linear Torsion Angle ... # 18
P1 -PT1 -P2 -C38 117.50 0.80 1.555 1.555 1.555 1.555
PLAT710_ALERT_4_G Delete 1-2-3 or 2-3-4 Linear Torsion Angle ... # 19
C59 -PT1 -C1 -C2 1.00 8.00 1.555 1.555 1.555 1.555
PLAT710_ALERT_4_G Delete 1-2-3 or 2-3-4 Linear Torsion Angle ... # 20
P2 -PT1 -C1 -C2 18.00 4.00 1.555 1.555 1.555 1.555
PLAT710_ALERT_4_G Delete 1-2-3 or 2-3-4 Linear Torsion Angle ... # 21
P1 -PT1 -C1 -C2 -159.00 4.00 1.555 1.555 1.555 1.555
PLAT710_ALERT_4_G Delete 1-2-3 or 2-3-4 Linear Torsion Angle ... # 22
PT1 -C1 -C2 -C3 31.00 6.00 1.555 1.555 1.555 1.555
PLAT710_ALERT_4_G Delete 1-2-3 or 2-3-4 Linear Torsion Angle ... # 26
C8 -RE1 -C5 -O1 164.00 5.00 1.555 1.555 1.555 1.555
PLAT710_ALERT_4_G Delete 1-2-3 or 2-3-4 Linear Torsion Angle ... # 27
C6 -RE1 -C5 -O1 76.00 5.00 1.555 1.555 1.555 1.555
PLAT710_ALERT_4_G Delete 1-2-3 or 2-3-4 Linear Torsion Angle ... # 28
C8A -RE1 -C5 -O1 -3.00 6.00 1.555 1.555 1.555 1.555
PLAT710_ALERT_4_G Delete 1-2-3 or 2-3-4 Linear Torsion Angle ... # 29
C7 -RE1 -C5 -O1 -12.00 7.00 1.555 1.555 1.555 1.555
PLAT710_ALERT_4_G Delete 1-2-3 or 2-3-4 Linear Torsion Angle ... # 30
N1 -RE1 -C5 -O1 -103.00 5.00 1.555 1.555 1.555 1.555
PLAT710_ALERT_4_G Delete 1-2-3 or 2-3-4 Linear Torsion Angle ... # 31
BR1A-RE1 -C5 -O1 163.00 5.00 1.555 1.555 1.555 1.555
PLAT710_ALERT_4_G Delete 1-2-3 or 2-3-4 Linear Torsion Angle ... # 32
BR1 -RE1 -C5 -O1 -17.00 5.00 1.555 1.555 1.555 1.555
PLAT710_ALERT_4_G Delete 1-2-3 or 2-3-4 Linear Torsion Angle ... # 33
C8 -RE1 -C6 -O2 2.00 0.00 1.555 1.555 1.555 1.555
PLAT710_ALERT_4_G Delete 1-2-3 or 2-3-4 Linear Torsion Angle ... # 34
C8A -RE1 -C6 -O2 17.00 0.00 1.555 1.555 1.555 1.555
PLAT710_ALERT_4_G Delete 1-2-3 or 2-3-4 Linear Torsion Angle ... # 35
C7 -RE1 -C6 -O2 11.00 0.00 1.555 1.555 1.555 1.555
PLAT710_ALERT_4_G Delete 1-2-3 or 2-3-4 Linear Torsion Angle ... # 36
C5 -RE1 -C6 -O2 8.00 0.00 1.555 1.555 1.555 1.555

PLAT710_ALERT_4_G Delete 1-2-3 or 2-3-4 Linear Torsion Angle ... # 37
N1 -RE1 -C6 -O2 123.00 38.00 1.555 1.555 1.555 1.555
PLAT710_ALERT_4_G Delete 1-2-3 or 2-3-4 Linear Torsion Angle ... # 38
BR1A-RE1 -C6 -O2 2.00 0.00 1.555 1.555 1.555 1.555
PLAT710_ALERT_4_G Delete 1-2-3 or 2-3-4 Linear Torsion Angle ... # 39
BR1 -RE1 -C6 -O2 16.00 0.00 1.555 1.555 1.555 1.555
PLAT710_ALERT_4_G Delete 1-2-3 or 2-3-4 Linear Torsion Angle ... # 40
C8 -RE1 -C7 -O3 -130.00 13.00 1.555 1.555 1.555 1.555
PLAT710_ALERT_4_G Delete 1-2-3 or 2-3-4 Linear Torsion Angle ... # 41
C6 -RE1 -C7 -O3 -42.00 13.00 1.555 1.555 1.555 1.555
PLAT710_ALERT_4_G Delete 1-2-3 or 2-3-4 Linear Torsion Angle ... # 42
C8A -RE1 -C7 -O3 38.00 13.00 1.555 1.555 1.555 1.555
PLAT710_ALERT_4_G Delete 1-2-3 or 2-3-4 Linear Torsion Angle ... # 43
C5 -RE1 -C7 -O3 46.00 15.00 1.555 1.555 1.555 1.555
PLAT710_ALERT_4_G Delete 1-2-3 or 2-3-4 Linear Torsion Angle ... # 44
N1 -RE1 -C7 -O3 137.00 13.00 1.555 1.555 1.555 1.555
PLAT710_ALERT_4_G Delete 1-2-3 or 2-3-4 Linear Torsion Angle ... # 45
BR1A-RE1 -C7 -O3 -129.00 13.00 1.555 1.555 1.555 1.555
PLAT710_ALERT_4_G Delete 1-2-3 or 2-3-4 Linear Torsion Angle ... # 46
BR1 -RE1 -C7 -O3 52.00 13.00 1.555 1.555 1.555 1.555
PLAT710_ALERT_4_G Delete 1-2-3 or 2-3-4 Linear Torsion Angle ... # 47
C6 -RE1 -C8 -O4 15.00 34.00 1.555 1.555 1.555 1.555
PLAT710_ALERT_4_G Delete 1-2-3 or 2-3-4 Linear Torsion Angle ... # 48
C8A -RE1 -C8 -O4 26.00 35.00 1.555 1.555 1.555 1.555
PLAT710_ALERT_4_G Delete 1-2-3 or 2-3-4 Linear Torsion Angle ... # 49
C7 -RE1 -C8 -O4 105.00 34.00 1.555 1.555 1.555 1.555
PLAT710_ALERT_4_G Delete 1-2-3 or 2-3-4 Linear Torsion Angle ... # 50
C5 -RE1 -C8 -O4 -75.00 34.00 1.555 1.555 1.555 1.555
PLAT710_ALERT_4_G Delete 1-2-3 or 2-3-4 Linear Torsion Angle ... # 51
N1 -RE1 -C8 -O4 -164.00 34.00 1.555 1.555 1.555 1.555
PLAT710_ALERT_4_G Delete 1-2-3 or 2-3-4 Linear Torsion Angle ... # 52
BR1A-RE1 -C8 -O4 98.00 34.00 1.555 1.555 1.555 1.555
PLAT710_ALERT_4_G Delete 1-2-3 or 2-3-4 Linear Torsion Angle ... # 53
BR1 -RE1 -C8 -O4 -164.00 22.00 1.555 1.555 1.555 1.555

PLAT710_ALERT_4_G Delete 1-2-3 or 2-3-4 Linear Torsion Angle ... # 147
C16 -RE2 -C14 -O5 -108.00 14.00 1.555 1.555 1.555 1.555
PLAT710_ALERT_4_G Delete 1-2-3 or 2-3-4 Linear Torsion Angle ... # 148
C15 -RE2 -C14 -O5 162.00 14.00 1.555 1.555 1.555 1.555
PLAT710_ALERT_4_G Delete 1-2-3 or 2-3-4 Linear Torsion Angle ... # 149
C11 -RE2 -C14 -O5 41.00 14.00 1.555 1.555 1.555 1.555
PLAT710_ALERT_4_G Delete 1-2-3 or 2-3-4 Linear Torsion Angle ... # 150
C9 -RE2 -C14 -O5 -15.00 14.00 1.555 1.555 1.555 1.555
PLAT710_ALERT_4_G Delete 1-2-3 or 2-3-4 Linear Torsion Angle ... # 151
C12 -RE2 -C14 -O5 64.00 14.00 1.555 1.555 1.555 1.555
PLAT710_ALERT_4_G Delete 1-2-3 or 2-3-4 Linear Torsion Angle ... # 152
C13 -RE2 -C14 -O5 31.00 14.00 1.555 1.555 1.555 1.555
PLAT710_ALERT_4_G Delete 1-2-3 or 2-3-4 Linear Torsion Angle ... # 153
C10 -RE2 -C14 -O5 4.00 14.00 1.555 1.555 1.555 1.555
PLAT710_ALERT_4_G Delete 1-2-3 or 2-3-4 Linear Torsion Angle ... # 154
C16 -RE2 -C15 -O6 116.00 20.00 1.555 1.555 1.555 1.555
PLAT710_ALERT_4_G Delete 1-2-3 or 2-3-4 Linear Torsion Angle ... # 155
C14 -RE2 -C15 -O6 -157.00 20.00 1.555 1.555 1.555 1.555
PLAT710_ALERT_4_G Delete 1-2-3 or 2-3-4 Linear Torsion Angle ... # 156
C11 -RE2 -C15 -O6 -57.00 20.00 1.555 1.555 1.555 1.555
PLAT710_ALERT_4_G Delete 1-2-3 or 2-3-4 Linear Torsion Angle ... # 157
C9 -RE2 -C15 -O6 19.00 20.00 1.555 1.555 1.555 1.555
PLAT710_ALERT_4_G Delete 1-2-3 or 2-3-4 Linear Torsion Angle ... # 158
C12 -RE2 -C15 -O6 -29.00 20.00 1.555 1.555 1.555 1.555
PLAT710_ALERT_4_G Delete 1-2-3 or 2-3-4 Linear Torsion Angle ... # 159
C13 -RE2 -C15 -O6 6.00 20.00 1.555 1.555 1.555 1.555
PLAT710_ALERT_4_G Delete 1-2-3 or 2-3-4 Linear Torsion Angle ... # 160
C10 -RE2 -C15 -O6 -42.00 20.00 1.555 1.555 1.555 1.555
PLAT710_ALERT_4_G Delete 1-2-3 or 2-3-4 Linear Torsion Angle ... # 161
C15 -RE2 -C16 -O7 -147.00 7.00 1.555 1.555 1.555 1.555
PLAT710_ALERT_4_G Delete 1-2-3 or 2-3-4 Linear Torsion Angle ... # 162
C14 -RE2 -C16 -O7 123.00 7.00 1.555 1.555 1.555 1.555
PLAT710_ALERT_4_G Delete 1-2-3 or 2-3-4 Linear Torsion Angle ... # 163
C11 -RE2 -C16 -O7 22.00 8.00 1.555 1.555 1.555 1.555

PLAT710_ALERT_4_G Delete 1-2-3 or 2-3-4 Linear Torsion Angle ... # 164
C9 -RE2 -C16 -O7 -9.00 7.00 1.555 1.555 1.555 1.555
PLAT710_ALERT_4_G Delete 1-2-3 or 2-3-4 Linear Torsion Angle ... # 165
C12 -RE2 -C16 -O7 -46.00 8.00 1.555 1.555 1.555 1.555
PLAT710_ALERT_4_G Delete 1-2-3 or 2-3-4 Linear Torsion Angle ... # 166
C13 -RE2 -C16 -O7 -42.00 8.00 1.555 1.555 1.555 1.555
PLAT710_ALERT_4_G Delete 1-2-3 or 2-3-4 Linear Torsion Angle ... # 167
C10 -RE2 -C16 -O7 23.00 8.00 1.555 1.555 1.555 1.555
PLAT710_ALERT_4_G Delete 1-2-3 or 2-3-4 Linear Torsion Angle ... # 264
C1 -PT1 -C59 -C64 128.00 5.00 1.555 1.555 1.555 1.555
PLAT710_ALERT_4_G Delete 1-2-3 or 2-3-4 Linear Torsion Angle ... # 267
C1 -PT1 -C59 -C60 -52.00 5.00 1.555 1.555 1.555 1.555
PLAT710_ALERT_4_G Delete 1-2-3 or 2-3-4 Linear Torsion Angle ... # 299
C6 -RE1 -N1 -N2 87.00 9.00 1.555 1.555 1.555 1.555
PLAT710_ALERT_4_G Delete 1-2-3 or 2-3-4 Linear Torsion Angle ... # 306
C6 -RE1 -N1 -C3 -89.00 9.00 1.555 1.555 1.555 1.555
PLAT809_ALERT_1_G Can not Parse the SHELXL Weighting Scheme String !
PLAT860_ALERT_3_G Note: Number of Least-Squares Restraints 5

CheckCIF report for **11**$^{+}$ TfO^{-}

Bond precision: C-C = 0.0108 A Wavelength=0.71073
Cell: a=12.815(3) b=24.031(6) c=24.532(6)
alpha=90 beta=102.149(12) gamma=90
Temperature: 296 K

	Calculated	Reported
Volume	7386(3)	7386(3)
Space group	P 21/n	P2(1)/n
Hall group	-P 2yn	?
Moiety formula	$C_{65}H_{48}F_5N_3O_8P_2Pt\ Re_2$,$CF_3O_3S$,$CH_2Cl_2$	?
Sum formula	$C_{67}H_{50}Cl_2F_8N_3O_{11}P_2PtRe_2S$	$C_{67}H_{50}Cl_2F_8N_3O_{11}P_2Pt\ Re_2S$
Mr	1957.51	1957.49
Dx,g cm^{-3}	1.760	1.760

Z	4	4
Mu (mm^{-1})	5.380	5.380
F000	3764.0	3764.0
F000’	3753.81	
h,k,lmax	15,28,29	15,28,29
Nref	13020	12983
Tmin,Tmax	0.603,0.650	0.615,0.673
Tmin’	0.578	

Correction method= MULTI-SCAN

Data completeness= 0.997 Theta(max)= 25.000

R(reflections)= 0.0429(9944) wR2(reflections)= 0.1023(12983)

S = 1.050 Npar= 880

The following ALERTS were generated. Each ALERT has the format
test-name_ALERT_alert-type_alert-level.

Alert level B

PLAT220_ALERT_2_B Large Non-Solvent C Ueq(max)/Ueq(min) ... 4.4 Ratio

Alert level C

PLAT094_ALERT_2_C Ratio of Maximum / Minimum Residual Density 2.17

PLAT213_ALERT_2_C Atom C41 has ADP max/min Ratio ..... 3.1 prola

PLAT222_ALERT_3_C Large Non-Solvent H Uiso(max)/Uiso(min) .. 4.9 Ratio

PLAT230_ALERT_2_C Hirshfeld Test Diff for C38 -- C39 .. 5.4 su

PLAT243_ALERT_4_C High ’Solvent’ Ueq as Compared to Neighbors of C90

PLAT244_ALERT_4_C Low ’Solvent’ Ueq as Compared to Neighbors of S80

PLAT244_ALERT_4_C Low ’Solvent’ Ueq as Compared to Neighbors of C84

PLAT342_ALERT_3_C Low Bond Precision on C-C Bonds ..... 0.0108 Ang

Alert level G

PLAT005_ALERT_5_G No _iucr_refine_instructions_details in CIF .... ?

PLAT007_ALERT_5_G Note: Number of Unrefined D-H Atoms 1

PLAT083_ALERT_2_G SHELXL Second Parameter in WGHT Unusually Large. 14.27

PLAT128_ALERT_4_G Alternate Setting of Space-group P21/c P21/n

PLAT371_ALERT_2_G Long C(sp2)-C(sp1) Bond C12 - C19 ... 1.42 Ang.

PLAT605_ALERT_4_G Structure Contains Solvent Accessible VOIDS of . 337 A**3

PLAT710_ALERT_4_G Delete 1-2-3 or 2-3-4 Linear Torsion Angle ... # 3

P2 -PT1 -P1 -C28 -4.40 1.00 1.555 1.555 1.555 1.555

PLAT710_ALERT_4_G Delete 1-2-3 or 2-3-4 Linear Torsion Angle ... # 6
P2 -PT1 -P1 -C35 -121.70 0.90 1.555 1.555 1.555 1.555
PLAT710_ALERT_4_G Delete 1-2-3 or 2-3-4 Linear Torsion Angle ... # 9
P2 -PT1 -P1 -C21 117.30 0.90 1.555 1.555 1.555 1.555
PLAT710_ALERT_4_G Delete 1-2-3 or 2-3-4 Linear Torsion Angle ... # 12
P1 -PT1 -P2 -C62 111.40 0.90 1.555 1.555 1.555 1.555
PLAT710_ALERT_4_G Delete 1-2-3 or 2-3-4 Linear Torsion Angle ... # 15
P1 -PT1 -P2 -C53 -6.60 1.00 1.555 1.555 1.555 1.555
PLAT710_ALERT_4_G Delete 1-2-3 or 2-3-4 Linear Torsion Angle ... # 18
P1 -PT1 -P2 -C55 -128.70 0.90 1.555 1.555 1.555 1.555
PLAT710_ALERT_4_G Delete 1-2-3 or 2-3-4 Linear Torsion Angle ... # 19
C2 -RE1 -C1 -O1 3.00 0.00 1.555 1.555 1.555 1.555
PLAT710_ALERT_4_G Delete 1-2-3 or 2-3-4 Linear Torsion Angle ... # 20
C3 -RE1 -C1 -O1 12.00 0.00 1.555 1.555 1.555 1.555
PLAT710_ALERT_4_G Delete 1-2-3 or 2-3-4 Linear Torsion Angle ... # 21
C4 -RE1 -C1 -O1 14.00 0.00 1.555 1.555 1.555 1.555
PLAT710_ALERT_4_G Delete 1-2-3 or 2-3-4 Linear Torsion Angle ... # 22
C5 -RE1 -C1 -O1 11.00 0.00 1.555 1.555 1.555 1.555
PLAT710_ALERT_4_G Delete 1-2-3 or 2-3-4 Linear Torsion Angle ... # 23
C8 -RE1 -C1 -O1 14.00 0.00 1.555 1.555 1.555 1.555
PLAT710_ALERT_4_G Delete 1-2-3 or 2-3-4 Linear Torsion Angle ... # 24
C7 -RE1 -C1 -O1 6.00 0.00 1.555 1.555 1.555 1.555
PLAT710_ALERT_4_G Delete 1-2-3 or 2-3-4 Linear Torsion Angle ... # 25
C6 -RE1 -C1 -O1 7.00 0.00 1.555 1.555 1.555 1.555
PLAT710_ALERT_4_G Delete 1-2-3 or 2-3-4 Linear Torsion Angle ... # 26
C3 -RE1 -C2 -O2 142.00 18.00 1.555 1.555 1.555 1.555
PLAT710_ALERT_4_G Delete 1-2-3 or 2-3-4 Linear Torsion Angle ... # 27
C1 -RE1 -C2 -O2 -132.00 18.00 1.555 1.555 1.555 1.555
PLAT710_ALERT_4_G Delete 1-2-3 or 2-3-4 Linear Torsion Angle ... # 28
C4 -RE1 -C2 -O2 26.00 18.00 1.555 1.555 1.555 1.555
PLAT710_ALERT_4_G Delete 1-2-3 or 2-3-4 Linear Torsion Angle ... # 29
C5 -RE1 -C2 -O2 -35.00 18.00 1.555 1.555 1.555 1.555
PLAT710_ALERT_4_G Delete 1-2-3 or 2-3-4 Linear Torsion Angle ... # 30
C8 -RE1 -C2 -O2 42.00 18.00 1.555 1.555 1.555 1.555

PLAT710_ALERT_4_G Delete 1-2-3 or 2-3-4 Linear Torsion Angle ... # 31
C7 -RE1 -C2 -O2 14.00 18.00 1.555 1.555 1.555 1.555
PLAT710_ALERT_4_G Delete 1-2-3 or 2-3-4 Linear Torsion Angle ... # 32
C6 -RE1 -C2 -O2 -22.00 18.00 1.555 1.555 1.555 1.555
PLAT710_ALERT_4_G Delete 1-2-3 or 2-3-4 Linear Torsion Angle ... # 33
C2 -RE1 -C3 -O3 -143.00 23.00 1.555 1.555 1.555 1.555
PLAT710_ALERT_4_G Delete 1-2-3 or 2-3-4 Linear Torsion Angle ... # 34
C1 -RE1 -C3 -O3 127.00 23.00 1.555 1.555 1.555 1.555
PLAT710_ALERT_4_G Delete 1-2-3 or 2-3-4 Linear Torsion Angle ... # 35
C4 -RE1 -C3 -O3 13.00 23.00 1.555 1.555 1.555 1.555
PLAT710_ALERT_4_G Delete 1-2-3 or 2-3-4 Linear Torsion Angle ... # 36
C5 -RE1 -C3 -O3 33.00 23.00 1.555 1.555 1.555 1.555
PLAT710_ALERT_4_G Delete 1-2-3 or 2-3-4 Linear Torsion Angle ... # 37
C8 -RE1 -C3 -O3 -24.00 23.00 1.555 1.555 1.555 1.555
PLAT710_ALERT_4_G Delete 1-2-3 or 2-3-4 Linear Torsion Angle ... # 38
C7 -RE1 -C3 -O3 -48.00 23.00 1.555 1.555 1.555 1.555
PLAT710_ALERT_4_G Delete 1-2-3 or 2-3-4 Linear Torsion Angle ... # 39
C6 -RE1 -C3 -O3 -11.00 24.00 1.555 1.555 1.555 1.555
PLAT710_ALERT_4_G Delete 1-2-3 or 2-3-4 Linear Torsion Angle ... # 136
C16 -RE2 -N11 -N10 60.00 5.00 1.555 1.555 1.555 1.555
PLAT710_ALERT_4_G Delete 1-2-3 or 2-3-4 Linear Torsion Angle ... # 141
C16 -RE2 -N11 -C12 -118.00 5.00 1.555 1.555 1.555 1.555
PLAT710_ALERT_4_G Delete 1-2-3 or 2-3-4 Linear Torsion Angle ... # 154
C16 -RE2 -C14 -O4 150.00 12.00 1.555 1.555 1.555 1.555
PLAT710_ALERT_4_G Delete 1-2-3 or 2-3-4 Linear Torsion Angle ... # 155
C18 -RE2 -C14 -O4 -121.00 12.00 1.555 1.555 1.555 1.555
PLAT710_ALERT_4_G Delete 1-2-3 or 2-3-4 Linear Torsion Angle ... # 156
C15 -RE2 -C14 -O4 57.00 12.00 1.555 1.555 1.555 1.555
PLAT710_ALERT_4_G Delete 1-2-3 or 2-3-4 Linear Torsion Angle ... # 157
C17 -RE2 -C14 -O4 13.00 14.00 1.555 1.555 1.555 1.555
PLAT710_ALERT_4_G Delete 1-2-3 or 2-3-4 Linear Torsion Angle ... # 158
N11 -RE2 -C14 -O4 -31.00 12.00 1.555 1.555 1.555 1.555
PLAT710_ALERT_4_G Delete 1-2-3 or 2-3-4 Linear Torsion Angle ... # 159
C16 -RE2 -C15 -O5 -135.00 26.00 1.555 1.555 1.555 1.555

PLAT710_ALERT_4_G Delete 1-2-3 or 2-3-4 Linear Torsion Angle ... # 160
C18 -RE2 -C15 -O5 25.00 31.00 1.555 1.555 1.555 1.555
PLAT710_ALERT_4_G Delete 1-2-3 or 2-3-4 Linear Torsion Angle ... # 161
C14 -RE2 -C15 -O5 -44.00 26.00 1.555 1.555 1.555 1.555
PLAT710_ALERT_4_G Delete 1-2-3 or 2-3-4 Linear Torsion Angle ... # 162
C17 -RE2 -C15 -O5 133.00 26.00 1.555 1.555 1.555 1.555
PLAT710_ALERT_4_G Delete 1-2-3 or 2-3-4 Linear Torsion Angle ... # 163
N11 -RE2 -C15 -O5 42.00 26.00 1.555 1.555 1.555 1.555
PLAT710_ALERT_4_G Delete 1-2-3 or 2-3-4 Linear Torsion Angle ... # 164
C18 -RE2 -C16 -O6 -70.00 10.00 1.555 1.555 1.555 1.555
PLAT710_ALERT_4_G Delete 1-2-3 or 2-3-4 Linear Torsion Angle ... # 165
C14 -RE2 -C16 -O6 21.00 10.00 1.555 1.555 1.555 1.555
PLAT710_ALERT_4_G Delete 1-2-3 or 2-3-4 Linear Torsion Angle ... # 166
C15 -RE2 -C16 -O6 110.00 10.00 1.555 1.555 1.555 1.555
PLAT710_ALERT_4_G Delete 1-2-3 or 2-3-4 Linear Torsion Angle ... # 167
C17 -RE2 -C16 -O6 -162.00 10.00 1.555 1.555 1.555 1.555
PLAT710_ALERT_4_G Delete 1-2-3 or 2-3-4 Linear Torsion Angle ... # 168
N11 -RE2 -C16 -O6 3.00 14.00 1.555 1.555 1.555 1.555
PLAT710_ALERT_4_G Delete 1-2-3 or 2-3-4 Linear Torsion Angle ... # 169
C16 -RE2 -C17 -O7 -85.00 12.00 1.555 1.555 1.555 1.555
PLAT710_ALERT_4_G Delete 1-2-3 or 2-3-4 Linear Torsion Angle ... # 170
C18 -RE2 -C17 -O7 -174.00 12.00 1.555 1.555 1.555 1.555
PLAT710_ALERT_4_G Delete 1-2-3 or 2-3-4 Linear Torsion Angle ... # 171
C14 -RE2 -C17 -O7 52.00 13.00 1.555 1.555 1.555 1.555
PLAT710_ALERT_4_G Delete 1-2-3 or 2-3-4 Linear Torsion Angle ... # 172
C15 -RE2 -C17 -O7 8.00 12.00 1.555 1.555 1.555 1.555
PLAT710_ALERT_4_G Delete 1-2-3 or 2-3-4 Linear Torsion Angle ... # 173
N11 -RE2 -C17 -O7 96.00 12.00 1.555 1.555 1.555 1.555
PLAT710_ALERT_4_G Delete 1-2-3 or 2-3-4 Linear Torsion Angle ... # 174
C16 -RE2 -C18 -O8 103.00 15.00 1.555 1.555 1.555 1.555
PLAT710_ALERT_4_G Delete 1-2-3 or 2-3-4 Linear Torsion Angle ... # 175
C14 -RE2 -C18 -O8 12.00 15.00 1.555 1.555 1.555 1.555
PLAT710_ALERT_4_G Delete 1-2-3 or 2-3-4 Linear Torsion Angle ... # 176
C15 -RE2 -C18 -O8 -57.00 19.00 1.555 1.555 1.555 1.555

PLAT710_ALERT_4_G Delete 1-2-3 or 2-3-4 Linear Torsion Angle ... # 177
C17 -RE2 -C18 -O8 -165.00 15.00 1.555 1.555 1.555 1.555
PLAT710_ALERT_4_G Delete 1-2-3 or 2-3-4 Linear Torsion Angle ... # 178
N11 -RE2 -C18 -O8 -74.00 15.00 1.555 1.555 1.555 1.555
PLAT710_ALERT_4_G Delete 1-2-3 or 2-3-4 Linear Torsion Angle ... # 181
C12 -C19 -C20 -PT1 -19.00 8.00 1.555 1.555 1.555 1.555
PLAT710_ALERT_4_G Delete 1-2-3 or 2-3-4 Linear Torsion Angle ... # 182
C42 -PT1 -C20 -C19 13.00 7.00 1.555 1.555 1.555 1.555
PLAT710_ALERT_4_G Delete 1-2-3 or 2-3-4 Linear Torsion Angle ... # 183
P2 -PT1 -C20 -C19 18.00 0.00 1.555 1.555 1.555 1.555
PLAT710_ALERT_4_G Delete 1-2-3 or 2-3-4 Linear Torsion Angle ... # 184
P1 -PT1 -C20 -C19 -4.00 4.00 1.555 1.555 1.555 1.555
PLAT710_ALERT_4_G Delete 1-2-3 or 2-3-4 Linear Torsion Angle ... # 233
C20 -PT1 -C42 -C43 -118.00 4.00 1.555 1.555 1.555 1.555
PLAT710_ALERT_4_G Delete 1-2-3 or 2-3-4 Linear Torsion Angle ... # 236
C20 -PT1 -C42 -C47 58.00 4.00 1.555 1.555 1.555 1.555
PLAT869_ALERT_4_G ALERTS Related to the use of SQUEEZE Suppressed !

CheckCIF report for **18**

Bond precision: C-C = 0.0183 A Wavelength=0.71073
Cell: a=12.4921(18) b=19.290(3) c=23.157(4)
alpha=84.348(9) beta=86.221(9) gamma=87.507(8)
Temperature: 296 K

	Calculated	Reported
Volume	5537.2(15)	5537.0(15)
Space group	P -1	P-1
Hall group	-P 1	?
Moiety formula	$C_{114}H_{94}F_{10}FeN_6P_4Pt_2$	?
Sum formula	$C_{114}H_{94}F_{10}FeN_6P_4Pt_2$	$C_{114}H_{94}F_{10}FeN_6P_4Pt_2$
Mr	2307.85	2307.86
Dx,g cm^{-3}	1.384	1.384
Z	2	2

Mu (mm^{-1})	2.772	2.772
F000	2304.0	2304.0
F000’	2299.68	
h,k,lmax	10,16,19	10,16,19
Nref	7303	7210
Tmin,Tmax	0.745,0.871	0.750,0.885
Tmin’	0.730	

Correction method= MULTI-SCAN
Data completeness= 0.987 Theta(max)= 17.730
R(reflections)= 0.0281(5864) wR2(reflections)= 0.0644(7210)
S = 1.013 Npar= 1246
The following ALERTS were generated. Each ALERT has the format
test-name_ALERT_alert-type_alert-level.
Alert level A
REFNR01_ALERT_3_A Ratio of reflections to parameters is < 6 for a
centrosymmetric structure
sine(theta)/lambda 0.4285
Proportion of unique data used 1.0000
Ratio reflections to parameters 5.7865
THETM01_ALERT_3_A The value of sine(theta_max)/wavelength is less than 0.550
Calculated sin(theta_max)/wavelength = 0.4285
PLAT088_ALERT_3_A Poor Data / Parameter Ratio 5.79
PLAT241_ALERT_2_A Check High Ueq as Compared to Neighbors for C65
PLAT241_ALERT_2_A Check High Ueq as Compared to Neighbors for C66
Alert level B
PLAT220_ALERT_2_B Large Non-Solvent C Ueq(max)/Ueq(min) ... 6.7 Ratio
PLAT234_ALERT_4_B Large Hirshfeld Difference C101 -- C102 .. 0.28 Ang.
PLAT241_ALERT_2_B Check High Ueq as Compared to Neighbors for C42
PLAT242_ALERT_2_B Check Low Ueq as Compared to Neighbors for C64
PLAT242_ALERT_2_B Check Low Ueq as Compared to Neighbors for C67
PLAT334_ALERT_2_B Small Average Benzene C-C Dist. C64 -C69 1.33 Ang.
Alert level C
PLAT213_ALERT_2_C Atom C9 has ADP max/min Ratio ..... 3.8 oblat
PLAT213_ALERT_2_C Atom C39 has ADP max/min Ratio ..... 3.6 prola

PLAT213_ALERT_2_C Atom C50 has ADP max/min Ratio ..... 3.1 oblat
PLAT213_ALERT_2_C Atom C65 has ADP max/min Ratio ..... 3.9 prola
PLAT213_ALERT_2_C Atom C66 has ADP max/min Ratio ..... 4.0 prola
PLAT213_ALERT_2_C Atom C102 has ADP max/min Ratio ..... 3.5 oblat
PLAT222_ALERT_3_C Large Non-Solvent H Uiso(max)/Uiso(min) .. 4.7 Ratio
PLAT230_ALERT_2_C Hirshfeld Test Diff for C55 -- C56 .. 5.9 su
PLAT234_ALERT_4_C Large Hirshfeld Difference F3 -- C50 .. 0.22 Ang.
PLAT234_ALERT_4_C Large Hirshfeld Difference F5 -- C52 .. 0.19 Ang.
PLAT234_ALERT_4_C Large Hirshfeld Difference N4 -- N5 .. 0.22 Ang.
PLAT234_ALERT_4_C Large Hirshfeld Difference N4 -- C56 .. 0.25 Ang.
PLAT234_ALERT_4_C Large Hirshfeld Difference N5 -- N6 .. 0.20 Ang.
PLAT234_ALERT_4_C Large Hirshfeld Difference N6 -- C55 .. 0.21 Ang.
PLAT234_ALERT_4_C Large Hirshfeld Difference C5 -- C10 .. 0.18 Ang.
PLAT234_ALERT_4_C Large Hirshfeld Difference C8 -- C9 .. 0.23 Ang.
PLAT234_ALERT_4_C Large Hirshfeld Difference C9 -- C10 .. 0.22 Ang.
PLAT234_ALERT_4_C Large Hirshfeld Difference C15 -- C16 .. 0.18 Ang.
PLAT234_ALERT_4_C Large Hirshfeld Difference C16 -- C17 .. 0.16 Ang.
PLAT234_ALERT_4_C Large Hirshfeld Difference C19 -- C24 .. 0.21 Ang.
PLAT234_ALERT_4_C Large Hirshfeld Difference C21 -- C22 .. 0.21 Ang.
PLAT234_ALERT_4_C Large Hirshfeld Difference C26 -- C31 .. 0.20 Ang.
PLAT234_ALERT_4_C Large Hirshfeld Difference C27 -- C28 .. 0.18 Ang.
PLAT234_ALERT_4_C Large Hirshfeld Difference C28 -- C29 .. 0.17 Ang.
PLAT234_ALERT_4_C Large Hirshfeld Difference C30 -- C31 .. 0.17 Ang.
PLAT234_ALERT_4_C Large Hirshfeld Difference C33 -- C34 .. 0.18 Ang.
PLAT234_ALERT_4_C Large Hirshfeld Difference C36 -- C39 .. 0.18 Ang.
PLAT234_ALERT_4_C Large Hirshfeld Difference C37 -- C38 .. 0.21 Ang.
PLAT234_ALERT_4_C Large Hirshfeld Difference C40 -- C45 .. 0.17 Ang.
PLAT234_ALERT_4_C Large Hirshfeld Difference C42 -- C43 .. 0.19 Ang.
PLAT234_ALERT_4_C Large Hirshfeld Difference C43 -- C44 .. 0.18 Ang.
PLAT234_ALERT_4_C Large Hirshfeld Difference C44 -- C45 .. 0.20 Ang.
PLAT234_ALERT_4_C Large Hirshfeld Difference C47 -- C52 .. 0.21 Ang.
PLAT234_ALERT_4_C Large Hirshfeld Difference C67 -- C68 .. 0.19 Ang.
PLAT234_ALERT_4_C Large Hirshfeld Difference C71 -- C72 .. 0.23 Ang.
PLAT234_ALERT_4_C Large Hirshfeld Difference C71 -- C76 .. 0.17 Ang.

PLAT234_ALERT_4_C Large Hirshfeld Difference C72 -- C73 .. 0.22 Ang.
PLAT234_ALERT_4_C Large Hirshfeld Difference C73 -- C74 .. 0.20 Ang.
PLAT234_ALERT_4_C Large Hirshfeld Difference C74 -- C75 .. 0.20 Ang.
PLAT234_ALERT_4_C Large Hirshfeld Difference C82 -- C83 .. 0.19 Ang.
PLAT234_ALERT_4_C Large Hirshfeld Difference C85 -- C86 .. 0.17 Ang.
PLAT234_ALERT_4_C Large Hirshfeld Difference C93 -- C94 .. 0.16 Ang.
PLAT234_ALERT_4_C Large Hirshfeld Difference C99 -- C100 .. 0.16 Ang.
PLAT234_ALERT_4_C Large Hirshfeld Difference C100 -- C101 .. 0.23 Ang.
PLAT234_ALERT_4_C Large Hirshfeld Difference C102 -- C103 .. 0.21 Ang.
PLAT234_ALERT_4_C Large Hirshfeld Difference C105 -- C106 .. 0.20 Ang.
PLAT234_ALERT_4_C Large Hirshfeld Difference C105 -- C109 .. 0.18 Ang.
PLAT234_ALERT_4_C Large Hirshfeld Difference C106 -- C107 .. 0.17 Ang.
PLAT234_ALERT_4_C Large Hirshfeld Difference C110 -- C111 .. 0.19 Ang.
PLAT234_ALERT_4_C Large Hirshfeld Difference C112 -- C113 .. 0.22 Ang.
PLAT241_ALERT_2_C Check High Ueq as Compared to Neighbors for N2
PLAT241_ALERT_2_C Check High Ueq as Compared to Neighbors for N3
PLAT241_ALERT_2_C Check High Ueq as Compared to Neighbors for N5
PLAT241_ALERT_2_C Check High Ueq as Compared to Neighbors for N6
PLAT241_ALERT_2_C Check High Ueq as Compared to Neighbors for C7
PLAT241_ALERT_2_C Check High Ueq as Compared to Neighbors for C9
PLAT241_ALERT_2_C Check High Ueq as Compared to Neighbors for C21
PLAT241_ALERT_2_C Check High Ueq as Compared to Neighbors for C37
PLAT241_ALERT_2_C Check High Ueq as Compared to Neighbors for C41
PLAT241_ALERT_2_C Check High Ueq as Compared to Neighbors for C44
PLAT241_ALERT_2_C Check High Ueq as Compared to Neighbors for C45
PLAT241_ALERT_2_C Check High Ueq as Compared to Neighbors for C69
PLAT242_ALERT_2_C Check Low Ueq as Compared to Neighbors for C8
PLAT242_ALERT_2_C Check Low Ueq as Compared to Neighbors for C22
PLAT242_ALERT_2_C Check Low Ueq as Compared to Neighbors for C29
PLAT242_ALERT_2_C Check Low Ueq as Compared to Neighbors for C33
PLAT242_ALERT_2_C Check Low Ueq as Compared to Neighbors for C36
PLAT242_ALERT_2_C Check Low Ueq as Compared to Neighbors for C40
PLAT242_ALERT_2_C Check Low Ueq as Compared to Neighbors for C43
PLAT242_ALERT_2_C Check Low Ueq as Compared to Neighbors for C49

PLAT242_ALERT_2_C Check Low Ueq as Compared to Neighbors for C60
PLAT242_ALERT_2_C Check Low Ueq as Compared to Neighbors for C71
PLAT242_ALERT_2_C Check Low Ueq as Compared to Neighbors for C81
PLAT242_ALERT_2_C Check Low Ueq as Compared to Neighbors for C85
PLAT242_ALERT_2_C Check Low Ueq as Compared to Neighbors for C88
PLAT242_ALERT_2_C Check Low Ueq as Compared to Neighbors for C92
PLAT242_ALERT_2_C Check Low Ueq as Compared to Neighbors for C95
PLAT242_ALERT_2_C Check Low Ueq as Compared to Neighbors for C101
PLAT242_ALERT_2_C Check Low Ueq as Compared to Neighbors for C102
PLAT334_ALERT_2_C Small Average Benzene C-C Dist. C5 -C10 1.37 Ang.
PLAT334_ALERT_2_C Small Average Benzene C-C Dist. C33 -C38 1.37 Ang.
PLAT334_ALERT_2_C Small Average Benzene C-C Dist. C40 -C45 1.36 Ang.
PLAT334_ALERT_2_C Small Average Benzene C-C Dist. C47 -C52 1.36 Ang.
PLAT334_ALERT_2_C Small Average Benzene C-C Dist. C57 -C62 1.37 Ang.
PLAT334_ALERT_2_C Small Average Benzene C-C Dist. C71 -C76 1.37 Ang.
PLAT334_ALERT_2_C Small Average Benzene C-C Dist. C78 -C83 1.37 Ang.
PLAT334_ALERT_2_C Small Average Benzene C-C Dist. C85 -C90 1.37 Ang.
PLAT334_ALERT_2_C Small Average Benzene C-C Dist. C92 -C97 1.37 Ang.
PLAT334_ALERT_2_C Small Average Benzene C-C Dist. C99 -C104 1.36 Ang.
PLAT342_ALERT_3_C Low Bond Precision on C-C Bonds ..... 0.0183 Ang
PLAT731_ALERT_1_C Bond Calc 1.33(3), Rep 1.330(13) ..... 2 su-Ra
C49 -C50 1.555 1.555 # 142
PLAT731_ALERT_1_C Bond Calc 1.37(3), Rep 1.374(14) ..... 2 su-Ra
C50 -C51 1.555 1.555 # 143
Alert level G
PLAT005_ALERT_5_G No _iucr_refine_instructions_details in CIF .... ?
PLAT371_ALERT_2_G Long C(sp2)-C(sp1) Bond C2 - C3 ... 1.46 Ang.
PLAT371_ALERT_2_G Long C(sp2)-C(sp1) Bond C54 - C55 ... 1.44 Ang.
PLAT380_ALERT_4_G Check Incorrectly? Oriented X(sp2)-Methyl Moiety C84
PLAT606_ALERT_4_G VERY LARGE Solvent Accessible VOID(S) in Structure !
PLAT710_ALERT_4_G Delete 1-2-3 or 2-3-4 Linear Torsion Angle ... # 3
P2 -PT1 -P1 -C33 -28.20 0.80 1.555 1.555 1.555 1.555
PLAT710_ALERT_4_G Delete 1-2-3 or 2-3-4 Linear Torsion Angle ... # 6
P2 -PT1 -P1 -C40 94.10 0.80 1.555 1.555 1.555 1.555

PLAT710_ALERT_4_G Delete 1-2-3 or 2-3-4 Linear Torsion Angle ... # 9
P2 -PT1 -P1 -C26 -147.60 0.80 1.555 1.555 1.555 1.555
PLAT710_ALERT_4_G Delete 1-2-3 or 2-3-4 Linear Torsion Angle ... # 12
P1 -PT1 -P2 -C19 16.40 0.90 1.555 1.555 1.555 1.555
PLAT710_ALERT_4_G Delete 1-2-3 or 2-3-4 Linear Torsion Angle ... # 15
P1 -PT1 -P2 -C12 135.40 0.80 1.555 1.555 1.555 1.555
PLAT710_ALERT_4_G Delete 1-2-3 or 2-3-4 Linear Torsion Angle ... # 18
P1 -PT1 -P2 -C5 -102.00 0.80 1.555 1.555 1.555 1.555
PLAT710_ALERT_4_G Delete 1-2-3 or 2-3-4 Linear Torsion Angle ... # 21
P4 -PT2 -P3 -C78 101.90 1.10 1.555 1.555 1.555 1.555
PLAT710_ALERT_4_G Delete 1-2-3 or 2-3-4 Linear Torsion Angle ... # 24
P4 -PT2 -P3 -C85 -139.20 1.00 1.555 1.555 1.555 1.555
PLAT710_ALERT_4_G Delete 1-2-3 or 2-3-4 Linear Torsion Angle ... # 27
P4 -PT2 -P3 -C92 -16.40 1.10 1.555 1.555 1.555 1.555
PLAT710_ALERT_4_G Delete 1-2-3 or 2-3-4 Linear Torsion Angle ... # 30
P3 -PT2 -P4 -C71 4.70 1.10 1.555 1.555 1.555 1.555
PLAT710_ALERT_4_G Delete 1-2-3 or 2-3-4 Linear Torsion Angle ... # 33
P3 -PT2 -P4 -C64 126.10 1.00 1.555 1.555 1.555 1.555
PLAT710_ALERT_4_G Delete 1-2-3 or 2-3-4 Linear Torsion Angle ... # 36
P3 -PT2 -P4 -C57 -113.50 1.10 1.555 1.555 1.555 1.555
PLAT710_ALERT_4_G Delete 1-2-3 or 2-3-4 Linear Torsion Angle ... # 43
C47 -PT1 -C1 -C2 19.00 10.00 1.555 1.555 1.555 1.555
PLAT710_ALERT_4_G Delete 1-2-3 or 2-3-4 Linear Torsion Angle ... # 46
PT1 -C1 -C2 -C3 3.00 11.00 1.555 1.555 1.555 1.555
PLAT710_ALERT_4_G Delete 1-2-3 or 2-3-4 Linear Torsion Angle ... # 49
C1 -C2 -C3 -C4 10.00 7.00 1.555 1.555 1.555 1.555
PLAT710_ALERT_4_G Delete 1-2-3 or 2-3-4 Linear Torsion Angle ... # 50
C1 -C2 -C3 -N3 -169.00 6.00 1.555 1.555 1.555 1.555
PLAT710_ALERT_4_G Delete 1-2-3 or 2-3-4 Linear Torsion Angle ... # 151
C1 -PT1 -C47 -C48 150.00 7.00 1.555 1.555 1.555 1.555
PLAT710_ALERT_4_G Delete 1-2-3 or 2-3-4 Linear Torsion Angle ... # 154
C1 -PT1 -C47 -C52 -26.00 7.00 1.555 1.555 1.555 1.555
PLAT710_ALERT_4_G Delete 1-2-3 or 2-3-4 Linear Torsion Angle ... # 181
C99 -PT2 -C53 -C54 -2.00 15.00 1.555 1.555 1.555 1.555

PLAT710_ALERT_4_G Delete 1-2-3 or 2-3-4 Linear Torsion Angle ... # 182
P3 -PT2 -C53 -C54 -62.00 8.00 1.555 1.555 1.555 1.555
PLAT710_ALERT_4_G Delete 1-2-3 or 2-3-4 Linear Torsion Angle ... # 183
P4 -PT2 -C53 -C54 114.00 8.00 1.555 1.555 1.555 1.555
PLAT710_ALERT_4_G Delete 1-2-3 or 2-3-4 Linear Torsion Angle ... # 184
PT2 -C53 -C54 -C55 -9.00 12.00 1.555 1.555 1.555 1.555
PLAT710_ALERT_4_G Delete 1-2-3 or 2-3-4 Linear Torsion Angle ... # 289
C53 -PT2 -C99 -C100 40.00 10.00 1.555 1.555 1.555 1.555
PLAT710_ALERT_4_G Delete 1-2-3 or 2-3-4 Linear Torsion Angle ... # 292
C53 -PT2 -C99 -C104 -136.00 10.00 1.555 1.555 1.555 1.555
PLAT869_ALERT_4_G ALERTS Related to the use of SQUEEZE Suppressed !